THE UNIVERSITY *of* EDINBURGH

The role of phenotype switching during biological evolution in static environments

Andrew Tadrowski

Doctor of Philosophy
The University of Edinburgh
2016

Abstract

Biological evolution is an inherently non-equilibrium process, by which a population acquires a new genetic composition, optimally suited to its present environment. Far from being the slow process it is traditionally viewed as, the rapid evolution of microbes is causing serious global concern in the acquisition of microbial resistance to antibiotics. Better understanding of the mechanisms that govern the evolution of microbes is therefore of paramount importance.

In many traditional models, evolution occurs over the space of all possible genetic states (genotypes). These are assigned a quantity called fitness, which quantifies that genotype's suitability over others to thrive within its present environment. A population of replicating cells can evolve over this space under the competing influences of random variations of the genotype (i.e. mutations) and the increased likelihood of success for fitter genotypes (i.e. selection).

Many of these models fail to account for the observation that biological diversity is rife, even amongst genetically identical cells that exist in the same environment. This diversity manifests itself as a difference in phenotype (the observable traits of an organism). It means that organisms with the same genotype, but a different phenotype, may have different fitnesses. Therefore, when phenotypic heterogeneity is apparent, evolution over genotype space should consider different fitness landscapes for each of the distinct phenotypic states that exist.

Phenotypic heterogeneity has long been observed in populations of microbes. Often these can switch between different phenotypic states for a number of reasons. A common example of this is stochastic phenotype switching, in which cells randomly switch between two phenotypic states, without any inducing influence. This has been shown to benefit populations of cells that are subject to fluctuating environmental conditions, or by creating a division of labour in the population.

In this work, I examine the possibility of another role for stochastic phenotype switching: as a mechanism that can accelerate evolution even in a static environment. During evolution, populations can spend large amounts of time trapped at local peaks on a fitness landscape. A cell that switches phenotype will change to a different fitness landscape, which may allow for faster genetic evolution.

I begin this work in Chapters 3 and 4, where I present a model of an evolving population of haploid cells, trapped at a local peak on a 1D fitness landscape. These cells have access to a second phenotypic state, in which the fitness landscape is uniform. The focus of this study is to see the effect that stochastic phenotype switching to this secondary phenotype has on the populations evolution of a target state. In Chapter 3 I study this numerically and identify an optimal range for the rate of phenotype switching, within which the time taken for the process can be reduced by many orders of magnitude. I also find that if the frequency of switching is allowed to evolve, then the likely evolutionary trajectory taken by a population is one that first evolves a switching frequency to within the identified optimal range, before escaping from the local peak.

In Chapter 4 I present an analytic study of the same model. The aim here is to recover the numerical results from Chapter 3. I employ numerous analytic techniques to show the existence of the optimal range, while developing an analytic approach that allows a study of the model at parameter values that are otherwise difficult to simulate.

This same model is extended in Chapter 5 to consider evolution over a more complex genotype space: that of a hypercube. Here, genotypes correspond to particular binary sequences, which can be used as representations of many biological states of interest; for example, nucleotide sequences in DNA or the presence and absence of important mutations in specific genes. My focus here is again on the effect that stochastic phenotype switching has on how a population of cells evolves over genotype space. This is studied numerically for various kinds of randomly generated fitness landscapes. I find that in some instances phenotype switching can significantly benefit a population. However, in other instances it can significantly hinder the evolution, increasing the time taken for the process by many orders of magnitude.

Finally, in Chapter 6 I present a model that explores how a population of the bacterium *Escherichia coli (E. coli)* evolves resistance to the antibiotic

ciprofloxacin. This work is motivated by the observed rapid acquisition of resistance of *E. coli* when exposed to sub-lethal concentrations of the antibiotic. Upon damage to their DNA, cells can induce a switch to a secondary phenotypic state (as part of the SOS response), in which DNA repair and an increased rate of mutations occur. Using this model, with empirical data for the fitness and susceptibility of genotypes, I numerically explore the dependence of rapid evolution on the existence of this secondary phenotypic state. I find that the model predicts, over the short timescales considered, that the evolution of sufficient resistance requires the existence of the secondary phenotypic state.

The findings of this work is that the phenotypic switching of cells can have a significant impact on how populations evolve in static environments. While stochastic phenotype switching can help populations escape from local peaks, it can also trap populations on sub-optimal landscapes if the frequency of switching is too low.

Declaration

I declare that this thesis was composed by myself, that the work contained herein is my own except where explicitly stated otherwise in the text, and that this work has not been submitted for any other degree or professional qualification except as specified.

(*Andrew Tadrowski, 2016*)

Some of the work contained in Chapter 3 has been prepared for publication and is available in preprint form [191].

Acknowledgements

This work is dedicated to the memories of my nana Mary Charteris and papa Ted Tadrowski: wonderful grandparents and great friends.

To my supervisors Bartłomiej Waclaw and Martin Evans: thank you for your help, guidance and enduring patience.

To my office-mate Toby Searle: thank you for your company, and for helping me to see the funny side of it all.

To my parents: thank you for your constant love and support, and for creating such a happy home.

To my sister Laura: thank you for always being there, making me laugh, and for setting such a good example.

And to my fiancée Jacqueline: thank you for making this experience such a happy one, and for making us a wonderful home. I could not have done this without you.

This work was generously supported by the CM-DTC[1], SUPA[2] and EPSRC[3].

[1]The Scottish Centre for Doctoral Training in Condensed Matter Physics
[2]The Scottish Universities Physics Alliance
[3]Engineering and Physical Sciences Research Council

Contents

List of Figures

List of Tables

Chapter 1

Introduction

1.1 Overview

Biological evolution has led to the startling variety of life that can be found on this planet. Of all life forms, perhaps the most important — and easily overlooked — are microbes. These are single-celled organisms that include bacteria and yeasts. In many ways microbes are the dominant life forms on earth. A recent estimate of the number of sub-seafloor sedimentary microbes was found to be 2.9×10^{29} ($\sim 10^{20}$ for every human on earth) [97]. Microbes have important roles in ecosystems, including the recycling of key atmospheric molecules such as in nitrogen fixation (converting relatively inert atmospheric N_2 into ammonium ions which are integral to molecular biosynthesis) [209]. They also have uses in industry such as in bioremediation [69].

Many microbes have a direct impact on us and positively affect our lives, such as the diverse intestinal microbial flora that benefit our health [50]. However, many have the capacity to grievously harm our individual lives and species as a whole. For example, the bacterium *Yersinia pestis* was the causative agent of the bubonic plague, killing an estimated 50 million people as the "Black Death" of the 14th century [40].

Microbes are the ideal subjects to use for experimental studies of biological evolution. They allow for highly controlled, repeatable experiments to be carried out [54]. Due to their quick reproduction rate, the process of biological evolution — normally associated with extremely large timescales — can be viewed as it

happens over a matter of hours and days. Through such studies, the growing problem of unwanted microbial evolution can be addressed.

The rapid evolution of resistance in microbes to antimicrobial drugs is a global health concern [95, 145, 146]. Resistance affects the treatment of infections, the success of surgical operations, and the quality of life of those afflicted. Worldwide resistance in the bacterium *Klebsiella pneumoniae*, a pathogenic cause of pneumonia, has already emerged [146, 170]. Treatment failures have also been reported for the last resort drugs for *gonorrhoea* [146], while the bacterium *Escherichia coli (E. coli)* continues to develop widespread resistance to the *fluoroquinolone* family of antibiotics [107, 128]. An improved understanding of the mechanisms and dynamics of microbial evolution can help to form combative strategies against the evolution of further unwanted resistance.

We consider the biological evolution of a population to occur as the result of the competing evolutionary mechanisms of *selection* and *mutation*. Mechanisms other than mutation, such as *gene transfer* and *migration*, also allow for variations in organism types to be explored but will not be considered here. Selection increases the likelihood of "better suited" organisms existing in the population, while new organism types are sampled through mutations. The net result is that populations move through the space of possible organism types towards an optimal (genetic) distribution. This is analogous to the temporal evolution that physical systems undergo, towards the ground state configuration that minimises their free energy.

In this chapter we begin by discussing key concepts from biology that are important to the work carried out in this thesis. As the focus is on microbial evolution, these discussions mainly concern populations of asexually reproducing cells. We begin at the very start, by defining the process of biological evolution. We will see why phenotypic heterogeneity exists even amongst isogenic populations, and how it can lead to the phenomenon of *stochastic phenotype switching*. We close this chapter with an overview of the research contained in this thesis. Throughout this chapter the relevant biology is often simplified for brevity. A more thorough explanation of the numerous molecular processes taking place in cells can be found in the preeminent text of [10].

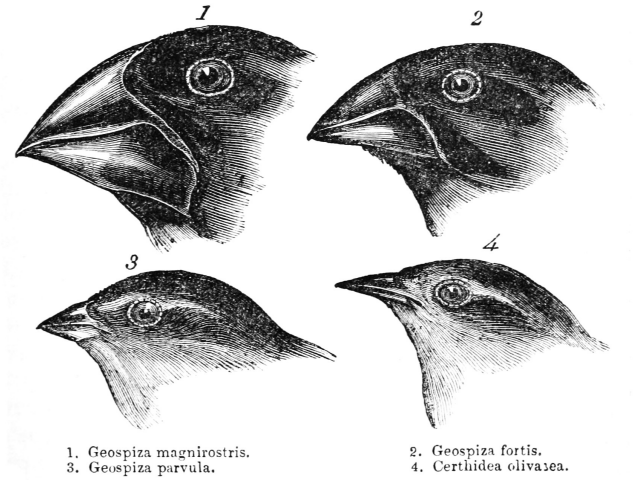

Figure 1.1 *"Darwin's finches", illustrated by J. Gould. Taken from [37]*

1.2 Biological evolution

If different species share the same environment and natural resources they can be competitors for survival. Those better suited to the challenges of life in the environment are likely to thrive and propagate, at the expense of those less able to. This same competition takes place between individuals of the same species, both when they are identical and when they differ as a result of some phenotypic variation (i.e. variations in physical traits such as height). If the variation is heritable, this trait can be passed to offspring and, over many generations, can propagate across the population.

Variations in phenotype can give individuals a benefit to survival, while allowing populations to adapt to exploit available ecological niches. A classic example of this are "Darwin's finches", shown in Fig. 1.1. The primary differences between the finches are in the size and shapes of their beaks, which appear highly adapted to different available food sources in their environments. A study found that the differences in beak morphology can result from heritable variations in the amount of a protein (Bmp4) present during the development of skeletal features, such as the beak [160].

The process by which organisms compete with one another for survival, while sampling new heritable traits through reproduction, is the essence of Darwins evolutionary theory of natural selection [38]. For biological evolution to take place, populations require variations in heritable phenotypic traits and mechanisms through which such variations can arise. Not until the work of

Mendel was rediscovered in the early 20th century was it accepted that heritable traits are passed from parent(s) to offspring in discrete units. These units were later identified to be genes — sequences of the genome that code for proteins or functional RNA chains.. Combined with Darwin's theory of natural selection, and the work of Fisher [59], Haldane [78] and Wright [214, 215], this lead to the *Modern evolutionary synthesis*, the evolutionary theory widely accepted today.

1.2.1 Genotypes and phenotypes

All living cells store their genetic information in DNA. This information relates to all aspects of cellular behaviour and functioning. DNA consists of two polynucleotide strands, connected together into the structure of a double helix. Each strand consists of a chain of nucleotides; composite molecules consisting of a deoxyribose sugar, phosphate group and a nitrogen containing base. The four possible bases in DNA are cytosine (C), guanine (G), adenine (A) and thymine (T). Genetic information is stored in the ordering of these bases. Both polynucleotide strands in DNA contain the same information and are bound together by hydrogen bonding of the complimentary bases of A with T and C with G. These pairings create four possible basepair (bp) combinations: A-T, T-A, G-C and C-G, which serve as the smallest units of genetic information.

Alternatively, RNA molecules are single polynucleotide strands that bond with themselves. RNA nucleotides use the sugar ribose (instead of the deoxyribose of DNA) and the same bases as DNA except for thymine, which is replaced by uracil (U). RNA is key to the cellular processes of *transcription* and *translation*. These are part of the complex process of *expression*, by which the information contained in the genome leads to the production of functional molecules (e.g. proteins) in the cell. RNA is also how genetic information is stored in RNA based viruses.

The length of genomes vary dramatically across organisms and viruses. For example, the genome length of humans (*Homo sapiens*) is 3.2×10^9 bp, a number which is doubled in somatic cells which contain two sets of chromosomes (as they are *diploid* cells). The genome length in the bacterium *E. coli* is 4.6×10^6 bp and the RNA based bacteriophage $Q\beta$ is 4.2×10^3 bp [44, 46].

An organism's phenotype (the collection of all observable traits) depends non-trivially on its genotype (genome), environment and history. An illustration of this can be seen in Fig. 1.2, which shows a cat alongside a kitten which is a clone

Figure 1.2 *A cat and its clone. Despite being genetically identical the kitten and cat exhibit different coat colourings and patterns. During development, the final form is decided by environmental factors as well as genotype. Taken from [1].*

of it [178]. Despite being genetically identical the coat pattern and colourings of the kitten do not match that of the cat. Coat patterns and pigmentations are affected not only by the genotype but environmental factors during early development.

The first kind of phenotypic changes we consider are those that occur due to changes of genotype. Unlike plants and animals, most microbes reproduce asexually [121]. During asexual reproduction, a cell creates a copy of its own genome which is passed to a daughter cell. Variations in genotype occur due to incorrect copying of the genome, resulting in DNA with a different base-pair sequence. In such instances the daughter is of a "mutant" genotype. The simplest kinds of mutations are point mutations in which one base-pair is replaced by a different one during DNA replication. Other mutation types can occur such as base-pair insertions and deletions (leading to *frame-shift* errors) and larger genotype rearrangements occurring through *recombination* [54]. However, our focus throughout will be on mutations occurring through base-pair substitutions.

The probability of mutations per nucleotide base during DNA replication varies between organisms. In *E. coli* it is on average 10^{-10} to 10^{-9} per replication [46, 116]. In general, replication fidelity is believed to be this efficient as most mutations are expected to be harmful [4]. However, both genome-wide mutation rates and site specific ones can reach far higher rates than this. In *mutator* strains, the rate of mutations can be orders of magnitude higher. These mutations can reach high frequencies in populations by producing compensatory beneficial mutations elsewhere in the genome (in a process termed *hitch-hiking*) [182, 190].

Mutation rates have also been observed to increase by as many as four orders of magnitude in the presence of antibiotics [28, 35, 76]. This can be due to the initiation of certain cellular responses, such as the SOS response which we discuss shortly. This increases the expression of error prone DNA polymerases (enzymes involved in DNA replication) and correspondingly the rate of mutations.

It is common practise to view and model the evolutionary process as occurring over genotype space. While the genotypes of organisms can be classed according to their exact (discrete) genomic sequences, it would be far more difficult to quantify them, and study them, by the extent to which they express continuous phenotypic traits. Alternative models that consider evolution to occur over the space of possible phenotypes, such as Fisher's *Geometric model* [59], are not considered in this thesis.

1.2.2 Fitness

Selection acts on a population through differences in the *fitness* of its members. Fitness is a measure of a cell's suitability to its present environment, which is normally decided by its reproductive success. Therefore a fitter cell is expected to propagate more offspring than a less fit one. In microbial experiments, fitness can be measured in numerous ways. One way is to measure it relative to another cell (such as an ancestral wild-type) by growing both cell types in equal conditions and measuring the ratio in density differences after a set amount of time (usually one day) [54]. While fitness is a property of an organism's phenotype, owing to the complexity of the genotype-phenotype map (discussed in the preceding section), it is often assigned directly to genotypes.

Assigning a numerical fitness value directly to each genotype produces a mapping between genotypes and fitness that is known as the *fitness landscape* [215]. For a 2D genotype space (in which nearest neighbour genotypes are those connected by mutations) the fitness landscape is often represented as a continuous 2D surface in 3D space, producing a familiar mountainous image upon which the high-climbing metaphor of evolution can be pictured. An example cartoon showing part of such a fitness landscape can be seen in Fig. 1.3. However, beyond 2D genotype spaces this familiar imagery can be misleading, as real fitness landscapes are multidimensional and discrete.

Driven by the competition between mutation and selection, populations move

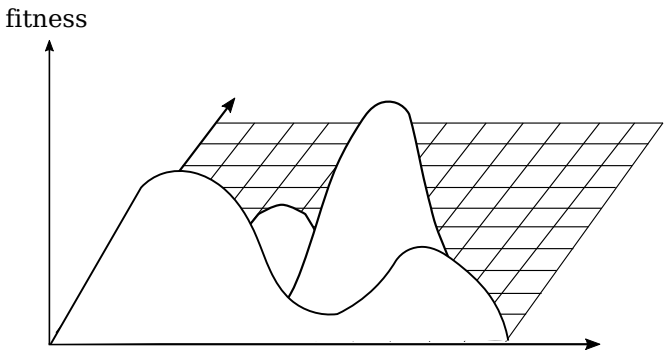

Figure 1.3 *A continuous fitness landscape for a 2D genotype space. The 2D grid identifies viable genotypes. To each genotype a fitness is directly assigned, which results in a mountainous topography over which the evolutionary process can be pictured to occur.*

over the fitness landscape (over the space of possible genotypes). Selection drives the motion to regions of increased fitness, while mutation provides the means by which new genotypes can be sampled. A balance between mutation and selection is reached at the steady-state distributions of the population. This often happens at local peaks of the fitness landscape.

Therefore during evolution, as the movement of the population is directed towards fitter genotypes, non-zero net currents of population (i.e. mass) will flow over the space of possible genotypes. The probability of the population existing in a specific genetic configuration is therefore likely to change in time. In such a case the flow of probability into and out of this configuration are not equal and the condition of *detailed balance* from equilibrium statistical mechanics is broken. This means the process of biological evolution is a "non-equilibrium" mass transport process. Numerous stochastic methods and models from both non-equilibrium and equilibrium statistical mechanics can be used in the study of features of evolving populations and their steady-state distributions. Some of these will be discussed in Chapter 2.

Fitness landscapes can consist of numerous peaks and valleys as a result of *epistasis*. Epistasis describes the fitness interaction between different loci, such that a mutation's effect on fitness will depend on what alleles are at other loci (i.e. the genetic background). As a result, two mutations that are independently beneficial can combine to have different effects on fitness. With *sign epistasis* the fitness effect can be positive or negative depending on the genetic background at the other allele. This type of epistasis is present in fitness landscapes that contain a single peak but for which not all direct trajectories towards the peak have fitness

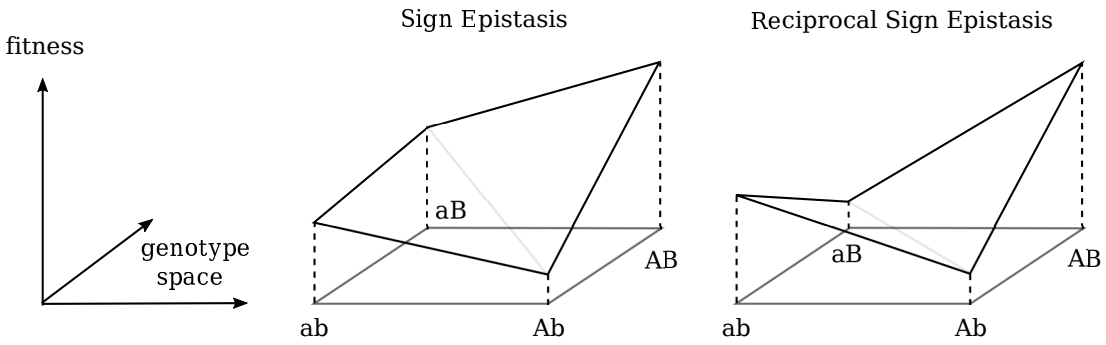

Figure 1.4 *Fitness landscapes that exhibit sign epistasis and reciprocal sign epistasis in a two locus model. With sign epistasis (left image) the fitness landscape has a single peak. Whether the mutation a→A has a positive effect on fitness depends on whether the allele at the other locus is b or B. In the reciprocal sign epistasis case (right image) the fitness landscape contains two peaks. This is due to both mutations a→A and b→B from genotype ab being deleterious, despite them combining to confer a fitness advantage.*

increasing monotonically along them [204]. Alternatively, landscapes that contain multiple peaks necessarily exhibit *reciprocal sign epistasis* [154]. With reciprocal sign epistasis two mutations that individually increase fitness will reduce it when combined (or vice versa). This type of epistasis has been observed experimentally in real fitness landscapes [108, 124, 197]. Figure 1.4 shows illustrations of the effects of sign epistasis and reciprocal sign epistasis in a model with two loci.

1.2.3 Phenotypic noise

Phenotypic heterogeneity is present even amongst populations of genetically identical cells that exist in a homogeneous environment. This is due to variations in the extent to which phenotypic traits are expressed. Heterogeneity in a particular trait can be classified as *quantitative* or *qualitative*. In quantitative heterogeneity the trait can take a continuous range of values, while in qualitative it can take one of at least two distinct values [3]. A demonstration of such heterogeneity in a population of *E. coli* can be seen in Fig. 1.5.

There are many reasons why isogenic cells exhibit phenotypic heterogeneity. Cellular age, defined as the time since certain sub-cellular structures were produced, can differ across a population of cells that divide asymmetrically. Age can then affect a cell's expression of certain phenotypic traits. For example, upon exposure to antibiotics the survival of the bacterium *Mycobacterium tuberculosis*

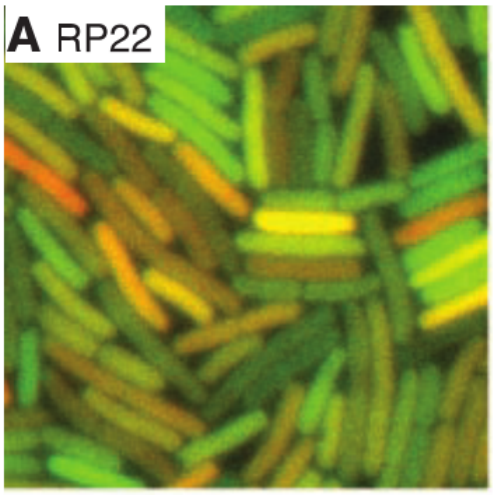

Figure 1.5 *Intrinsic noise in an isogenic E. coli population. Genes present code for cyan and yellow fluorescent proteins (cfp and yfp respectively), controlled by identical promoters. Cells with the same amount of each protein will appear yellow, otherwise differences in the abundances cause them to look red or green. Taken from [55]. Reprinted with permission from AAAS.*

(M. tuberculosis) was found to depend on the age of the cells in the population [11]. Alternatively, heterogeneity can arise due to oscillations of cellular functions [118]. This is observed in *unicellular cyanobacteria* which oscillate over a 24 hour period between expressing genes for nitrogen fixation and photosynthesis as a metabolic process [123]. Finally, the interaction of bacteria with their environment, such as through chemical signalling, can affect gene expression. For example, cells can communicate with one another through quorum sensing and react to changing population densities by altering gene expression [200].

However, more fundamentally, phenotypic heterogeneity arises from the stochasticity of the biochemical processes involved in gene expression. This results in fluctuations in the abundance of proteins produced which affects a cell's phenotype. We refer to this kind of phenotypic heterogeneity as *phenotypic noise*, of which there are two sources. First, the processes involved in expression require molecules (e.g. regulatory proteins and polymerases) which exist at limited numbers in the cells and which vary between them. These differences result in a stochasticity in gene expression between cells known as *extrinsic noise* [158]. During cellular division the segregation of molecular material is stochastic and largely asymmetric, which results in this kind of noise [88]. It was shown in the soil bacterium *Bacillus subtilis (B. subtilis)*, following genetic modification that

increased the size of cells, that there was a drop in the degree of phenotypic noise. This was attributed to the increased number of molecular components in these larger cells, which reduced the stochasticity in expression [186]. Extrinsic noise also occurs due to factors independent of the cell, such as the subtle environmental differences that exists between cells [158].

The second source of phenotypic heterogeneity can be seen by examining a single cell. Its properties will fluctuate indicating that genes are not expressed at a constant rate. This is due to the low rates of occurrence of the random microscopic events that initiate the necessary reactions in expression. This sort of stochasticity is *intrinsic noise* and can be seen in Fig. 1.5 [55, 149, 158]. The cells contain two fluorescent proteins, the expression of which are controlled by the same promoter. In the absence of intrinsic noise there should be an equal rate of expression of both genes causing the cells to appear yellow.

Phenotypic noise can be amplified or dampened by a gene's regulatory networks. Studies of *E. coli* and the budding yeast *Saccharomyces cerevisiae (S. cerevisae)* have measured the extent of variations in phenotypic noise across different genes [142, 179]. High levels of noise are often associated with stress-related or metabolic genes [17], while lower levels of noise are observed in essential genes, such as those coding for essential or complex-forming proteins [66]. This is likely due to *negative feedback loops* in the regulatory networks [23]. Such feedback loops dampen noise that might otherwise be harmful to the organism's fitness [117].

Gene regulatory networks can also have *positive feedback loops* to amplify phenotypic noise. This can result in the emergence of distinct phenotypic states (i.e. qualitative phenotypic heterogeneity). This kind of feedback loop occurs in the bistable lactose utilisation network of *E. coli* [34, 148, 177]. The uptake and metabolism of lactose in *E. coli* requires the expression of the *lac* operon, which consists of three genes, *lacZ*, *lacY* and *lacA*. A random increase in the gene product of one of these, LacY, leads to an increase in an inducer molecule (TMG) which binds to and inhibits the action of *repressors*. This results in a further increase in the production of LacY, allowing the cell to metabolize lactose [148]. However, if glucose is present it can interfere with the activity of LacY and inhibit *lac* expression. While the *lac* genes are expected to be expressed for all cells at high concentrations of inducers (an example of induced phenotypic switching), at intermediate concentrations they are expressed in only a fraction of the population [34]. The results in a stochastic ON/OFF switch between two

distinct phenotypic states, in which the cells can and cannot metabolize lactose. This is an example of stochastic phenotype switching in bacteria [177].

Some phenotypic switching is not stochastic but is induced as a result of cellular sensory mechanisms detecting changes to the environment or damage to the cell. The latter is the case in the *SOS response*, a DNA repair and survival mechanism found in many bacterial species [94] and the focus of the work in Chapter 6. Following DNA damage in the cell, the SOS response is induced which, along with other consequences, causes the arrest of conventional symmetric cell division. Cell division arrest is a common bacterial response to a range of environmental stresses, such as nutrient deficiencies [153], high pressures [220], dessication [183], immune responses of the host [96], UV exposure [171] and antibiotic treatments [126, 131, 168]. In the SOS response, while conventional division has stopped, the cells are still able to grow and replicate genetic material, causing them to become filamentous. In this filamentous state cells can produce budded offspring at their tips which may continue conventional growth [28].

Clearly a cell's ability to regulate expression levels and induce phenotypic switches will be of benefit to its survival. However, these are both responsive mechanisms to detected changes, such as a change in the environment or cellular damage. Such a process of detection and response takes time to occur and will be less useful the more rapid changes are, such as those experienced by pathogenic bacteria in a host. *Stochastic phenotype switching (SPS)* is a random switching between distinct phenotypic states that occurs independently of any sensing mechanism instructing the cell to do so. We have already seen an example of this in the ON/OFF switch for the metabolization of lactose in *E. coli*, which was due to a bistable gene regulatory network [148].

1.2.4 Stochastic phenotype switching

There are two widely accepted explanations for the existence of SPS. First, it can benefit populations that are subject to rapid environmental changes. Through signal transduction, cells can normally detect cues from the environment and respond by regulating their level of expression of certain genes. However, environmental changes may be too rapid, or the number of possible changes too many for a signal transduction pathway to exist for each one [99]. In these instances populations may benefit if a fraction of the population express phenotypes suited to other environments. This is known as the *bet hedging*

strategy [22, 122, 152, 157, 193]. Following this strategy, some fraction of the population will be maladapted to the present environment. However, upon changes to the environment this fraction may stand a better chance of propagating, or at least surviving until conditions change again, than the original phenotype [210].

The other common explanation for SPS is that it can benefit populations through a *division of labour* [2, 162, 196]. This allows different cells to carry out different functions in the population, with the population gaining increased functionality as a whole. Unlike the bet hedging strategy it does not require environmental fluctuations to be beneficial. Examples of this include self-destructive cooperation [5] and the coexistence of virulent and avirulent *Salmonella Typhimurium (S. Typhimurium)* bacteria due to a bistable network expressing for virulence [14]. The virulent bacteria induce an inflammatory response in a host, which is beneficial for the survival of the avirulent bacteria. *S. Typhimurium* also experiences SPS between states that do and do not code for the formation of flagella [185]. Flagella trigger defence mechanisms in eukaryotic hosts, making those without them more virulent.

A common example of SPS in *E. coli* and many other bacterial species takes place between *normal* and *persister* states. Upon exposure to sufficiently strong antibiotics, most of a bacterial population will be killed. However, some can survive if they are in the persistent phenotypic state, which is sufficiently tolerant to the antibiotics despite having acquired no genetic resistance to them [16]. This tolerance comes from having a reduced, but not necessarily zero, growth rate. In *E. coli*, SPS between these states occur due to a toxin-antitoxin module *hipBA* [166]. Genes in this module express for both the toxin HipA and the antitoxin HipB. If the expression of HipA exceeds a certain threshold (without being nullified by HipB), growth arrest in the cell is triggered and the cell enters the persister phenotypic state. The variability in expression of the hipBA toxin-antitoxin module causes cells to switch back and forth between the normal and persister states.

A final two examples of SPS occur in the soil bacterium *B. Subtilis*. The first is *competence* to *non-competence* switching, which occurs during the stationary phase of growth [125]. Upon reaching this stage the expression of the *comK* gene becomes bistable, causing cells to switch between the two phenotypic states. In the competent state, cells cease growth but can take up DNA from their environment. This allows them to continue to explore genetic variations at a phase

of growth in which they otherwise could not easily achieve it through replication. The other example of SPS in *B. subtilis* is between motile and sessile (i.e. non-motile) cells that occurs during exponential growth [102]. Sessile cells can exploit the existing environment, while motile cells can explore the surroundings for a better/future one.

In this thesis we aim to question the role that SPS can have in the process of genetic evolution when the environment is static. We suspect it may be an important feature when genetic mutations are essential for a population's long-term survival, or when an evolving population has reached a point of stasis (such as becoming trapped at a local fitness peak). Microbial experiments with antibiotics provide examples for both these situations in which the environment can be engineered to be approximately static. *E. coli* and the opportunities for survival offered by its persister state, discussed above, is an example of the former situation. Another example we have already discussed is when bacteria can switch to a secondary (filamentous) phenotypic state as part of the SOS response following an applied stress [28, 218]. Within this phenotype genetic mutations occur at an increased rate and while not strictly a case of SPS the potential for benefit to the population's evolution of the secondary phenotypic state remains. Alternatively, consider a bacterial population that has just been exposed to antibiotics. The bacteria will experience a reduced growth rate (i.e. fitness). Genetic mutations are likely to exist that will reduce the efficiency of the antibiotic (for example through the production of antibiotic degrading enzymes or an increased production of multi-drug efflux pumps). However, studies suggest this sort of resistance frequently requires combinations of mutations, which themselves are not advantageous. This is commonly seen in the fitness landscapes of both *E. coli* and *S. Typhimurium* [127, 128, 174, 175]. Therefore the process of the genetic evolution of resistance begins as that of escape from a local fitness peak which may take considerable time. However, SPS may be able to accelerate such a process.

1.2.5 The evolution of stochastic phenotype switching

For SPS to be an evolvable feature, the level of phenotypic noise must be a heritable trait that selection can act upon. This has been shown to be the case for the yeast *S. cerevisiae*. It was shown that the level of noise in particular traits is controlled, either directly or indirectly, by the genotype which is itself subject

to mutations that selection acts upon [13, 216]. This same yeast has also been used to show positive selection for high levels of phenotypic noise [219].

Experimental studies support that SPS can evolve as a response to fluctuating selection (i.e. fluctuating environments). For example when populations of *S. cerevisiae* were subjected to repeated fluctuations between two nutrient sources (glucose and maltose), mutants were obtained with shortened lag phases [140]. This is the time in which growth stops while cells de-repress genes to allow for metabolism of a new nutrient. The shortened time suggests that the cells had evolved to switch phenotype before they could sense that there had been a nutrient change.

Another example of directly observed evolution of SPS was seen using the bacterium *Pseudomonas fluorescens* [22]. Populations spent time periodically growing in static and shaken microcosms. Some of the populations evolved SPS between different colony morphology traits that are suited to each type of microcosm.

Various computational and mathematical models have been used to examine the evolution of SPS under fluctuating selection. This includes the evolution of a bistable gene regulatory network from one that is initially monostable [112]. Mathematical models have focussed on the evolution of the optimal SPS rate when switching is already present between two phenotypic states. These have considered various scenarios of symmetric switching between symmetric landscapes [113], asymmetric landscapes [67] and when both switching rates and landscapes are asymmetric [169]. With symmetric switching and landscapes the optimal switching rate matches the rate with which the environments switch [113]. When asymmetries are included in either the SPS rate or between the landscapes numerous outcomes for the optimal SPS rate occur, including the possibility of it being zero [67, 169]. However, all of these models consider only optimising the growth rate through phenotype switching at a single genotype. They do not consider the additional effect that SPS may have on the process of genetic evolution.

1.2.6 Phase Variation

Phase variation is a type of high frequency reversible stochastic phenotype switching that is commonly found in commensal and pathogenic bacteria [212,

213]. This switching involves the heritable alteration or deactivation (frequently ON/OFF switches) of key genes that code for cellular surface macromolecules that affect the interaction between cell and host. Different phase variations can combine to produce numerous distinct phenotypic states [81]. Mechanisms for the switches can be both genetic and epigenetic. Epigenetic phase variation can occur due to DNA methylation. An example of this is the ON/OFF switch in the *agn43* gene in *E. coli*. This gene codes for the outer membrane protein Ag43, one of the consequences of which is an autoaggregative property in the cells (allowing them to stick to epithelial cells). The expression of the Ag43 protein may result in both an increase in virulence and persistence of the cells [58, 172, 212].

Genetic phase variations occur as a result of genetic changes that take place during DNA replication or repair. These changes include *gene inversion* (e.g. leading to fimbriae switching in *E. coli* [6]) and the mutation types of *transposition* and *slipped-strand mispairing (SSM)*. In the following we look at the SSM mutation type as the cause of this is easily identified by study of the genome alone.

Contingency loci are regions of hypermutable DNA common to commensal and pathogenic bacteria [136, 165, 184, 205]. Such bacteria exist in host environments where they are subject to rapid, unpredictable changes in the host's immune response (and upon transfer between hosts). Genome-wide hypermutation is likely to lead to mutants that are deleterious. However, local hypermutation in contingency loci allow the organisms to explore specific variants. These variants often have different cellular surface structures which affect the interaction between the cell and host [135]. This is an effective preemptive strategy used by bacteria to survive in a stressful host environment.

Hypermutation in contingency loci is due to the presence of *simple sequence repeats* (SSRs) in the DNA sequence. These are adjacent repeated nucleotide sequences that increase the likelihood of polymerase slippage, particularly as the number of repeats increase [39, 195]. After slippage, SSM can occur upon reattachment (due to the repetitive nature of the SSRs). This results in an increase or decrease in the number of repeat units in the SSRs and a corresponding frame-shift that can stop gene transcription or alter the gene output (by frequently resulting in the creation of a premature "stop" codon [4]). SSRs are commonly found in pathogenic bacteria [136] and eukaryotic cells (where they are more commonly called *microsatellites*). Otherwise, studies suggest there is positive selection against SSRs in most bacteria [4]. This is backed-up by a lack of them identified in *E. coli*, although they are still present [98, 164].

Typical switching probabilities of genes containing contingency loci are around 10^{-5} to 10^{-2} per DNA replication [20, 42, 217], but are higher in the presence of stresses that cause DNA damage [21, 151, 187]. Unlike some examples of SPS, such as between normal and persister states, phase variation is not associated with any form of cell division arrest or reduced growth rate.

A common example of phase variation takes place in the bacterium *Haemophilus influenzae (H. influenzae)*. *H. influenzae* is an obligate commensal bacteria which is part of the microbial flora of the upper respiratory tract in humans. However, it is also a major cause of pneumonia, meningitis and septicemia [135]. *H. Influenzae* contains more tetranucleotide repeats than any other known bacterial genome, much more than would be expected to have evolved by chance [85]. Most of these repeats occur in genes involved in the biosynthesis of lipopolysaccharide (LPS) [87]. LPS is a complex macromolecule which is essential to the functioning and integrity of the cell wall and is integral to advancing infections. It is also a target for the immune response of the host and directly affects the pathogenicity of the bacteria [85]. Similarly, a phase variation in the number of fimbriae, which are beneficial at different stages of infection, occurs due to SSRs [79].

1.2.7 Microbial evolution experiments

Microbes are ideal organisms to use in the study of biological evolution [54]. They can reproduce quickly (*E. coli* can have a doubling time as low as ~ 20 minutes [61]) allowing evolution over many generations to be viewed in real time. The mostly asexual form of reproduction is useful in comparing results from replicate experiments (as the extent of possible genetic variation is much smaller than with sexual reproduction). Organisms can also be stored, at various points in the process, in suspended animation. This allows for direct comparisons to be made between evolved and ancestral genotypes.

Experimental techniques allow for precise genetic manipulation of genotypes. This level of control over the specific genetic composition of the starting population allows for specific questions to be asked. Laboratory settings are large enough to host experiments involving large population numbers and can ensure as controlled an environment for the experiment as possible. These benefits of microbial evolution also ensure that experiments are highly reproducible.

Two experimental procedures to study adaptive evolution in microbes are

continuous culture methods (e.g. by using a *chemostat*) and a *serial transfer process* [18]. These two process are represented schematically in Fig. 1.6. In a continuous culture method using a chemostat, the growth medium remains chemically static and well-mixed. A steady flow of nutrients into the chemostat is matched by the same flow of depleted medium and cells out of it. The population size remains approximately constant at an equilibrium density for which the growth rate is the same as the flow through the system.

In a serial transfer process, the population is maintained indefinitely in the log (exponential) phase of growth. Upon depletion of the resources in the present media (signalling the end of the exponential growth phase) a fraction of the population is transferred to fresh media where it resumes exponential growth. This process is repeated for as many transfers as necessary. Serial transfer processes can keep the population in a perpetual state of growth. The experimental set-up is simpler than that of a chemostat and allows for replicate experiments to be run easily. In order for this procedure to work, the fraction of the transferred population must be large enough to contain the same genetic diversity as the entire population.

1.3 Outline of research

The aim of the research carried out in this thesis is to explore an additional possible role in the evolutionary process for stochastic phenotype switching (SPS): that of facilitating genetic evolution in a static environment. The consequence of cells having n distinct phenotypic states, accessible through SPS, is that there are n distinct fitness landscapes. Cells can switch between these landscapes to the same genotype in each one. The process of evolving a particular genotype can then be undertaken over some or all of these landscapes. Specifically what happens will depend on the relative topographies of the available landscapes. In the research carried out here we restrict ourselves to the case of two distinct phenotypic states (i.e. $n = 2$).

We can expect that with access to more than one fitness landscape, fitness barriers in a single landscape can be avoided by cells switching to another landscape in which the obstacle is less costly or absent entirely. Therefore we expect SPS will be of particular benefit to populations that, without it, are trapped at local peaks on a fitness landscape.

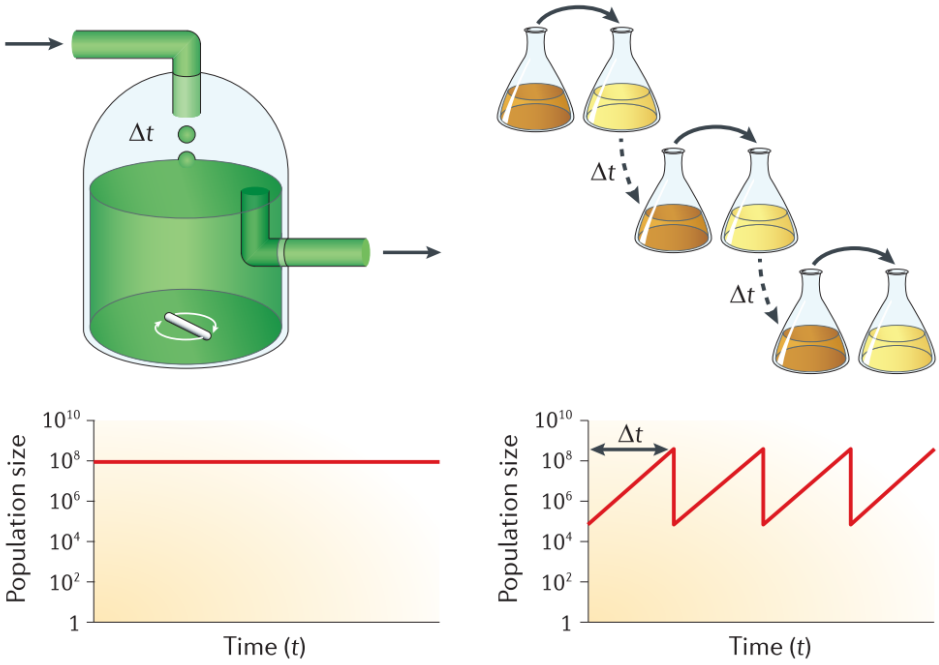

Figure 1.6 *Two different experimental techniques used to study the adaptive evolution of microbes. (A) Growth in a chemostat provides a continuous culture technique to study the stationary phase of microbial growth. (B) Serial transfer process allows for the log phase (exponential growth) to be studied by the continual transfer of a fraction of the population to fresh media. Reprinted by permission from Macmillan Publishers Ltd: Nature Reviews. Genetics [18], copyright 2013.*

We begin this research in Chapter 3, in which we undertake a numerical analysis of the effect that SPS has on a population trapped at a local peak on a 1D fitness landscape. We consider the simplest case in which a single mutation is costly (forming a fitness "valley"), while a second can be compensatory and provides the target state for the evolving population. The population has access to a secondary phenotypic state, which does not experience the same fitness effects upon genetic changes. Therefore the secondary phenotype has a uniform fitness landscape. We examine the effect this secondary phenotype has on the time taken for the evolutionary process in a chemostat, as well as the expected evolutionary trajectories that cells follow to the target. In Chapter 4 we consider the same model but undertake an analytical study of it. We do this to confirm the earlier numerical results, while it also enables us to look at results for parameter values that would otherwise be difficult to simulate.

In Chapter 5 this model is extended to a more expansive and realistic genotype space and fitness landscapes. The space considered is that of a hypercube and the evolution of populations of binary sequences, as in the quasispecies model. We undertake a numerical study of how the population's crossing of genotype space can be affected by the inclusion of a secondary phenotypic state. We consider this for different combinations of randomly generated landscape models. To begin with one fitness landscape is of the House of Cards (HoC) [101, 106] landscape type, while the other is a uniform landscape. This is an extension to higher dimensions of the model considered in Chapters 3 and 4. We then go on to consider combinations of the HoC and Rough Mount Fuji [9, 139] landscape models for both landscapes. The aim throughout remains to understand how the inclusion of phenotypic switching affects the population's evolution of a predetermined target genotype.

In Chapter 6 we present a model for the acquisition of resistance of *E. coli* to the antibiotic *ciprofloxacin*, a member of the *fluoroquinolone* family of antibiotics. Using empirical data for the fitness and resistance of genotypes, we consider evolution over a hypercube space of genotypes. All genotypes consist of combinations of 5 mutations that are frequently observed experimentally. In the presence of *ciprofloxacin*, DNA damage can cause *E. coli* to induce the SOS response, transferring them to a secondary phenotypic state. Although not an example of SPS, this shares similarities with our earlier model, in that genetic evolution is facilitated through cells having access to a secondary phenotype. With this model, we numerically predict the expected behaviour of a population

evolving as part of a serial transfer process. Our aim is to test for the rapid evolution of resistance that has been observed experimentally [28, 35].

We begin in the next chapter by considering some key concepts and evolutionary models. We will also consider there the common analytic and numerical techniques that will be used throughout this thesis.

Chapter 2

Concepts, Models and Methods

2.1 Introduction

In this chapter we consider an overview of some common concepts, evolutionary models and methods (both mathematical and numerical) that will be used throughout this thesis. This overview is intended to serve as a general introduction to a reader unfamiliar with the modelling of biological evolution. It is by no means exhaustive and instead focusses only on what is required to follow the work in this thesis.

Numerous texts have been important in compiling the information contained in this and the upcoming chapters. These receive special mention here. For the mathematical modelling of evolution this includes the texts by Nowak [144], Murray [137] and Ewens [56], while that of Hartl and Clark [80] has been useful in developing an understanding of population genetics. In the analysis of stochastic processes, the texts by Gardiner [70] and Redner [159] have been important, while that by Press *et al.* [155] and Griffiths and Higham [77] have been useful sources for numerical techniques.

2.2 Evolutionary models

We begin this overview by looking at various evolutionary models that are useful to the following work. First we consider deterministic models, beginning with

simple models of population growth. We then proceed to models describing the competition of species through selection and mutations, ending up with the *quasispecies model*. We will then consider the stochastic process of biological evolution and various models and features of importance within it. Throughout the following, evolution and adaptation are the interchangeable terms given to the process whereby a population changes its genetic distribution in order to maximise its fitness in the present environment (which remains static).

2.2.1 Deterministic models

Single species growth

We start with one of the earliest deterministic models for the population growth of a single species. Consider a species with the population size $N(t)$ at time t, which undergoes birth and death events with the rates b and d respectively. The simplest continuous description of the population growth is one of unbounded deterministic growth. This is described by the following differential equation

$$\frac{dN}{dt} = (b-d)N, \tag{2.1}$$

which has the solution

$$N(t) = N_0 e^{(b-d)t} \qquad \text{where} \qquad N(t=0) = N_0. \tag{2.2}$$

This was originally proposed by T. R. Malthus in his "Principles of Population" towards the end of the 18th century [137]. The solution is simple, such that if the net growth rate $r = (b-d) < 0$ the population will die out, while if $r = (b-d) > 0$ it will grow exponentially. Exponential population growth is unrealistic in the long term, although it can suitably describe population growth over short-times, such as the log (i.e. exponential) phase of bacterial growth.

The unrealistic long term exponential growth of (2.2) was motivation for P. F. Verhulst to propose an alternative type of growth, in which the population is limited from becoming too large. This was termed *logistic growth* and is of the form [137]

$$\frac{dN}{dt} = rN\left(1 - \frac{N}{K}\right). \tag{2.3}$$

The factor $(1-N/K) \to 0$ as $N \to K$ which stops the population growing beyond

$N = K$. K here is termed the *carrying capacity* and is the upper bound on the population size due to, e.g., a capacity on available resources or space in the system. Given the initial condition $N(t = 0) = N_0$, the solution to (2.3) can be found by separation of variables to be

$$N(t) = \frac{N_0 K e^{rt}}{[K + N_0(e^{rt} - 1)]}. \tag{2.4}$$

This solution tends to K in the limit $t \to \infty$ provided $N_0 \neq 0$. This can be seen by noting that (2.3) has two equilibrium solutions (in which $dN/dt = 0$), the stable $N = K$ and the unstable $N = 0$. Note that for initial population sizes $N_0 > K$, the population size $N(t)$ decays to the solution in (2.4).

Coupled population growth

Consider now the coupled deterministic growth of two species involved in a mutation-selection process, as considered in [144]. The coupling is through mutations that occur during replication. Mutations are such that a species creates offspring of the other species instead of its own.

Consider two species, A and B, in which A has the fitness $(1 + s)$ and species B has unity fitness. Both species undergo replication and with the probability μ create offspring of the other species. Let n_A and n_B be the frequencies of the two species in the population, such that $n_A + n_B = 1$. The dynamics of n_A is such that

$$\dot{n}_{\mathrm{A}}(t) = \overbrace{[(1+s)(1-\mu)]n_{\mathrm{A}}(t)}^{succesful\ replication} - \underbrace{[sn_{\mathrm{A}}(t)+1]n_{\mathrm{A}}(t)}_{loss} + \overbrace{\mu[1-n_{\mathrm{A}}(t)]}^{mutational\ gain}. \tag{2.5}$$

The "loss" term equals $\phi(n_{\mathrm{A}}, n_{\mathrm{B}})n_{\mathrm{A}}(t)$ where $\phi(n_{\mathrm{A}}, n_{\mathrm{B}}) = (1 + s)n_{\mathrm{A}} + n_{\mathrm{B}}$ is the average fitness of the population. This term is necessary to ensure the condition $n_{\mathrm{A}} + n_{\mathrm{B}} = 1$ is valid at all t. It also results in (2.5) being nonlinear.

The steady-state solution of (2.5), in which $\dot{n}_{\mathrm{A}}(t) = 0$, is

$$n_{\mathrm{A}} = \frac{1}{2}\left[1 - \mu - \frac{2\mu}{s} \pm \sqrt{\left(1 - \mu - \frac{2\mu}{s}\right)^2 + \frac{4\mu}{s}}\right]. \tag{2.6}$$

Setting $\mu = 0$ recovers the necessary solutions in the absence of mutations which

are ($n_{\mathrm{A}} = 1, n_{\mathrm{B}} = 0$) and ($n_{\mathrm{A}} = 0, n_{\mathrm{B}} = 1$). In the former solution species A takes over the population (and species B in the latter). Which solution is valid depends on the initial state of the population and the value of s. This result illustrates the *principle of competitive exclusion* in which two species, competing for the same resources, cannot coexist at constant population values and which often results in one of the species becoming extinct [137].

However, consider now when $\mu \neq 0$ and $s > 0$ such that species A has a fitness advantage (i.e. a larger growth rate) over species B. The positive square root solution of (2.6) predicts that n_B is nonzero and will initially increase as μ increases from zero. Despite species B being less fit its survival no longer depends on itself alone. Mutations have coupled its success to that of species A. As long as species A survives, it will support species B through mutations. The steady-state solution of (2.6) balances the competition between mutation and selection, the extent of which is decided by the strength of the coupling μ.

Quasispecies model

The dynamics of two species coupled by mutations, as described above, can be extended to incorporate any number of species with mutations occurring between them. This leads us to the concept of a *quasispecies*, which was first presented in studies of the evolution of self-replicating prebiotic molecules (such as RNA) [51, 53].

A quasispecies is an ensemble of genetically similar species produced by a mutation-selection process. As we saw in the two-species case above, when mutation rates are large a species' success depends not only on itself but on the other species that can mutate into it. Therefore selection acts on the quasispecies as a whole rather than the individuals within it [53].

The *quasispecies model* describes the evolution of a population over the space of all possible sequences of length L. Instead of species, we will refer to these possible sequences as genotypes. Each site (i.e. locus) in a genotype's sequence can have a possible $k \geq 2$ alleles, with $k = 2$ being the commonly studied case of binary sequences [68, 91].

The genetic similarity between two genotypes can be measured by the *Hamming distance* h between them. This counts the number of point mutation differences between the sequences that these genotypes represent. Therefore the Hamming

distance $h(\sigma, \sigma')$ between the genotypes $\sigma = \{\sigma_1, ..., \sigma_L\}$ and $\sigma' = \{\sigma'_1, ..., \sigma'_L\}$ is given by

$$h(\sigma, \sigma') = \sum_{k=1}^{L} (1 - \delta_{\sigma_k, \sigma'_k}) \tag{2.7}$$

The quasispecies model is a deterministic, infinite population model that describes the evolutionary dynamics of the population over the space of all possible genotypes (i.e. sequences of which there are $M = k^L$ in total). The population undergoes a mutation-selection process over a static landscape and eventually reaches a steady-state distribution.

Let the population distribution at time t be given by the vector $\vec{n}(t) = \{n_1(t), ..., n_M(t)\}$, where n_i is the frequency of genotype i which has fitness r_i. Let the matrix Q be the stochastic mutation matrix in which the element q_{ji} is the probability that an individual of genotype i (sequence σ^i) produces a mutant of genotype j (sequence σ^j) during replication. Note that this is the *coupled* quasispecies model. Alternative, *paramuse* models, consider mutations and reproduction to be independent processes [15]. As the elements of Q are probabilities, the matrix Q is doubly stochastic such that $\sum_{i=1}^{M} q_{ji} = \sum_{i=1}^{M} q_{ij} = 1$. If μ is the probability that the allele at a single locus in a sequence is incorrectly copied (to another specific allele), and all mutations have the same probability of occurring, then the element q_{ji} is given by

$$q_{ji} = \mu^{h(\sigma^i, \sigma^j)} (1 - \mu)^{L - h(\sigma^i, \sigma^j)} \tag{2.8}$$

The frequency of the ith genotype $n_i(t)$ in the population evolves in time by the following differential equation

$$\dot{n_i} = \sum_{j=1}^{M} q_{ij} r_j n_j - \phi(\vec{n}) n_i \qquad i = 1, ..., M. \tag{2.9}$$

As in (2.6), $\phi(\vec{n}) = \sum_{i=1}^{M} n_i r_i$ is the average fitness of the population and is included in a term that ensures the normalisation condition $\sum_{i=1}^{M} n_i = 1$ is satisfied. Note that the form this loss term takes is a particular choice to ensure that n_i is a frequency. Other choices for $\phi(\vec{n})$ are possible but they all lead to qualitatively similar dynamics and hence we will not discuss them here.

Equation (2.9) is quadratic in n_i through the ϕn_i loss term. An equivalent linear

form can be found by transforming from the variables n_i to x_i by

$$x_i = n_i e^{\psi(t)} \quad \text{where} \quad \psi(t) = \int_0^t \phi(s)ds. \tag{2.10}$$

If we differentiate and substitute (2.10) into (2.9) we get that

$$\begin{aligned} \dot{x}_i &= \left[\dot{n}_i(t) + n_i(t)\phi(t)\right] e^{\psi(t)} && (2.11) \\ &= \sum_{j=1}^{M} q_{ij} r_j n_j e^{\psi(t)}. && (2.12) \end{aligned}$$

Therefore x_i evolves by the following linear differential equation

$$\dot{x_i} = \sum_{j=1}^{M} q_{ij} r_j x_j \qquad i = 1, ..., M. \tag{2.13}$$

Now defining $X = \sum_{i=1}^{M} x_i$ means that $X = e^{\psi(t)}$ and therefore $x_i = n_i X$ according to the definition in (2.10). Therefore X_i can be interpreted as the abundance (i.e. number) of individuals of genotype i, while X is the total size of the population, which obeys the following differential equation

$$\dot{X} = \phi X. \tag{2.14}$$

Therefore the total population size X grows exponentially at a rate controlled by the average fitness of the population ϕ.

It is evident from (2.9) that the steady-state distribution of the quasispecies can be found by solving the following eigenvalue problem

$$W\vec{n} = \phi\vec{n}, \tag{2.15}$$

where the matrix W is the mutation-selection matrix with elements $w_{ij} = q_{ij} r_j$. The largest eigenvalue of W is the average fitness ϕ and the eigenvector corresponding to it is the principal eigenvector of W. This eigenvector describes the steady-state distribution of the quasispecies for which the average fitness ϕ is maximised in a mutation-selection process.

This result leads to some of the non-trivial behaviour of quasispecies. The "survival of the flattest" effect, shown in Fig. 2.1, results in the fittest genotype vanishing from the population in favour of a distribution about a group of individually less-fit genotypes that manage to maximise the average fitness ϕ.

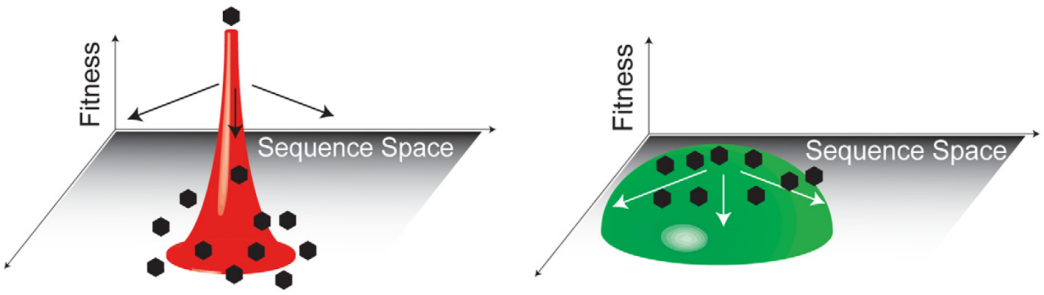

Figure 2.1 *Survival of the flattest effect. The genetic diversity at high mutation probabilities means that the population distribution on the left, centred about the fitness maximum, has a lower average fitness ϕ than the distribution on the right. Therefore the population has the steady-state distribution on the right, in which the fittest genotype is lost from the population. Taken from [115].*

A feature of the quasispecies model is the existence of an error threshold μ_c. For mutation probabilties $\mu < \mu_c$ the population remains localised enough to undergo adaptation to regions that maximise the average fitness ϕ. However, for $\mu > \mu_c$ the quasispecies no longer "feels" the effect of the fitness peaks in the landscape and adaptation can no longer take place. This results in the population losing genetic integrity by delocalising over genotype space. As the number of genotypes considered tends to infinity (as $L \to \infty$) this transition between the localised and delocalised behaviours can behave as a first order phase transition [27, 68]. This transition has been studied in a number of ways, for example by mapping the quasispecies model to the 2D Ising model [119, 120, 192], a 1D quantum chain [12] and a model of directed polymers [68].

Not all fitness landscapes contain an error threshold. The simplest landscape that does have one consists of a single peak with the fitness advantage W_0 over the remaining genotypes. The critical error threshold in this case is [53, 68, 91]

$$\mu_c \approx \frac{\ln W_0}{L} \sim \frac{1}{L} \quad \text{when} \quad \ln W_0 \sim 1 \tag{2.16}$$

from which we see that in order for the population to adapt the likelihood of sequence wide mutation cannot exceed $\mu L \sim 1$ (i.e. approximately one mutation per genome).

The existence of a critical error threshold can be studied for classes of fitness landscapes through methods such as the *Maximum Principle* [84, 211]. This involves finding an exact solution (in the limit $L \to \infty$) for the dominant

eigenvalue of the mutation-selection matrix, by translating the problem to an optimisation problem of a single scalar function. The presence of singularities in the dominant eigenvalue can then identify parameter values for which a critical error threshold exists.

Consider a class of fitness landscapes in which epistatic effects are incorporated through a nonlinear dependence of a genotype's fitness on its Hamming distance from the optimal genotype. In this case the fitness can be written as

$$r_h = r_0 - bh^\alpha, \tag{2.17}$$

where r_h is the fitness of a genotype with hamming distance h from the optimal genotype which has fitness r_0. The parameter $b > 0$ and α is here the *epistasis exponent*. When $\alpha = 0$ the landscape in (2.17) consists of a single peak of fitness r_0 while the remaining genotypes have fitness $r_0 - b$. An error threshold exists for such a single peak landscape as we have already discussed. Alternatively when $\alpha = 1$ the landscape is non-epistatic and no error threshold exists. For the range of values $\alpha > 1$, the occurrence of additional mutations away from the optimal genotype exacerbates the fitness reduction from r_0. The opposite is true when $\alpha < 1$, in which the fitness reduction is diminished by subsequent mutations away from the optimal genotype. Using the maximum principle it has been shown that fitness landscapes created from the class in (2.17) contain a critical error threshold if $\alpha \leq 1/2$ [84, 211].

Adaptation occurs fastest when the mutation rate is close to the error threshold. Numerous RNA based viruses, such as HIV and the Hepatitis C virus, can be described as behaving like quasispecies [43, 60, 115]. With low fidelity RNA polymerase they have very high mutation rates, orders of magnitude greater than DNA based organisms. These mutation rates are typically close to the error threshold, with probabilities of error during replication of $\sim 10^{-4}$ per nucleotide base [86, 115]. These high mutation rates allow them to rapidly adapt in order to survive attacks from the immune system of the host. A possible way to combat such viruses is by *lethal mutagenesis* [60, 115]. This involves increasing the quasispecies' mutation rate, through the action of mutagens, causing it to exceed the error threshold. This has been shown experimentally to result in less viable viral populations [86].

We end this section by considering a specific example of the quasispecies model in which the number of alleles $k = 2$ (i.e. the sequences are binary) and at most a

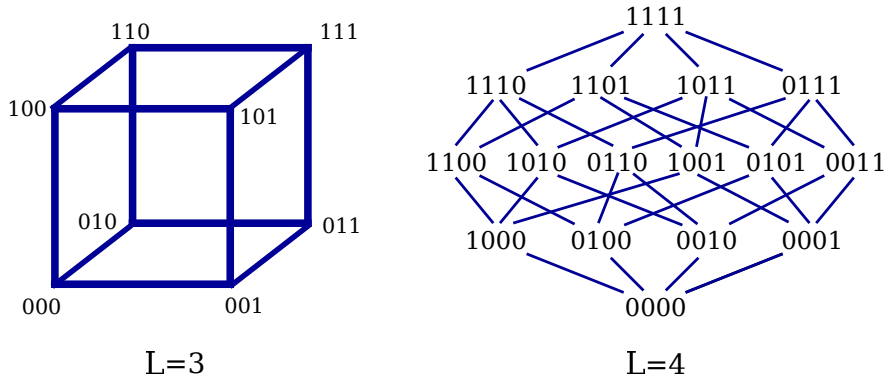

Figure 2.2 *The hypercubic genotype spaces for binary sequences of length $L = 3$ and $L = 4$. Each genotype is connected (through mutations) to all others that differ to it in sequence by the value at a single locus*

.

single point mutation can occur during the replication of a sequence. This is likely to be the case if the mutation probability μ is very small according to (2.8). In this case the genotype space is a hypercube of dimension L. Examples of this for sequences of length $L = 3$ and $L = 4$, with links connecting genotypes that can mutate to one another, are shown in Fig. 2.2. In this scenario each genotype has L nearest neighbours and the number of possible trajectories connecting antipodal genotypes, by single point mutations, is $L!$. This structure of genotype space and the possible mutations between them are used in the models of Chapters 5 and 6.

2.2.2 Stochastic Evolution

We now consider features and examples of stochastic models of biological evolution. *Genetic drift* is one such feature which concerns the randomness in the process of reproduction [80]. It is absent from deterministic formulations and can result in genotypes that are selectively favoured being lost to the population. Its effect is strongest at low population numbers (either in total or at a specific genotype) where fluctuations in population numbers about their mean values are most significant.

With this in mind, given that a mutant arises what is the probability that it will take over the population? If it manages this then the mutant has *fixed*, having undergone the process of *fixation*. In the following we consider the likelihood of this happening.

The Wright-Fisher and Moran models

Two classic models of populations genetics are the Wright-Fisher and Moran models [59, 134, 214]. They are both discrete time, fixed population size models that describe the evolution of genotype frequencies (i.e. population numbers) in a reproducing population. They are distinguished by their update algorithms that randomly decide the change to the population distribution in the next time step. We only describe the Wright-Fisher model here but we will use the Moran model in the next section to calculate the probability of mutant fixation. Throughout the following we stick to the language we have adopted of "cells" and "genotypes" instead of the more traditional "genes" and "alleles" that are associated with these models.

In the Wright-Fisher model, evolution takes place over discrete (non-overlapping) generations. The population distribution in the $(m+1)^{th}$ generation is found by randomly sampling (with replacement) cells from the m^{th} generation for all N members in the population. This sampling is random and selective differences (i.e. differences in fitness) and mutations between cells can be incorporated.

Alternatively, in the Moran model the generations overlap. In each time step a single cell is selected for replacement by another (that can include itself). In contrast to the Wright-Fisher model the population number of each genotype can change by at most one in a single time step. The evolution of the population at each genotype can therefore be described as varying by a birth-death process.

The probability of fixation

Consider the probability of mutant fixation in the Moran model for the simplest case of two genotypes (A and B) without mutations occurring between them. Let there be a total of N cells in the population with the initial condition that $(N-i)$ are of genotype A and i are mutants of genotype B. The state of the population is therefore given by the value of i which can change over time. Let ϵ_i be the probability of fixation of genotype B given that there are i cells presently of that genotype. This quantity satisfies the boundary conditions $\epsilon_N = 1$ and $\epsilon_0 = 0$.

Let p_i and q_i be the probability that in a single time step the number of cells of genotype B increases and decreases by 1. The fixation probability ϵ_i obeys the

following recurrence relation

$$\epsilon_i = q_i\epsilon_{i-1} + (1 - p_i - q_i)\epsilon_i + p_i\epsilon_{i+1}. \tag{2.18}$$

This can be re-expressed in terms of the difference in successive fixation probabilities, $\Delta\epsilon_i = \epsilon_{i+1} - \epsilon_i$, to give the recurrence relation

$$\Delta\epsilon_i = \left(\frac{q_i}{p_i}\right)\Delta\epsilon_{i-1} = \prod_{j=1}^{i}\left(\frac{q_j}{p_j}\right)\epsilon_1. \tag{2.19}$$

Here we have used that $\Delta\epsilon_0 = \epsilon_1$ due to the boundary condition $\epsilon_0 = 0$. Therefore the fixation probability ϵ_i is

$$\epsilon_i = \Delta\epsilon_{i-1} + \epsilon_{i-1} = \epsilon_1\sum_{k=0}^{i-1}\prod_{j=1}^{k}\left(\frac{q_j}{p_j}\right) \tag{2.20}$$

$$= \frac{\sum_{k=0}^{i-1}\prod_{j=1}^{k}\left(\frac{q_j}{p_j}\right)}{\sum_{k=0}^{N-1}\prod_{j=1}^{k}\left(\frac{q_j}{p_j}\right)}, \tag{2.21}$$

where the quantity ϵ_1 used in (2.21) comes from substituting the boundary condition $\epsilon_N = 1$ into (2.20) to get

$$\epsilon_1 = \frac{1}{\sum_{k=0}^{N-1}\prod_{j=1}^{k}\left(\frac{q_j}{p_j}\right)}. \tag{2.22}$$

If there is no selective difference between genotypes (i.e. evolution is neutral) then the quantities p_i and q_i are both given by

$$p_i = q_i = \left(\frac{i}{N}\right)\left(\frac{N-i}{N}\right), \tag{2.23}$$

where the left and right factors are the probability that a cell of genotype B and A are chosen respectively. This means that the ratio $q_i/p_i = 1$ and according to (2.21) the fixation probability is $\epsilon_i = i/N$.

Alternatively, consider the case of a selective difference between the genotypes, such that the fitnesses of genotypes A and B are $r_A = 1$ and $r_B \neq 1$ respectively. We will consider the selective difference to affect the chance that cells are selected for reproduction but not for death. In this case the probabilities p_i and q_i are

usually assumed to be

$$p_i = \left(\frac{ir_{\mathrm{B}}}{ir_{\mathrm{B}} + N - i}\right)\left(\frac{N-i}{N}\right) \qquad q_i = \left(\frac{N-1}{ir_{\mathrm{B}} + N - i}\right)\left(\frac{i}{N}\right), \tag{2.24}$$

where the left factors in both p_i and q_i are the probabilities that a cell of genotype B and A are selected for reproduction respectively (while the right factors are the probabilities that cells of the other genotype are selected for death). In this case the ratio $q_i/p_i = 1/r_{\mathrm{B}}$. Substituting this ratio into (2.21) gives the probability of fixation ϵ_i to be

$$\epsilon_i(N, r_{\mathrm{B}}) = \frac{1 - 1/r_{\mathrm{B}}^i}{1 - 1/r_{\mathrm{B}}^N} \tag{2.25}$$

This monotonically increases with r_{B} and tends to i/N in the neutral limit of $r_{\mathrm{B}} \to 1$. Importantly, it predicts non-zero probabilities of mutant fixation, owing to genetic drift, when $r_{\mathrm{B}} < 1$ and genotype B is deleterious. This model can be generalised to include more genotypes with mutations occurring between them, as we will do in Section 3.4.4.

An alternative form for the fixation probability in the approximate continuum limit (i.e. of population frequency) was derived originally by Kimura [56, 104]. In it the probability of fixation ϵ_1 of a single mutant, with relative selective advantage s to the remaining population, is given by

$$\epsilon_1(N, s) = \frac{1 - e^{-s}}{1 - e^{-Ns}}. \tag{2.26}$$

This recovers the same result of $\epsilon_1 = 1/N$ as (2.22) in the neutral limit of $s \to 0$, as well as the ϵ_1 value when $s \neq 0$ in (2.25) when $|s| \ll 1$ such that $\ln(r_B) = \ln(1 + s) \approx s$. The result in (2.26) is frequently used in Chapter 4.

Evolutionary Dynamics

The stochastic evolution of a population over a complex fitness landscape is difficult to predict. It depends on dynamical parameters such as the strength of mutation and selection, the population size and the local topography of the underlying fitness landscape [92, 189]. However, within certain *evolutionary regimes* predictions can be made for the expected behaviour of evolving populations.

In the following let N be the total population number, u the rate that mutants are created (not to be confused with the mutation probability μ) and s the

selective advantage of a mutant under consideration (compared to the fitness of the remaining population). The *strong selection weak mutation* (SSWM) regime occurs when $Ns \gg 1$ and $Nu \ll 1$, such that mutations are rare and likely to establish only if beneficial [74]. In this regime the population is localised about a single genotype (with only a single mutant expected at any given time) and restricted to follow trajectories along which the fitness never decreases [75]. These kind of trajectories are known as *accessible* [62]. The conditions for the SSWM regime make it applicable at low mutation probabilities, while the population is large enough to ensure the selection condition is satisfied.

The *Greedy Adaptive* regime occurs when mutations are more frequent but still rare ($Nu \sim L \gg 1$ while $Nu^2 \ll 1$) while selection remains strong ($Ns \gg 1$) [92, 147]. In this regime a population located at a single genotype will sample the mutants at all adjacent genotypes before moving to the fittest. Therefore the population is expected to move over genotype space by taking the individual steps that maximally increase its fitness. The trajectories taken in this regime are therefore highly predictable (almost deterministic) and a property of the fitness landscape. Populations in this regime are more likely to become trapped at local fitness peaks than smaller populations [92]. This is due to them being trapped within the peak's *basin of attraction*, in which the path of steepest fitness increase leads to the peak [63, 114].

When a population becomes trapped at a local fitness peak it can be a considerable time before stochastic fluctuations are significant enough for it to escape. This can result in the observation of *punctuated evolution*, the dynamical pattern of long periods of population stasis interspersed with periods of rapid change [19, 110, 141]. When this occurs the evolutionary dynamics can be compared with that of record statistics [109], where the waiting time for a new record is comparable to the time it takes for random mutations to locate a genotype of improved fitness.

An example of punctuated evolution occurring in a simulation run (using the sequence-based model of Chapter 5) can be seen in Fig. 2.3, for evolution over the $L = 5$ hypercubic genotype space. The fitnesses of all states are uniform except for two genotypes which have an equal fitness advantage and a Hamming distance of $h = 3$ separating them. The bulk of the population can be seen to transition between these two peaks due to stochastic fluctuations and random drift. In the absence of stochastic fluctuations, such as in the deterministic quasispecies model, punctuated evolution to larger peaks is still possible. However, in these

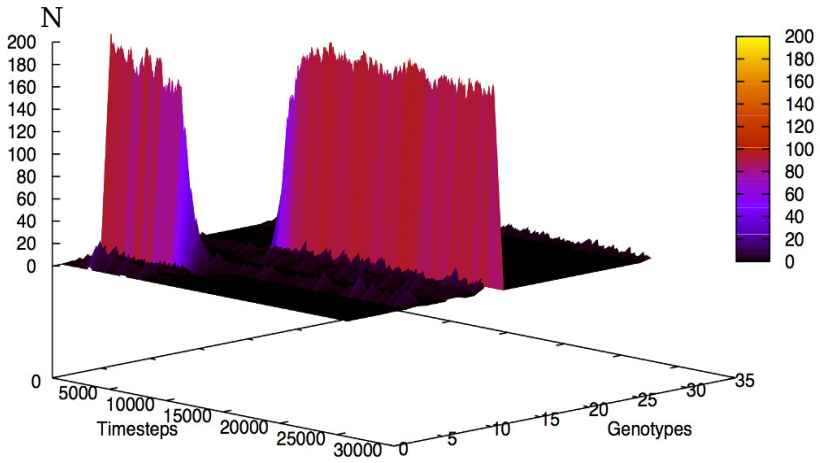

Figure 2.3 *Punctuated evolution in the quasispecies model with two peaks for binary sequences of length $L = 5$. The plot shows the population number N as a function of time T for the 32 possible genotypes. All genotypes have uniform fitness except for two which form equal sized fitness peaks, between which the bulk of the population jumps due to stochastic fluctuations.*

instances its due to the considerable time it takes to build up significant mutant populations that eventually reach a fitter peak, at which point the new fitter mutant population can outcompete those at the original peak [91].

An alternative evolutionary scenario that can be studied analytically is how a population evolves a fixed sequence of mutants (i.e. along genotypes A→B→C→...). Well studied problems of this kind in population genetics are *valley crossing* problems [201, 206]. Such problems concern how a population acquires a beneficial double-mutant given that the intermediate mutant (or mutants) is deleterious or neutral. This process has also been considered for sequences of more than two mutants [89, 176, 206]. This is the situation we consider in Chapters 3 and 4 for a population that is also able to switch phenotype.

Similar to the SSWM regime, for small population sizes the population can obey *sequential fixation* dynamics [33, 201, 206]. Here, the population remains localised at a single genotype and moves collectively following the production of a mutant that will fix. The time it takes this to happen will be significant if the mutant is deleterious but the fixation of such mutants is not impossible according to (2.25) and (2.26) owing to random drift. In this regime the population can be described as performing a random walk across genotype space. The distinguishing feature of this dynamics is that the rate with which a compensatory double mutant is produced is inversely proportional to the population size.

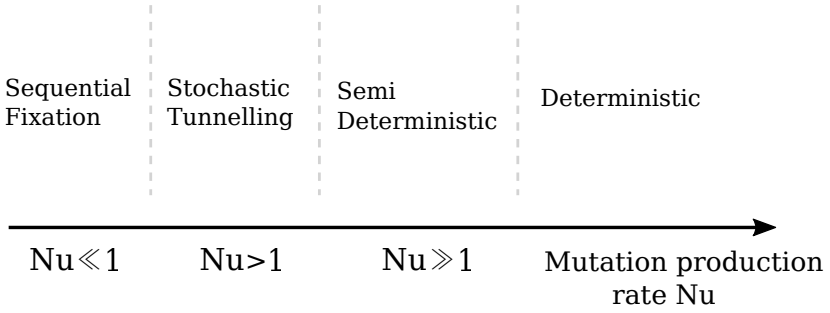

Figure 2.4 *The evolutionary regimes that a population evolving a fixed sequence of mutants may experience as a function of the mutant production rate Nu (at each intermediate state). Note this is for illustrative purposes only and the specific boundaries between the regimes, and whether or not each regime exists at all depends on the parameters of the model being considered, specifically the underlying fitness landscape.*

As the rate of mutant production Nu increases, intermediate mutant populations do not need to fix before producing the next mutant in the sequence. This is the dynamics of *stochastic tunnelling* [90], initially termed *simultaneous fixation* [75]. If we can assume that intermediate mutant lineages behave independently (ruling out models with frequency dependent fitnesses) the production of further mutants created by drifting mutant lineages can be described by branching processes [89, 90, 206]. Obeying this dynamics the time taken to produce a compensatory double mutant varies inversely with population size.

Upon further increase in the rate of mutant production the evolution can first be described by a joint stochastic and deterministic description (*semi-deterministic* dynamics) before moving to a fully deterministic regime in which the dynamics is captured by a system of ordinary differential equations [206]. A general illustration of how these evolutionary regimes are moved through as a function of the rate of mutant production Nu is shown in Fig. 2.4.

A final feature of stochastic evolution that requires mention is *clonal interference* [54, 80, 132]. Clonal interference is important in asexually reproducing populations and occurs when mutants that carry different beneficial mutations compete with one another for dominance of a population. In general, the resulting rate with which the successful mutant achieves propagation through the population will be lower than if it had been the only beneficial mutation. Hence clonal interference can result in the slowing down of the adaptation process in asexual populations.

2.2.3 Random landscape models

Experimental studies into the structure of real fitness landscapes, due to the astronomical sizes of genotype spaces, have focussed on only a small subset of viable genotypes [128, 197, 198, 202, 207]. Therefore the available information regarding the structure of real fitness landscapes, while growing, remains limited [188] and uncertainty remains regarding the expected features that larger fitness landscapes will have. Will they consist of many peaks and troughs which provide obstacles to evolution (originally proposed by Wright [215])? Or does the high dimensionality of real genotype spaces, which results in an abundance of mutational pathways between any two genotypes, mean that it is statistically likely for accessible paths to exist (an hypothesis attributed to Fisher [59])? An alternative theory, the *neutral theory of molecular evolution* [103], proposes that in molecular evolution the majority of mutations will be deleterious and those that are not are likely to be neutral [181]. Therefore pathways taken through genotype space are likely to be neutral, along which populations evolve under the effect of random drift alone following a mutation.

In evolutionary models it is useful to consider evolution over ensembles of fitness landscapes, rather than specific ones. These landscapes are different realisations of a *random landscape model* which reflects some statistical feature of interest, of which we mention a few here. Some of these have similarities with models from statistical physics, such as models of spin glasses [114] and of percolation [71].

In the *House of Cards* model [93, 101], which was originally proposed by Kingman [106], all the fitnesses are uncorrelated. Therefore a single point mutation has the capacity to drastically alter the fitness of a cell. An example of such a fitness landscape is shown in Fig. 2.5A. This is considered to be a null model in that biological fitness landscapes are expected to exhibit some correlation between genotypes [62]. Nevertheless this landscape can be used as a lowest degree approximation, specifically if the real landscape is expected to be rugged (i.e. containing many peaks and troughs), which many have been found to be [82, 167, 188]. This model is equivalent to the Random Energy Model (REM) of spin glasses [41].

The effect that epistatic interactions between loci can have on the fitness landscape can be studied in the LK model (also known as the NK model) proposed by Kauffman and Weinberger [100]. This model has tunable ruggedness

and can be applied to real fitness landscapes to provide a measure of their degree of epistasis [62, 82, 167]. In this model each locus in the sequence of a genotype is assigned K *interaction partners*. These are K unique loci (different to the locus being considered) which are randomly or otherwise selected. For locus p let the set consisting of its interaction partners and itself be $\nu_p = \{p, \nu_{(p,1)}, \nu_{(p,2)}, ..., \nu_{(p,K)}\}$ where $\nu_{(p,j)}$ is the j'th interaction partner of locus p. An example illustration of interaction partners can be seen in Fig. 2.5B.

In the LK model the fitness of genotype σ is equal to a sum of contributions from each locus. The contribution from locus p will depend on what the alleles are in genotype σ at the loci contained in the set ν_p. Therefore the total fitness $r(\sigma)$ of genotype $\sigma = \{\sigma_1, \sigma_2, ..., \sigma_L\}$ can be written as

$$r(\sigma) = \sum_{p=1}^{L} r_p\left(\{\sigma_j\}_{j\in\nu_p}\right), \tag{2.27}$$

where $r_p\left(\{\sigma_j\}_{j\in\nu_p}\right)$ is the fitness contribution of locus p. There are 2^{K+1} possible combinations (for binary sequences) that the alleles contained at the loci in the set ν_p can be in. Each of these combinations is assigned an independently drawn random number and the fitness contribution $r_p\left(\{\sigma_j\}_{j\in\nu_p}\right)$ from locus p is equal to that which has the combination of alleles to match the genotype σ being considered. Therefore 2^{K+1} random numbers are drawn for each of the L loci in the genotype sequence. A change at a single locus (i.e. mutation) results in a different fitness contribution from not just that locus but from all others that have that locus as one of its interaction partners. The parameter K therefore controls the strength of interactions between loci in determining the fitness of the genotypes. In the case when $K = L - 1$ there is maximum interaction between loci, such that a mutation anywhere in the genotype changes all contributions to the total fitness $r(\sigma)$. This situation is equivalent to the House of Cards random landscape model. Alternatively when the interaction between loci is minimised at $K = 0$ this model is equivalent to the *Mount Fuji* model, which we will look at an extension of shortly [63].

A model that explores the neutral theory of evolution is the *Holey Landscape* model [71], an example of which is shown in Fig. 2.5C. In this model genotypes are randomly assigned one of two values (say 0 and 1) and the connectivity of genotypes in the space can be explored [62]. This is similar to models of percolation from statistical physics.

The final model of interest to us, with tunable ruggedness, is the *Rough Mount Fuji* model [9, 139]. This was developed by Aita *et al.* [9] in the context of protein evolution, as an extension of their earlier *Mount Fuji* model [8]. This model considers fitnesses to be (on average) additive within the vicinity of local fitness peaks but subject to fluctuations (and is equivalent to the REM model in an external field). This is considered to be somewhat biologically realistic and can also be used to quantify properties of empirical fitness landscapes [9, 62]. An example of part of such a fitness landscape is shown in Fig. 2.5D.

Numerous studies have been carried out into the accessibility of landscapes created using such random landscape models [24, 62, 83, 173]. In many instances as the sequence length L increases (for large L) the probability of there being at least one accessible path (connecting a genotype and its antipodal state) increases [62, 83]. However, this is not the case in the House of Cards model unless the fitnesses of specific genotypes are constrained in some way. The accessibility of these landscapes will be discussed more in Chapter 5 where we consider models that incorporate the House of Cards and Rough Mount Fuji landscape types.

2.3 Mathematical methods

We now consider several of the common mathematical methods that are used in this thesis. These are general methods which are well documented in texts such as [70, 155, 159, 163].

2.3.1 Poisson process and distribution

Throughout this thesis we describe cellular actions, such as births and deaths as obeying Poisson processes. We take some time here to remind ourselves of Poisson processes, the Poisson distribution and how to generate Poisson distributed random numbers [70].

If the number of occurrences of an event is greater than or equal to zero, the events are independent of one another, and the number occurring in any interval is describable by a Poisson distribution, then the occurrence of such events can be described as obeying a Poisson process. Common examples of situations that can be described by Poisson processes are the number of calls received at a call

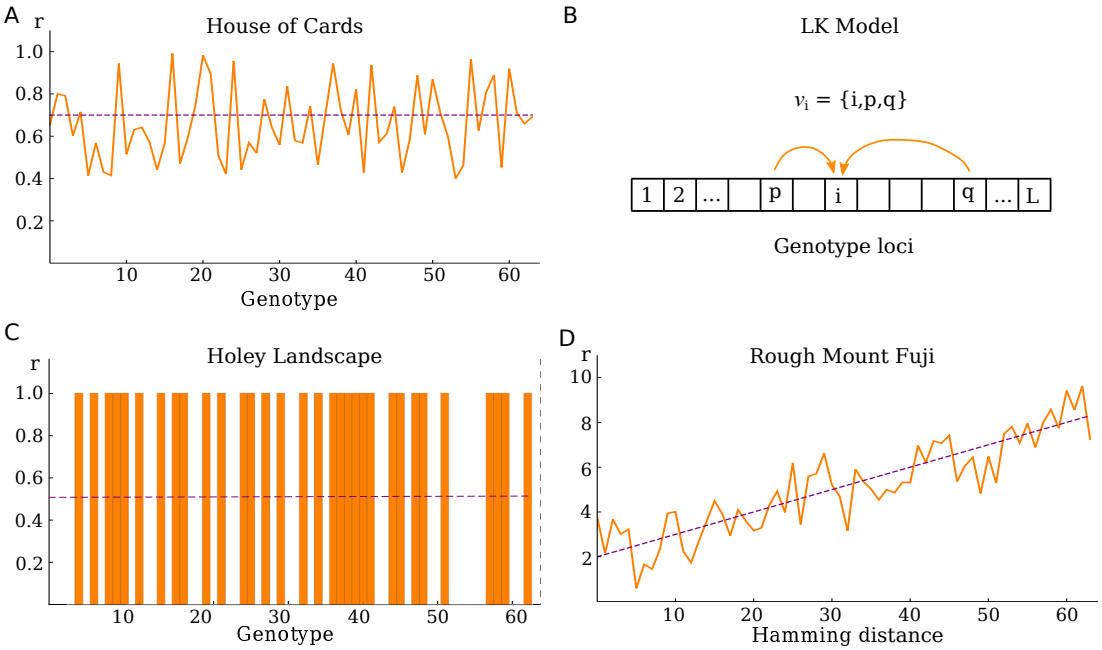

Figure 2.5 *Features of random landscape models. (A) and (C) show random fitness landscapes for the House of Cards (HoC) and Holey Landscape models respectively and plot the fitness r as a function of the genotypes (which are labelled in some chosen way). In (A) the fitnesses are selected from a continuous distribution of values while in (C) they are selected from one of only two values (often 0 and 1). (B) Interaction partners (loci p and q) are chosen for locus i in the LK model when $K = 2$. The state of these three loci (collected in set ν_i) will decide the fitness contribution of locus i to the total fitness of the genotype. (D) A section of a Rough Mount Fuji (RMF) landscape demonstrating how the genotype fitness can vary with Hamming distance away from a chosen genotype (designated here to be genotype 0). The fitness, on average, increases by a fixed amount with Hamming distance from genotype 0. Dashed purple lines in the plots show the average fitness values where relevant.*

centre, or the number of electrons in a current arriving at an anode, in a given time.

Let X be a discrete random variable that equals the number of occurrences of an event, while λ is the expected number of occurrences per unit time. $P_n(t)$ is the probability distribution that the number of occurrences $X = n$ in time interval t.

In a Poisson process the probability that an event occurs in a small time interval Δt is $\lambda \Delta t$ and that no event occurs is $(1 - \lambda \Delta t)$. Therefore the distribution $P_n(t)$ evolves in time Δt by

$$P_n(t + \Delta t) = P_n(t)(1 - \lambda \Delta t) + P_{n-1}(t)\lambda \Delta t. \tag{2.28}$$

Rearranging (2.28) and letting $\Delta t \to 0$ yields the differential equation

$$\frac{dP_n(t)}{dt} = -\lambda P_n(t) + P_{n-1}(t)\lambda. \tag{2.29}$$

Equation (2.29) can be rewritten in terms of the generating function $G(s,t) = \sum_{n=0}^{\infty} s^n P_n(t)$ as

$$\frac{\partial G(s,t)}{\partial t} = \lambda(s-1)G(s,t), \tag{2.30}$$

which has the solution

$$G(s,t) = G(s,0)e^{\lambda(s-1)t}. \tag{2.31}$$

Now the initial condition $P_0(t = 0) = 1$ as when no time has passed no events can have occurred. This translates to the initial condition for $G(s,t)$ to be $G(s,0) = 1$. Therefore

$$G(s,t) = e^{\lambda s t} e^{-\lambda t} \tag{2.32}$$

$$= \sum_{n=0}^{\infty} \frac{(\lambda s t)^n}{n!} e^{-\lambda t}. \tag{2.33}$$

Recalling the definition of the generating function $G(s,t)$, we can read from (2.33) the form that the probability distribution $P_n(t)$ must take. This is

$$P_n(t) = \frac{(\lambda t)^n e^{-\lambda t}}{n!}, \tag{2.34}$$

which is the standard form of the Poisson distribution.

Our interest is in $P_0(t)$, the probability that no events occur in interval t. Therefore the probability $P(t)$ that at least one event occurs by time t is

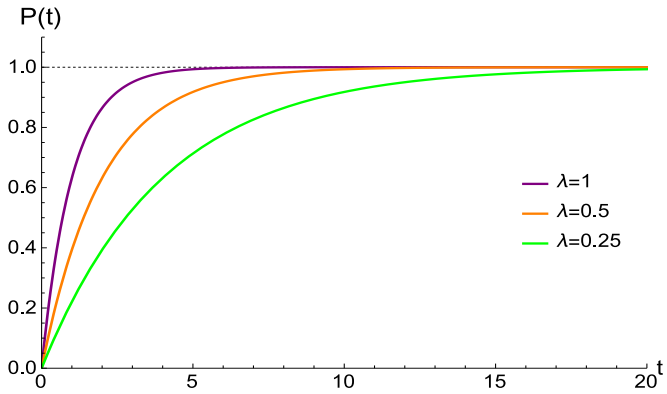

Figure 2.6 *A plot of the probability $P(t)$ that at least one event has occurred by time t. The occurrences of events obey a Poisson process. Curves are for different values of λ, the expected rate with which the events occur.*

$P(t) = 1 - P_0(t) = 1 - e^{-\lambda t}$. A plot of $P(t)$ for different values of λ can be seen in Fig. 2.6. Rearranging this expression for $P(t)$ for t gives us

$$t = -\frac{1}{\lambda} \ln[1 - P(t)], \tag{2.35}$$

in which necessarily $(1 - P(t)) \in [0, 1]$. A uniformly distributed random number $u \in (0, 1]$, substituted for $(1 - P(t))$ into (2.35), produces a Poisson distributed random time t for the first event to occur. This method is used to calculate the time until the next event occurs in the stochastic algorithms discussed later.

2.3.2 Master equations

We now look at the common technique of formulating *master equations* to describe stochastic processes such as random walks [70, 159]. In a random walk, a system exists in one of a finite number of states from which it can transition ("hop") to other states with known probabilities (discrete time processes) or rates (continuous time processes). Master equations describe the rate of change of the probability that a system is in a given state at a given time. From these equations, properties of the random walk can be calculated such as the *mean first passage time*, which is the average time it takes the random walker to first visit a particular state.

We consider first the *forward master equation*. Let $P(C, t)$ be the probability distribution that the system is in state C at time t, while $\omega(C \to C')$ is the rate

of the transition from state C to C', which is treated as a Poisson process. In an infinitesimal time $\tau \ll 1$ a system in state C transitions to state C' with the probability $\omega(C \to C')\tau$ and remains in state C with probability $(1 - \omega(C \to C')\tau)$. Therefore

$$P(C, t+\tau) = \sum_{C' \neq C} \left[P(C', t)\omega(C' \to C)\tau + \left[1 - \omega(C \to C')\tau\right] P(C, t) \right], \quad (2.36)$$

where the sum is over all states in the system. Note that $\omega(C'' \to C) = 0$ for a state C'' which cannot transition in a single hop to C and therefore does not contribute to (2.36).

Rearranging (2.36) and taking the limit $\tau \to 0$ yields the following differential equation for the rate of change of $P(C, t)$

$$\frac{\partial P(C,t)}{\partial t} = \sum_{C' \neq C} \left[P(C', t)\omega(C' \to C) - P(C, t)\omega(C \to C') \right], \quad (2.37)$$

which is the standard form of the forward master equation. The first term in (2.37) describes the flow of probability into the state C (from C'), while the second term is the flow of probability out of C (into C').

A random walk is a *Markov process*, such that the future evolution of the system depends only on its present state (and not its history). Therefore to arrive at (2.37) it was not necessary to specify the history of the system from time $t = 0$ until time t. However, the *backwards master equation* is a different description of the same Markov process which uses this earlier information. It produces a different rate of change equation for the probability distribution, which is arrived at by considering the variability in the initial state. To consider this we amend our notation slightly. Let $P(C, t|C_0, t_0)$ be the probability distribution that the system is in state C at time t given that it was in state C_0 at time t_0. The transition rate from state C to C' is still given by $\omega(C \to C')$.

Consider if the system is in state C_0 at some infinitesimal time $\tau \ll 1$ before t_0. In the time interval τ until t_0 is reached, the system can transition to state C' with the probability $\omega(C_0 \to C')\tau$, or remain in state C_0 with the probability $(1 - \omega(C_0 \to C')\tau)$. Therefore

$$\begin{aligned} P(C, t|C_0, t_0 - \tau) &= \sum_{C' \neq C} \left[\omega(C_0 \to C')\tau P(C, t|C', t_0) \right. & (2.38) \\ &\qquad \left. + (1 - \omega(C_0 \to C')\tau) P(C, t|C_0, t_0) \right], & (2.39) \end{aligned}$$

which can be rearranged and in the limit $\tau \to 0$ yields

$$\frac{\partial P(C,t|C_0,t_0)}{\partial t_0} = -\sum_{C' \neq C} \omega(C_0 \to C') \left[P(C,t|C',t_0) - P(C,t|C_0,t_0)\right]. \quad (2.40)$$

Equation (2.40) is the backward master equation, giving the rate of change of $P(C,t|C_0,t_0)$ with respect to the initial condition t_0. To re-express (2.40) as a rate of change equation with respect to the time t (i.e. an alternative forward master equation to the one in (2.37)) we can note the following: for Markov processes, in which the transition rates are independent of time, the time dependence of $P(C,t|C_0,t_0)$ is on the time interval $(t - t_0)$ and not on the specific values of t and t_0. Therefore for any time interval τ, such that $(t_0 - \tau) \geq 0$

$$P(C,t+\tau|C_0,t_0) = P(C,t|C_0,t_0-\tau). \quad (2.41)$$

Subtracting $P(C,t|C_0,t_0)$ from both sides of this equation, dividing through by τ and taking the limit $\tau \to 0$ we get that

$$\frac{\partial P(C,t|C_0,t_0)}{\partial t} = -\frac{\partial P(C,t|C_0,t_0)}{\partial t_0}. \quad (2.42)$$

Therefore we can write an alternative form for the forward master equation, using (2.40), as

$$\frac{\partial P(C,t|C_0,t_0)}{\partial t} = \sum_{C' \neq C} \omega(C_0 \to C') \left[P(C,t|C',t_0) - P(C,t|C_0,t_0)\right]. \quad (2.43)$$

This is the form that we will use for the forward master equation in Chapter 4. It will be used to calculate quantities such as the mean first passage time, which we defer consideration of until then.

2.3.3 Systems of differential equations

We consider now how vector differential equations can be solved through an eigendecomposition of the Markov matrix [155]. Let $\mathbf{P}(t)$ be a vector that obeys the following differential equation

$$\frac{d\mathbf{P}(t)}{dt} = \mathrm{M}\mathbf{P}, \quad (2.44)$$

where M, referred to as a Markov matrix, is a square matrix that is not diagonal (otherwise the solution is trivial) but is diagonalizable. This has the solution

$$\mathbf{P}(t) = e^{\mathrm{Mt}}\mathbf{P}(0), \tag{2.45}$$

where e^{Mt} is a matrix exponential. To arrive at a meaningful form for $\mathbf{P}(t)$ we can re-express e^{Mt} by performing an eigen-decomposition of M. This expresses the diagonalisable matrix M in terms of its eigenvalues and left and right eigenvectors by

$$\mathrm{M} = \sum_{\mathrm{i}} |\psi_{\mathrm{i}}\rangle \langle\phi_{\mathrm{i}}| \lambda_{\mathrm{i}}, \tag{2.46}$$

where we have switched to Dirac's *bra-ket* notation for vectors. The sum runs over all eigenvalues λ_i, which are eigenvalues of both the left and right eigenvectors ($\langle\phi_i|$ and $|\psi_i\rangle$ respectively). If the matrix M is non-symmetric then provided the eigenvalues are not degenerate the left and right eigenvectors are orthogonal to one another, i.e. $\langle\psi_i|\phi_j\rangle = \delta_{ij}$ in the case in which they are normalised also.

Expressing the matrix exponential in (2.45) in series form and replacing the matrix M with its eigenvalue decomposition we get

$$\begin{aligned} \mathbf{P}(t) &= \sum_{k=0}^{\infty} \frac{t^k}{k!} \mathrm{M}^{\mathrm{k}} |0\rangle & (2.47) \\ &= \sum_{k=0}^{\infty} \frac{t^k}{k!} \left(\sum_i |\psi_i\rangle \langle\phi_i| \lambda_i \right)^k |0\rangle & (2.48) \end{aligned}$$

Due to the orthogonality between the left and right eigenvectors

$$\left(\sum_i |\psi_i\rangle \langle\phi_i| \lambda_i \right)^k = \sum_i |\psi_i\rangle \langle\phi_i| \lambda_i^k. \tag{2.49}$$

Substituting this into (2.48) gives the solution

$$\mathbf{P}(t) = \sum_i \langle\phi_i|0\rangle e^{t\lambda_i} |\psi_i\rangle , \tag{2.50}$$

where we have gathered the sum over k and other terms into an exponential again. Alternatively, if the eigenvectors are not normalised the solution becomes

$$\mathbf{P}(t) = \sum_i \frac{\langle\phi_i|0\rangle}{\langle\phi_i|\psi_i\rangle} e^{t\lambda_i} |\psi_i\rangle \tag{2.51}$$

Therefore by calculating the eigenvalues and eigenvectors of the Markov matrix M the solution for (2.44) is that of (2.51). In Chapter 3 we use this method to perform a numerical eigen-decomposition in order to solve a system of master equations.

2.4 Numerical Methods

Most of the results that are presented in this thesis are numerical. Here we outline the three commonly used numerical methods. The first method solves ordinary differential equations (ODEs) while the remaining two are used for stochastic simulations.

2.4.1 Euler's method

Euler's method is the most general algorithm used to numerically solve ordinary differential equations (ODE's) [77]. Given an initial value problem of the form

$$\dot{x}(t) = f(t, x(t)), \quad x(t_0) = x_0, \quad t > t_0, \tag{2.52}$$

we want to solve for the true curve $x(t)$. Euler's method constructs a set of points $\{x_n\}$ which are approximations to points on the true curve. These points are separated by intervals of fixed size h (the step size) beginning from the initial value x_0. Each point can be calculated from the preceding one by Taylor expanding to first order in h, such that

$$x_{n+1} = x_n + hf(t_n, x_n(t_n)) + \mathcal{O}(h^2). \tag{2.53}$$

Each step carries a local truncation error of the order of h^2, while the process carries a global truncation error of order h.

Any set of points $\{x_n\}$ obtained using this method is an approximation. The validity of results obtained using this method will always be tested for convergence to the true solution by repeating the method with a reduced step size.

2.4.2 Stochastic simulation algorithms

Here we introduce two algorithms that are used in stochastic simulations throughout the following chapters. As an example system we will consider a well mixed environment of chemicals (in thermal but not chemical equilibrium). This system alters its state through reactions that occur between the constituents. This setting of chemical kinetics is frequently the context these algorithms are presented in literature [32, 72, 73] and is appropriate for our upcoming models.

Consider a system with N chemical species $\{S_1, ..., S_N\}$ and M possible reactions $\{R_1, ..., R_M\}$ that involve them. These reactions change the state of the system $\vec{X}(t) = (X_1(t), ..., X_N(t))$, in which $X_i(t)$ is the abundance (number of particles) of species i in the system at time t. In the following, for shorthand we refer to the state of the system at time t as $\vec{x} = \vec{X(t)}$.

Reaction R_i has the *propensity* $a_i(\vec{x})$, which is the rate with which reactions of the type R_i occur when the system is in state $\vec{x}$. The total propensity in the system, being the total rate of all reactions, is therefore $a_0(\vec{x}) = \sum_{j=1}^{M} a_j(\vec{x})$. If reaction R_i occurs, the state of the system will change by the vector $\vec{v}_i = (v_{1i}, ..., v_{Ni})$, in which v_{ji} is the change in abundance to species j due to reaction R_i.

Let $P(\vec{x}, t|\vec{x}_0, t_0)$ be the probability that the system is in state $\vec{x} = \vec{X}(t)$, given that it was in state $\vec{x}_0 = \vec{X}(t_0)$. The rate of change of $P(\vec{x}, t|\vec{x}_0, t_0)$ is given by the following master equation

$$\frac{\partial P}{\partial t}(\vec{x}, t|\vec{x}_0, t_0) = \sum_{j=1}^{M} \left[a_j(\vec{x} - \vec{v}_j)P(\vec{x} - \vec{v}_j, t|\vec{x}_0, t_0) - a_j(\vec{x})P(\vec{x}, t|\vec{x}_0, t_0)\right]. \quad (2.54)$$

Solving (2.54) will give you an exact solution for the probability that the system is in state $\vec{x}$ at time t. However, this is not always possible and instead the following methods are used to simulate stochastically how the system evolves.

Kinetic Monte Carlo

The Kinetic Monte Carlo (KMC) algorithm, and in particular its most known implementation the Gillespie algorithm, is an *exact* stochastic simulation algorithm [73]. This means the trajectories it generates for the system (through phase space) have the same likelihood of occurrence as predicted by the solution

of (2.54).

In each step of the algorithm, a single reaction R_i is chosen to occur and a time-step τ for it to happen in. The system is then updated by $\vec{X}(t+\tau) = \vec{x} + \vec{v}_i$ and the process repeats until a predetermined target is reached. The time-step τ is described as the waiting time for the first event in a Poisson process. Therefore τ is an exponentially distributed random number with mean $1/a_0(\vec{x})$, which is calculated by

$$\tau = -\frac{1}{a_0(\vec{x})} \ln(u_1) \quad \text{with random} \quad u_1 \in (0, 1]. \tag{2.55}$$

That this selects a Poisson distributed random time was shown earlier in (2.35).

Reaction R_i has the probability $a_i(\vec{x})/a_0(\vec{x})$ of being the reaction that occurs. Therefore by drawing a second (uniformly distributed) random number $u_2 \in [0, 1)$, the reaction is found to be R_j, in which j is the smallest integer in $\{1, ..., M\}$ that satisfies

$$\sum_{k=1}^{j} a_k(\vec{x}) > u_2 a_0(\vec{x}). \tag{2.56}$$

The KMC algorithm described above is the *rejection free* KMC. Variations on this method include the *rejection* KMC and a fixed time step KMC. In the rejection KMC, the potentially time consuming iterative process to calculate which reaction occurs in (2.56) is bypassed. The reaction R_i is randomly selected (with all reactions equally likely) and a uniform random number $u_2 \in (0, 1]$ decides if it should happen by testing if $u_2 \leq a_i(\vec{x})/a_0(\vec{x})$. If this condition is not satisfied then the action is rejected and a new one is selected and tested in the same way.

Alternatively, in the fixed time step KMC algorithm, the selection of τ in (2.55) is replaced by using a fixed time step $\tau = 1/a_0(\vec{x})$, the average of the distribution of selected times. This method is more precise the greater $a_0(\vec{x})$ is (i.e. at larger population sizes).

A drawback of KMC algorithms is that they update the system a single reaction at a time. This can be time consuming if, e.g. the process being simulated involves waiting on rare events to occur (such as mutations during reproduction). In these instances the τ *leaping* algorithm may be more suitable.

Tau leaping

The tau leaping algorithm (also known as τ leaping) is an approximate stochastic simulation algorithm which can evolve the system by more than one reaction at a time [72]. In each time step τ it calculates how many times each of the reaction types $\{R_1, ..., R_M\}$ occur. It does this by describing each reaction as obeying a Poisson process and draws a random number for each one to decide how many of that reaction type occurs. The system is then simultaneously updated with the changes due to all reactions.

Let $K_j(\tau|\vec{x}, t)$ be the number of the times that reaction R_j is expected to occur in time interval τ when the system is in state $\vec{x} = \vec{X}(t)$. If τ is small enough, then $K_j(\tau|\vec{x}, t)$ can be approximated by a Poisson distributed random variable $p_j(a_j(\vec{x}), \tau)$ with mean $a_j(\vec{x})\tau$. By calculating $p_j(a_j(\vec{x}), \tau)$, independently for all M reactions, the state of the system can be updated according to

$$\vec{X}(t + \tau) = \vec{x} + \sum_{j}^{M} \vec{v}_j p_j(a_j(\vec{x}), \tau). \tag{2.57}$$

As introduced earlier the vector $\vec{v}_j$ details how a single reaction of type R_j changes the abundance of the species in the system. The accuracy of this method relies on the time step τ being small enough that the system does not change in an "appreciable" way during the update. This condition is the *leap condition* which ensures that the change to the propensity functions $\{a(\vec{x})\}$ are small enough to justify the simultaneous initiation of all reactions in the way described. How great a change is before it becomes "appreciable" is open to interpretation. However, in the following work this condition is satisfied implicitly by using a fixed time step τ and then testing the solution has converged using smaller time steps. Note that this is an approximate method that does not guarantee that the leap condition is satisfied in every step. However, in what follows we always tested that τ was sufficiently small in simulations by running them again at lower values to ensure that the results did not noticeably change.

Alternatively, effective methods have been created that test for the maximum step size τ that satisfy different interpretations of the leap condition. These result in dynamic time step methods, an effective overview of which can be found in [32]. Dynamic time step methods were tested for the simulations in this thesis but were found to slow down simulation time in a way that did not justify the algorithm's use.

2.4.3 Algorithm implementation

The algorithms described in this section are utilised throughout the following chapters and are identified alongside any results shown. In stochastic models, when the population sizes are small ($\leq$ 100 cells), or alternatively when the growth is exponential as in Chapter 6, results are gathered using the rejection free KMC algorithm and occasionally the fixed time step KMC. This exact method is also used whenever the trajectory information of cells is stored.

For larger population sizes the total propensity in the system $a_0(\vec{x})$ is large enough that the estimated time τ until the next reaction occurs, as given by (2.55), is too small to use to simulate the entire process. Therefore for larger population sizes ($K > 100$ cells) a fixed time step tau leaping algorithm is often used. Results generated using this algorithm, as well as Euler's algorithm used to solve deterministic equations, are always tested for convergence. This involves the numerical results being tested for equivalence with results obtained using a smaller time step (this is normally an order of magnitude smaller but may be greater if the data is particularly time consuming to generate). Proof of convergence is normally excluded from results in order to avoid unnecessary confusion.

Chapter 3

Stochastic phenotype switching in a 1D valley crossing model - Numerical study

3.1 Introduction

In this chapter we consider a computational model of microbial evolution in a chemostat. The model describes how a population of haploid cells are able to overcome a fitness valley in genotype space to escape from a local fitness peak. The cells have access to a second phenotypic state in which the fitness effects are not as deleterious as in the original phenotype. The existence of this second phenotypic state allows for a significant reduction in the time it takes the population to escape from the local peak to evolve a compensatory double mutant; providing the population with a "safe niche" in which genetic mutations can be acquired more quickly. This chapter focusses on a numerical study of the model, which is then analytically studied in Chapter 4.

We consider the simplest case of a 1D genotype space, with a *fitness valley* (i.e. an intermediate state with reduced fitness) separating the initial ("wild-type") genotype from the global peak of a fitness landscape. Cells undergo stochastic phenotype switching between the original landscape and the landscape of the second phenotype (in which the fitness valley does not exist). In the absence of phenotype switching the population, or some fraction of it, must cross the fitness

valley in order to reach the optimal state. This can be a time consuming process, particularly at small population sizes. However, phenotype switching can open up alternative trajectories to the optimal state, which can optimise the evolutionary process.

Our initial focus in this chapter will be on understanding how the second phenotypic state affects the time taken for a member of the population to reach the global optimal state, which we refer to as the adaptation time T. We will see that there exists an optimal range for the rate of stochastic phenotype switching, in which evolution is the fastest. We will then examine the trajectories that successful cells take to see if they are predictable and, if so, to understand why. Finally, we will close this chapter by considering an extension of the model, in which cells can evolve their own rate of stochastic phenotype switching. We do this to answer the following question: will a population of cells, initially without stochastic phenotype switching, evolve it in order to accelerate its evolutionary escape from a local fitness peak?

3.2 Background and motivation

Stochastic phenotype switching (SPS) can benefit microbial populations that frequently undergo environmental changes. In this case, the phenotypic heterogeneity in the population provides a preemptive "bet-hedging" strategy against the population being maladapted should the environment change [22, 111]. SPS can also benefit populations in static environments through the division of labour, in which different functions are carried out by different groups in the population. For example, this can be when some cells sacrifice themselves for the benefit of other cells [5], or when cells of a single phenotype secrete a compound to the benefit of the entire population [196].

SPS can thus provide selective advantage on the level of both individual cells, and whole populations of related cells. Thus, naturally occurring mechanisms that lead to spontaneous SPS can be favoured by selection. For example, SPS can be due to noise amplification in multistable gene regulatory networks, which through the inherent noise in gene expression [55, 142] can result in switching between distinct phenotypic states [34, 177]. Interestingly, genes that code for essential cellular functions are often protected against such potentially harmful phenotypic noise (e.g. by negative feedback loops) [23, 117]. Alternatively,

repeated nucleotide sequences in the genomes of pathogenic bacteria can result in *slipped strand mispairing*, a common mechanism for the stochastic phenotype switching of *phase variation*. This can lead to ON/OFF stochastic switches in bacteria for expressing genes that are responsible for the production of different surface appendages [213]. These can aid the survival of bacteria in the rapidly changing environment of a host [212]. For example, the bacterium *Escherichia coli (E. coli)* can switch between states that do and do not code for the protein Ag43, the presence of which allows them to autoaggregate and can lead to increased virulence [58].

In this chapter we consider the possibility of whether SPS can also accelerate the genetic evolution of populations when the environment is static. To do this we study the scenario of a population that is struggling to continue evolution through being trapped at a local peak in the fitness landscape. Due to the high dimensionality of real genotype spaces, it is expected that many fitness landscapes will contain *accessible paths*, along which fitness increases monotonically [62, 203]. However, real fitness landscapes have also been found to consist of numerous local fitness peaks [31, 54, 108, 208]. During the evolutionary process, populations (particularly large ones) can be attracted to local peaks and become trapped [92]. If this happens, the population must cross a fitness valley if evolution is to continue. This can be a very time consuming process [201, 206].

The simplest scenario of escape from a local fitness peak is a 1D genotype space, in which a single deleterious genotype separates a population of cells from the global optimum. The first mutation reduces a cell's fitness, which can be recovered (and exceeded) by a compensatory second mutation. Such situations have been found to exist in bacterial landscapes of *E. coli* and *Salmonella typhimurium (S. typhimurium)* in the evolution of resistance to antibiotics [127, 174, 175]. For example, in the presence of the antibiotic, the wild-type genotype will have a reduced growth rate. The first genetic mutation can make the target enzyme of the antibiotic less susceptible to it but also less efficient (causing a reduction in fitness relative to the wild-type). A secondary mutation could compensate for this loss of efficiency and in doing so increase the genotype's fitness beyond that of the wild-type.

On the other hand, having a secondary phenotypic state which is more resistant to environmental stresses is common in bacteria. For example, switching between normal and persister states in the presence of antibiotics has been observed for many microbes [14, 16]. However, the resistance property of persisters often

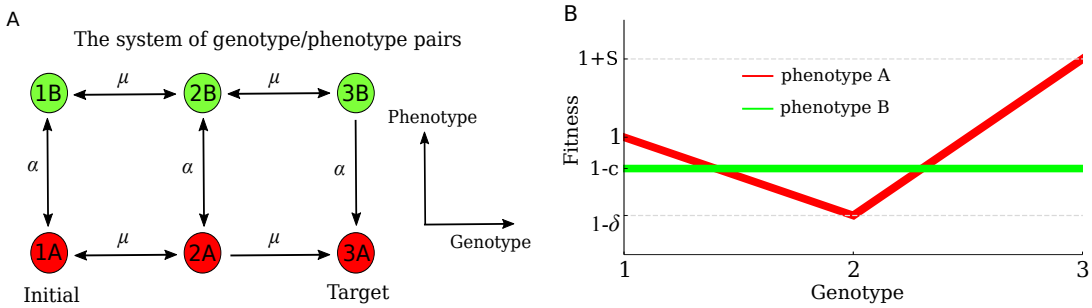

Figure 3.1 *The model we consider. (A) The* 6 *state system of genotype/phenotype pairs that cells can exist in and the available transitions between them. Genotypes are labelled* $1, 2$ *and* 3 *and phenotypes as* A *and* B*. Transitions that alter the genotype and phenotype are labelled by* μ *and* α *respectively. A population of cells start in state* $1A$ *and evolves until an individual reaches state* $3A$*. (B) The fitness landscapes for both phenotypes. Phenotype* A *has a fitness valley at state* $2A$ *while phenotype* B *has uniform fitness across all genotypes, at a cost* c *when compared to the fitness of* $1A$*.*

follows from having a reduced growth rates. Alternatively, remaining on the example of antibiotic resistance, the secondary phenotypic state could be one with an increased level of gene expression for antibiotic degrading enzymes or multi-drug efflux pumps (that flush the antibiotic from the cell). A switch to such a state is observed in the bacterium *Pseudomonas aeruginosa (P. aeruginosa)* upon exposure to antibiotics [30, 48].

3.3 Model

In the model, all cells in the population can exist as one of three genotypes ("genetic states" labelled 1, 2 and 3) and two phenotypes (labelled A and B). These combine to form six possible cellular states of genotype/phenotype pairs. This network of states can be seen in Figure. 3.1A.

These cells stochastically undergo the actions illustrated in Fig. 3.2. These are: replication, death and phenotype switching. Replication occurs at the rate $r_i(1 - \frac{N_T}{K})$ where r_i is the fitness (with arbitrary units) of a cell in state i, $N_T = N_T(t)$ is the total population of cells at time t and K is the carrying capacity of the environment. The logistic factor $(1 - \frac{N_T}{K})$ controls the growth of the population and tends to zero as N_T approaches K. Therefore K represents a limit to the population's size due to a lack of available resources or free space

Figure 3.2 *Actions available to each cell and the parameters that control the rates they occur. These are: successful replication, unsuccessful replication (producing a mutant offspring of a neighbouring genotype), switching phenotype and death.*

in the environment etc. During replication, with the probability μ, the offspring produced is of a neighbouring genotype to that of the parent cell (but the same phenotype). For each neighbouring genotype, there is a probability μ that the offspring is a mutant created there.

Stochastic phenotype switching (SPS) occurs independently of the replication process at the rate α. This rate is uniform across all genotypes in each phenotype. For most of the following, α is also symmetric (i.e the rate of switching from phenotype A$\rightarrow$B is the same as from B$\rightarrow$A). However, in Section 3.7 we will consider the effect of an asymmetric switching rate. Finally, with rate d cells are removed from the system. This action is referred to as "death" but corresponds to the flushing away of biological matter that takes place in a chemostat.

The fitness landscapes for both phenotypes are shown in Fig. 3.1B. The landscape for phenotype A is deleterious at state 2A (i.e. it has reduced fitness with respect to the wild-type state 1A) and has the global fitness maximum of both landscapes at 3A (with fitnesses $r_{2\mathrm{A}} = 1-\delta$ and $r_{3\mathrm{A}} = 1+s$ respectively). Phenotype B has a uniform landscape with fitnesses $1-c$. Therefore the parameter c is the fitness cost (relative to 1A) for a cell being in phenotype B. Table 3.1 provides a quick reference of some of the commonly used parameters and variables in the model.

A population of cells that starts in the wild-type state 1A will, if it avoids extinction, evolve some final distribution about the optimal state 3A. However, here we are interested in the process by which the population of cells first evolves a cell in state 3A. The time taken for this process is the adaptation time T. The

Symbol	description	Details
N_i	population at state i	Total population number $N_T = \sum_i N_i$
K	carrying capacity	Limiting value of N_T through the factor $(1 - \frac{N_T}{K})$ in the growth rate
r_i	fitness of state i	Rate with values $\{1, 1-\delta, 1+S\}$ for phenotype A cells and $1-c$ for pxhenotype B
d	death	Rate set to $d = 0.1$ throughout
μ	mutation probability	Probability - during replication - of mutation to each neighbouring genotype
α	switching rate	Rate a cell changes its own phenotype between states A and B. Symmetric for cells in both phenotypes
δ	valley depth	Fitness reduction of state 2A compared to 1A ($r_{2A} = r_{1A} - \delta$)
c	cost	Fitness cost of states in phenotype B compared to state 1A

Table 3.1 *Key parameters and variables in the model.*

probability that beneficial mutants fix in a population of cells is well understood [56, 104]. Therefore we will not concern ourselves here with whether the cell produced at 3A takes over the population or not. Instead we are interested in how the population first manages to overcome the fitness valley and what the expected evolutionary trajectory is.

In the following results, unless otherwise stated, the population begins at size $(1 - (d/r_1))K$ in state 1A. This is the equilibrium size of a population confined to state 1A, which we will discuss in Chapter 4. We consider mainly the case of zero fitness costs for phenotype B (i.e. $c = 0$) but will later look at the effect of having $c > 0$. Different simulation techniques are used to study different aspects of the model and will be identified when used.

In the following results, the time presented is a simulation time (with arbitrary units we'll refer to as *sim units*). The rate with which cells replicate in the model is $\sim (1 - (N_T/K))r_i \approx d = 0.1$ $(sim\ units)^{-1}$. Therefore cells in the model have an average generational time of ~ 10 *sim units*, from which we can infer a physical time from results.

3.4 How phenotype switching affects the time to adaptation

3.4.1 Phenotype switching can speed up evolution

We begin by considering the general effect that phenotype switching can have on the adaptation time T. This can be seen in Fig. 3.3A, which shows a series of bar charts comparing T with and without phenotype switching (for the case of $\alpha = 10^{-5}$ and 0 respectively). It demonstrates that, for different parameter combinations, low frequency phenotype switching often results in a lower adaptation time. The extent of this reduction is sensitive to the parameters of the model, as shown for each pair of bars.

Figure 3.3B looks at how T varies as a function of the mutation probability μ, again comparing results with and without phenotype switching (here $\alpha = 10^{-4}$ and $\alpha = 0$ respectively). We observe that above a certain μ value, μ_c, there is no observable difference between the two curves. For $\mu < \mu_c$, phenotype switching reduces the adaptation time T, with a greater reduction the smaller μ is. This occurs due to the reduced rate with which genetic mutants are created in the system as μ is reduced. This reduction therefore affects the waiting time for the population to follow the trajectory across the valley more than by other trajectories to 3A.

The rate with which genetic mutants are produced in the system is $\sim \mu dK$. Therefore plots of T as a function of K, comparing curves with and without phenotype switching, will be qualitatively similar to the plot of $T(\mu)$ in Fig. 3.3B. We conclude that for $\mu > \mu_c$, trajectories that involve phenotype B are not quicker than evolving 3A directly by 1A$\rightarrow$2A$\rightarrow$3A. However, for $\mu < \mu_c$ phenotype B opens up alternative trajectories that are quicker than the direct evolution of 3A.

A power law is evident between the adaptation time T and the mutation probability μ in the curves in Fig. 3.3B. This only appears to be the case for the $\alpha = 10^{-4}$ curve until its convergence with the $\alpha = 0$ curve at μ_c. T scales with μ for these curves by approximately $T \sim 1/\mu^2$ and $T \sim 1/\mu$ in the case of $\alpha = 0$ and $\alpha = 10^{-4}$ respectively. These relationships can both be verified through the analytical work contained in Chapter 4.

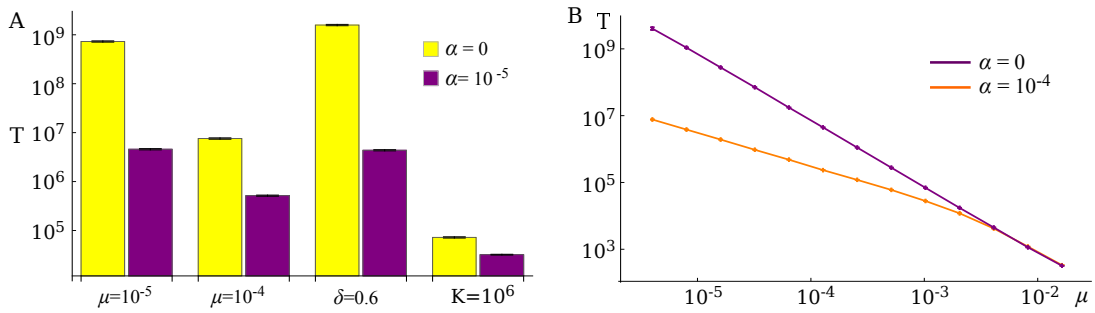

Figure 3.3 *Phenotype switching can reduce the adaptation time T. (A) A bar chart comparing pairs of T values with and without phenotype switching for different parameter values. Left-most pair of bars: $K = 100, \mu = 10^{-5}, \delta = 0.4$ and $d = 0.1$. Underneath each pair of bars is a label that indicates any changed variable with respect to the left-most pair. (B) Comparing T as function of μ for two different α values ($\alpha = 0$ and 10^{-4}). The remaining parameter values are $K = 100$ and $\delta = 0.4$. All results are average over $250 \to 10^4$ runs and collected using both KMC and τ leap algorithms.*

3.4.2 Existence of an optimal range for the switching rate

Holding all other parameters fixed and varying only the switching rate α reveals that there exists an optimal range for α. In this range the adaptation time T can be reduced by orders of magnitude when compared to the system without switching. However, this only occurs if direct evolution through 2A is slow enough that phenotype B offers quicker trajectories, as discussed above for Fig. 3.3B. Figures 3.4A and B demonstrate this by showing various curves of T as a function of α.

Figure 3.4A shows plots of $T(\alpha)$ for different μ values in the case of a deep valley ($\delta = 0.4$). The optimal α range can be observed here at the lower μ values and its significance noted to increase (see the log scale) as μ reduces. Alternatively, Fig. 3.4B is a typical plot of $T(\alpha)$ when the valley depth is small ($\delta = 0.1$). Switching is shown to ultimately reduce T, following an initial minor peak in the curve of $T(\alpha)$. We can surmise that this peak occurs at low enough frequency of switching α, that following at least one cell switching, the population (or some fraction of it) can become trapped in phenotype B waiting for a return switch. This leaves (at most) a reduced population in phenotype A to evolve the target state, which can take longer than in the case without switching.

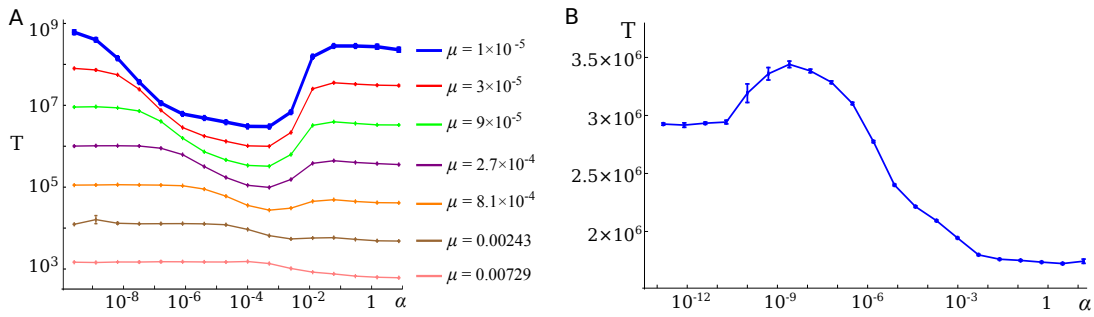

Figure 3.4 *The adaptation time T as a function of the switching rate α. (A) A log-log plot comparing T as function of α for different values of the mutation probability μ and a deep valley ($\delta = 0.4$). (B) A semi-log plot of T as a function of α for a system with a shallow valley ($\delta = 0.1$) and $\mu = 10^{-5}$. Remaining parameters are $d = 0.1$, while $K = 100$ for (A) and $K = 20$ for (B). All results are averaged over at least $10^3 \to 10^4$ simulation runs and collected using a KMC algorithm.*

3.4.3 Without phenotype switching at the intermediate genotype

To understand the optimal α range in Fig. 3.4A, we consider now the effect of removing the action of phenotype switching for cells in genotype 2 (i.e. at the states 2A and 2B). This creates the network of states and transitions shown in Fig. 3.5A, which we refer to as the *reduced system*.

The adaptation time T as a function of α in this reduced system can be seen in Fig. 3.5B. It is compared with a curve for the full system when $\mu = 10^{-5}$ (the blue curve in Fig. 3.4A). In the reduced system, T decreases monotonically, losing the optimal α range the full system has and tending at large α to a T value lower than the minimum value in the full system. Therefore phenotype switching between cells in the intermediate states (2A and 2B) is the cause of the optimal α range.

3.4.4 An alternative Moran model

To test that the observed behaviour is not specific to our choice of model, we look briefly now at a fixed-population model that describes approximately the same valley crossing process. In this model, the system is updated as in the Moran model. We use this to reproduce the characteristic small and large δ curves in

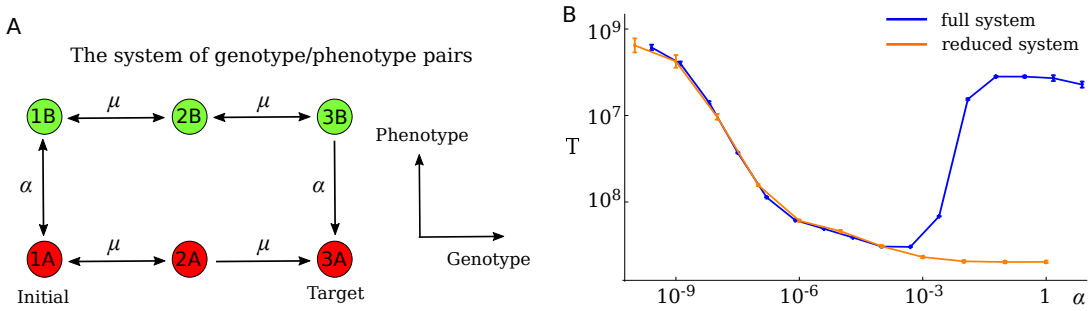

Figure 3.5 *Removing phenotype switching between states 2A and 2B. (A) The modified network of states and transitions considered, referred to as the reduced system. (B) A plot comparing the adaptation time T as a function of α when the system does and does not feature the transition between 2A and 2B (the full and reduced system respectively). The remaining parameters are $K = 100, \mu = 10^{-5}, \delta = 0.4$ and $d = 0.1$. Results are averaged over 10^3 simulation runs and collected using a KMC algorithm.*

Fig. 3.4.

There can be no death action in this model. Instead, with every iteration of the update algorithm a single individual is selected for removal and another to take its place (allowing that the same individual can be selected for both roles). The algorithm considers that all cellular actions increase the population number. However, this is not true in the action of phenotype switching (which is uncoupled from the replication process, see Fig. 3.2). Therefore for this Moran model only, we will change the action of phenotype switching to be the production of offspring of the switched phenotype (instead of a cell switching itself). With normal replication rates in the system of order $\sim d = 0.1$ the primary way that new cells will be produced, at low α, is by the usual replication action and not this amended phenotype switching one. Therefore for $\alpha \ll 0.1$, this algorithm should approximately describe the same process as the original model with varying total population number.

Results using this Moran model are shown in Fig. 3.6, which presents two curves of the adaptation time T as a function of α. Figure 3.6A shows this curve when the valley is deep ($\delta = 0.4$) and Fig. 3.6B when it is shallow ($\delta = 0.1$). These plots can be directly compared with the curves in Fig. 3.4 from the original model (where it is the blue curve in Fig. 3.4A that matches the parameters used for Fig. 3.6A). Figure 3.6 reproduces qualitatively the curves in Fig. 3.4 for all but the largest α values. However, this discrepancy at large α is expected due to the changed action of phenotype switching. The units of T in Fig. 3.6 are the

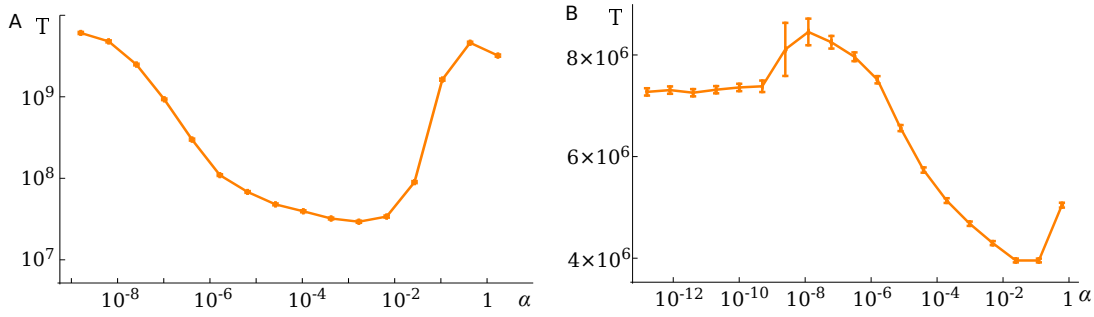

Figure 3.6 *Results for a fixed population model, updated using a Moran process, that is equivalent to the model with actions of Fig. 3.2. The plots show curves of the adaptation time T as a function of α in the case of (A)$\delta = 0.4$ and (B)$\delta = 0.1$. The remaining parameters are $\mu = 10^{-5}$, while $K = 100$ for (A) and $K = 20$ for (B). Results are averaged over $800 \to 10^4$ simulation runs.*

number of iterations of the update algorithm that occurred to reach the target. This is unlike the T calculated in the KMC algorithm, hence the quantitative difference between T in Figs. 3.4 and 3.6 is expected.

3.4.5 Eigen-decomposition analysis

We consider now an alternative numerical method that solves exactly for the adaptation time T. This is used to test some results we have seen so far in stochastic simulations.

For a system that can exist in a finite number of states, if we know the transition rates between the states then we can analytically calculate the mean time for the system to move from any (non-absorbing) state to another (provided that these two states are connected in some way). Let $q_j^{(i)}(t)$ be the probability that the system has not visited an absorbing state and is in state j at time t, given that it started in state i at $t = 0$. The expected time it takes to evolve to state j, conditioned on it doing so is given by

$$T_j^{(i)} = \frac{\sum_m W_{m\to j} \int_0^\infty t q_m^{(i)}(t) dt}{\sum_m W_{m\to j} \int_0^\infty q_m^{(i)}(t) dt}. \tag{3.1}$$

This expression is used in the analytic derivations of Chapter 4 and we leave its justification until then. The sum in (3.1) runs over all states that can transition to state j in a single step, while $W_{m\to j}$ is the transition rate to go from state m to j. The denominator in 3.1 accounts for the "conditioned on it doing so"

caveat, which is required as the system has a second absorbing state that does not correspond to the target being reached: that of the population going extinct. In simulations, as we only collect finite numbers for the adaptation time T (which we then average over) this condition is necessary.

We can solve (3.1) numerically for the model considered in this chapter. In this case each state of the system corresponds to a unique distribution of the population (with cells treated as indistinguishable) over the network of states in Fig. 3.1A. For a given carrying capacity K the possible states are those featuring from zero to K cells distributed over the network, with zero corresponding to the absorbing state of the population having gone extinct. Note that this method is only suitable for small carrying capacities K for which the number of states is not too great, which we will discuss more about shortly. In the following, to reduce the number of states that the system has we consider only the case $\alpha = 0$. However the same method can be applied to the case $\alpha \neq 0$.

We start by writing, for each possible state the system can be in, a backward master equation that describes how the survival probability of being in that state (given the system started in state i at time $t = 0$) changes in time. For the model we are considering state i corresponds to the entire population being in state 2A in Fig. 3.1A. This system of backward master equations can be written as the following vector differential equation

$$\frac{d\mathbf{q}^{(i)}(t)}{dt} = M\mathbf{q}^{(i)}(t). \tag{3.2}$$

Here $\mathbf{q}^{(i)}(t)$ is the vector whose $j'th$ element is the survival probability $q_j^{(i)}(t)$, while M is the Markov matrix of transition rates into and out of each state. Equation (3.2) can be solved by an eigen-decomposition of the matrix M, as outlined in Section 2.3.3, which we perform numerically using *Mathematica*. The solution gives us $\mathbf{q}^{(i)}(t)$, from which the integrals in (3.1) can be numerically calculated for the target state (being a single cell in state 3A) to give us the adaptation time T.

Figure 3.7A compares the numerical solution of (3.1) with simulation data for the adaptation time T as a function of μ (when $\alpha = 0$). It shows excellent agreement between the two curves. This same method can also confirm the $T(\alpha \to 0)$ limit of the earlier curve shown in Fig. 3.4B. This is shown in Fig. 3.7B, which shows the curve of Fig. 3.4B alongside the $T(\alpha = 0)$ numerical solution obtained using the above method.

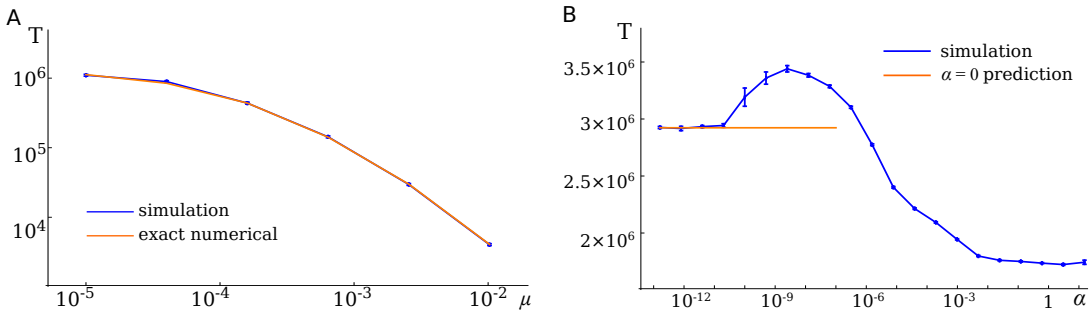

Figure 3.7 *Calculating numerically the exact solution for the adaptation time T from the system of backward master equations. (A) The plot compares curves of the adaptation time T as a function of μ gathered using simulations and by numerically integrating solutions of the backward master equations. The parameters used are $K = 10, \delta = 0.4, \alpha = 0$ and $d = 0.1$ (B) Simulation data showing a plot of T as a function of α alongside the predicted numerical value for $T(\alpha = 0)$. The parameters used here are $K = 20, \mu = 10^{-5}, \delta = 0.1$ and $d = 0.1$. All simulation results are collected using a KMC algorithm and averaged over 10^3 simulation runs.*

This process is unsuitable for large population sizes (i.e. carrying capacities K) due to the large number of states that would need considered. By the *stars and bars* problem of combinatorics [57] there are $\binom{n+l-1}{n}$ ways of distributing n indistinguishable cells about l lattice sites, allowing for sites to contain no cells. Therefore in our system of Fig. 3.1A there are $\Gamma = \sum_{n=0}^{K} \binom{n+4}{n} = \binom{K+5}{5}$ possible population distributions (i.e. states) for nonzero α about the non-target states and the significantly smaller $\Gamma = \sum_{n=0}^{K}(n+1) = \binom{K+2}{2}$ when $\alpha = 0$. The matrix M in (3.2) is size $\Gamma \times \Gamma$ and the process of performing a numerical eigen-decomposition with it quickly becomes intractable for $\Gamma \sim 10^4$. However, if the model had a fixed population size the number of states would be significantly reduced. In such a case this method could be used to consider greater population sizes.

3.5 Trajectory Analysis

In order to understand the plots we have seen of the adaptation time T, we look now at which trajectories are taken by *successful cells*. Successful cells are those which reach the target 3A in each simulation run (of which there is only one). To do this in simulations, we store for each cell, along with its current state, the sequence of states that its ancestors were in, beginning from the wild-type state

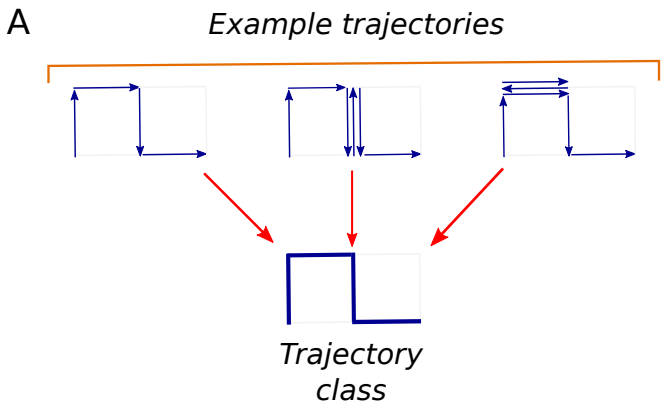

Figure 3.8 *Different trajectories can belong to the same trajectory class. The diagram shows three different trajectories that belong to the same trajectory class. The purpose is to remove closed loop information that otherwise distinguishes cells that followed the same basic trajectory.*

1A. We then assign each successful cell to belong to one of twenty one possible *trajectory classes*. These classes identify only whether or not each step between states occurred in a trajectory (and do not distinguish between the direction of the step). Trajectory classes therefore ignore any closed loops that are part of the full trajectory.

Each trajectory class is represented by a unique symbol showing which steps this class includes. An example of different trajectories that are all assigned to the same trajectory class can be seen in Fig. 3.8. In the following we use the terms trajectories and trajectory classes interchangeably.

Using trajectory information we now examine how the trajectories taken by successful cells are expected to change with α. Figures 3.9A and C show plots of T as a function of α for different valley depths (being shallow and deep respectively). These are the same typical kinds of curves shown earlier in Fig. 3.4. Included in each plot, above each datapoint, is a column of trajectory symbols. Each column displays the most probable trajectories that are observed at this α value. Note that all trajectories began at the wild-type state 1A but can appear otherwise in this representation due to back-steps being taken in some trajectories. The trajectories are arranged in order of prevalence with the most probable trajectory at the bottom of the column and the least probable at the top. Only trajectories appearing more than 5% of the time have been included.

For each value of α, the statistics of these observed trajectories can be examined. Figures 3.9 B and D do this, each for three of the α values from Figs. 3.9 A

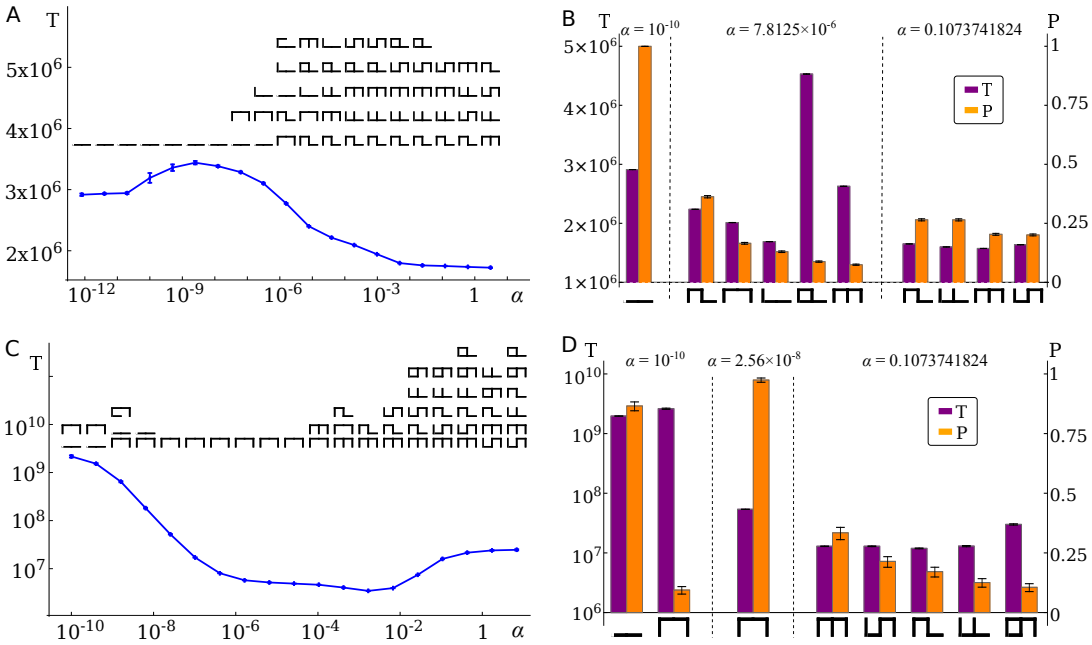

Figure 3.9 *Examining the most probable trajectories taken by successful cells. (A) and (C) show plots of the adaptation time T as a function of α, with and without the optimal α range, being the case of $\delta = 0.1$ (Fig. (A)) and $\delta = 0.5$ (Fig. (C)) respectively. Above each datapoint is a column of symbols that identify the trajectory classes of successful cells. Listed from the bottom of each column to the top are the most probable trajectories by which cells evolve to 3A. (B) and (D) show trajectory statistics for three α values taken from (A) and (C) respectively. For each α value there is a horizontal list of the most probable trajectories (running left to right from most to least probable). Above each trajectory symbol is a pair of bars that show the probability of that trajectory being taken (orange bars) and the average time it takes (purple bars). Trajectories occurring less than 5% of the time are omitted from all plots. The remaining parameters used are $K = 20, \mu = 10^{-5}$ and $d = 0.1$. Results are gathered using a KMC algorithm and averaged over 10^4 simulation runs for (A) and $500 \rightarrow 10^4$ runs for (B).*

and C respectively. For each α value shown, there is a horizontal list of the most probable trajectories (the same as were listed above the relevant point in Figs. 3.9A and C). Above each trajectory symbol is a pair of bars that show the probability of this trajectory being taken and the average time T it took for successful cells to evolve by it.

Figure 3.9A shows that, over the entire α range considered, the most probable trajectories often feature genotype mutations in phenotype A and/or visit state 2A. There is large variability in the trajectories (at each α value) from mid to large α, with no single trajectory dominating. This is unlike at lower α, where the direct trajectory 1A→2A→3A necessarily dominates. The small peak at low α values is the only example of when phenotype switching increases T. Earlier we hypothesised that this was caused by some cells becoming stuck in phenotype B, leaving a smaller population in phenotype A, with a reduced mutation supply rate there, to evolve the target state 3A. By considering trajectories with a less than 5% chance of likelihood (in results which are not presented), we find the direct trajectory 1A→2A→3A to be almost exclusively taken at the peak. As no other trajectory is represented as occurring, the time increase must be due to the direct trajectory 1A→2A→3A taking, on average, longer to occur. This supports our hypothesis that some of the population must be trapped in phenotype B.

Figure 3.9B illustrates the differences in the observed trajectories in Fig. 3.9A for three values of α. At the largest α value, the observed trajectories are equally likely to occur and cells take approximately the same time to evolve along any of them. At the intermediate α value, the adaptation times are different for the different trajectories. We can see here that the quickest trajectories are not always the most likely to occur. The lowest α value is trivial, showing the certainty with which cells will evolve directly to 3A.

Figure 3.9C shows the alternative scenario of a curve of $T(\alpha)$ when the valley depth is deep ($\delta = 0.5$) and the optimal α range exists. Compared to Fig. 3.9A, there is a high probability of a single trajectory being taken for much of the α range. The onset of the optimal α range corresponds to when the trajectory that avoids state 2A (⊓) becomes the only one of considerable likelihood. This trajectory continues to dominate into the valley floor of the $T(\alpha)$ curve, where it remains the only trajectory observed. At larger α values it is unavoidable that trajectories visit state 2A. We therefore observe an increased variability in the trajectory types as α increases. These trajectories include ones that both do and do not feature mutations in phenotype A.

Figure 3.9D confirms these observations. At the lowest α value, the most probable trajectory is that which evolves directly to 3A (⎯). The trajectory that avoids the valley (⌐¬) is still present here though, taking a slightly greater time but still comparable enough to justify the trajectory having a non-zero probability of occurrence. At the intermediate α value, there is a large reduction in the time taken to evolve by the trajectory that avoids 2A (⌐¬). Therefore it outcompetes the other trajectories and becomes almost certainly the trajectory that is taken. At the largest α value, numerous trajectories are again likely. These feature mutations in both phenotypes, with comparable times and likelihoods of occurrence between them. These times are larger than the time for the trajectory that avoids 2A (in results not shown). However, the probability of that trajectory occurring is vanishingly small here, leaving only the trajectories with larger times to contribute to the larger T value observed.

3.5.1 The most probable trajectory

We have identified that the optimal α range coincides with when the most probable trajectory is that which avoids state 2A. We now want to look for when this trajectory is the most likely to occur. Fig. 3.10 shows a plot of the most probable trajectory in the space of (μ, α). As expected, evolution favours different trajectories depending on the values of μ and α. This allows the space of (μ, α) to be separated into three distinct regions of trajectory types. The straight line separating regions 1 and 2 predicts a power law relationship (of $\mu \sim \sqrt{\alpha}$) existing between μ and α at the transition between these two regions.

Region 1 corresponds to cells that evolve 3A directly (⎯). Here genetic mutations are frequent enough to offset the reduction in fitness from state 2A. Upon reduction of μ (at low enough α), a transition to a different trajectory type can occur when the increasing time spent at 2A is less than the waiting time for two phenotype switching events to occur. This new region is region 2, which consists of successful cells that evolve 3A by the trajectory that avoids 2A (⌐¬). As we observed in Fig. 3.9C, this region corresponds to the beginning of the valley and its basin in the curve of $T(\alpha)$. Therefore this trajectory can be used to identify the existence of the optimal α range.

Region 3 consists of a mixture of trajectory types that use both phenotypes and may or may not visit state 2A. Occurring at large α, these trajectories are unlikely to avoid state 2A as the rate of switching becomes larger than that of genetic

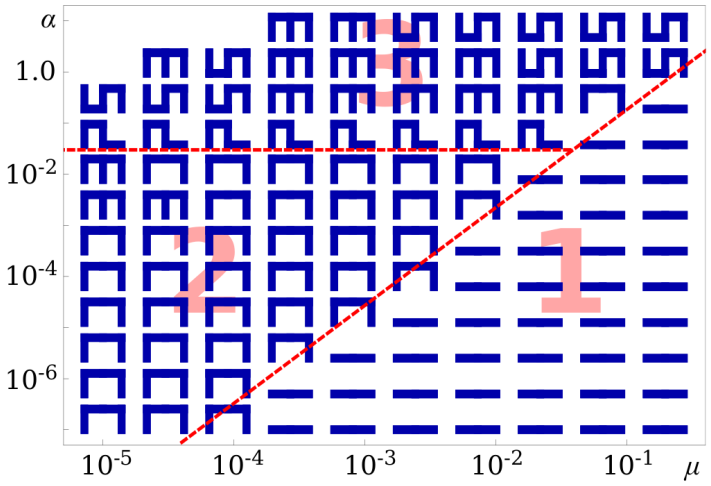

Figure 3.10 *The most probable trajectories for cells to take in the space of* (μ, α)*. Three distinct regions of different likely trajectory behaviour are identified. Parameter values are* $K = 100, \delta = 0.4$ *and* $d = 0.1$*. The population started here from a single cell in state 1A. Results are gathered using a KMC algorithm and averaged over at least* $10^3 \rightarrow 10^4$ *simulation runs.*

mutations. The subsequent increased adaptation time identifies this region to be the large α region that ends the valley in Fig. 3.9C.

In region 3 there is uncertainty in which trajectory a successful cell will take. However, in regions 1 and 2 a single trajectory is predicted to dominate (see also Fig. 3.9C). The diversity of possible trajectories can be explored further by considering the *inverse participation ratio* IPR for a list of trajectories, such as those collected for each (μ, α) point in Fig. 3.10. We define IPR to be the following

$$IPR = \frac{\sum_i \eta_i^2}{(\sum_i \eta_i)^2}, \tag{3.3}$$

where the sums in both the numerator and denominator are over all trajectory classes present in the trajectory list and η_i is the number of instances of trajectory i that occurred. When $IPR = 1$ only a single trajectory class is present and it increases the more trajectory classes there are. The maximum value of IPR when there are n trajectory classes present in the list is n. This occurs when all trajectory classes have an equal abundance in the list.

A plot of the inverse participation ratio IPR over the space of (μ, α) can be seen in Fig. 3.11. This uses the same data that was used to produce Fig. 3.10. We can see that for regions 1 and 2 (originally identified in Fig. 3.10) that $IPR \approx 1$ indicating that there is negligible diversity in the trajectories taken in these regions. This

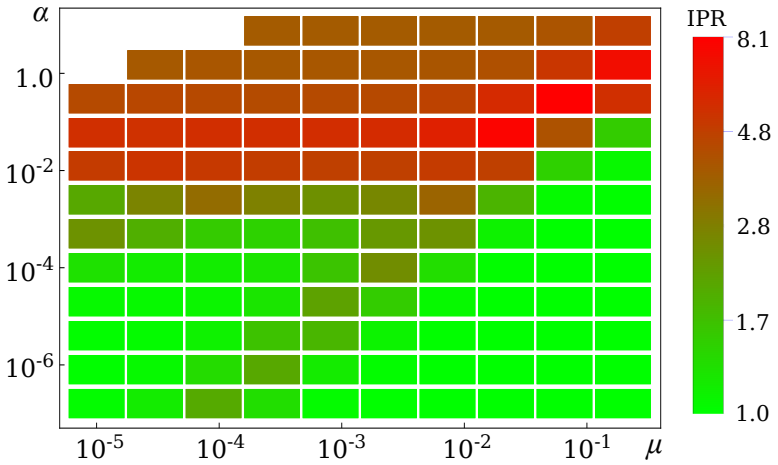

Figure 3.11 *The distribution of trajectory classes taken in the space of* (μ, α)*. Each tile corresponds to specific value of* (μ, α) *in which the colour of the tile identifies the inverse participation ratio* IPR *at those values (see the bar legend, which is scaled logarithmically). Parameter values are* $K = 100, \delta = 0.4$ *and* $d = 0.1$*. The population started here from a single cell in state 1A. Results are gathered using a KMC algorithm and averaged over at least* $10^3 \rightarrow 10^4$ *simulation runs.*

is consistent with our expectations for the trajectories taken in these regions (as discussed in our analyses of Figs. 3.9 and 3.10).

The boundary between regions 1 and 2 (estimated in Fig. 3.10 by a dashed line) can be identified in Fig. 3.11 due to the slight increase in IPR along it. This increase is due to the trajectories of regions 1 and 2 (i.e. trajectory types ▁ and ⊓ respectively) competing with one another, rather than other trajectory types also being present for which we would expect larger values of IPR.

The boundary between region 3 and that of regions 1 and 2 accounts for the largest IPR values observed in Fig. 3.11. This is again consistent with the earlier observation of increased trajectory diversity as α increases beyond the optimal α range (as seen in Fig. 3.9C). However, in Fig. 3.11 we can also observe that the value of IPR reduces away from the boundary in region 3. This reduced IPR value is by roughly a half (compared to that at the boundary) and is not as low as the IPR in regions 1 and 2 (being $IPR \approx 1$, indicating a single trajectory is most likely). However, this lowered but still significant IPR value in region 3 makes qualitative sense. The larger α is (moving into region 3 away from the boundary) the less likely it will be that a successful cell can evolve to state $3A$ without switching phenotype at each genotype along the way. Therefore the likely trajectories will tend to being one of four types (⊓⊓, ⊔⊔, ⊓⊔ or ⊔⊓). If we consider

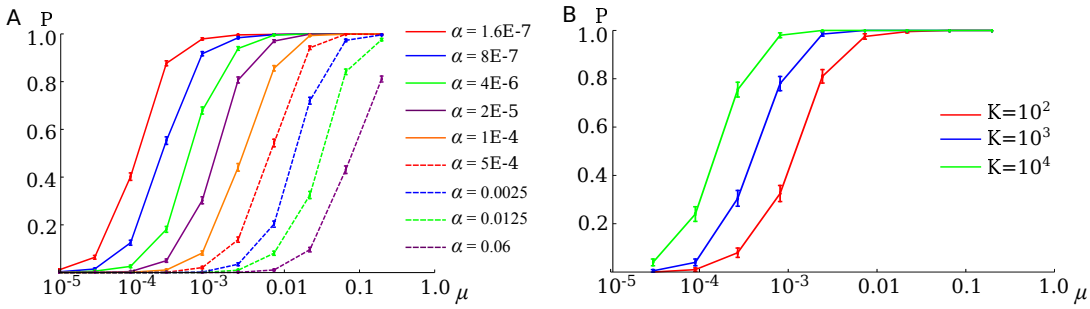

Figure 3.12 *Probing the boundary between regions of uniform most probable trajectory behaviour. (A) Plot shows the probability P that cells evolve by 1A→2A→3A as a function of μ for different α values when $K = 100$. (B) Comparing plots of P as a function of μ for different K when $\alpha = 2 \times 10^{-5}$. The remaining parameters used are $\delta = 0.4$ and $d = 0.1$. All results are gathered using a KMC algorithm and averaged over 10^3 simulation runs.*

there to be four trajectories that are tending towards an equal abundance in the list of trajectories, then the IPR value is tending towards $IPR = 4$. This is approximately the IPR value we observe away from the boundary in region 3 in Fig. 3.11.

As we have seen, there is little trajectory variability in regions 1 and 2 from the trajectory class that defines the region. Therefore the probability that these trajectory classes are taken can be used, in a way that is similar to an order parameter, to identify the boundaries of these regions in phase space. Figure 3.12A demonstrates this for the boundary between regions 1 and 2. It shows the probability P (that the direct trajectory 1A→2A→3A is taken) as a function of μ. This is compared for various α values, using the same data as in Fig. 3.10. The point of transition for each curve (i.e. where P goes from 0 to 1) can be used to estimate the boundary line separating regions 1 and 2. A similar search, this time for the trajectory ⊓, can be used to estimate the boundary between regions 2 and 3 in Fig. 3.10.

Figure 3.12B compares one of these curves ($\alpha = 2 \times 10^{-5}$) for different values of the carrying capacity K ($K = 10^2, 10^3$ and 10^4). As K increases there is no observed sharpening of this transition that we would expect if P behaved like an order parameter of statistical mechanics. Therefore we can deduce that there will always be a significant amount of mixed-trajectory behaviour existing in the vicinity of the region boundaries in Fig. 3.10.

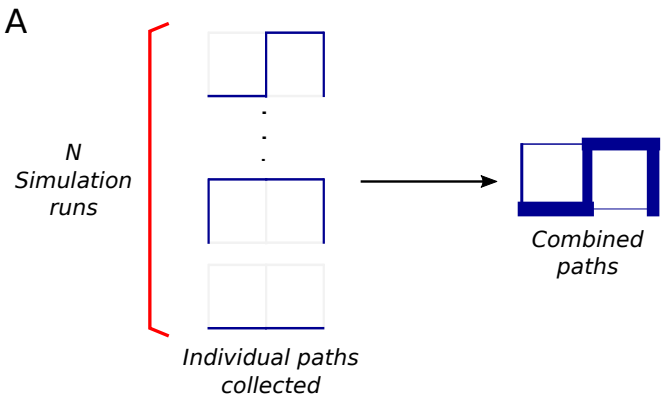

Figure 3.13 *Combining individual trajectories to construct diagrams of the probability that each step is taken. The composite diagram consists of links of different thickness, corresponding to the probability of that step being taken.*

3.5.2 The most probable steps

We can look in more detail at the trajectory information by looking at the probability that successful cells take each step in genotype/phenotype space. This information can be represented as a diagram of links that connect the different states of the system. The thickness of each link is proportional to the probability that the step it represents is taken. Figure 3.13 demonstrates how composite trajectory images are created from individual trajectories.

Figure 3.14 shows the probability that individual steps are taken by successful cells in (μ, α) space (with the same data that was used in Fig. 3.10). The plot recovers the dominant features of the trajectories that were predicted by Fig. 3.10 and that prompted the decomposition of (μ, α) space into 3 regions of distinct behaviour. This supports our use of the single most probable trajectory as a suitable representative for the trajectory data.

3.5.3 Searching for the optimal α range

In order to explore the role stochastic phenotype switching can play in real microbial populations we now look at how the existence of the optimal α range changes with population size (i.e. carrying capacity K). For K larger than $\sim 10^4$ storing all trajectory information becomes numerically intractable. However, as the optimal α range coincides with the most probable trajectory avoiding state 2A (see Fig. 3.9C), we can narrow our search to look only for when this is expected

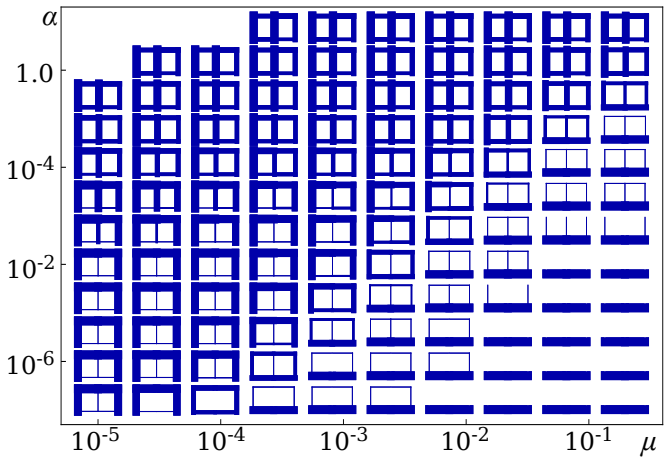

Figure 3.14 *The probability that each step is taken in* (μ, α) *space. Parameters used are* $K = 100, \delta = 0.4$ *and* $d = 0.1$ *and the population began as a single cell of type 1A. Results are collected using a KMC algorithm and averaged over at least* $10^3 \rightarrow 10^4$ *simulation runs.*

to happen. Each trajectory will now be classified as one of two types: one that visits state 2A or one that avoids it. The symbols used to identify each of these are shown in Fig. 3.15A. Keeping track of only this aspect of trajectories allow us to search for the optimal α range at much larger values of K.

Figure 3.15B shows a plot of (K, α) space, where each point is assigned one of the two trajectory symbols depending on whether or not the most probable trajectory type avoids state 2A or not. The background of each point also has a colour showing the probability with which the valley state is visited. This tells us how well the trajectory type symbol represents the trajectories at that point. We observe a large central region (green) that favours trajectories avoiding state 2A. This region corresponds to the beginning of the valley descent and basin in a curve of $T(\alpha)$. Here, the adaptation time T is significantly reduced when compared to the process in the absence of switching, or when switching becomes too frequent at large α. This region narrows but remains observable up to $K \sim 10^9$, at which the population sizes are becoming more applicable to microbial populations. The boundaries of this green region show significant variability in the trajectory type, as seen by the mixing in background colours. This is expected following the observation of the trajectory variability near the region boundaries in Fig. 3.12B.

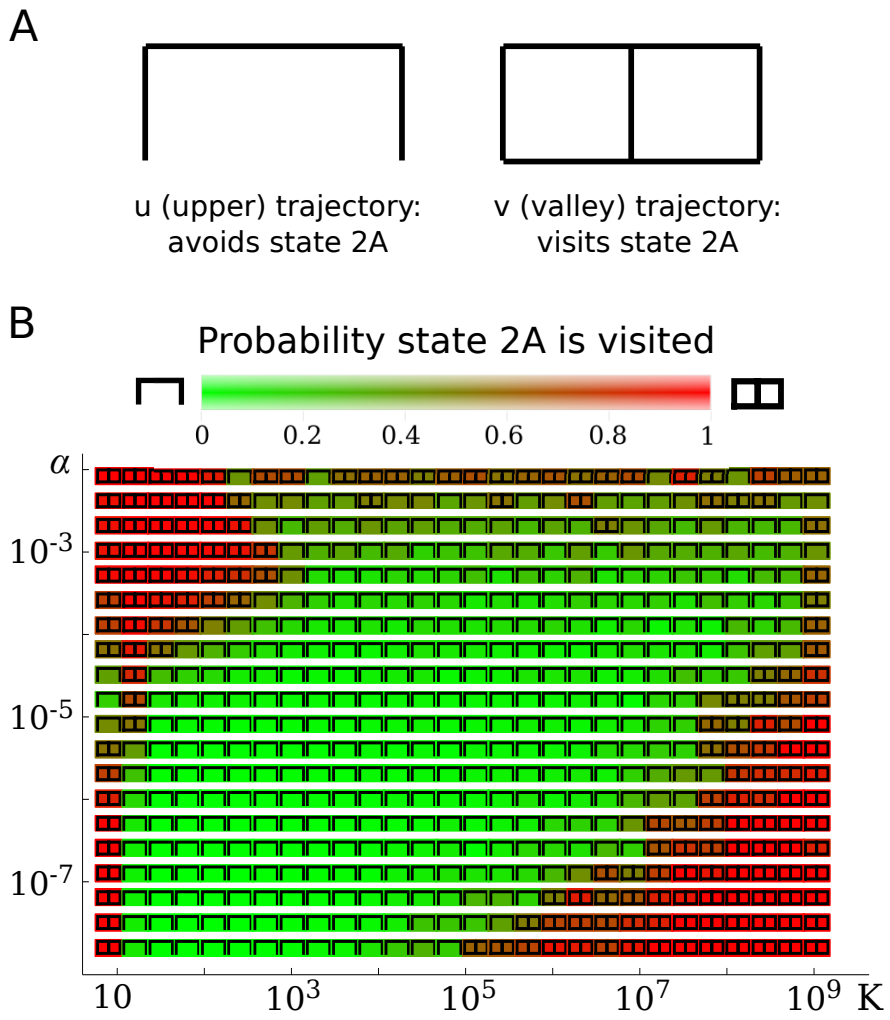

Figure 3.15 *Searching for the optimal α range at larger carrying capacity K. (A) Trajectories are grouped together by whether they visit (trajectory "v") or avoid (trajectory "u") state 2A and are represented by the symbols shown. (B) The most probable trajectory type as a function of (K, α). Included for each point is the probability (see the colour bar) that the trajectory type shown is a valid representation of all trajectories at that point. Parameters used are $\mu = 10^{-6}, \delta = 0.4$ and $d = 0.1$. Results are averaged over at least $10^2 \rightarrow 10^3$ simulation runs and collected using a τ-leap algorithm.*

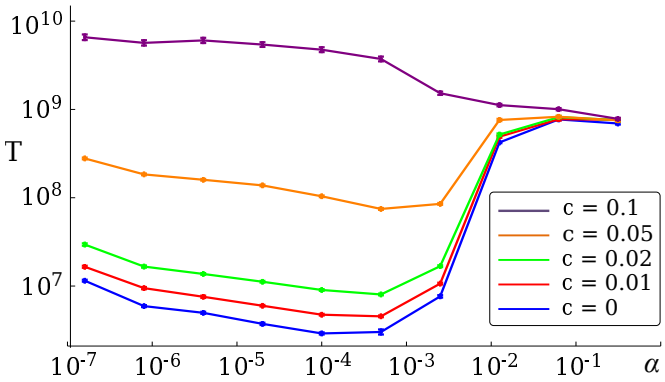

Figure 3.16 *Applying a fitness cost to the states in phenotype B. Shown is a plot of the adaptation time T as a function of α for different fitness costs c ($c = \{0, 0.01, 0.02, 0.05, 0.1\}$) that are applied to states in phenotype B. Parameters used are $K = 100, \mu = 10^{-5}, \delta = 0.9$ and $d = 0.1$. Results are gathered using a KMC algorithm and averaged over $10^2 \to 10^4$ simulation runs.*

3.6 Fitness costs for phenotype B

Stochastic phenotype switching is often observed in microbes in the presence of an applied stress that affects one phenotype more than the other. The resilience of the less-affected phenotype often follows from a reduction in normal cellular functions such as growth. For example, in bacteria this is the case in switching between normal and persister states in *Escherichia coli* [16] and in the competence to non-competence switching in *Bacillus subtillus* [125]. We now incorporate this into the model by including a non-zero fitness cost $c \neq 0$ to cells in phenotype B.

Figure 3.16 shows curves of the adaptation time T as a function of α for different values of the cost c. We observe that an optimal range for the phenotype switching rate remains, provided c is small enough, but reduces in depth with increasing values of the cost c. As we know that the optimal range exists because the trajectory that avoids state 2A is quicker, it is clear that as c increases the time taken for this trajectory decreases until it offers no benefit to T and the optimal range ceases to exist.

A reduction in T still exists in the large α limit. However, this is due to the high frequency of phenotype switching mitigating the effects of the valley state, not by avoiding it.

3.7 Asymmetric rates of phenotype switching

The results presented so far have focussed on when switching between phenotypes is symmetric and occurring at the rate α. We consider now how results change with asymmetric switching rates. Let the parameter β be the switching rate from states in phenotype B $\rightarrow$ A, while α remains the switching rate from states in phenotype A $\rightarrow$ B.

Figure 3.17 looks at how the adaptation time T changes with the degree of this asymmetry between the switching rates. Figure 3.17A shows a curve of T as a function of β when $\alpha = 1$. As we saw earlier in 3.9C, for α values this large, when $\alpha = \beta$ the system is in the large α limit. However, in Fig 3.17A we observe significant variation in T with varying β. The resultant curve is similar to that of $T(\alpha)$ when switching is symmetric, in that an optimal range exists for β values in which T is minimised.

The increase in T as $\beta \rightarrow 0$ is expected. In this limit the population is unable to switch from phenotype B$\rightarrow$A and yet cells will still switch to phenotype A and therefore become trapped. Otherwise, for $\beta < \alpha$, provided β is not too close to zero, we observe a reduction in T compared with when $\alpha = \beta$. We observed earlier in Fig. 3.9C that the optimal α range starts to end, through an increase in α, when populations cannot avoid state 2A as they evolve to 3A. When $\beta < \alpha$, without being too small to exclude the population travelling by it, the rate with which individuals in a population at 2B switch to 2A is reduced. Therefore for a population existing at genotype 2, there should be a reduction in the amount at the deleterious state 2A, when compared to the case $\alpha = \beta$. This accounts for the lower adaptation times seen here. The opposite is true for when $\beta > \alpha$ in which case switching to state 2A is more frequent. Therefore for a population at genotype 2, more will be expected to be in state 2A than when $\alpha = \beta$. This accounts for the increased T when $\beta > \alpha$.

Included above each datapoint in Fig. 3.17A is a list of the most probable trajectories. This is the same type of plot that was shown earlier in Figs. 3.9A and C. Only trajectories that were observed at least 10% of the time are shown here. The trajectory data shows that the ⊓⊓ shaped trajectory is dominant for most of the valley basin. This is in contrast to what we saw in Fig. 3.9C where this trajectory preceded the ending of the valley. The large value of α considered here ($\alpha = 1$) accounts for this; if a cell at 2B switches to 2A it is likely to switch

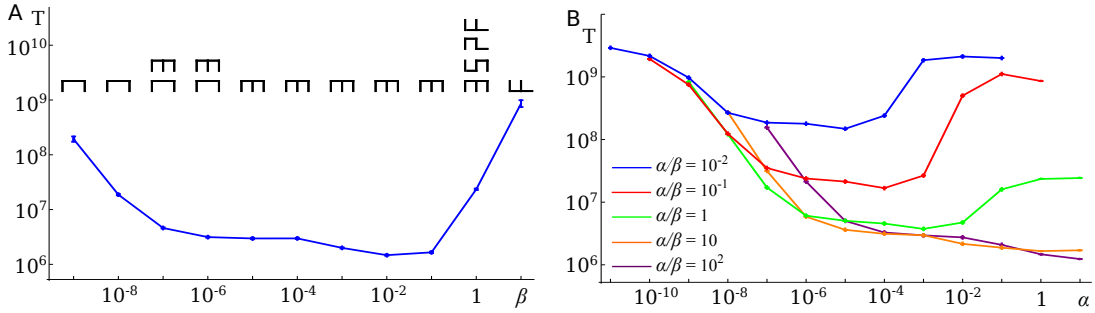

Figure 3.17 *The effect that asymmetric switching has on the adaptation time T. (A) A plot of T as a function of switching rate β from $B \to A$ when $\alpha = 1$. Above each datapoint is a column of the most probable trajectories taken by successful cells. These columns run from bottom to top as the most to least probable trajectories. Only trajectories that occur more than 10% of the time are included. (B) A plot comparing curves of T as a function of α for different values of the ratio (α/β). Parameters used are $K = 20, \mu = 10^{-5}, \delta = 0.5$ and $d = 0.1$. Results are gathered using a KMC algorithm and averaged over $500 \to 10^3$ runs.*

back before the genetic mutation to state 3A occurs.

Consider now Fig. 3.17B, which plots curves of T as a function of α for different values of the ratio (α/β), which measures the asymmetry in the switching rates. In all cases phenotype switching leads to a reduction in T compared to the case without switching ($\alpha = 0$). An optimal range occurs when $\alpha/\beta \leq 1$, while for $\alpha/\beta \geq 1$ the curves monotonically decrease. These latter curves are expected to increase, if only by a small amount, at larger α than are considered here.

For large α in Fig. 3.17B, the adaptation time T decreases with increasing values of α/β. At large α, when the switching A→B is fast, the quasi-equilibrium distribution of a population at genotype 2 (between phenotype A and B) is expected to be of the ratio β/α. Therefore for larger α/β, more cells should be in 2B than 2A, which increases the average fitness of the population. This leads to the observed reduction in the adaptation time T.

We look now at the trajectory behaviour of successful cells over (α, β) space. Figure 3.18A shows a plot of the most probable trajectory that successful cells will take, in which each datapoint is represented by a symbol that identifies the most probable trajectory. We see that, in general, as α increases then so does the value of β with which the trajectories ⊓ or ⊓⊓ stop being most likely. With asymmetric switching, this signals the end of the optimal β values that can significantly reduce T.

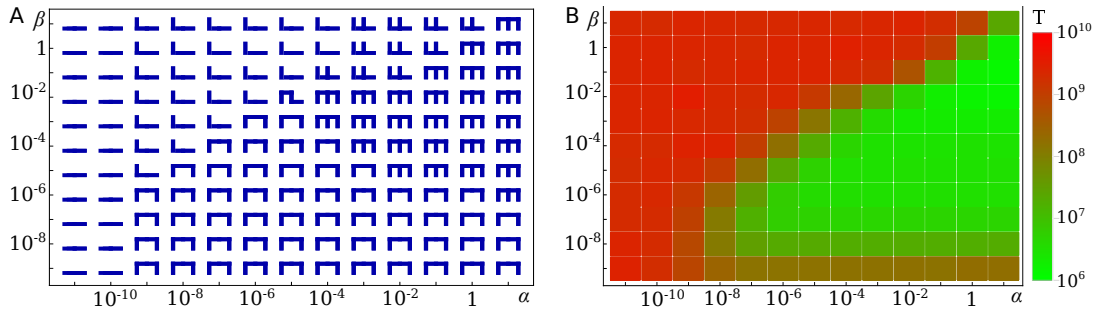

Figure 3.18 *The behaviour of successful cells in* (α, β) *space. (A) A plot of the most probable trajectory taken by successful cells. Each value of* (α, β) *is represented by a symbol that identifies the most probable trajectory. (B) A plot of the adaptation time for each value of* (α, β)*. Each point is represented by a tile — the colour of which identifies* T *(see the legend). Parameters used are* $K = 20, \mu = 10^{-5}, \delta = 0.5$ *and* $d = 0.1$*. Results were gathered using a KMC algorithm and averaged over* $500 \rightarrow 10^3$ *simulation runs.*

At very low α, the direct trajectory 1A→2A→3A is inevitably the most likely, as switching to phenotype B is rare. A new region of uniform trajectory behaviour can also be seen in Fig. 3.18A, with the trajectory type ⌊_. This occurs when $(\alpha/\beta) < 1$, while α is large enough for trajectories that visit phenotype B to not be uncommon. This trajectory still concerns the creation of a double mutant in phenotype A by crossing the deleterious state 2A. Therefore this trajectory is expected to be indistinguishable, in terms of the adaptation time T, to that of the direct evolution of 3A.

We now consider the differences in adaptation times T in (α, β) space. This is presented in a density plot in Fig. 3.18B, which uses the same data as in Fig. 3.18A. Each datapoint is represented by a tile which has a background colour that identifies the value of T at that point (see the bar legend with a logarithmic scale). As expected from our earlier observations, we see a large green region for $\alpha/\beta \geq 1$, which coincides with the most probable trajectories being ⊓ and ⊓⊓. In this region T is reduced by many orders of magnitude (as much as 4 for only $K = 20$) compared to the case without switching ($\alpha = 0$).

For $\alpha/\beta \ll 1$ in Fig. 3.18B, there is little observable change in T. This agrees with what was observed in Fig 3.17B where we saw that as (α/β) reduced the optimal α range became less significant (i.e. the valley in the curve of $T(\alpha)$ became shallower). Figure 3.18B shows that quite quickly (with varying β) the optimal range vanishes altogether, leaving phenotype switching to have no observable effect on the evolution.

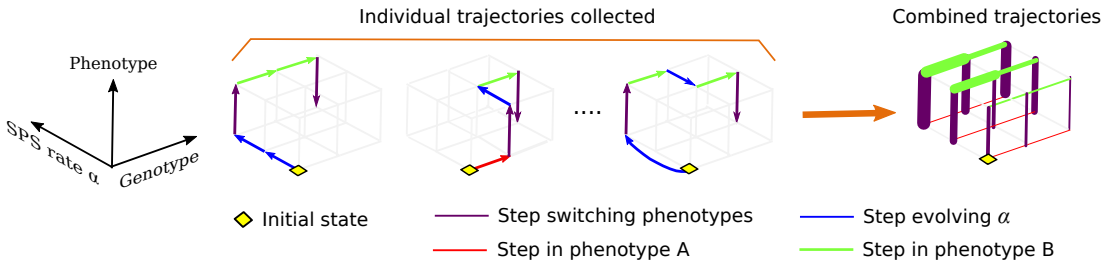

Figure 3.19 *Visualising the trajectories of successful cells that can evolve their switching rate α. Individual trajectories contain changes in the state and α value of a cell. Combined trajectories ignore α changes to show only the probability of steps being taken in genotype/phenotype space.*

3.8 Evolving the rate of phenotype switching

So far we have observed the optimal range for the phenotype switching rate α to be a persistent feature of the model that can significantly reduce the adaptation time. We now explore the same evolutionary process — the evolution of a cell in state 3A — when cells are able to evolve their phenotype switching rates. The question we want to answer is the following: does the optimal α range benefit evolving populations enough for it to be possible that stochastic phenotype switching can randomly arise in a population in order to take advantage of it?

The evolution of α is incorporated into the model as follows: During replication, offspring are assigned a new α value with the probability μ (i.e. the same for genetic mutation). The set of possible α values I consider is $\{\alpha = 2.56 \times 10^{-10} \times 5^i$ for integer $i \in [0, 15]\}$ which covers the range of different effects which α can have on the process. We will consider later the specific ways that a new α value is selected from this set.

The population begins in the wild-type state 1A with the lowest α value ($\alpha \approx 0$). It evolves until a cell in the target state 3A is produced, regardless of its α value. As before, the trajectories of successful cells are collected, which here span three dimensions: two for the cellular states and one for the α value. In visualising these trajectories steps evolving α are ignored, as they overcomplicate the visuals, and we look again at the most probable steps taken by successful cells. Figure 3.19 shows how composite plots of this kind are constructed.

3.8.1 Evolving α randomly

We consider first the case in which, to select a new α value, this value is randomly chosen from the set of allowed values (excluding the existing value), with equal likelihood of selection. The simulation results for this can be seen in Fig. 3.20. Figure 3.20A shows the probabilities that each step is taken as links of different thicknesses, in which the thickness of a link represents the probability of that step being taken. We observe here (by the absence of red links) that successful cells are not likely to mutate their genotype while in phenotype A. Instead, most cells will switch to phenotype B to cross genotype space, then switch back to phenotype A and the target 3A. The α values most common for crossing genotype space are those falling within the optimal α range (see the green links). This can be seen by observing the blue curve in Fig. 3.20B which shows the curve of $T(\alpha)$ when cells cannot evolve α.

Included in Fig. 3.20B, alongside the curve of T vs α, is a bar chart showing the probability that successful cells experience genotype mutations for the different allowed α values. A correlation can be seen between the depth of the valley and the probability of crossing genotype space at that α. Figure 3.20A also shows that cells that evolve α above the optimal range (note the thick purple links at high α) are unlikely to be successful in crossing genotype space at that α (due to the absence of green links at those α values). As we discovered earlier this is due to the high frequency of transitions that occur between states 2A and 2B which slow down adaptation through effectively creating a new, albeit weaker, fitness valley that must be crossed.

Perhaps unexpectedly, trajectories are likely to cross genotype space at α values below the optimal range, where we expect this to be a slow process. However, this can be explained if we assume that the slow part of this process — the waiting time for the cells to switch phenotype twice — is accelerated by cells evolving a large α value, switching to phenotype B, then evolving α to a low value again with which it can more easily cross genotype space. It can be confirmed that this is occurring by observing, in Fig. 3.20A, that there is little phenotype switching at low α values (i.e. thin or no purple links) and yet the likelihood of mutations crossing genotype space there (green links) remains high. This proposes an alternative kind of quick trajectory that populations can take, which also makes use of phenotype switching. However, such trajectories require at least one extra mutation compared to those that evolve α directly to the optimal

range. Therefore the dominant evolution in this model is still observed to be by trajectories of the latter type.

3.8.2 Evolving α incrementally

Consider now the alternative scenario in which evolution of the switching rate α is a gradual process that accumulates through numerous mutations. Upon mutation of α, the new selected value neighbours the original in the set of allowed α values. This corresponds to α changing by a constant factor, equally likely to be an increase or decrease.

Figure 3.21 shows simulation results where, as in Fig. 3.20, Fig. 3.21A shows the probability that steps are taken in genotype/phenotype space for different values of α. Figure 3.21B shows a bar chart of the probability that genotype space is crossed for each α value. This is the normalized product of the probabilities that the steps from genotypes 1→2 and 2→3 featured in trajectories at that value of α, regardless of the phenotype. This bar chart is superimposed with a curve of T vs α for the model in which α cannot evolve.

Mutations in phenotype A are more likely to occur here (there are more red lines) than we observed in Figure 3.20. This is presumably due to the additional waiting time for cells to evolve α large enough to switch phenotypes. This is also the reason that fewer cells cross genotype space at larger α than was observed in Fig. 3.20. Otherwise the populations in both scenarios (concerning how a new α value is selected) behave in a consistent way. In both cases the most probable trajectories are those that evolve α to within the optimal range in order to accelerate the crossing of genotype space.

3.9 Discussion and conclusions

In this chapter we examined computational results from a model that explores the effect that stochastic phenotype switching has on an evolving population of haploid cells that are trapped at a local fitness peak in 1D genotype space.

We found that there often exists an optimal range for the rate of stochastic phenotype switching, in which the evolutionary process is optimized (by a reduction in the adaptation time T, by potentially orders of magnitude). This

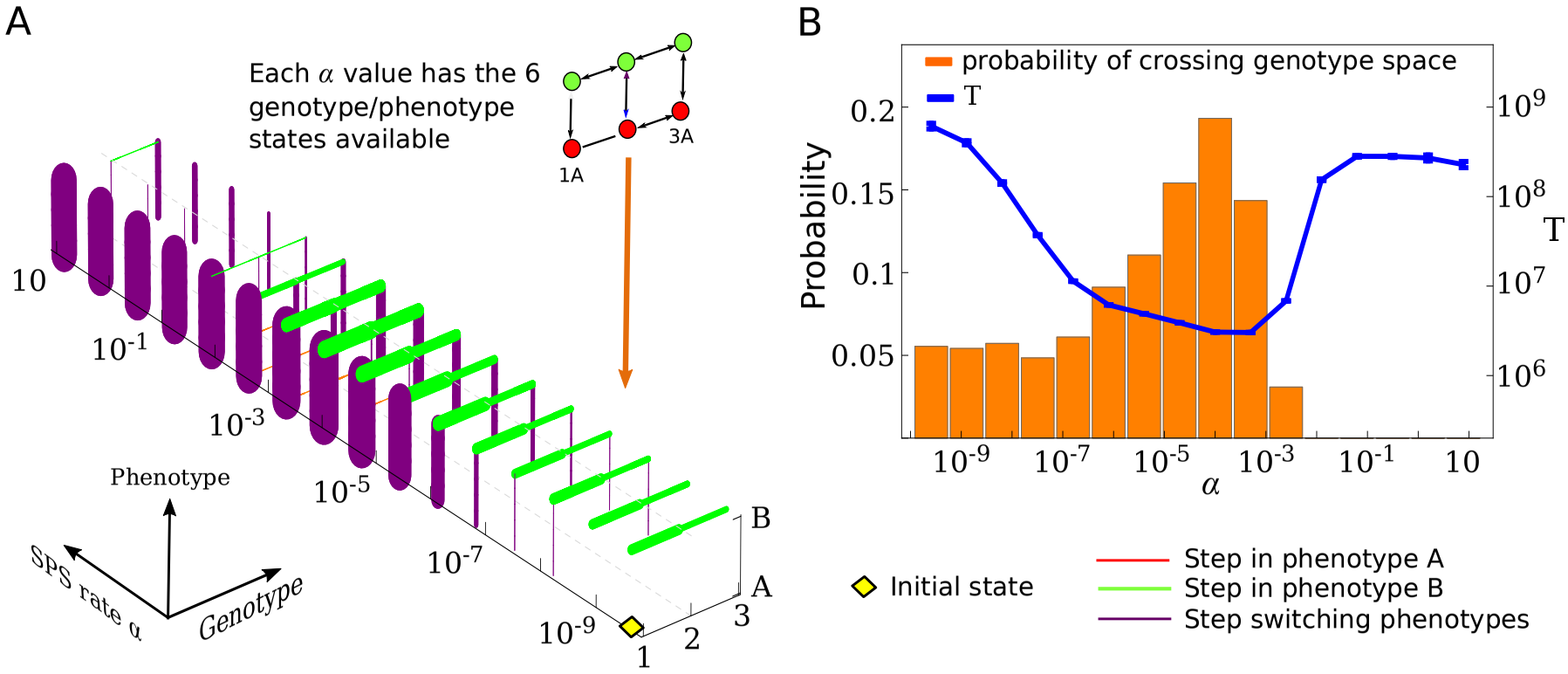

Figure 3.20 *The probability that steps are taken by successful cells when α evolves randomly. (A) A graph of step probabilities in genotype/phenotype space for different α values. Steps that evolve α are excluded from the visualisation. The thickness of each link is proportional to the probability that that step is taken by successful cells. The population begins in state 1A with $\alpha = 2.56 \times 10^{-10}$ and evolves until a cell in state 3A is produced. (B) A bar chart showing the probability that genotype space was crossed at each value of α, regardless of the phenotype. Superimposed on this is the curve of T as a function of α for the model that cannot evolve α. Parameters used are $K = 100, \mu = 10^{-5}, \delta = 0.4$ and $d = 0.1$. Results are gathered using a KMC algorithm and averaged over at least 10^4 simulation runs.*

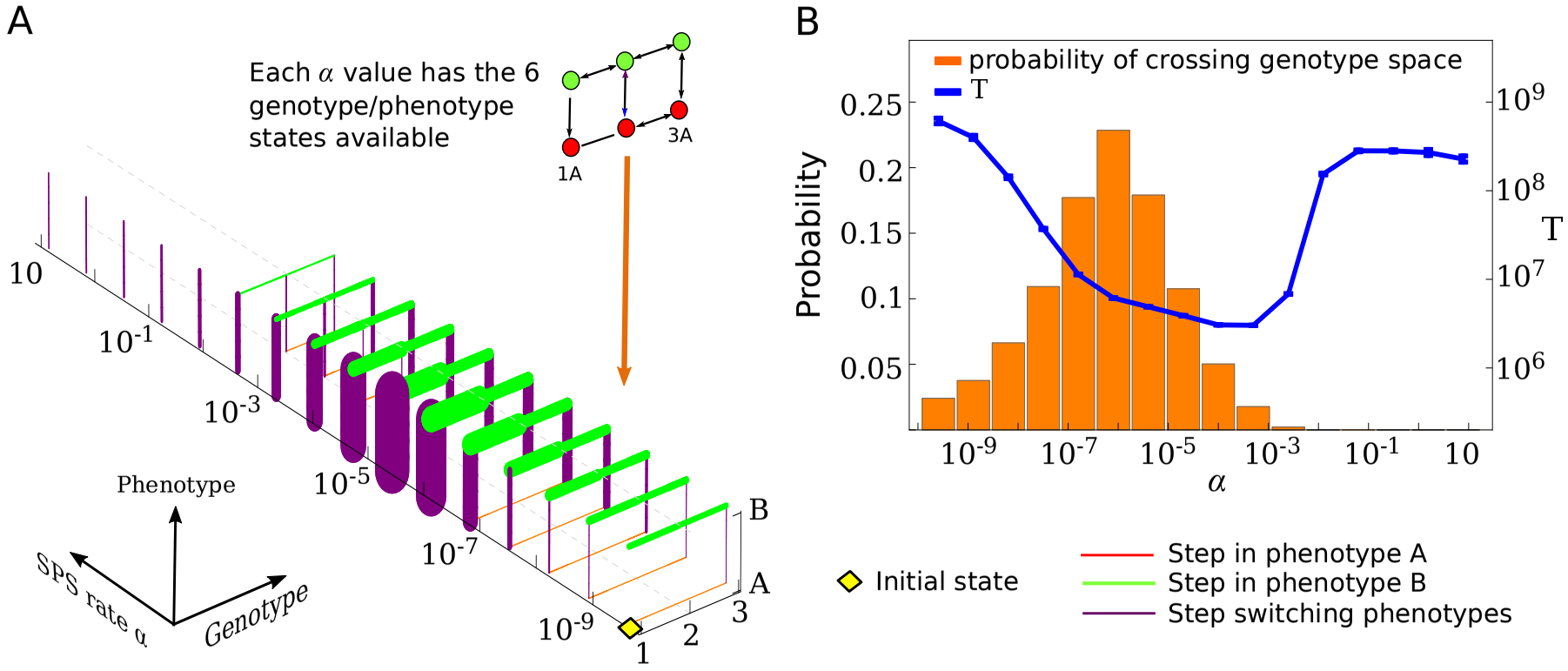

Figure 3.21 *The probability of steps being taken when α evolves by a constant factor. (A) A graph of step probabilities in genotype/phenotype space for the available α values. Steps that evolve α are excluded from the visualisation. The thickness of each link is proportional to the probability that that step is taken by successful cells. The population begins in state 1A with $\alpha = 2.56 \times 10^{-10}$ and evolves until a cell in state 3A is produced. (B) A bar chart showing the probability that genotype space was crossed at each value of α, regardless of the phenotype. Superimposed on this is the curve of T as a function of α when the model cannot evolve α. Parameters used are $K = 100, \mu = 10^{-5}, \delta = 0.4$ and $d = 0.1$. All results are gathered using a KMC algorithm and averaged over at least 10^4 simulation runs.*

optimization corresponds to the emergence of a new viable trajectory to the target state that allows the population to avoid the deleterious valley state. The benefit to the population increases in significance as the mutation production rate lowers. This reduction in T was observed to be as large as several orders of magnitude while the mutation probability μ was still at very large values (e.g. $\mu = 10^{-5}$ in Figs. 3.4A and 3.9C) compared to the values expected in microbes [47, 116]. This reduction is expected to become more significant as μ decreases, suggesting that stochastic phenotype switching could be a significant mechanism in the evolutionary process in microbes.

We went on to see that this feature is resistant to asymmetry in the rate of switching, as well as to when minor costs are applied to states of the second phenotype. However, to observe a significant reduction in T, beyond the usual one at high α, it is necessary that phenotype B provides an "easier" route to the target state.

Finally, the model predicted that if the rate of stochastic phenotype switching is allowed to evolve, successful cells will consist mainly of those that have evolved significant rates of switching, to within the optimal switching rate range identified.

Therefore this model supports the hypothesis that stochastic phenotype switching could evolve as a strategy to aid the evolution of cells that are struggling to evolve in their current environment. This can be a result of being trapped at local fitness peaks, which have been observed in real microbial fitness landscapes [108] as a result of reciprocal sign epistasis [154]. Extending our considerations beyond the simple 3 state genotype space, we can hypothesise that if the maxima and minima in the two fitness landscapes are not correlated, the adaptation time could be reduced by populations following trajectories that utilise both landscapes, using phenotype switching as a means to avoid deleterious intermediate states in each landscape.

We can use results from this chapter to make predictions of the expected behaviour in real microbial systems that this model could apply to. This requires a microbial system that meets a number of conditions: First, the population must be trapped at a local fitness peak. It must also have access to a second phenotypic state in which the intermediate genotypes have significantly reduced deleterious fitness effects compared to the original phenotype. Examples of microbial systems that may satisfy these conditions were discussed in Section 3.2.

The final condition for phenotype switching to play a role in the evolution of

real microbial populations is that the switching rates between phenotypes should be sufficiently large. This point is concluded from Fig. 3.15, which presented results for a mutation probability $\mu = 10^{-6}$. In microbes the probability of single nucleotide mutation per replication is 10^{-10} to 10^{-9} [47, 116]. However, in mutator strains [182, 190], or in the presence of antibiotics [76], this can increase to as high as $\approx 10^{-7}$. Therefore a mutation probability of $\mu = 10^{-6}$ could correspond to ~ 10 possible point mutations in a mutator strain. Alternatively, a mutation probability this high could correspond to a loss of function (assuming a typical gene length of $\sim$ 1kbp) mutation in a non-mutator strain.

According to Fig. 3.15, when $\mu = 10^{-6}$ stochastic phenotype switching could play an important role in evolution over a large range of K and α values, in which it is the preferred mode of travel. This is the case for small populations ($K \sim 10^3$) for switching rates up to $\alpha \approx 10^{-4}$, for intermediate populations ($K = 10^6$) in which $10^{-7} < \alpha < 10^{-3}$ and for larger populations ($K = 10^9$) when $\alpha \approx 10^{-3}$. At lower values of μ, this region is expected to extend to lower switching rates and larger K values as the rate of mutant production reduces. This trend was seen in Fig. 3.4A and is explored further in Chapter 4. Across all K values, upon increasing α, the valley ends when the switching rate obtains a characteristic value which is observed to be independent of μ. Therefore the end of this region is expected to remain at approximately $\alpha \approx 10^{-3}$ to 10^{-2}. Switching rates in nature have been observed to be as fast as this [6, 212]. Therefore this mode of evolution in microbes could be significant.

The model we studied in this chapter is general and considers only a small genotype space. It was not intended to describe any particular experimental system — e.g. in the number of genotypes considered or in the nature of the switching between phenotypes. Nevertheless the effect of the mechanisms involved here may already have been observed in experimental work. The bacterium *E. coli* has been observed to switch to a filamentous phenotypic state following induction of the SOS response, (see Chapter 1 and 6) upon exposure to sub-inhibitory concentrations of the antibiotic ciprofloxacin [29, 218]. *E. coli* populations resistant to ciprofloxacin have been observed following the production of normal cells (ie the non-filamentous cells and our phenotype A) which have acquired rapid genetic resistance. While not an example of stochastic phenotype switching, like we consider in this model, the observed effect appears to be the same: the facilitation of genetic evolution by the opening up of a second phenotypic state (our phenotype B), within which genetic evolution can more easily occur.

A similar example occurs in the bacterium *Staphylococcus aureus* which, upon exposure to the anitibiotic gentamicin, can switch reversibly to a phenotype known as small colony variants (SCV) [129]. SCVs are believed to have mutated a defect that makes them resistant to aminoglycosides and have reduced (but nonzero) growth rate from which resistance can be evolved.

We now consider how these conclusions could be tested. With the example of *E. coli* switching to a filamentous phenotype (SOS response) we can predict that, in the absence of the second phenotypic state, a population of cells will evolve resistance much slower. This can be tested if — instead of stopping the SOS response from taking place in cells — such filamentous cells are instead removed from the population. Evolution experiments using a chemostat, with continuous removal of cells through them being flushed away, could be used to separate filamentous cells from normal cells which will be left to evolve resistance slowly. This very observation has already been made in experiments in which the induction of the SOS response was inhibited [28, 35].

Chapter 4

Stochastic phenotype switching in a 1D valley crossing model - Analytic study

4.1 Introduction

In this chapter we undertake a mathematical analysis of the model that was introduced in Chapter 3 (see Section 3.3) where it was studied numerically. The model describes how a population of asexual haploid cells, which have access to a second phenotypic state, is able to escape from a local peak in a 1D fitness landscape. The states available to the cells and the actions each cell can undergo are those shown in Figs. 3.1 and 3.2 respectively. We are interested in the adaptation time T in which a population of cells, beginning in the wild-type state 1A, evolves the first cell in the target state 3A.

In Chapter 3 we observed the existence of an optimal range for the rate of phenotype switching α. In this range the adaptation time T can be reduced by orders of magnitude compared to in the absence of phenotype switching. This is due to alternative trajectories to the target state 3A becoming more viable to an evolving population. In this work it was necessary to use parameter values that were appropriate to a limited number of biological scenarios. The smallest mutation probability considered ($\mu = 10^{-6}$) was insufficient to consider the probability of single nucleotide mutations, which occur on average 10^{-10} to

10^{-9} times per replication in E. coli [46, 116].

The focus of the work in this chapter is to validate analytically the existence of the optimal range for the phenotype switching rate α, as well as to develop an approach to search for it at more biologically relevant parameter values. Therefore in this chapter we seek to analytically solve for T, which we will compare with numerical results throughout. The solutions we find for T will often be restricted to the particular case in which $c = 0$, i.e. zero fitness costs for states of phenotype B. However, the methods described in this chapter can be adapted to consider when $c \neq 0$.

Direct calculation of T is not always possible. This is due to the complexity of analytically describing an evolving population's dynamics over a 2D state space (even one that is as small as we consider here). However, in Chapter 3 we saw that two trajectories are particularly important in the evolution of a cell of type 3A: that which evolves 3A directly via 1A→2A→3A (represented by the symbol: ⎽⎽) and that which avoids state 2A entirely (represented by the symbol: ⎍). We will refer to these as trajectories A and B respectively, with the corresponding adaptation times T_A and T_B. These trajectories must be taken by populations that are constrained to evolve from 1A to 3A over the networks of states A and B, shown in Fig. 4.1.

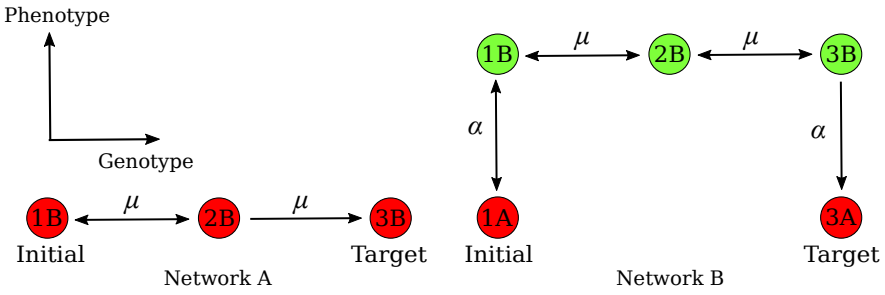

Figure 4.1 *Subnetworks A and B of the full network shown in Fig. 3.1A. Populations starting at state 1A are constrained to evolve directly to 3A (trajectory A), or by avoiding 2A entirely (trajectory B), with the adaptation times T_A and T_B respectively. At low α, we approximate the full system's adaptation time T to be $T \approx \min[\mathrm{T_A}, \mathrm{T_B}]$*

.

At low values of α, if the valley depth δ is large enough that the optimal α range exists, successful cells will travel to 3A almost exclusively by trajectories A and B. We saw an example of this occurring earlier in Fig. 3.9C. This significantly simplifies the calculation of T as it means that $T \approx \min[\mathrm{T_A}, \mathrm{T_B}]$ for low enough α. When this approximation is valid, all we need to do is calculate T_A and T_B.

This greatly simplifies the problem to that of a population acquiring a particular sequence of mutations.

Mathematical descriptions of how asexual populations acquire a sequence of as few as two mutations are already surprisingly complex [206]. This complexity arises from the uncertainty in the population's dynamics, which are sensitive to parameters such as mutation probability μ and carrying capacity K, as well as the particular fitness landscape being considered. However, there are instances in which populations evolve in a way that is predictable, in which they conform to the behaviour of a specific *dynamical regime*. In each dynamical regime, the population behaves, in general, in a way that is both unique and quantifiable, allowing it to be described analytically. Varying parameters that affect the population's dynamics, such as the rate of mutant production, moves the system from one dynamical regime to another. This makes a general solution for the adaptation time T unlikely to be found for the system. Instead, each of these regimes requires its own analysis and calculation of T for when the system is in it.

In this chapter, we begin by considering each dynamical regime for which we can calculate the adaptation times T, T_A and T_B. Each regime will be introduced and it will be shown how the relevant adaptation times can be calculated in them. We will also calculate for each regime the boundary conditions that separate it from its neighbouring regimes.

Increasing α results in an increase in the variability of trajectories taken by successful cells, in which they eventually stop travelling exclusively by trajectories A and B. When this happens, above some characteristic switching rate α_c, the approximation $T \approx \min[\mathrm{T_A}, \mathrm{T_B}]$ is no longer valid. In the following we will explore when this is expected to happen. For $\alpha \gg \alpha_c$, it is difficult to calculate T until the limit of large α is reached. At this point, the two phenotype system can be mapped to that of a single phenotype, at which point we can calculate T again.

At the end of this chapter, we will combine together all of the analytic solutions to produce plots of the adaptation time T as a function of the switching rate α. We will compare these results with those of Chapter 3, as well as explore results at parameter values that would be otherwise difficult to simulate. From these solutions, the existence of the optimal α range can be established and its presence at lower mutation probabilities explored.

4.2 Background

Complex interactions between different genetic loci can result in mutations that, despite being individually deleterious, combine to confer a fitness advantage. This is the result of reciprocal sign epistasis in the system — a necessary feature of landscapes containing multiple fitness peaks [154]. Such landscapes with numerous peaks have been shown to exist experimentally [31, 54, 108, 207].

This chapter concerns a classic problem in population genetics, of how an asexually reproducing population can acquire a beneficial double mutant. For this to happen the population must cross a "fitness valley" caused by deleterious intermediate states. In the absence of recombination, which we do not consider, it is necessary for a mutant lineage at one of the intermediate states to produce the target double mutant, which must then establish (i.e. reach a considerable frequency) in the population.

Wright originally believed that it was necessary for sequences of mutants to sequentially fix, in order to avoid them being lost due to genetic drift [214]. However, this behaviour is representative of only a single type of population dynamics, which we refer to as *sequential fixation* (SF). The problem with this dynamics is that it would hinder the escape from a local fitness peak of larger populations, as the probability of fixation for neutral or deleterious mutants varies inversely with the population size [104]. Wright partly overcame the problem of evolution stalling at local fitness peaks as a result of this in his *shifting balance theory*, in which the negative effects of selection can be mitigated in populations that are divided (into demes) [133, 215].

Later it was proposed that populations can acquire double mutants, without the deleterious intermediate mutant having to first fix [75]. Under certain dynamical conditions, drifting lineages of the intermediate mutation are more likely to produce the double mutant than fix. This behaviour was termed *simultaneous fixation* [75], but later became more commonly known as *stochastic tunnelling* (ST) [90], a term which we will use throughout this chapter. In stochastic tunnelling, the time taken to cross the valley varies inversely with population size. Therefore this is the dominant dynamics at larger populations sizes. In this dynamics, how a drifting mutant lineage produces a further mutant (i.e. the double mutant) can be described as a branching process [90, 206]. As the population size increases further, the valley crossing process can first be treated

semi-deterministically [206] before a fully deterministic description is required.

The valley crossing problem for the establishment of a double-mutant (i.e. with a single intermediate state) has been studied in a number of models. These have focused on variations of the problem, such as when the states (either the intermediate or compensatory ones) are neutral [49, 105], or for small or large population sizes for which the regimes are different. Notable works include those focussing on the ST regime [89], or both the SF and ST regimes allowing for the crossover between the regimes to be observed [33, 201].

The valley crossing problem with more than a single intermediate mutation has also been studied. This has been considered for the ST regime alone [89, 176], as well as in a formulation for all regimes [206] (including beyond the ST regime in which a semi-deterministic formulation is employed). The work in [206] has been an important influence for the mathematical analysis in this chapter.

4.3 Deterministic Analysis

We begin our analysis with the deterministic description of the model. We start here as various properties that we define here will be used in the later stochastic analysis. In the *deterministic* (Det) regime, occurring at large population sizes at which stochastic effects are minimized, the adaptation times can be calculated as follows.

For the full system of states, the population at each of the states obey the following deterministic differential equations

$$\begin{aligned}
\dot{N}_{1A}(t) &= \xi r_{1A}(1-\mu)N_{1A} + \xi r_{2A}\mu N_{2A} - \alpha N_{1A} + \alpha N_{1B} - dN_{1A} && (4.1)\\
\dot{N}_{2A}(t) &= \xi r_{2A}(1-2\mu)N_{2A} + \xi r_{1A}\mu N_{1A} - \alpha N_{2A} + \alpha N_{2B} - dN_{2A} && (4.2)\\
\dot{N}_{3A}(t) &= \alpha N_{3B} + \xi r_{2A}\mu N_{2A} && (4.3)\\
\dot{N}_{1B}(t) &= \xi r_{1B}(1-\mu)N_{1B} + \xi r_{2B}\mu N_{2B} - \alpha N_{1B} + \alpha N_{1A} - dN_{1B} && (4.4)\\
\dot{N}_{2B}(t) &= \xi r_{2B}(1-2\mu)N_{2B} + \xi r_{1B}\mu N_{1B} + \xi r_{3B}\mu N_{3B} - \alpha N_{2B} && (4.5)\\
&\quad +\alpha N_{2A} - dN_{2B}\\
\dot{N}_{3B}(t) &= \xi r_{3B}(1-\mu)N_{3B} + \xi r_{2B}\mu N_{2B} - \alpha N_{3B} - dN_{3B}, && (4.6)
\end{aligned}$$

where the quantity $\xi = \left(1 - \frac{N_T}{K}\right)$. Note that $N_{3\mathrm{A}}$ can only increase by mutants produced there by the population at 2A, as well as by cells switching phenotypes

from the population in 3A. This ignores cells at 3A replicating or dying which is the best description for the process up until $N_{3A} = 1$. This ensures that the adaptation time T is independent of r_{3A} (the fitness of the state 3A) which it will be in the stochastic process.

The total population size N_T evolves in time through the equation

$$\dot{N}_T(t) = \xi \sum_{i \in \mathrm{S}} r_i N_i - d N_T, \tag{4.7}$$

where i identifies a state in the set of all possible states S. The contribution of each state's fitness (r_i) to the evolution of N_T changes with the distribution of the population. We will use the approximation that $\sum_i r_i N_i \approx R \sum_i N_i = R N_T$, which substitutes the individual fitnesses r_i with a representative value R. With this replacement, the steady state distributions of (4.7) are the trivial $N_T = 0$ and when $\xi R \approx d$ for which we get that

$$N_T \approx \left(1 - \frac{d}{R}\right) K. \tag{4.8}$$

We will refer to the approximate value given for N_T in (4.8) as the *saturation value* N_T^*. This is a useful quantity as it linearises the replication terms in (4.1) to (4.6) through the substitution $\xi \approx d/R$. The value R that we use is the average fitness of the states that the population is expected to be distributed over. As we do not expect there to be a large frequency of cells in either 2A or 3A these states can be ignored from the value of R with no observable difference to results. Therefore, when $c = 0$, $R \approx 1$.

The validity of the linearisation that results from setting $\xi \approx d/R$ can be argued in a number of ways. Firstly, in the analyses that follow we will always consider the population to begin from the saturation value given in (4.8). At this value of N_T the birth and death rates approximately balance in the system (subject to random fluctuations in the stochastic system). Therefore the variable nature of ξ will be (on average) lost such that $\xi(N_T) = \xi$. Secondly, as we will shortly see, for most of the dynamics the population is expected to exist primarily in a single state. This supports our use of the approximation that $\sum_i r_i N_i \approx R N_T$ with R being the state that we know the population is mainly in. Finally, as we consider there to be no fitness cost (i.e. $c = 0$) the fitness is $r_i = 1$ for all states $i \neq$ 2A. As we do not expect a significant population to exist at state 2A (due to it being deleterious) most of the population will have the same fitness which

again supports the approximation $\sum_i r_i N_i \approx R N_T$.

By linearising the system of differential equations we can attempt to solve for the adaptation times. We first consider this for the trajectories over networks A and B, solving for the adaptation times T_A and T_B respectively. In all cases the adaptation time is the value of t such that $N_{3A}(t) = 1$. Note that in each case the solutions presented are for the direct trajectories A and B (i.e. we do not consider back steps in the trajectory despite them appearing in the networks in Fig. 4.1). In the deterministic regime, where the rate of mutant production is large, this is expected to make little difference to the results.

4.3.1 Trajectory A

We first consider trajectory network A shown in Fig. 4.1. The dynamics of the populations at states 1A, 2A and 3A obey the following differential equations

$$\dot{N}_{1\mathrm{A}}(t) = \xi r_{1\mathrm{A}}(1-\mu)N_{1\mathrm{A}} - dN_{1\mathrm{A}} \tag{4.9}$$

$$\dot{N}_{2\mathrm{A}}(t) = \xi r_{2\mathrm{A}}(1-2\mu)N_{2\mathrm{A}} + \xi r_{1\mathrm{A}}\mu N_{1\mathrm{A}} - dN_{2\mathrm{A}} \tag{4.10}$$

$$\dot{N}_{3\mathrm{A}}(t) = \xi r_{2\mathrm{A}}\mu N_{2\mathrm{A}}. \tag{4.11}$$

Again $\xi = (1 - (N_T/K))$, which upon substitution of the saturation value for N_T from (4.8), simplifies to $\xi \approx d$. The initial conditions are $N_{1\mathrm{A}}(0) = C_0 = (1-d)K, N_{2\mathrm{A}}(0) = 0$ and $N_{3\mathrm{A}}(0) = 0$ and the differential equations can be solved sequentially to produce

$$N_{1\mathrm{A}}(t) = C_0 e^{g_1 t} \tag{4.12}$$

$$N_{2\mathrm{A}}(t) = \frac{\xi\mu r_{1\mathrm{A}} C_0}{(g_1 - g_2)}(e^{g_1 t} - e^{g_2 t}) \tag{4.13}$$

$$N_{3\mathrm{A}}(t) = \frac{\xi^2\mu^2 r_{1\mathrm{A}} r_{2\mathrm{A}} C_0}{g_1 g_2 (g_1 - g_2)}\left[g_1(1 - e^{g_2 t}) - \underbrace{g_2(1 - e^{g_1 t})}_{\text{dominant}}\right] \tag{4.14}$$

$$\approx \frac{\xi^2\mu^2 r_{1\mathrm{A}} r_{2\mathrm{A}} C_0}{g_1(g_1 - g_2)}(e^{g_1 t} - 1), \tag{4.15}$$

where the values g_1 and g_2 are

$$g_1 = \xi r_{1\mathrm{A}}(1-\mu) - d \qquad g_2 = \xi r_{2\mathrm{A}}(1-2\mu) - d. \tag{4.16}$$

The final solution of (4.15) is an approximate solution, found by considering only the "dominant" term in (4.14). To prove that this is the dominant term, in the large timescales we are interested in, consider the ratio Λ of the two terms in the square brackets in (4.14):

$$\Lambda = \left\| \frac{-g_1(1-e^{g_2 t})}{g_2(1-e^{g_1 t})} \right\| \approx \frac{\mu(1-e^{-d\delta t})}{\delta(1-e^{-d\mu t})}. \tag{4.17}$$

Here we have made the approximations that $g_1 \approx -\mu d$ and $g_2 \approx -\delta d$ following the substitution of $r_{1\mathrm{A}} = 1$ and $r_{2\mathrm{A}} = 1-\delta$ into (4.16). The approximation $g_2 \approx -\delta d$ requires that $\mu \ll 1$ which we always consider to be true. The expression for Λ in (4.17) can be expanded to first order in μdt to give

$$\Lambda \approx \frac{1-e^{-d\delta t}}{\delta dt} \quad \text{when} \quad t \ll \frac{1}{\mu d}. \tag{4.18}$$

The condition on t included in (4.18) is required for the expansion to obtain the expression for Λ in Fig. 4.18 to be valid. To prove the second term in (4.14) is dominant at large times we require that $\Lambda \ll 1$. From (4.18) this is true when the denominator is appropriately large (i.e. $\delta dt \gg 1$), which gives us a second condition for t (a lower bound this time) such that

$$\Lambda \approx \frac{1-e^{-d\delta t}}{\delta dt} \ll 1 \quad \text{when} \quad \frac{1}{\delta d} \ll t \ll \frac{1}{\mu d}. \tag{4.19}$$

The upper bound in (4.19) is a condition only for the validity of the Λ expansion in (4.18), not for whether or not $\Lambda \ll 1$ at t values exceeding this upper bound. The original expression for Λ from (4.17) is a decaying function in time (which tends to the value μ/δ as $t \to \infty$) and therefore it must also be true that $\Lambda \ll 1$ for t values exceeding the upper bound in (4.19). Therefore (4.19) predicts that the second term in (4.14) will dominate when $t \gg 1/\delta d \approx 5/\delta d$. If we consider a valley depth of approximately $\delta \approx 0.5$ and $d = 0.1$, this predicts that the second term in (4.14) should become dominant at $t \approx 10^2$.

What remains to be checked is whether or not the target will have been reached by the time $t \approx 10^2$ (i.e. whether or not $N_{3\mathrm{A}}(t = 10^2) \geq 1$). To check this we

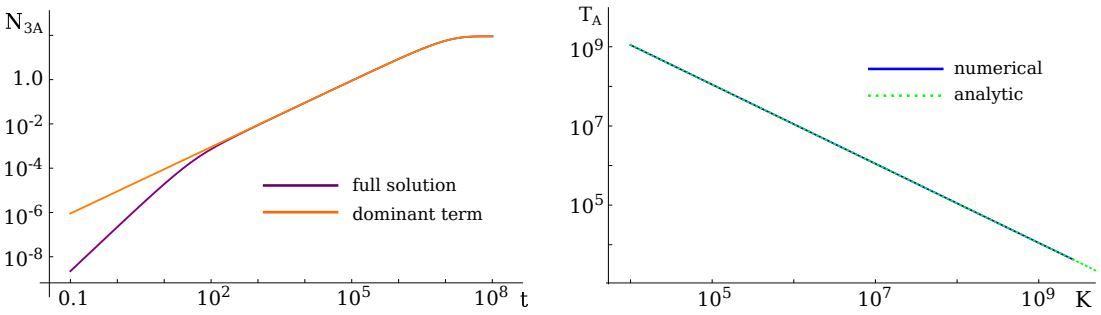

Figure 4.2 *Calculating the adaptation time T_A. (A) Compares curves of N_{3A} — the population size at state 3A — as a function of time for $K = 10^8$. The purple curve is the full analytic solution from (4.14), while the orange curve is the "dominant" term in (4.14). (B) Compares curves of the numerical solution for T_A (blue curve) from the original set of differential equations with the analytic solution (green curve). The remaining parameters used are $\mu = 10^{-6}, \delta = 0.5$ and $d = 0.1$.*

simply substitute $t = 10^2$ into (4.14), along with $d = 0.1$, to get

$$N_{3A}(t = 10^2) \approx \left[\frac{\mu(1-\delta)(1-d)K}{\delta(\delta-\mu)}\right][-\mu(1-e^{-10\delta}) + \delta(1-e^{-10\mu})] \quad (4.20)$$

$$\approx \left[\frac{\mu^2(1-\delta)(1-d)K}{\delta(\delta-\mu)}\right][-(1-e^{-10\delta}) + 10\delta] \quad (4.21)$$

$$\approx \frac{\mu^2(1-\delta)(1-d)K(10\delta-1)}{\delta(\delta-\mu)} \quad (4.22)$$

$$\sim 10\mu^2 K \quad (4.23)$$

where we have expanded $e^{-10\mu} \approx 1 - 10\mu$ to get the second line. Therefore as long as $10\mu^2 K \ll 1$ the population at 3A is not expected to have reached the target by the time the second term in (4.14) becomes dominant.

Figure 4.2A shows a curve of the "dominant" term in (4.14) plotted as a function of time t. Alongside this is the full solution for $N_{3A}(t)$ from (4.14). As the above analytics predicted, the curve for the full solution for $N_{3A}(t)$ converges with the curve of the "dominant" term at $t \approx 10^2$, at which point the population at state 3A has not yet reached the target size of $N_{3A} = 1$. Therefore at larger t values the solution in (4.15) can be used.

Using the solution in (4.15) we can calculate the adaptation time T_A. This is the time such that $N_{3A}(T_A) = 1$ and is found to be

$$T_A = \frac{r_{1A}(1-\mu) - r_{2A}(1-2\mu)}{\xi\mu^2 r_{1A} r_{2A} C_0} = \frac{\delta + \mu(1-2\delta)}{\xi\mu^2(1-\delta)(1-d)K} \sim \frac{1}{d\mu^2 K}, \quad (4.24)$$

where the fitnesses $r_{1A} = 1$ and $r_{2A} = 1 - \delta$ and the initial population size $C_0 = (1 - (d/r_{1A}))K = (1 - d)K$ have been substituted into (4.24) to get the second form.

In order to get (4.24), we must expand the exponential in (4.15) to first order in $g_1 t$. This requires that $|g_1 t| \approx \mu dt \ll 1$ up until $t = T_A$, which places the following condition on K for (4.24) to be valid:

$$K \gg \frac{1}{\mu}. \tag{4.25}$$

This condition is expected to be satisfied in the deterministic regime; we will see later that it is a necessary condition of this regime. It states that $\mu K \gg 1$ ensuring a large mutation production rate. The final form for T_A in (4.24) makes physical sense as it scales inversely with $d\mu^2 K$, which is the rate with which double mutants are produced by the population.

Figure 4.2B compares a curve of the analytic solution in (4.24) with the numerical solution (calculated using *Mathematica*) of the equations in (4.9) to (4.11). We can see there is excellent agreement between the two solutions.

4.3.2 Trajectory B

Consider now the system of differential equations for the populations at the states along trajectory B in Fig. 4.1. These describe how the populations at states 1A, 1B, 2B, 3B and 3A change in time and are

$$\begin{aligned}
\dot{N}_{1A}(t) &= \xi r_{1A}(1-\mu)N_{1A} - \alpha N_{1A} - dN_{1A} && (4.26)\\
\dot{N}_{1B}(t) &= \xi r_{1B}(1-\mu)N_{1B} + \alpha N_{1A} - dN_{1B} && (4.27)\\
\dot{N}_{2B}(t) &= \xi r_{2B}(1-2\mu)N_{2B} + \xi r_{1B}\mu N_{1B} - dN_{2B} && (4.28)\\
\dot{N}_{3B}(t) &= \xi r_{3B}(1-\mu)N_{3B} + \xi r_{2B}\mu N_{2B} - \alpha N_{3B} - dN_{3B} && (4.29)\\
\dot{N}_{3A}(t) &= \alpha N_{3B}, && (4.30)
\end{aligned}$$

with the initial conditions $N_{1A} = C_0 = (1-d)K, N_{1B} = 0, N_{2B} = 0, N_{3B} = 0$ and $N_{3A}(0) = 0$. As we did for T_A in Section 4.3.1, these can be solved sequentially, after first linearising them using the saturation value for N_T from (4.8) so that $\xi = (1 - (N_T/K)) \approx d$. The solution for $N_{3A}(t)$ is not short, or particularly insightful, and has therefore been relegated to Appendix A. A consequence of

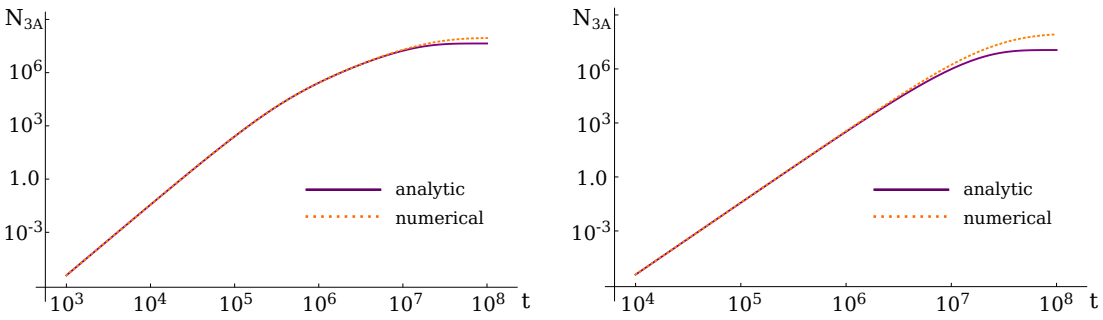

Figure 4.3 *Comparing the analytic and numerical solution for the size of the population at state 3A (N_{3A}) as a function of time. These curves are compared in (A) when $\alpha \neq \mu d$ and (B) when $\alpha = \mu d$. The parameters used are $K = 10^8, \mu = 10^{-6}, d = 0.1$, while $\alpha = 10^{-5}$ in (A) and $\alpha = 10^{-7}$ for (B).*

this is that we are unable to rearrange it into an acceptable form in order to solve analytically for the adaptation time T_{B} (such that $N_{3A}(t = T_B) = 1$).

However, Fig. 4.3 shows plots of the analytically calculated $N_{3A}(t)$ (contained in Appendix A) alongside numerical solutions of equations (4.26) to (4.30) (obtained using *Mathematica*). There are two solutions for $N_{3A}(t)$, depending on the relationship between α and μd. In Figs. 4.3A and B, $\alpha \neq \mu d$ and $\alpha = \mu d$ respectively. Both plots show good agreement between the analytic and numerical solutions over a large range of intermediate t values, in which the population at N_{3A} grows and in which the target value of $N_{3A} = 1$ is reached. However, in both plots there is a disagreement between analytic and numerical solutions as to the steady-state size that the population reaches at state 3A.

4.3.3 Full system

To conclude this section, we now look again at the full system of states (see Fig. 3.1), in which the growth of the population at all states is described deterministically by the equations in (4.1) to (4.6). These equations are difficult to solve analytically for the adaptation time T. Therefore instead we will look at the numerical result of the system of equations, which we can compare with the results for T_A and T_B.

Figure 4.4A shows the numerical solution for the adaptation time T as a function of switching rate α. We see here that the optimal α range is predicted to exist in the deterministic description of the system as well as in the stochastic. For the parameters considered, T is reduced by approximately three orders of magnitude

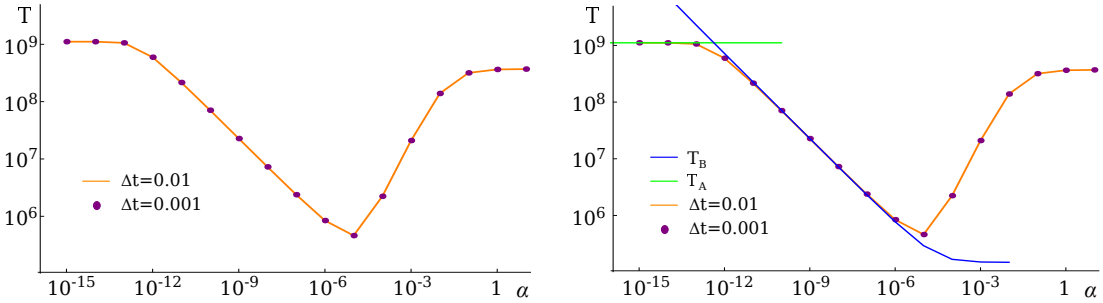

Figure 4.4 *The adaptation time T as a function of α in the deterministic regime. (A) A plot showing the numerical solution for T using the Euler update algorithm with stepsize Δt. Purple dots show results for smaller Δt than the orange curve and confirm convergence of the solution. (B) The same plot as (A) but including the deterministic adaptation times T_A and T_B. T_A is an analytic solution while T_B is solved numerically from the set of differential equations describing trajectory B. Parameters used are $K = 10^{10}, \mu = 10^{-9}, \delta = 0.5$ and $d = 0.1$.*

when compared to the limits of low and high α.

Figure 4.4B plots the full numerical solution for T (i.e. the same curve as in Fig. 4.4A) alongside the adaptation times T_A and T_B. The curve for T_A is the analytic solution from (4.24), while the curve for T_B is calculated numerically (using *Mathematica*). We can see that, as posited at the beginning of this chapter, the full system T is well approximated by the lowest of T_A and T_B over a large range of α values. For α beyond this range (i.e. at large α) the population begins to follow more trajectories than just A and B and a different approach must be considered.

4.4 Sequential fixation regime

We begin the stochastic analysis of the model by looking at the *sequential fixation* regime. This regime occurs at small population sizes when the total rate of mutant production is very small: $\mu dK \ll 1$ (with μd being the approximate rate with which individual cells produce mutants when the population is at saturation size). If a mutant lineage is to exist long enough to produce the next mutant in the sequence, it is likely that it has become significant in the population (i.e. it has approximately fixed). Otherwise we expect it to be lost due to random drift, particularly if the mutant state is deleterious. In this regime, the adaptation time T is dominated by the waiting time for the population to produce mutants

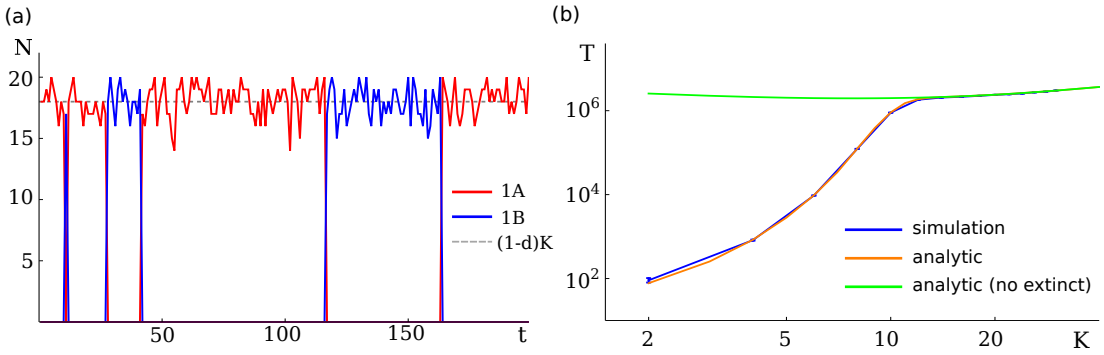

Figure 4.5 *Population dynamics in the sequential fixation (SF) regime. (A) A plot demonstrating that the population remains approximately localized at a single state. It shows the number of cells (N) in states 1A and 1B as a function of time t in a typical simulation run. The population at the remaining four states is approximately zero throughout. The dashed grey line indicates the total population saturation value $N_T^* = (1-d)K$. (B) A plot comparing curves of the adaptation time T as a function of carrying capacity K. A curve showing simulation data (blue line) is compared with the analytic solutions for the full system when population extinctions are included (orange line) and excluded (green line). The parameters used in both plots are $K = 20, \mu = 10^{-5}, \delta = 0.1$, while $\alpha = 10^{-5}$ for (A) and 10^{-6} for (B). Simulation data was collected using a KMC algorithm and averaged over 10^3 runs in (B).*

that are likely to fix. Therefore we can ignore the intermediate dynamics of the cells, such as drift times (being the time it takes for the mutant population to reach fixation).

In this regime, the population remains highly localized and — over large timescales — has the appearance of moving collectively from one state to another upon the event of a mutant fixing. Figure 4.5A demonstrates this behaviour in a single simulation run. It shows the population number at states 1A and 1B varying in time as the population moves back and forth between these two states. We can also see in Fig. 4.5A that the total population size N_T fluctuates about the saturation value N_T^* from (4.8).

In the sequential fixation regime we will describe the population as a single random walker traversing the state space of Fig. 3.1A. However, as the total population number N_T is a variable, significant fluctuations (about the saturation value N_T^*) can lead to the population going extinct. This is particularly likely to occur at small values of K. To account for this we add an additional absorbing state — the extinction state E — to the considered network of states. This new network of states, and the transitions between them, is shown in Fig. 4.6.

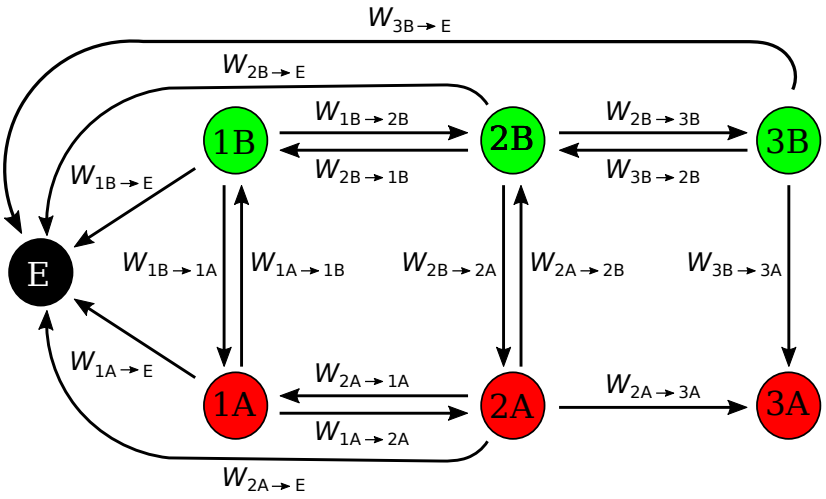

Figure 4.6 *The network of states when the possibility of population extinction is included. Two absorbing states exist: the target state 3A and the extinction state E. All transient states can transition to the extinction state. $W_{i\to j}$ is the rate with which the population transitions from state i to state j.*

For small populations synonymous with this regime, the possibility of population extinction affects the calculation of the adaptation time T. A simulation run in which the population goes extinct will contribute an infinite time to any average T calculated. Therefore we will condition against the population going extinct in this regime and define T to be as follows: "the mean time it takes a random walker, starting in state 1A, to be absorbed in state 3A, conditioned on it not previously having been absorbed in state E". To illustrate why this is an important distinction to make Fig. 4.5B skips ahead in our discussion to plot curves of the analytic solution when the possibility of extinction is both included and excluded. Curves of T as a function of carrying capacity K are plotted for both these scenarios alongside simulations results. At large K there is no observable difference between the three curves. However, for K below ~ 12, the analytic solutions produce different results, with the one that includes extinction matching with the simulation results. When the analytic solutions differ, the reason the one including extinction is smaller than the one without it is that populations that can go extinct have to, on average, reach the target 3A quicker in order to avoid absorption at state E.

In the following section we consider how to calculate the mean first passage time for a random walker to be absorbed at a specific state, conditioned on it being absorbed there and not at some other absorbing state.

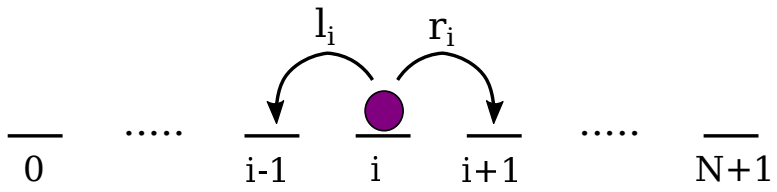

Figure 4.7 *A random walker on a 1D network of states, labelled from 0 to N+1, in which states 0 and N+1 are absorbing. A random walker (purple circle), beginning at some arbitrary state i, transitions to states $i-1$ and $i+1$ with rates l_i and r_i respectively. We are interested in the mean first passage time for the walker to be absorbed at state N+1 conditioned on it not having previously been absorbed at state 0.*

4.4.1 Conditioned mean first passage time

In deriving the adaptation time T we begin by considering the mean first passage time for a random walker to be absorbed at a particular state, conditioned on it doing so, for a 1D network of states. This is the situation shown in Fig. 4.7. A random walker begins at state i at $t = 0$ and traverses the network of which states 0 and $N + 1$ are absorbing. The rates of transition from state i to $i - 1$ and $i + 1$ are l_i and r_i respectively. We want to calculate the mean time it takes for the walker to be absorbed at state $N + 1$, conditioned on it being absorbed there and not at state 0. We begin by considering a standard approach to solve for the mean first passage time [159].

Let $q(n, t|i)$ be the probability that the walker has survived (i.e. has not yet been absorbed anywhere) and is at state n at time t, given that it started at state i at time $t = 0$. The total probability that the walker has survived by time t is therefore $Q(t|i) = \sum_n q(n, t|i)$, where the sum is over all transient (i.e. non-absorbing) states. In the small time interval Δt this changes by

$$Q(t + \Delta t|i) = Q(t|i) - \rho(t|i)\Delta t, \tag{4.31}$$

where $\rho(t|i)$ is the probability density of absorption at time t given the walker started at state i. The minus before the second term accounts for the survival probability necessarily decreasing in time. By expanding (4.31) to first order in Δt we can deduce that

$$\rho(t|i) = -\frac{\partial Q(t|i)}{\partial t}. \tag{4.32}$$

Therefore in time $t \to t + dt$ the probability of absorption is $\rho(t|i)dt$. The mean

first passage time until absorption anywhere is therefore

$$\tau(i) = \int_0^\infty t\rho(t|i) = -\int_0^\infty t\frac{\partial Q(t|i)}{\partial t}dt = \int_0^\infty Q(t|i)dt, \tag{4.33}$$

where the final form is found through integration by parts.

Now we want to consider the contribution to (4.33) from each absorbing state. The probability density is additive such that $\rho(t|i) = \rho_0(t|i) + \rho_{\mathrm{N}+1}(t|i)$, where $\rho_0(t|i)$ and $\rho_{\mathrm{N}+1}(t|i)$ are the probability densities of absorption at time t in states 0 and N+1 respectively. These are equal to the probability that the walker has survived and is in the adjacent state to the absorbing state at time t, multiplied by the rate of transition to the absorbing state (i.e. $\rho_0(t|i) = q(1,t|i)l_1$ and $\rho_{\mathrm{N}+1}(t|i) = q(N,t|i)r_{\mathrm{N}}$).

Let us define $P(0,t|i)$ and $P(N+1,t|i)$ to be the probabilities of absorption at 0 and $N+1$ respectively in time $t \to t+dt$, given that the walker starts in state i at $t = 0$. These can be written as

$$P(0,t|i) = \rho_0(t|i)dt = q(1,t|i)l_1 dt \tag{4.34}$$

$$P(N+1,t|i) = \rho_{\mathrm{N}+1}(t|i)dt = q(N,t|i)r_{\mathrm{N}}dt, \tag{4.35}$$

while the total probability of absorption at state 0 and N+1, called $P(0|i)$ and $P(N+1|i)$ respectively, must satisfy

$$1 = P(0|i) + P(N+1|i) \tag{4.36}$$

$$= \int_0^\infty P(0,t|i)dt + \int_0^\infty P(N+1,t|i)dt. \tag{4.37}$$

Going back now to the mean first passage time $\tau(i)$ in (4.33), this can be split into contributions from absorption at states 0 and N+1, called $\tau(0|i)$ and $\tau(N+1|i)$ respectively, by

$$\tau(i) = \overbrace{\int_0^\infty tP(0,t|i)dt}^{\tau(0|i)} + \overbrace{\int_0^\infty tP(N+1,t|i)dt}^{\tau(N+1|i)}. \tag{4.38}$$

Now, to condition upon absorption at $N+1$ we divide $\tau(N+1|i)$ by the probability that $N+1$ is the state that the walker is absorbed in. Therefore the mean time until absorption at $N+1$, conditioned on it being absorbed there, which we will

call $T(i)$ to coincide later with the adaptation time, is

$$T(i) = \frac{\tau(N+1|i)}{P(N+1|i)} = \frac{\int_0^\infty tP(N+1,t|i)dt}{\int_0^\infty P(N+1,t|i)dt}. \tag{4.39}$$

The condition in the denominator has the effect of reducing $T(i)$ compared to when $N+1$ is the only absorbing state. This is not immediately obvious from (4.39) where the denominator $P(N+1|i) \leq 1$ and only becomes one when $N+1$ is the only absorbing state. However, the numerator in (4.39) depends on the survival probability of the walker, which is expected to decrease the more absorbing states are added.

The justification of (4.39) can be extended to a general network of states, to consider conditioned absorption at any subset of them. For conditioned absorption at any state in the subset of absorbing states μ, the adaptation time $T(i)$ is

$$T(i) = \frac{\sum_{j\in\mu}\tau(j|i)}{\sum_{j\in\mu}P(j|i)}. \tag{4.40}$$

All quantities in (4.40) can be calculated, without the need to perform any integration, by considering systems of master equations (as discussed in Section 2.3.2). For example, consider the contribution to (4.40) from the absorbing state $\xi \in \mu$, which can be transitioned into from the transient state n. The forward master equation (using the form of (2.43)) describing how the survival probability of the random walker being in state n (given that it started in state i) changes in time, is

$$\frac{\partial q(n,t|i)}{\partial t} = \sum_j W_{i\to j}[q(n,t|j) - q(n,t|i)]. \tag{4.41}$$

The sum is over all states that an individual in state i could transition to, while the initial condition is $q(n,t=0|i) = \delta_{ni}$. Integrating (4.41) over all values of time t and defining $S(n|i) = \int_0^\infty q(n,t|i)dt$ we get

$$-\delta_{ni} = \sum_j W_{i\to j}[S(n|j) - S(n|i)]. \tag{4.42}$$

The left hand side of this equation is obtained from performing integration by parts on (4.41) and applying the initial condition. Alternatively, multiplying

(4.41) by t and integrating over all time gives us

$$-S(n,t|i) = \sum_j W_{i\to j}\left[\int_0^\infty tq(n,t|j)dt - \int_0^\infty tq(n,t|i)dt\right], \tag{4.43}$$

where again the left hand side comes from integration by parts. Multiplying (4.43) by $W_{n\to\xi}$ we get

$$-W_{n\to\xi}S(n,t|i) = \sum_j W_{i\to j}[\overbrace{\int_0^\infty W_{n\to\xi}tq(n,t|j)dt}^{\tau(\xi|i)} - \overbrace{\int_0^\infty W_{n\to\xi}tq(n,t|i)dt}^{\tau_(\xi|j)}]. \tag{4.44}$$

If we consider (4.42) and (4.44) for all possible initial states i, we will get two systems of equations from which the quantities $\tau(\xi|i)$ and $P(\xi|i) = W_{n\to\xi}S(n|i)$ can be found through rearrangement alone. These quantities are the contributions to the adaptation time in (4.40) that come from the absorbing state ξ.

As an example we will consider the 1D network of states in Fig. 4.7 and the simple case in which $N = 2$. States 0 and 3 are absorbing and by (4.40) the mean time until absorption at state 3, conditioned on it being absorbed there, by a walker starting at state 1, is

$$T(1) = \frac{\tau(3|1)}{P(3|1)} = \frac{\tau(3|1)}{r_2S(2|1)} = \frac{\int_0^\infty tq(2,t|1)r_2dt}{r_2\int_0^\infty q(2,t|1)dt}. \tag{4.45}$$

The system of forward master equations, concerning the survival probability that the walker is at state 2 at time t, is

$$\frac{\partial q(2,t|1)}{\partial t} = r_1q(2,t|2) - (l_1+r_1)q(2,t|1) \tag{4.46}$$

$$\frac{\partial q(2,t|2)}{\partial t} = l_2q(2,t|1) - (l_2+r_2)q(2,t|2). \tag{4.47}$$

Integrating to get these into the form of (4.42) gives us

$$0 = r_1S(2|2) - (l_1+r_1)S(2|1) \tag{4.48}$$

$$-1 = l_2S(2|1) - (l_2+r_2)S(2|2), \tag{4.49}$$

while multiplying (4.46) and (4.47) by t and integrating, to get them into the

form of (4.44), gives

$$-r_2 S(2|1) = r_1\tau(3|2) - (l_1 + r_1)\tau(3|1) \quad (4.50)$$

$$-r_2 S(2|2) = l_2\tau(3|1) - (l_2 + r_2)\tau(3|2). \quad (4.51)$$

Equations (4.48) to (4.50) can be rearranged to express $S(2|1)$ and $\tau(3|1)$ in terms of the transition rates in the system. By doing this we find the adaptation time $T(1)$ to be

$$T(1) = \frac{l_1 + l_2 + r_1 + r_2}{r_1 r_2 + l_1(l_2 + r_2)}. \quad (4.52)$$

4.4.2 Adaptation time for the full system

We now apply the method presented in Section 4.4.1 to calculate T for the network of states in Fig. 4.6. The absorbing state is 3A and there are two transient states from which it can be reached: by the transition 2A→3A or 3B→3A. We will begin by considering what all the transition rates included in Fig. 4.6 are.

The transition rate from a transient state i to the target (i.e $W_{i\to 3A}$) is simply the rate with which mutants are produced at 3A when all the population is at i. However, the transition rate $W_{i\to j}$ between two transient states i and j, is the rate that mutants are produced at state j (from the population at i) multiplied by the probability they have of fixing at j. In a population of fixed size N the probability that a mutant fixes in a state with relative fitness disadvantage δ is [56, 104]

$$P(N,\delta) = \begin{cases} \frac{1}{N} \text{ for } \delta = 0 \\ \frac{1-e^{\delta}}{1-e^{\delta N}} \text{ for } \delta > 0. \end{cases} \quad (4.53)$$

The model we are looking at does not have a fixed population size. However, the population size fluctuates about the saturation value N_T^* which we will treat as the fixed population size to be used in (4.53).

The extinction rate $W_{i\to E}$ for state i, is the rate with which the population at i transitions to state E in Fig. 4.6. To estimate this we consider the total population size N_T at i to be a discrete variable that undergoes a random walk. This random walk occurs between the values $N_T = 0$ and $N_T = K$ and describes the fluctuations of N_T when the population is at state i. The random walker (being the value of N_T), begins at the saturation value N_T^* for that state. It has asymmetric hop rates (due to the $(1-N_T/K)$ factor that increases the growth rate

when N_T is small), an absorbing boundary at $N_T = 0$ and a reflective boundary at $N_T = K$.

Therefore the extinction rate is the rate with which the walker, starting at the saturation value N_T^*, is absorbed at $N_T = 0$. This rate is different for states with different growth rates, i.e. for different transient states in the system. To calculate this we use the following, discrete time, result from [138]: In a 1D asymmetric random walk, with site dependent transition probabilities, the number of steps it takes a walker to go from site 0 to M (in which 0 is a reflecting boundary) is

$$\bar{t}_{(0,M)} = \sum_{k=0}^{M-1} \frac{1}{p_k} + \sum_{k=0}^{M-2} \frac{1}{p_k} \sum_{i=k+1}^{M-1} \prod_{j=k+1}^{i} \frac{q_j}{p_j} \tag{4.54}$$

Here p_i and q_i are the probabilities that in each timestep the walker transitions from site i to $i+1$ and $i-1$ respectively. The continuous mean first passage time (MFPT) takes the same form but replaces probabilities with transition rates. The inverse of $\bar{t}_{(0,M)}$ will give us the rate with which the walker goes from 0 to M.

In our model, the random walker starts at $N_T = N_T^* \approx (1 - (d/r_i))K$ for state i. For ease of notation the dependence of N_T^* on the state i is never explicitly shown (but it should be remembered that N_T^* is state-dependent). Using (4.54) the MFPT until absorption (i.e. extinction), $\bar{t}_E$ is equal to

$$\bar{t}_E = \bar{t}_{(N_T=K, N_T=0)} - \bar{t}_{(N_T=K, N_T=N_T*)}, \tag{4.55}$$

the inverse of which is the extinction $W_{i\to E}$ rate for the state i being considered. A list of the transition rates used in this model, as well as a more thorough discussion on the extinction rates, can be found in Appendix B.

Now from (4.40) the adaptation time T for the full system in this regime can be written as

$$T = \frac{\int_0^\infty t W_{2\mathrm{A}\to 3\mathrm{A}} q(2\mathrm{A}, \mathrm{t}|1\mathrm{A})\mathrm{dt} + \int_0^\infty \mathrm{tW}_{3\mathrm{B}\to 3\mathrm{A}} \mathrm{q}(3\mathrm{B}, \mathrm{t}|1\mathrm{A})\mathrm{dt}}{W_{2\mathrm{A}\to 3\mathrm{A}} \int_0^\infty q(2\mathrm{A}, \mathrm{t}|1\mathrm{A})\mathrm{dt} + \mathrm{W}_{3\mathrm{B}\to 3\mathrm{A}} \int_0^\infty \mathrm{q}(3\mathrm{B}, \mathrm{t}|1\mathrm{A})\mathrm{dt}}. \tag{4.56}$$

The first terms in both the numerator and denominator are the contributions from the route to the target 2A→3A, while the second terms are from the route 3B→3A.

As we saw earlier, for a general network of states the system of forward master equations can yield all terms in (4.56) without the need to perform any

integration. Consider calculating the two terms in (4.56) relating to absorption via 2A→3A (i.e. the first terms in the numerator and denominator). We begin with the system of forward master equations describing how the survival probability $q(2\mathrm{A}, \mathrm{t}|\mathrm{j})$ changes in time:

$$\begin{aligned}
\frac{\partial}{\partial t}q(2\mathrm{A},\mathrm{t}|1\mathrm{A}) &= W_{1\mathrm{A}\to 2\mathrm{A}}q(2\mathrm{A},\mathrm{t}|2\mathrm{A}) + \mathrm{W}_{1\mathrm{A}\to 1\mathrm{B}}\mathrm{q}(2\mathrm{A},\mathrm{t}|1\mathrm{B}) \\
&\quad - (W_{1\mathrm{A}\to 2\mathrm{A}} + W_{1\mathrm{A}\to 1\mathrm{B}} + W_{1\mathrm{A}\to \mathrm{E}})q(2\mathrm{A},\mathrm{t}|1\mathrm{A})
\end{aligned} \tag{4.57}$$

$$\begin{aligned}
\frac{\partial}{\partial t}q(2\mathrm{A},\mathrm{t}|2\mathrm{A}) &= W_{2\mathrm{A}\to 1\mathrm{A}}q(2\mathrm{A},\mathrm{t}|1\mathrm{A}) + \mathrm{W}_{2\mathrm{A}\to 2\mathrm{B}}\mathrm{q}(2\mathrm{A},\mathrm{t}|2\mathrm{B}) \\
&\quad - (W_{2\mathrm{A}\to 1\mathrm{A}} + W_{2\mathrm{A}\to 2\mathrm{B}} + W_{2\mathrm{A}\to \mathrm{E}} + W_{2\mathrm{A}\to 3\mathrm{A}})q(2\mathrm{A},\mathrm{t}|2\mathrm{A})
\end{aligned} \tag{4.58}$$

$$\begin{aligned}
\frac{\partial}{\partial t}q(2\mathrm{A},\mathrm{t}|1\mathrm{B}) &= W_{1\mathrm{B}\to 1\mathrm{A}}q(2\mathrm{A},\mathrm{t}|1\mathrm{A}) + \mathrm{W}_{1\mathrm{B}\to 2\mathrm{B}}\mathrm{q}(2\mathrm{A},\mathrm{t}|2\mathrm{B}) \\
&\quad - (W_{1\mathrm{B}\to 1\mathrm{A}} + W_{1\mathrm{B}\to 2\mathrm{B}} + W_{1\mathrm{B}\to \mathrm{E}})q(2\mathrm{A},\mathrm{t}|2\mathrm{B})
\end{aligned} \tag{4.59}$$

$$\begin{aligned}
\frac{\partial}{\partial t}q(2\mathrm{A},\mathrm{t}|2\mathrm{B}) &= W_{2\mathrm{B}\to 1\mathrm{B}}q(2\mathrm{A},\mathrm{t}|1\mathrm{B}) + \mathrm{W}_{2\mathrm{B}\to 2\mathrm{A}}\mathrm{q}(2\mathrm{A},\mathrm{t}|2\mathrm{A}) \\
&\quad + W_{2\mathrm{B}\to 3\mathrm{B}}q(2\mathrm{A},\mathrm{t}|3\mathrm{B}) \\
&\quad - (W_{2\mathrm{B}\to 1\mathrm{B}} + W_{2\mathrm{B}\to 2\mathrm{A}} + W_{2\mathrm{B}\to \mathrm{E}} + W_{2\mathrm{B}\to 3\mathrm{B}})q(2\mathrm{A},\mathrm{t}|2\mathrm{B})
\end{aligned} \tag{4.60}$$

$$\begin{aligned}
\frac{\partial}{\partial t}q(2\mathrm{A},\mathrm{t}|3\mathrm{B}) &= W_{3\mathrm{B}\to 2\mathrm{B}}q(2\mathrm{A},\mathrm{t}|2\mathrm{B}) \\
&\quad - (W_{3\mathrm{B}\to 2\mathrm{B}} + W_{3\mathrm{B}\to 3\mathrm{A}} + W_{3\mathrm{B}\to \mathrm{E}})q(2\mathrm{A},\mathrm{t}|3\mathrm{B}).
\end{aligned} \tag{4.61}$$

Integrating these equations over all t and applying the initial conditions

$q(2\mathrm{A},0|\mathrm{i}) = \delta_{2\mathrm{A,i}}$ gives us

$$\begin{aligned} 0 &= W_{1\mathrm{A}\to 2\mathrm{A}}S(2\mathrm{A}|2\mathrm{A}) + \mathrm{W}_{1\mathrm{A}\to 1\mathrm{B}}\mathrm{S}(2\mathrm{A}|1\mathrm{B}) \\ &\quad - (W_{1\mathrm{A}\to 2\mathrm{A}} + W_{1\mathrm{A}\to 1\mathrm{B}} + W_{1\mathrm{A}\to \mathrm{E}})S(2\mathrm{A}|1\mathrm{A}) \end{aligned} \tag{4.62}$$

$$\begin{aligned} -1 &= W_{2\mathrm{A}\to 1\mathrm{A}}S(2\mathrm{A}|1\mathrm{A}) + \mathrm{W}_{2\mathrm{A}\to 2\mathrm{B}}\mathrm{S}(2\mathrm{A}|2\mathrm{B}) \\ &\quad - (W_{2\mathrm{A}\to 1\mathrm{A}} + W_{2\mathrm{A}\to 2\mathrm{B}} + W_{2\mathrm{A}\to \mathrm{E}} + W_{2\mathrm{A}\to 3\mathrm{A}})S(2\mathrm{A}|2\mathrm{A}) \end{aligned} \tag{4.63}$$

$$\begin{aligned} 0 &= W_{1\mathrm{B}\to 1\mathrm{A}}S(2\mathrm{A}|1\mathrm{A}) + \mathrm{W}_{1\mathrm{B}\to 2\mathrm{B}}\mathrm{S}(2\mathrm{A}|2\mathrm{B}) \\ &\quad - (W_{1\mathrm{B}\to 1\mathrm{A}} + W_{1\mathrm{B}\to 2\mathrm{B}} + W_{1\mathrm{B}\to \mathrm{E}})S(2\mathrm{A}|2\mathrm{B}) \end{aligned} \tag{4.64}$$

$$\begin{aligned} 0 &= W_{2\mathrm{B}\to 1\mathrm{B}}S(2\mathrm{A}|1\mathrm{B}) + \mathrm{W}_{2\mathrm{B}\to 2\mathrm{A}}\mathrm{S}(2\mathrm{A}|2\mathrm{A}) + \mathrm{W}_{2\mathrm{B}\to 3\mathrm{B}}\mathrm{S}(2\mathrm{A}|3\mathrm{B}) \\ &\quad - (W_{2\mathrm{B}\to 1\mathrm{B}} + W_{2\mathrm{B}\to 2\mathrm{A}} + W_{2\mathrm{B}\to \mathrm{E}} + W_{2\mathrm{B}\to 3\mathrm{B}})S(2\mathrm{A}|2\mathrm{B}) \end{aligned} \tag{4.65}$$

$$\begin{aligned} 0 &= W_{3\mathrm{B}\to 2\mathrm{B}}S(2\mathrm{A}|2\mathrm{B}) \\ &\quad - (W_{3\mathrm{B}\to 2\mathrm{B}} + W_{3\mathrm{B}\to 3\mathrm{A}} + W_{3\mathrm{B}\to \mathrm{E}})S(2\mathrm{A}|3\mathrm{B}). \end{aligned} \tag{4.66}$$

Here we have used the notation introduced earlier in (4.42), that $S(2\mathrm{A}|\mathrm{j}) = \int_0^\infty \mathrm{q}(2\mathrm{A},\mathrm{t}|\mathrm{j})\mathrm{dt}$. Alternatively, if we first multiply (4.57) to (4.61) by $W_{2\mathrm{A}\to 3\mathrm{A}}t$, before then integrating over all t we get

$$\begin{aligned} -W_{2\mathrm{A}\to 3\mathrm{A}}S(2\mathrm{A}|1\mathrm{A}) &= W_{1\mathrm{A}\to 2\mathrm{A}}\tau(3\mathrm{A}|2\mathrm{A}) + \mathrm{W}_{1\mathrm{A}\to 1\mathrm{B}}\tau(3\mathrm{A}|1\mathrm{B}) \\ &\quad - (W_{1\mathrm{A}\to 2\mathrm{A}} + W_{1\mathrm{A}\to 1\mathrm{B}} + W_{1\mathrm{A}\to \mathrm{E}})\tau(3\mathrm{A}|1\mathrm{A}) \end{aligned} \tag{4.67}$$

$$\begin{aligned} -W_{2\mathrm{A}\to 3\mathrm{A}}S(2\mathrm{A}|2\mathrm{A}) &= W_{2\mathrm{A}\to 1\mathrm{A}}\tau(3\mathrm{A}|1\mathrm{A}) + \mathrm{W}_{2\mathrm{A}\to 2\mathrm{B}}\tau(3\mathrm{A}|2\mathrm{B}) \\ &\quad - (W_{2\mathrm{A}\to 1\mathrm{A}} + W_{2\mathrm{A}\to 2\mathrm{B}} + W_{2\mathrm{A}\to \mathrm{E}} + W_{2\mathrm{A}\to 3\mathrm{A}})\tau(3\mathrm{A}|2\mathrm{A}) \end{aligned} \tag{4.68}$$

$$\begin{aligned} -W_{2\mathrm{A}\to 3\mathrm{A}}S(2\mathrm{A}|1\mathrm{B}) &= W_{1\mathrm{B}\to 1\mathrm{A}}\tau(3\mathrm{A}|1\mathrm{A}) + \mathrm{W}_{1\mathrm{B}\to 2\mathrm{B}}\tau(3\mathrm{A}|2\mathrm{B}) \\ &\quad - (W_{1\mathrm{B}\to 1\mathrm{A}} + W_{1\mathrm{B}\to 2\mathrm{B}} + W_{1\mathrm{B}\to \mathrm{E}})\tau(3\mathrm{A}|2\mathrm{B}) \end{aligned} \tag{4.69}$$

$$\begin{aligned} -W_{2\mathrm{A}\to 3\mathrm{A}}S(2\mathrm{A}|2\mathrm{B}) &= W_{2\mathrm{B}\to 1\mathrm{B}}\tau(3\mathrm{A}|1\mathrm{B}) + \mathrm{W}_{2\mathrm{B}\to 2\mathrm{A}}\tau(3\mathrm{A}|2\mathrm{A}) \\ &\quad + W_{2\mathrm{B}\to 3\mathrm{B}}\tau(3\mathrm{A}|3\mathrm{B}) \\ &\quad - (W_{2\mathrm{B}\to 1\mathrm{B}} + W_{2\mathrm{B}\to 2\mathrm{A}} + W_{2\mathrm{B}\to \mathrm{E}} + W_{2\mathrm{B}\to 3\mathrm{B}})\tau(3\mathrm{A}|2\mathrm{B}) \end{aligned} \tag{4.70}$$

$$\begin{aligned} -W_{2\mathrm{A}\to 3\mathrm{A}}S(2\mathrm{A}|3\mathrm{B}) &= W_{3\mathrm{B}\to 2\mathrm{B}}\tau(3\mathrm{A}|2\mathrm{B}) \\ &\quad - (W_{3\mathrm{B}\to 2\mathrm{B}} + W_{3\mathrm{B}\to 3\mathrm{A}} + W_{3\mathrm{B}\to \mathrm{E}})\tau(3\mathrm{A}|3\mathrm{B}). \end{aligned} \tag{4.71}$$

which uses the notation that $\tau(3\mathrm{A}|\mathrm{j}) = \mathrm{W}_{2\mathrm{A}\to 3\mathrm{A}}\int_0^\infty \mathrm{tq}(2\mathrm{A},\mathrm{t}|\mathrm{j})\mathrm{dt}$. The first term

in the numerator of (4.56) is equal to $\tau(3A|1A)$, while the first term in the denominator is equal to $W_{2A\to 3A}S(2A|1A)$. These quantities can be expressed in terms of the rates in the system, by rearranging the equations from (4.62) to (4.71). For the following results this rearrangement was carried out using *Mathematica*.

The other two terms in (4.56) can be found the same way, beginning with the system of forward master equations for the survival probabilities $q(3B, t|j)$ with the initial conditions $q(3B, 0|i) = \delta_{3B,i}$. As this derivation offers nothing new it is excluded from presentation here.

Due to the complicated form of the extinction rates, for small K (i.e. $K < 20$) a general solution has not been obtained for the adaptation time T. For $K \geq 20$ the extinction rates are approximately zero and (4.56) can be solved for a general T. However, this formula is long and not illuminating and is therefore also excluded from being presented here. However, Fig. 4.5B, which we looked at earlier, contains a plot of this adaptation time T as a function of K. It is compared with a curve (green) in which the possibility of extinction was not considered (i.e. zero extinction rates) and with simulation data (blue curve). We can see that the full solution matches very well with the simulation data, for the entire range of K values considered. This is remarkable considering the conflicting assumptions it was necessary to make regarding the dynamics of the population. For example, in calculating the transition rates between transient states we assume the population size to be fixed, yet its fluctuation is integral in calculating the non-zero transition rates to extinction.

4.4.3 Trajectories A and B

We consider now evolution in the SF regime when the population is forced to travel by trajectories A and B in Fig. 4.1. In each case we calculate the adaptation time (so T_A and T_B for trajectory A and B respectively). We restrict our considerations to when the costs $c = 0$ and the extinction rates are zero. Therefore the following solutions are only valid for larger population sizes (i.e. $K \gtrsim 20$). When these conditions are not met, the analytic solutions can still be calculated using e.g. *Mathematica*. We exclude most steps of the calculation in the following as they are very similar to those we have just seen.

For trajectory A, the general equation for the adaptation time T_A is

$$T_A = \frac{\int_0^\infty tW_{2\mathrm{A}\to 3\mathrm{A}} q(2\mathrm{A}, \mathrm{t}|1\mathrm{A})\mathrm{dt}}{W_{2\mathrm{A}\to 3\mathrm{A}} \int_0^\infty q(2\mathrm{A}, \mathrm{t}|1\mathrm{A})\mathrm{dt}}. \tag{4.72}$$

Following the approach laid out in the preceding section, if we start with a system of forward master equations for the survival probabilities $q(2\mathrm{A}, \mathrm{t}|\mathrm{i})$, the following solution can be found

$$T_A = \frac{(1 + P_{1\mathrm{A}} + P_{2\mathrm{A}})r_{1\mathrm{A}}r_{2\mathrm{A}} - d[r_{1\mathrm{A}}(1 + P_{1\mathrm{A}}) + r_{2\mathrm{A}}P_{2\mathrm{A}})]}{dK\mu P_{2\mathrm{A}}(r_{1\mathrm{A}} - d)(r_{2\mathrm{A}} - d)}. \tag{4.73}$$

The quantities $P_{1\mathrm{A}}$ and $P_{2\mathrm{A}}$ are the probabilities that mutants will fix at states 1A and 2A respectively. Using the equation in (4.53) these are

$$P_{1\mathrm{A}} = \frac{1 - e^{-\delta}}{1 - e^{-\delta(1-(d/r_{2\mathrm{A}}))K}} \approx \delta \quad , \quad P_{2\mathrm{A}} = \frac{1 - e^{\delta}}{1 - e^{\delta(1-(d/r_{1\mathrm{A}}))K}} \tag{4.74}$$

The solution in (4.73) is only valid for $K \gtrsim 20$. At these values $P_{2\mathrm{A}} \approx 0$ and by making the substitution $r_{2\mathrm{A}} = (r_{1\mathrm{A}} - \delta)$ into (4.73) we find that

$$T_A \approx \frac{r_{1\mathrm{A}}(1 + \delta)}{dK\mu(r_{1\mathrm{A}} - d)P_{2\mathrm{A}}} \sim \frac{1}{dK\mu P_{2\mathrm{A}}}. \tag{4.75}$$

Therefore the adaptation time T_A scales with the waiting time for a mutant to be created at 2A that will fix there (the rate of this happening from a population at 1A is approximately $dK\mu P_{2\mathrm{A}}$). This makes sense as it is the part of the process expected to take the longest time to occur.

Figure 4.8A shows a plot of the adaptation time T_A as a function of carrying capacity K. It compares the analytic solution from (4.72) when extinction rates are included with a curve of simulation data. The valley depth $\delta = 0.01$ used here is very small, causing the population to behave in a way consistent with the SF regime up to the large values of K considered ($K = 10^2$). Over this range we can see that the analytic solution matches very closely with simulation results.

We consider now trajectory B and the analytic solution for the adaptation time T_B in the SF regime. The general form of this is

$$T_B = \frac{\int_0^\infty tW_{3\mathrm{B}\to 3\mathrm{A}} P_{3\mathrm{B}}^{(1\mathrm{A})} dt}{W_{3\mathrm{B}\to 3\mathrm{A}} \int_0^\infty P_{3\mathrm{B}}^{(1\mathrm{A})}(t) dt}. \tag{4.76}$$

Again, following the approach of the preceding section, starting with the forward

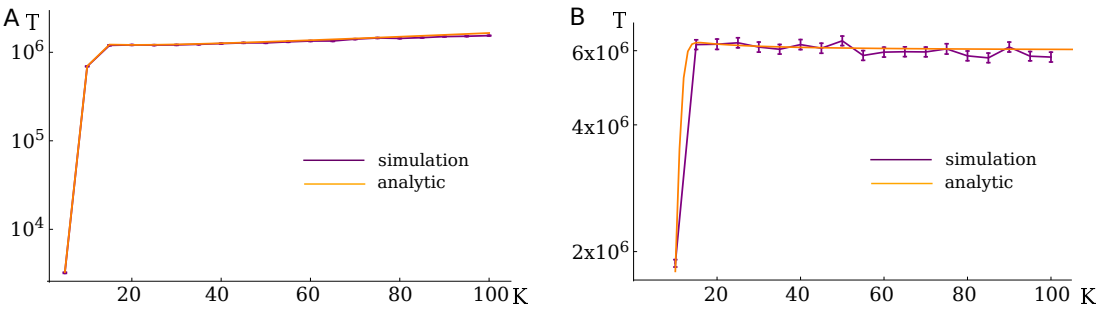

Figure 4.8 *Comparing simulation data with the analytic solutions for the adaptation time as function of K in the SF regime. (A) and (B) show curves for T_A and T_B over trajectory networks A and B respectively with simulation data. Parameter values are $\mu = 10^{-5}, \delta = 0.01, \alpha = 10^{-5}$ and $d = 0.1$. Simulation data was gathered using a KMC algorithm and averaged over 10^3 runs.*

master equations for the survival probabilities $q(3\mathrm{B}, \mathrm{t}|\mathrm{i})$, we find that

$$T_B = \frac{(5\alpha + d\mu)K(d - r_1) - 4d\mu r_1}{dK\alpha\mu(d - r_1)} \sim \frac{1}{\alpha}\left[1 + \frac{5\alpha}{d\mu} + \frac{1}{K}\right]. \tag{4.77}$$

Where we have used that the probability of fixation at a mutant state with no fitness difference is $1/N_T$ and the saturation value N_T is the same for all states in trajectory B (making (4.77) only valid in the case of costs $c = 0$). In the event that the rate of switching is comparable to the rate in which mutants are produced, such that $\alpha \approx \mu d$, this simplifies to $T_B \sim [6 + 1/K]/\mu d$. As in (4.75), this solution contains a term that is inversely proportional to the product μdK. However, as this term is part of a sum in (4.77), lowering K cannot reduce T_B below $\sim 6/\mu d$.

Figure 4.8B compares curves of T_B as a function of K. One curve is the analytic solution which includes the possibility of extinction. The analytic solution in (4.77) is approximately equal to this when $K \gtrsim 20$. This curve is presented alongside simulation data, which it shows good agreement with.

All of the methods and solutions contained in this section are only valid for the system in the SF regime. In the following section we will derive a condition for when this regime is expected to end.

4.5 Stochastic tunnelling regime

We look now at the *stochastic tunnelling* (ST) regime [75, 90, 201, 206]. In this regime, mutants are produced at greater rates than in the SF regime. Therefore cells are likely to be produced further along a sequence of mutations before cells in the earlier states reach fixation. This process, in which only a small subset of the population at an intermediate state produces the next mutant in the sequence, is referred to as stochastic tunnelling [90]. When this happens, the mutant lineages can be described as undergoing branching processes.

The behaviour characterising this regime typically occurs when the mutant production rate is large $\mu dK > 1$ but μ is still small enough for the dynamics to be stochastic. As $K \gg 1$ in this regime (and $\mu \ll 1$), extinction of the population is unlikely and can be ignored. In general, the adaptation time in this regime varies inversely with population size — due to the increased rate of mutant production at larger K. Therefore the adaptation times are often smaller than in the SF regime and we find that the drift dynamics of the mutant populations must now be incorporated.

We will begin by outlining the calculation of the adaptation time T for the generation of a double mutant by stochastic tunnelling. This can itself be part of a larger mutational process. To do this we follow the same approach as in [206] for the three states shown in Fig. 4.9. The population begins in state $i-1$, at time $t = 0$, and evolves by tunnelling through state i, to produce a cell in the target state $i+1$. We want to calculate the expected time it takes for the first cell to be produced at $i+1$. A mutant at state i that is termed "successful" is one that will go on to produce offspring in state $i+1$. Each mutant at i produces an independent lineage of cells that evolves by a continuous time branching process. All mutants therefore have the same probability of being successful (note this would not be the case if states had frequency dependent fitnesses). The following calculates properties for a single mutant lineage at i. We must therefore exclude the possibility of competing mutant lineages at the same state. This requirement will be used later to derive the conditions for being in this regime.

For the two step process in Fig. 4.9, the adaptation time T in the ST regime is

$$T = T_{i-1\to i|\mathrm{suc}} + \tau_i. \tag{4.78}$$

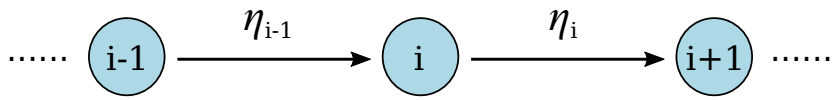

Figure 4.9 *A general two step process to acquire a double mutant. Cells in state $i-1$ can produce mutants in state i, which can produce mutants in state $i+1$. η_j is the rate that a cell in state j produces a mutant in state $j+1$.*

Here $T_{i-1\to i|\text{suc}}$ is the expected time it takes the population at $i-1$ to produce the first successful mutant at i, which will dominate T. τ_i is the expected time a successful mutant lineage at state i will drift before producing a cell at state $i+1$. To determine whether a mutant produced at i is successful we will calculate $P_i(t)$ — the probability that a mutant lineage at i, created at $t=0$, is successful (i.e. produced a cell at $i+1$) by time t. The probability of a mutant at i being at all successful is therefore $P_i = \lim_{t\to\infty} P_i(t)$. Furthermore if we know $P_i(t)$, the drift time τ_i can be calculated by

$$\tau_i = \int_0^\infty \left(1 - \frac{P_i(t)}{P_i}\right) dt. \tag{4.79}$$

To calculate $P_i(t)$ consider a mutant produced at state i. Let $n(t)$ be the number of mutant cells in this lineage at time t, with initial condition $n(t=0)=1$. The size of the lineage fluctuates in time until it dies out ($n(t)=0$) or produces a cell in the next mutant state $i+1$. In a single realisation of the stochastic process, i.e. one particular trajectory $n(t)$ out of the set of possible trajectories $\{n(t)\}$, the probability that the lineage produces the mutant $i+1$ in time interval $t\to t+dt$ is $\eta_i n(t)dt$, where η_i is the rate with which a cell of type i produces a cell of type $i+1$ (see Fig. 4.9).

The waiting time for a cell to be created at $i+1$, from a fluctuating population at i, can be described by an inhomogeneous Poisson process. The probability that a particular trajectory $n(t)$ produces a mutant at $i+1$ by time t is therefore

$$\begin{aligned} P_i(n(t)) &= 1 - \exp\left(-\int_0^t \eta_i n(t')dt'\right) \\ &= 1 - \exp\left(-\eta_i W(t)\right), \end{aligned} \tag{4.80}$$

where $W(t) = \int_0^t n(t')dt'$. If we average (4.80) over all possible lineage trajectories

$\{n(t)\}$ we get the following expression for $P_i(t)$

$$\begin{aligned} P_i(t) &= \int P_i(n(t))D[n(t)] && (4.81)\\ &= \int \left[1-\exp\left(-\eta_i W(t)\right)\right] D[W(t)] && (4.82)\\ &= \int_0^\infty \left(1-e^{-\eta_i w}\right) P_i(n,w,t)dwdn. && (4.83)\end{aligned}$$

Here $P_i(n,w,t)$ is the probability density function, such that $P_i(n,w,t)dt$ equals the probability that for a realisation of the process $W(t)=w$ and $n(t)=n$ in time $t \to t+dt$.

Let us now introduce $\Phi_i(x,y,t)$ as the Laplace transform of the probability density function $P_i(n,w,t)$. The variables n and w are discrete and continuous respectively and therefore

$$\Phi_i(x,y,t) = \sum_{n=0}^{+\infty} \int_0^\infty P_i(n,w,t)e^{-xn-yw}dw. \qquad (4.84)$$

If we can calculate $\Phi_i(x,y,t)$, then $P_i(t)$ can be found by (4.83) to be $P_i(t) = 1-\Phi_i(x=0,y=\eta_i,t)$. Now $\Phi_i(x,y,t)$ can be calculated as follows. For a lineage, consider how $P_i(n,w,t)$ evolves in time $t \to t+dt$ through the birth and death of cells in it.

$$\begin{aligned} P_i(n,w,t+dt) = \quad & \overbrace{(n+1)d_iP_i(n+1,w-ndt,t)dt}^{\text{death}} \\ & + \underbrace{(n-1)b_iP_i(n-1,w-ndt,t)dt}_{\text{birth}} \\ & + \underbrace{\left[1-n(d_i+b_i)dt\right]P_i(n,w-ndt,t)}_{\text{no change}}. \qquad (4.85)\end{aligned}$$

Here b_i and d_i are the rates that cells of type i reproduce (i.e. produce offspring of their own type — not mutants) and die respectively. By expanding the terms $P_i(\ldots,w-ndt,t)$ about w, to first order in dt we get that

$$\begin{aligned} P_i(n,w,t+dt) &= (n+1)d_iP_i(n+1,w,t)dt + (n-1)b_iP_i(n-1,w,t)dt \\ &\quad + \left(1-n(d_i+b_i)dt\right)P_i(n,w,t) - ndt\frac{\partial P_i(n,w,t)}{\partial w}. \qquad (4.86)\end{aligned}$$

This can be rearranged to get the following differential equation describing the

evolution of $P_i(n, w, t)$ in time

$$\begin{aligned}\frac{\partial P_i(n,w,t)}{\partial t} &= (n+1)d_iP_i(n+1,w,t) + (n-1)b_iP_i(n-1,w,t) \\ &\quad -n(d_i+b_i)P_i(n,w,t) - n\frac{\partial P_i(n,w,t)}{\partial w}. \end{aligned} \tag{4.87}$$

If we multiply this by $\exp(-xn - yw)$, then integrate over w and sum over n we get

$$\begin{aligned}\frac{\partial \Phi_i(x,y,t)}{\partial t} &= \sum_{n=0}^{+\infty}\int_0^{\infty}\Big[(n+1)d_iP_i(n+1,w,t) + (n-1)b_iP_i(n-1,w,t) \\ &\quad - n(d_i+b_i)P_i(n,w,t) - n\frac{\partial P_i(n,w,t)}{\partial w}\Big]e^{-xn-yw}dw. \end{aligned} \tag{4.88}$$

This can be expressed as the following PDE, using the definition of $\Phi_i(x, y, t)$ from (4.84).

$$\frac{\partial \Phi_i}{\partial t} = \left[-d_ie^x - b_ie^{-x} + (d_i+b_i) + y\right]\frac{\partial \Phi_i}{\partial x}. \tag{4.89}$$

This is of a form that can be solved by the method of characteristics, which is carried out in Appendix C. Doing this gives us

$$\Phi_i(x, y=\eta_i, t) = \frac{\sigma_i^+(e^{-x}-\sigma_i^-)e^{-b_i(\sigma_i^+-\sigma_i^-)t} - \sigma_i^-(e^{-x}-\sigma_i^+)}{(e^{-x}-\sigma_i^-)e^{-b_i(\sigma_i^+-\sigma_i^-)t} - (e^{-x}-\sigma_i^+)}, \tag{4.90}$$

where

$$\sigma_i^{\pm} = \frac{(d_i+\eta_i+b_i) \pm \sqrt{(d_i+\eta_i+b_i)^2 - 4d_ib_i}}{2b_i}. \tag{4.91}$$

From (4.90) the form of $P_i(t)$ can be calculated to be

$$\begin{aligned} P_i(t) &= 1 - \Phi_i(x=0, y=\eta_i, t) \\ &= \frac{(1-\sigma_i^+)(1-\sigma_i^-)(e^{-b_i(\sigma_i^+-\sigma_i^-)t}-1)}{\sigma_i^+ - 1 + (1-\sigma_i^-)e^{-b_i(\sigma_i^+-\sigma_i^-)t}}, \end{aligned} \tag{4.92}$$

while the probability of a mutant at i being successful is

$$P_i = \lim_{t\to\infty} P_i(t) = 1 - \sigma_i^-. \tag{4.93}$$

Having calculating $P_i(t)$, all terms in (4.78) can now be calculated, giving the

adaptation time T to be

$$T = \overbrace{\frac{1}{\eta_{i-1}N_{i-1}P_i}}^{T_{i-1\to i|\mathrm{suc}}} + \overbrace{\int_0^\infty \left(1 - \frac{P_i(t)}{P_i}\right) dt}^{\tau_i} \tag{4.94}$$

$$= \frac{1}{\eta_{i-1}N_{i-1}(1-\sigma_i^-)} + \frac{1}{\eta_i(1-\sigma_i^-)} \ln\left[\frac{\sigma_i^+ - \sigma_i^-}{\sigma_i^+ - 1}\right]. \tag{4.95}$$

Here we have defined the population size at the initial state $i-1$ to be N_{i-1}. The dependence of T on N_{i-1} only appears in the first term in (4.95), in which it is inversely proportional to T. All other quantities in (4.95), such as $\sigma_i^\pm$ depend only on the rates of cellular actions and not population size. Therefore this predicts that $T(N_i)$ is a monotonically decreasing function. This makes sense: as the mutation production rate increases, then it should take less time for a population to tunnel stochastically.

This method, carried out here for a general two-step process (Fig. 4.9), can be applied to sequences of mutations that exceed a length of two. In what follows we do this when calculating T_B for trajectory B in Fig. 4.1. Note, despite Fig. 4.9 only showing mutations occurring in one direction, this method does not exclude mutant lineages from producing mutants "backwards" (i.e. to the preceding state in the mutational sequence). Such an inclusion would only affect the rates involved in the process (e.g. the growth rate of the lineage at i) and not the method itself.

4.5.1 Boundary between the SF and ST regime

We now calculate the boundary between the SF and ST regimes. For the general sequence of mutations in Fig. 4.9, we consider the boundary for state i to be when the probability of a mutant fixing at i is comparable to the probability P_i that it is successful by tunnelling (4.93). Therefore the boundary is considered to be when

$$P_i = \begin{cases} \frac{1}{\left(1-\frac{d}{r_i}\right)K} & \text{if } \delta = 0 \\ \frac{1-e^{\delta}}{1-e^{\delta\left(1-\frac{d}{r_i}\right)K}} & \text{if } \delta > 0. \end{cases} \tag{4.96}$$

Expressing these as conditions for K, which we label as $K^{\times}_{\mathrm{SF/ST}}$, gives us

$$K^{\times}_{\mathrm{SF/ST}} = \begin{cases} \frac{1}{\left(1-\frac{d}{r_i}\right)P_i} & \text{if } \delta = 0 \\ \frac{1}{\left(1-\frac{d}{r_i}\right)\delta} \ln\left(\frac{\delta}{P_i}\right) & \text{if } \delta > 0. \end{cases} \tag{4.97}$$

For sequences of mutations with more than one transient state, such as trajectory B, these states can exist in different regimes to one another. When this happens the system is in a *mixed regime*.

Consider a population and sequence of mutations in which all states are in the SF regime. On increasing K, the boundary condition of (4.97) is normally first satisfied by the final transient state in the sequence, before proceeding backwards along the sequence of remaining states. This is due to P_i being significantly smaller the further along the sequence of mutations that the state i is.

4.5.2 Trajectory A

We now apply this method to calculate the adaptation time T_A for network A in Fig. 4.1. This process is identical to the generation of a double mutant that we went through above, which culminated in (4.95). Therefore we can directly say that the adaptation time T_A is of the form

$$T_A = T_{1\mathrm{A}\to 2\mathrm{A}|\mathrm{suc}} + \tau_{2\mathrm{A}}, \tag{4.98}$$

in which

$$T_{1\mathrm{A}\to 2\mathrm{A}|\mathrm{suc}} = \frac{1}{\left(1-\frac{d}{r_{1\mathrm{A}}}\right) K d\mu (1-\sigma^{-}_{2\mathrm{A}})} \tag{4.99}$$

$$\tau_{2\mathrm{A}} = \frac{r_{1\mathrm{A}}}{r_{2\mathrm{A}} d(1-2\mu)(1-\sigma^{-}_{2\mathrm{A}})} \ln\left[\frac{\sigma^{+}_{2\mathrm{A}} - \sigma^{-}_{2\mathrm{A}}}{\sigma^{+}_{2\mathrm{A}} - 1}\right] \tag{4.100}$$

and from (4.91) we know that

$$\sigma^{\pm}_{2\mathrm{A}} = \frac{r_{1\mathrm{A}} + r_{2\mathrm{A}}(1-\mu) \pm \sqrt{(r_{1\mathrm{A}} + r_{2\mathrm{A}}(1-\mu))^2 - 4 r_{1\mathrm{A}} r_{2\mathrm{A}}(1-2\mu)}}{2 r_{2\mathrm{A}}(1-2\mu)}. \tag{4.101}$$

We shall now compare this solution for T_A, with the equivalent one for T_A in the SF regime in (4.75). The ST solution contains an extra term, being the

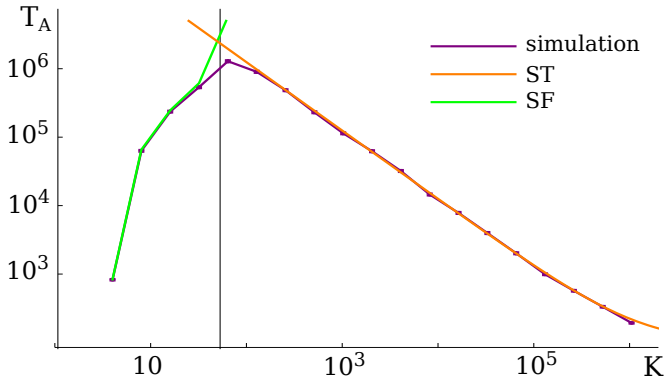

Figure 4.10 *The adaptation time T_A as function of K across the SF and ST regimes. Plot shows the analytic T_A in the SF and ST regimes alongside simulation data. A vertical line indicates the analytically predicted boundary between the SF and ST regime. Parameters used are $\mu = 10^{-4}, \delta = 0.1$ and $d = 0.1$. Simulation data is gathered using a KMC algorithm and averaged over 10^3 runs.*

contribution from the drift time of the successful mutant lineage at 2A. Otherwise both equations are approximately the same, predicting T_A to be dominated by the time it takes the population at 1A to produce a successful mutant, which is $\sim 1/(\mu d K P_{2\mathrm{A}})$. The key difference between the two solutions, leading to the quantitatively different behaviour in these regimes, is the form that $P_{2\mathrm{A}}$ takes. In (4.75) this is the probability that a mutant at 2A reaches fixation, which decreases with increasing K according to (4.74). However, in the ST regime, $P_{2\mathrm{A}}$ is independent of K which leads to a monotonically decreasing $T_A(K)$.

Figure 4.10 compares analytic curves of T_A in the SF and ST regimes as a function of K. These are plotted alongside simulation data and a vertical line predicting the boundary between the SF and ST regimes, using the condition in (4.97). This boundary prediction matches approximately where the two analytic solutions intersect. Away from the boundary, the analytic solutions in both regimes match well with the simulation data. However, for K values near the boundary there is some disagreement between the analytic and simulation results. This is not surprising however, as in the cross-over region between the SF and ST regimes, a population's dynamics will be less predictable and unable to be characterised by a single type of behaviour.

Note that the solution for T_A derived in this section can be used to describe the $\alpha = 0$ curve observed earlier in Fig. 3.3B, along with the approximate $T \sim 1/\mu^2$ relationship we observed in it.

4.5.3 Trajectory B

We now calculate the adaptation time T_B for trajectory B in Fig. 4.1. To do this we apply the same method as for calculating T_A but extend it to consider more than one transient state (3 in this case) between the initial and target states (1A and 3A respectively). As mentioned earlier, the system can exist in a number of mixed regimes that share SF and ST dynamics. In the following we begin by calculating the solution for T_B in the full ST regime. From there we will go on to calculate T_B for the two mixed regimes.

In the full ST regime the adaptation time T_B is of the general form

$$T_B = T_{1\text{A}\to 1\text{B}|\text{suc}} + \tau_{1\text{B}} + \tau_{2\text{B}} + \tau_{3\text{B}}. \tag{4.102}$$

This sum includes $T_{1\text{A}\to 1\text{B}|\text{suc}}$, the expected time to produce a successful mutant at 1B, and a drift time τ_i for each intermediate state. Note that $P_{1\text{B}}$ — the probability that a mutant is successful at 1B — will be a function of the probabilities that mutants at the later states are successful, i.e. $P_{2\text{B}}$ and $P_{3\text{B}}$. The quantities $P_i(t)$ are all calculated in the same way as described for the general process in Fig. 4.9. Therefore the specifics of their derivations are excluded in the following.

Note that when calculating how mutant lineages at state 1B can change, we ignore the possibility of cells being able to phenotype switch back to 1A. Alternatively, such an action could be included and considered equivalent to a cell "death" in the lineage. However, the evolving mutant lineage at 1B will be a small population compared to the main population at 1A. Therefore if switching 1B→1A is frequent enough to concern us, then even more frequent will be the switch 1A→1B, at which point the system would not be in the ST regime to begin with (as we would predict competing lineages at 1B). Therefore switches 1B→1A can be ignored in this regime.

By calculating all of the quantities P_i (which are listed in Appendix D), these can be substituted into (4.102), to give the solution

$$T_B = \frac{1}{(1-\frac{d}{r_{1\text{A}}})K\alpha P_{1\text{B}}} + \sum_i \frac{1}{b_i(1-\sigma_i^-)} \ln\left[\frac{\sigma_i^+ - \sigma_i^-}{\sigma_i^+ - 1}\right]. \tag{4.103}$$

The sum here is over states 1B, 2B and 3B. The specific values for all σ_i^+ and σ_i^- values can also be found in Appendix D.

With three transient states there are two possible regimes mixing both SF and ST dynamics. In discussing these regimes we will adopt the notation that the adaptation time T_B^{ijk} is for when states 1B, 2B and 3B are in the regimes denoted by i, j and k respectively. If all states are in the same regime then this regime will be identified by the single superscript i in T_B^i.

On increasing K from the full SF regime, state 3B first breaks the regime condition of (4.97). This creates the regime in which states 1B and 2B are in the SF regime while 3B is in the ST regime. The adaptation time in this regime T_B^{SFSFST} is given by

$$T_B^{SFSFST} = \tau_{SF} + \tau_{3B}. \tag{4.104}$$

Here τ_{3B} is the drift time at state 3B, while τ_{SF} is the contribution to the time by the population behaving as it does in the SF regime over the relevant part of the network. Therefore τ_{SF} is the time it takes the entire population to perform a random walk to 2B and then produce a successful mutant at 3B. Note that this includes the possibility of the population reaching 2B and then leaving it before producing the successful mutant at 3B.

We jump straight to results for τ_{SF} and τ_{3B} here, as the derivations are similar to what we considered before. When the fitness costs $c = 0$, these terms are given by the following

$$\tau_{SF} = \frac{P_{3B}d^2K\mu + (3 - 2P_{3B}K)\alpha r_1 + P_{3B}dK(2\alpha - \mu r_1)}{P_{3B}dK\alpha\mu(d - r_1)} \tag{4.105}$$

$$\tau_{3B} = \frac{1}{b_{3B}(1 - \sigma_{3B}^-)} \ln\left[\frac{\sigma_{3B}^+ - \sigma_{3B}^-}{\sigma_{3B}^+ - 1}\right]. \tag{4.106}$$

Continuing to increase K, state 2B is the next one to break condition (4.97). This puts state 1B in the SF regime while 2B and 3B are in the ST regime. The adaptation time T_B^{SFSTST} is therefore

$$T_B^{SFSTST} = \tau_{1B}^{SF} + \tau_{2B} + \tau_{3B}, \tag{4.107}$$

which is a sum of the drift times at states 2B and 3B, plus the time it takes the population (moving as a random walker) to reach 1B, from which it produces a successful mutant at 2B.

Again, skipping these repetitive derivations, we find that for no fitness costs (i.e.

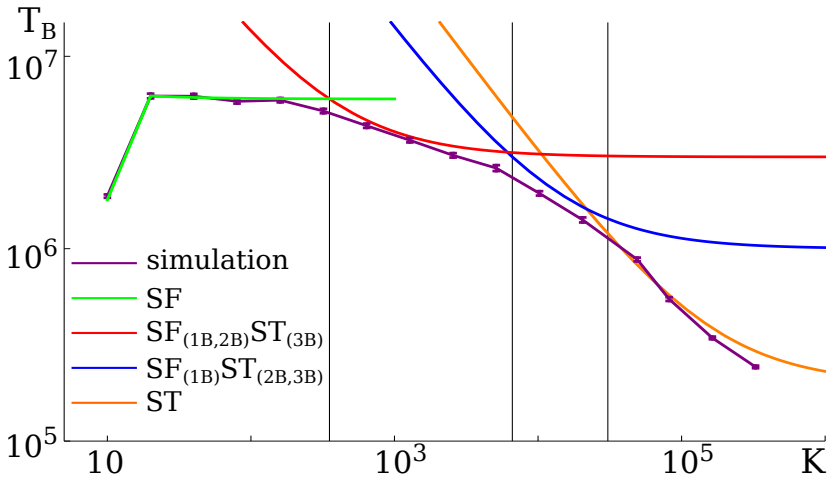

Figure 4.11 *The adaptation time T_B as function of K as the system moves from the SF to ST regimes. Curves shows the analytic derived T_B in the SF, ST and mixed regimes alongside simulation data. Vertical lines indicate the analytically predicted boundaries between regimes. Parameters used are $\mu = 10^{-5}, \alpha = 10^{-6}$ and $d = 0.1$. Simulation data is gathered using a KMC algorithm and averaged over 10^3 runs.*

$c = 0$), the terms in (4.107) are equal to

$$\tau_{1B}^{SF} = \frac{P_{2B} dK\mu(r_1 - d) + 2\alpha r_1}{P_{2B} dK\alpha\mu(r_1 - d)} \tag{4.108}$$

$$\tau_{2B} + \tau_{3B} = \sum_i \frac{1}{b_i(1 - \sigma_i^-)} \ln\left[\frac{\sigma_i^+ - \sigma_i^-}{\sigma_i^+ - 1}\right], \tag{4.109}$$

where the sum runs over the states 2B and 3B.

Presented in Fig. 4.11 is a plot of simulation data alongside numerous analytic curves of T_B as a function of K. The range of K values considered shows the system progressing from the full SF regime, through the two mixed SF/ST regimes, to finish in the full ST regime. Vertical lines are included, which identify the analytic boundaries between the regimes. These were predicted by considering when each state breaks the condition in (4.97). In general we observe a good match between the analytic curves and simulation data. There is also a good match between where the curves intersect and the predicted regime boundaries, except for at the regime boundary at the largest K value. In the vicinity of the boundaries we see deviation between the curves and simulation data, but this is expected.

The analytic solutions derived in this section can be used to understand the

curve of $\alpha = 10^{-4}$ that we saw earlier in Fig. 3.3B. In Chapter 3 we numerically identified the relationship $T \sim 1/\mu$ in the curve prior to its convergence with the $\alpha = 0$ curve at large μ. The results of this section support this as being consistent with the analytic solution for T_B^{SFSFST} (with the parameters used to produce the results of Fig. 3.3B placing the system in this dynamical regime). Note however, the results shown in Fig. 3.3B are for the full network of states shown in Fig. 3.1A, not the subnetwork in Fig. 4.1B that this analytic solution was derived for. Nevertheless this chapter seeks to demonstrate that this solution is often applicable to describe the full system adaptation time T. Therefore we can hypothesise that in Fig. 4.1B the significantly lower curve of $T(\mu)$ when phenotype switching is present (compared with the $\alpha = 0$ curve) is due to the population travelling to the target state primarily by trajectory B. A numerical study of the trajectories taken by successful cells would be able to verify if this is the case.

4.6 Semi-deterministic regime

Consider now the same general process shown in Fig. 4.9. If we continue to increase the rate of mutant production (e.g. by increasing K) then the population at state i will eventually leave the ST regime. This happens when mutants are produced at state i (from $i-1$) frequently enough that competing successful lineages are expected to exist there simultaneously. This violates the conditions of the ST regime, putting the system in the *semi-deterministic* (SD) regime [206].

In the SD regime, we can employ a joint deterministic and stochastic description for the process. The growth of the population at i is treated deterministically. However, the waiting time for it to produce a successful mutant at $i+1$ remains described by an inhomogeneous Poisson process.

We will define the boundary between the ST and SD regimes, $K^{\times}_{ST/SD}$ for state i, to occur when the drift time at i is comparable to the time it takes for a successful mutant to be produced there. Therefore this is when

$$T_{i-1\to i|\text{suc}} = \tau_i. \tag{4.110}$$

If there are more transient states than just i in the mutational sequence, then we will expand the right hand side of (4.110) to be the sum of the drift times at the

remaining transient states.

For trajectory A this regime is not significant. In this case condition (4.110) becomes $T_{1\mathrm{A}\to 2\mathrm{A}|\mathrm{suc}} = \tau_{2\mathrm{A}}$ and yields the following boundary condition for K

$$K^{\times}_{\mathrm{ST/SD}} \sim \frac{(1-\delta)}{\mu \ln\left[\dfrac{\sigma^{+}_{2\mathrm{A}} - \sigma^{-}_{2\mathrm{A}}}{\sigma^{+}_{2\mathrm{A}} - 1}\right]}. \tag{4.111}$$

In general this is an extremely large quantity, predicting a boundary value by which point the system is better described deterministically. This is due to the comparatively large likelihood that a population at 2A will produce a successful mutant at 3A, given that a successful mutant at 3A is simply one that is produced there.

On the other hand, for trajectory B this can be a significant regime. It occurs when

$$\frac{1}{\alpha \underbrace{(1-\frac{d}{r_{1\mathrm{B}}})K^{\times}_{\mathrm{ST/SD}}}_{N_{1\mathrm{A}}} P_{1\mathrm{B}}} = \tau_{1\mathrm{B}} + \tau_{2\mathrm{B}} + \tau_{3\mathrm{B}}, \tag{4.112}$$

which predicts the following boundary value

$$K^{\times}_{\mathrm{ST/SD}} = \frac{1}{\alpha\left(1-\frac{d}{r_{1\mathrm{B}}}\right) P_{1\mathrm{B}} \sum_i \tau_i}. \tag{4.113}$$

The drift terms, τ_i, remain those that were calculated for the ST regime, which are included in Appendix D. We now calculate the adaptation time T_B in the SD regime, which is of the form

$$T_B = \tau_{SD1B} + \tau_{2\mathrm{B}} + \tau_{3\mathrm{B}}. \tag{4.114}$$

Here τ_{SD1B} is the waiting time for the deterministically growing population at 1B to produce a successful mutant at 2B. While $\tau_{2\mathrm{B}}$ and $\tau_{3\mathrm{B}}$ remain the drift times of successful mutants at 2B and 3B respectively.

Consider the deterministic growth of the population at 1B ($N_{1\mathrm{B}}$). This is governed

by

$$\frac{dN_{1\mathrm{B}}}{dt} = \xi r_{1\mathrm{B}} N_{1\mathrm{B}}(1-\mu) - \alpha N_{1\mathrm{B}} + N_{1\mathrm{A}}\alpha - N_{1\mathrm{B}} d \tag{4.115}$$

$$\approx \underbrace{\left[\left(\frac{r_{1\mathrm{B}}}{r_{1\mathrm{A}}}\right)(1-\mu)d - 2\alpha - d\right]}_{-\gamma} N_{1\mathrm{B}} + \underbrace{(1-d)K\alpha}_{\rho}, \tag{4.116}$$

with the initial condition that $N_{1B}(0) = 0$. Here ξ again represents the logistic factor $(1 - \frac{N_T}{K})$, which with the saturation value of (4.8) becomes $\xi \approx d$. The first order linear ODE of (4.116) is trivial to solve and has the solution

$$N_{1\mathrm{B}}(t) = \frac{\rho}{\gamma}(1 - e^{-\gamma t}). \tag{4.117}$$

Therefore the waiting time τ_{SD1B} for the population at 1B to produce a successful mutant at 2B, described by an inhomogeneous Poisson process is

$$\tau_{\mathrm{SD1B}} = \int_0^\infty \exp[-\lambda \int_0^{t'} N_{1\mathrm{B}}(t'')dt'']dt' \tag{4.118}$$

$$= \int_0^\infty \exp[-\lambda \frac{\rho}{\gamma}[t' + \frac{1}{\gamma}(e^{-\gamma t'} - 1)]]dt' \tag{4.119}$$

$$\approx \sqrt{\frac{\pi}{2\lambda\rho}} \quad \text{if} \quad |\gamma t| \ll 1. \tag{4.120}$$

Where the rate $\lambda = \eta_{1\mathrm{B}\to 2\mathrm{B}} P_{2\mathrm{B}} \approx \mu d P_{2\mathrm{B}}$. The approximation that was used to get (4.120) involved expanding $e^{-\gamma t'}$ to second order in $\gamma t'$ and solving the resultant Gaussian integral. Therefore (4.120) is only valid when $t \ll 1/(\mu d + 2\alpha)$. In general, times this low are common in the SD regime. However, as we cannot guarantee this condition will always be satisfied, in the following results we will use the numerical solution of (4.119).

Figure 4.12 compares curves of the adaptation time T_B as a function of the carrying capacity K. One of these curves (orange) is the numerical solution to (4.119) while the other is simulation data (purple curve). Included are two vertical lines; the one at smaller K identifies the boundary between the ST and SD regimes ($K^{\times}_{\mathrm{ST/Det}}$) while the other is the boundary between the SD and full Det regime, which we will discuss shortly. Very good agreement is shown between the solution for T_B and simulation data in the range identified for the SD regime.

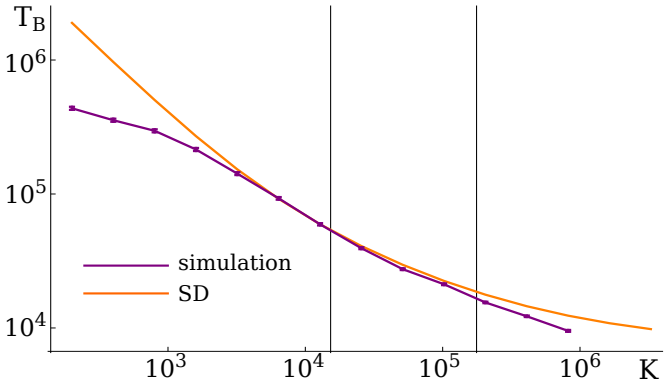

Figure 4.12 *The adaptation time T_B as function of K for the system in the SD regime. The curves shows T_B, calculated numerically from 4.119, alongside simulation data. Vertical lines indicate the predicted boundaries of this regime — with the analytic ST/SD boundary on the left and the numerical SD/Det boundary on the right. The parameters used are $\mu = 10^{-4}, \alpha = 10^{-5}$ and $d = 0.1$.*

4.6.1 Boundary between the SD and Det regimes

We consider now the parameter values at which the SD regime ends, at which point we describe the system as entering the *deterministic* (Det) regime. The analysis in the Det regime was already considered at the beginning of this chapter. The boundary between the SD and Det regimes happen when successful mutants are produced at 2B quicker than successful cells take to drift at states 2B and 3B. This leads again to a competition between successful mutant lineages and causes our analytic method to break down. In work that is not presented we attempted to extend the analysis of the SD regime by considering the population at state 2B to grow deterministically, while the population still stochastically tunnelled through 3B. However, the analytic results derived did not match the observed behaviour of the population in simulations. Therefore at this point we concede to a fully deterministic description.

The boundary between the SD and Det regime will therefore occur when

$$\frac{1}{N_{1\mathrm{B}}(\tau_{\mathrm{SD1B}})\mu d} = \tau_{2\mathrm{B}} + \tau_{3\mathrm{B}}. \tag{4.121}$$

The function $N_{1\mathrm{B}}(t)$ was found in (4.117) and is here evaluated at the time τ_{SD1B} from (4.119). This will be dependent on K and can therefore be used to extract from (4.121) a boundary condition for K separating the SD and Det regimes. This is trivial to find if we can use (4.120). However, in the results that follow, due to our uncertainty regarding the validity of (4.120), it is calculated numerically

using (4.119). We have already seen one prediction for this boundary in Fig. 4.12.

The boundary value predicted by (4.121) is likely to be an overestimate (i.e. predicting the boundary to be at a larger K value than it should be). This is because it uses the quantity $N_{1B}(\tau_{SD1B})$, which is the size of the population at 1B when the first successful mutant is created at 2B. However, after this mutant arises the population at 1B is still expected to grow deterministically. Therefore the second mutant, which causes unwanted competition between lineages, is likely to arrive quicker than (4.121) predicts.

4.7 Beyond the two trajectory approximation

For values of α larger than the characteristic value α_c, variability increases in the trajectories taken by successful cells. This was demonstrated earlier in Fig. 3.9C. For $\alpha > \alpha_c$, successful cells no longer travel exclusively by trajectories A or B and the approximation that the adaptation time for the full system $T \approx \min[T_A, T_B]$ breaks down.

The optimal α range ends when α becomes large enough that cells travelling by phenotype B are unlikely to avoid the switch 2B→2A. This leads to the most probable ⊓⊓ trajectory in Fig. 3.9C. To calculate α_c we consider the following question: when do we expect the pool of cells at 2B — from which successful cells at 3B are produced — to include cells that have undergone the switch from states 2B→2A→2B?

To answer this we compare the time it takes for a population of cells at 2B to undergo the following processes. Process 1 involves the population producing a successful cell at state 3B (in time τ_1). Process 2 involves a cell, or its offspring, arriving back at state 2B having switched 2B→2A→2B (in time τ_2). Both of these processes are shown in Fig. 4.13. We consider the approximation $T \approx \min[T_A, T_B]$ to be invalid when $\tau_1 \gg \tau_2$.

When $\tau_1 \gg \tau_2$ is satisfied, the population at 2B, before producing a successful cell at 3B, is likely to contain cells that have switched to 2A and back. Whether these cells become a significant portion of the population or are lost through random drift is unknown to us. It is therefore at this point that our confidence in our knowledge of cell ancestries, as well as the validity of the mathematical description of the evolving lineages at 2B, must break down.

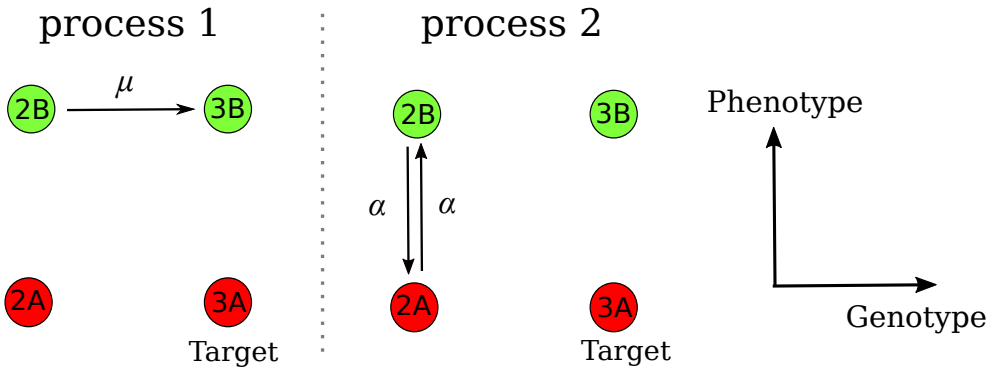

Figure 4.13 *The two processes that are compared to estimate the characteristic switching rate α_c. Process 1 involves a population of cells at 2B producing a successful cell — i.e. one expected to have progeny reach 3A — at state 3B. Process 2 involves a cell returning to state 2B having undergone the switches 2B→2A→2B.*

Note that when calculating τ_1 and τ_2 it is necessary to consider which dynamical regime the system is in for each process. For process 1 in the Det regime, we change the process slightly to be the time it takes a cell to appear at 3A rather than 3B. Describing the dynamics of single cells deterministically is inherently flawed, but this description seems more analogous to the stochastic scenario of a successful cell being produced at 2B.

The calculations for τ_1 and τ_2 are similar to those we considered earlier to calculate T_A and T_B. Therefore details of their calculations are excluded from here. In the upcoming results, α_c is calculated using an numerical algorithm that incrementally increases α and tests if the condition $\tau_1 \gg \tau_2 = 5\tau_2$ is satisfied. The α value it is first satisfied at is set to be α_c.

We expect α_c calculated in this manner to produce a crude underestimate of the actual α value at which this behaviour occurs. Testing if a single cell in the population at 2B has undergone 2B→2A→2B fails to account for two things: the first is whether this cell is expected to proliferate in the population once it returns to 2B. The second is that, at larger population sizes at 2B (e.g. when K is larger), it becomes less likely that this individual (or one of its progeny) will produce the first successful mutant at 3B. However, this estimate of α_c is still enough to demonstrate whether trajectory B is the most likely trajectory for intermediate α values. Therefore we will use it later in probing for the optimal α range.

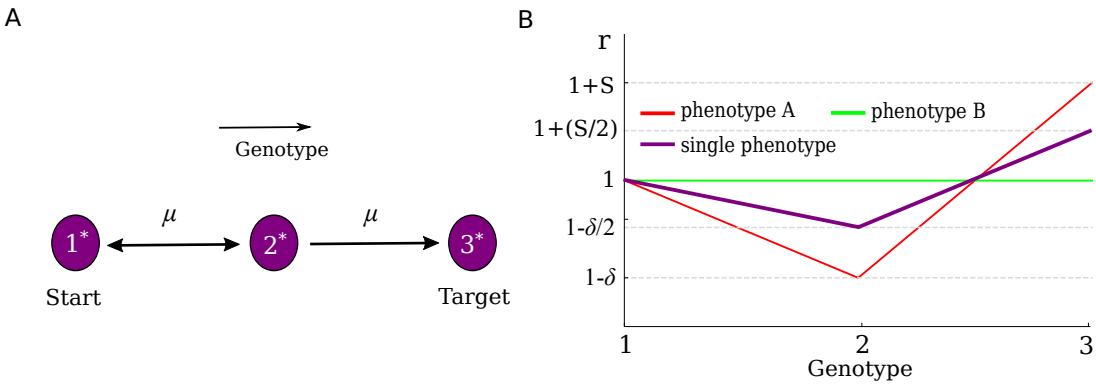

Figure 4.14 *Mapping from the two-phenotype model to a single phenotype model in the limit of large α. (A) The three state network in the single phenotype model that is mapped to. The new states $1^*, 2^*$ and 3^* are composed of both phenotypic states in the full model. (B) The fitness landscape of the single phenotype model compared with the landscapes of the two phenotype model. The single phenotype landscape has a reduced valley depth due to the averaging of the fitnesses of the deleterious state 2A with the fitter state 2B.*

4.8 Large switching rate limit

For $\alpha > \alpha_c$ we are unable to analytically calculate the full system adaptation time T until the large α limit α^* is reached. In this limit the two phenotype model can be mapped to a single phenotype model. This is shown in Fig. 4.14 where the new genotypes are labelled 1^*, 2^* and 3^*. The adaptation time in this limit is denoted T^*.

In this limit, the frequency of switching between phenotypes is too large for the selective differences between phenotypes to affect the population distribution between them. Instead, the population at a genotype is equally distributed between phenotypes A and B, regardless of the fitness differences between them. However, fitness differences between genotypes are still felt and the fitness of the "new" genotypes (i.e. 1^*, 2^* and 3^*) will be the average fitness of the (original) two states that make it up, i.e. $r_i = (r_{i\mathrm{A}} + r_{i\mathrm{B}})/2$. Therefore in this limit, the model maps to that of a single-phenotype model with a reduced valley depth compared to the original depth δ. The adaptation time T^* in this model can be calculated using the same methods as outlined earlier for T_A, for the same dynamical regimes.

We want to calculate how large α must be to observe this limiting behaviour. For this we calculate when α is large enough to result in approximately equal

population distributions between states 2A and 2B. We do this deterministically, which appears to hold up well even at small population sizes.

For a population confined to genotype 2, the population sizes $N_{2\mathrm{A}}$ and $N_{2\mathrm{B}}$ obey the following differential equations

$$\dot{N}_{2\mathrm{A}} = \xi N_{2\mathrm{A}} r_{2\mathrm{A}}(1-2\mu) + \alpha N_{2\mathrm{B}} - \alpha N_{2\mathrm{A}} - dN_{2\mathrm{A}} \tag{4.122}$$

$$\dot{N}_{2\mathrm{B}} = \xi N_{2\mathrm{B}} r_{2\mathrm{B}}(1-2\mu) + \alpha N_{2\mathrm{A}} - \alpha N_{2\mathrm{B}} - dN_{2\mathrm{B}}, \tag{4.123}$$

where $\xi = [1-(N_T/K)] \approx d$ is the logistic factor. These can be solved analytically to find the steady-state values of $N_{2\mathrm{A}}$ and $N_{2\mathrm{B}}$ as a function of α. The solution for the steady state distribution at 2B, expressed as a frequency $n_{2\mathrm{B}}$ such that $n_{2\mathrm{B}} = N_{2\mathrm{B}}/(N_{2\mathrm{A}} + N_{2\mathrm{B}})$, is

$$n_{2\mathrm{B}} = \frac{\delta d - (2-3\delta)\alpha + \sqrt{4\alpha^2(1-\delta) + (d+\alpha)^2\delta^2}}{2\delta(d+2\alpha)}. \tag{4.124}$$

The steady-state frequency of the population in state 2A is then just $n_{2\mathrm{A}} = 1 - n_{2\mathrm{B}}$. With these we set the fitness r_{2^*} of the new state 2^* to be the average such that

$$r_{2^*}(\alpha) = \frac{N_{2\mathrm{A}} r_{2\mathrm{A}} + N_{2\mathrm{B}} r_{2\mathrm{B}}}{N_{2\mathrm{A}} + N_{2\mathrm{B}}} = n_{2\mathrm{A}} r_{2\mathrm{A}} + n_{2\mathrm{B}} r_{2\mathrm{B}}. \tag{4.125}$$

It is straightforward to show in the limit of $\alpha \to \infty$ that $r_{2^*} = 1 - (\delta/2)$ when $r_{2\mathrm{A}} = 1 - \delta$ and $r_{2\mathrm{B}} = 1$, as expected. As this limit is approached, the curve of T^* as a function of α (related by the variable fitness $r_{2^*}(\alpha)$ at 2^*) captures well the levelling-off behaviour we observe in simulations. This can be observed in Fig. 4.15, which compares curves of simulation data with the analytic solution (i.e. T_A from earlier) using the variable fitness r_{2^*} for state 2^*.

In order to calculate a value for α^*, at which this limit is reached, we compare the single-phenotype adaptation time $T^*(r_{2^*}(\alpha))$ with the analytic solution for $T^*(\alpha \to \infty)$. $T(r_{2^*})$ will approach $T^*(\alpha \to \infty)$ from below as α increases (see Fig. 4.14). When $T(r_{2^*})$ is some multiple of $T^*(\alpha \to \infty)$, we will select that α value to be α^*. In the results that follow this multiple value is chosen to be 90%. For $\alpha \geq \alpha^*$, we will consider the large α regime to have been reached, beyond which the single phenotype model with variable fitness r_{2^*} can be used and there is little change in the curve of $T(\alpha)$.

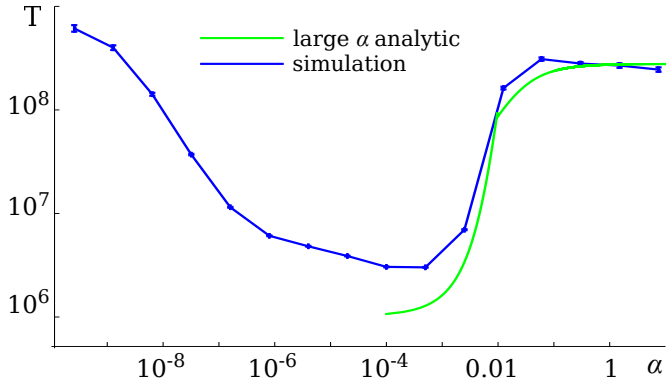

Figure 4.15 *Capturing the large α behaviour by mapping to a single-phenotype model. The plot compares curves of T as a function of α for simulation data with the single-phenotype analytic solution with variable valley depth $r_{2^*} = r_{2^*}(\alpha)$. The solution moves between the SF and ST regimes at $\alpha \sim 0.01$. Parameters used are $K = 100, \mu = 10^{-5}, \delta = 0.4$ and $d = 0.1$. Simulation data is averaged over 10^3 runs and collected using a KMC algorithm.*

4.9 Results

We now consider analytic (and some numerical) results that combine all of the solutions derived above, to predict how the adaptation time T varies with certain parameters. Data points were generated using an automated process (in *Mathematica*), which for each set of parameters, proceeds through the following algorithm:

1. If $\alpha < \alpha_c$
   (a) For trajectories A and B:
      i. Calculate the regime the system is in
      ii. Calculate the adaptation time in this regime (i.e. T_A and T_B)
   (b) The full system adaptation time $T = \min[\mathrm{T_A}, \mathrm{T_B}]$
2. If $\alpha_c \leq \alpha < \alpha^*$
   (a) No known value exists for T
3. If $\alpha \geq \alpha^*$
   (a) Using the single phenotype approximation with varying fitness $r_{2^*}(\alpha)$:
      i. Calculate the regime the system is in
      ii. Calculate the adaptation time T in this regime

4.9.1 Analytic predictions for the adaptation time T

We begin by testing the approximation that for $\alpha < \alpha_c$, the full system adaptation time $T \approx \min[\mathrm{T_A}, \mathrm{T_B}]$. Using an α value within this range, Fig. 4.16 shows various plots of the adaptation times (i.e T, T_A and T_B) as a function of K. Figure 4.16A shows the analytic curve of T_A as it moves through the SF and ST dynamical regimes. The regime boundary is identified as a dashed vertical line and the curve is a composite of the solutions in each regime. The third dynamical regime, the Det regime, is predicted to occur at larger K values ($K \sim 10^{11}$) than we consider here.

Figure 4.16B shows a similar composite curve but this time for T_B. This passes through all six possible regimes in the K range considered. Again, dashed vertical lines identify the regime boundaries and each regime is identified by text. For mixed regimes, subscripts identify which states are in which regime.

Figure 4.16C compares the curves of Figs. 4.16A and B in the same plot. As K increases, which curve has the lowest adaptation time proceeds as $T_A \to T_B \to T_A$. As $\alpha < \alpha_c$, this predicts that the population will travel by trajectory A, then B, then A again as each curve becomes the smallest.

Figure 4.16D plots a curve of $\min[\mathrm{T_A}, \mathrm{T_B}]$ as function of K, along with simulation data for the full system adaptation time T. We can see that the approximation $T \approx \min[\mathrm{T_A}, \mathrm{T_B}]$ matches very well with the simulation data for the entire K range considered. Therefore this approximation provides a good estimate for T when $\alpha < \alpha_c$, without the need to consider the complexity of the full network of states (Fig. 3.1A).

We consider now generating curves of T as a function of α using this composite method (outlined at the beginning of Section 4.9). Figure 4.17A shows independently predicted curves, valid within the regions that are identified. Included are three analytic solutions (T_A, T_B and T for when $\alpha \geq \alpha^*$) expected to be valid at different values of α. Dashed vertical lines identify the range $\alpha_c \leq \alpha < \alpha^*$ in which there is no analytic solution. The line at α_c (left line) indicates where the approximation $T \approx \min[\mathrm{T_A}, \mathrm{T_B}]$ breaks down, while the line at α^* (right line) identifies when the large α limit solution (with varying fitness r_{2^*}) can be used. Here this is estimated to be when T is 90% of the $T(\alpha \to \infty)$ value).

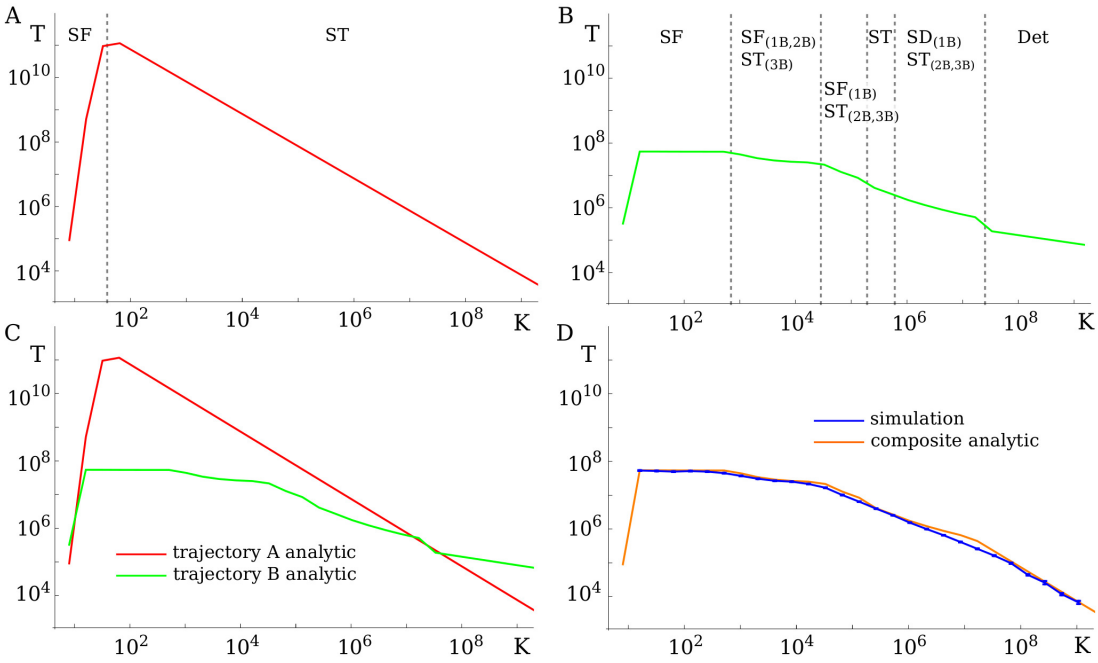

Figure 4.16 *Testing the approximation that the full system adaptation time* $T \approx \min[\mathrm{T_A}, \mathrm{T_B}]$ *when* $\alpha < \alpha_c$. *(A) and (B) show composite analytic curves of* T_A *and* T_B *as a function of* K *where the population evolves by trajectories A and B respectively. Vertical lines indicate the regime boundaries, where one solution for* T *ends and the next begins. Text identifies what regime the system is in at each* K *value, with mixed regimes including subscripts that identify which states are in which regime. (C) Compares the curves of (A) and (B), in which the smallest of* T_A *and* T_B *can be identified over the range of* K *values. (D) A plot comparing the quantity* $\min[\mathrm{T_A}, \mathrm{T_B}]$ *as a function of* K *with the full system adaptation time* T. *Parameters used are* $\mu = 10^{-6}, \delta = 0.4, \alpha = 2.56 \times 10^{-7}$ *and* $d = 0.1$. *All simulation data is averaged over* $10^2 \rightarrow 10^3$ *runs and collected using a* τ *leap algorithm.*

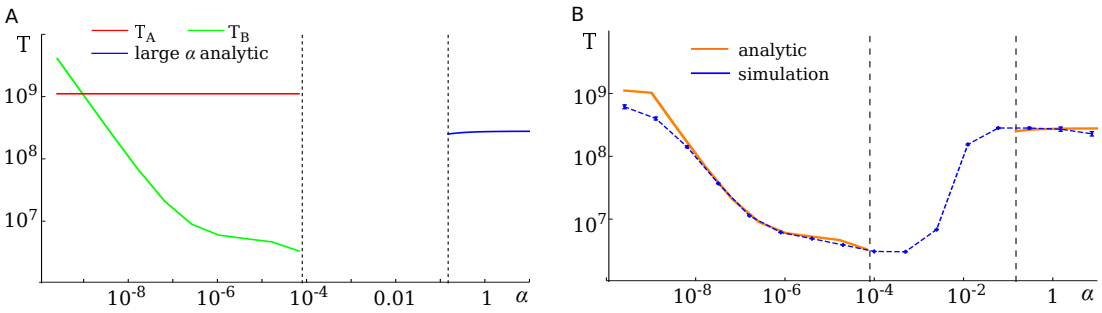

Figure 4.17 *Constructing a curve of the adaptation time T as a function of α. (A) A plot presenting curves that consist of all known information on the shape of the final curve. This includes the analytic solutions T_A, T_B and the solution when $\alpha \geq \alpha^*$ which corresponds to mapping to the single phenotype problem with varying fitness. Dashed vertical lines indicate α_c (left line) where we expect the approximation $T = \min[\mathrm{T_A}, \mathrm{T_B}]$ to breakdown, and α^* (right line). (B) A composite plot of T vs α that combines the curves in (A) alongside simulation data. Parameters used are $K = 100, \mu = 10^{-5}, \delta = 0.4$ and $d = 0.1$. All simulation data is averaged over 10^3 runs and gathered using a KMC algorithm.*

These solutions combine to form the broken curve of $T(\alpha)$ in Fig. 4.17B. Simulation data is included for comparison. We observe there to be a good match between the analytic and simulation curves, except at very low α values where the transition between two solutions occurs (that of T_A and T_B) and there is therefore some discrepancy.

This same approach is used to produce the plots of T as a function of α in Fig. 4.18. The plots here are for a much lower value of the mutation probability, $\mu = 10^{-9}$, and consider two values of K ($K = 10^6$ and 10^9 in Figs. 4.18A and B respectively). This value of μ is a more biologically relevant one than we have previously considered; being comparable with the probability of base pair mutation during DNA replication in microbes [47][116]. The plots also look at larger values of K, which are closer to the kind of microbial population sizes studied in the laboratory. Both these plots show the optimal α range to exist and result in a significant reduction in T (by orders of magnitude).

The magnitude of the reduction in $T(\alpha)$ in the optimal α range predicted in Fig. 4.18 is similar to that seen in Fig. 4.17. We can hypothesise that this magnitude depends strongly on the valley depth parameter δ, which we do not explore different values of in this chapter. Nevertheless, as δ reduces, the adaptation time T_A will also reduce, while T_B will remain unchanged (as trajectory B avoids the valley state and T_B will therefore be independent of δ).

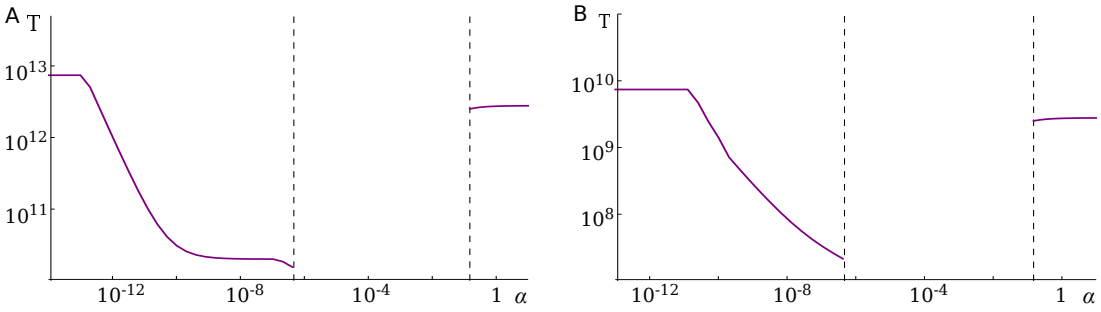

Figure 4.18 *Composite analytic curves predicting the adaptation time T as a function of α. (A) considers this for $K = 10^6$ while (B) is for $K = 10^9$. The remaining parameters are $\mu = 10^{-9}, \delta = 0.4$ and $d = 0.1$.*

Therefore we expect as δ reduces, that the magnitude of the reduction in $T(\alpha)$ in the optimal α range will increase.

4.9.2 The existence of the optimal α range

Following our observation of the optimal α range in Fig. 4.18, we will now search for it in (K, α) space. In the following, the optimal range is identified as being when the most probable trajectory is type B (i.e. when $T_B < T_A$) and $\alpha < \alpha_c$. These conditions are satisfied at the initial decrease of the $T(\alpha)$ curve, which α_c falls at the minimum of (see Fig. 4.18). Therefore the optimal range is expected to extend to larger α values than these conditions predict (in which we have no analytic solution for T). Nevertheless, these conditions are suitable to identify whether the optimal range exists at all.

We begin by considering (K, α) space when only one of these conditions is satisfied; that of $T_B < T_A$. In the following, each data point is represented by an icon. Each icon includes a trajectory symbol of ▁ or ⊓, identifying trajectory A or B respectively as the most likely. The icons also have background colours, which identify the dynamical regime the system is in at that value of (K, α).

Figures 4.19A and B show (K, α) space for $\mu = 10^{-6}$ and $\mu = 10^{-9}$ respectively. Each data point is represented by an icon, as explained above. We observe large regions of (K, α) space in which T_B is lower than T_A. In Fig. 4.19B, with the lower mutation probability μ, this region extends to much larger values of K, reaching values of interest for microbial experiments. We can observe that, for fixed α, as K is increased the system moves through the dynamical regimes in the order predicted. Some types of dynamics (i.e. dynamical regimes) become

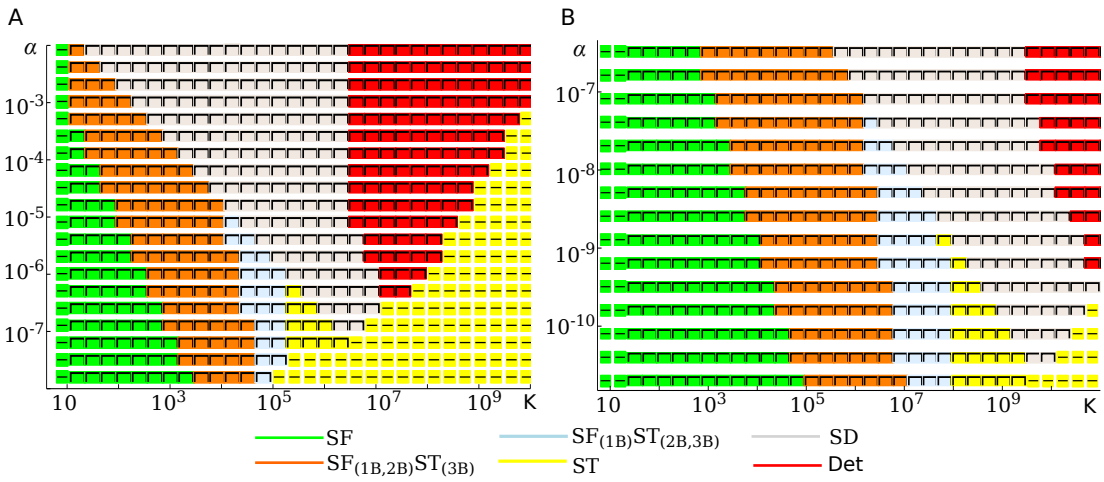

Figure 4.19 *The space of (K, α) in which each point is represented by an icon. Each icon identifies which of T_A and T_B is the lowest and the dynamical regime the system is in. In (A) the mutation probability μ is 10^{-6}, while in (B) it is 10^{-9}. The remaining parameters used are $\delta = 0.4, d = 0.1$.*

more important as α increases, while others disappear altogether. In both plots, two dynamical regimes for trajectory B disappear altogether (being the ST and a mixed regime).

We consider now the regions in Figs. 4.19A and B that satisfy the condition $\alpha < \alpha_c$. When this condition is satisfied, the results can be used as an approximation for the full system's behaviour. In looking at this we ignore what dynamical regime the system is in and represent data points as the icons shown in Fig. 4.19A. Again these have a trajectory symbol and background colour, both of which identify whether trajectory B is taken or not (but the latter now includes all trajectory types that are not trajectory B). These were chosen to allow comparison with Fig. 3.15B.

The results can be seen in Fig. 4.20. They show the same data as in Fig. 4.19 but focus only on whether state 2A is visited. Upon increasing α, the region of trajectories that avoid 2A (i.e. the green region) come to an end when $\alpha = \alpha_c$. At this point, avoiding state 2A becomes unlikely for trajectories. As we can see, both plots in Fig. 4.20 predict there to be large regions corresponding to the optimal α range. This is particularly true in Fig. 4.20B where, with the exception of very small K, or large K and small α, successful cells are expected to be travelling by phenotype B to the target.

As discussed earlier, the value predicted for α_c is expected to be an underestimate

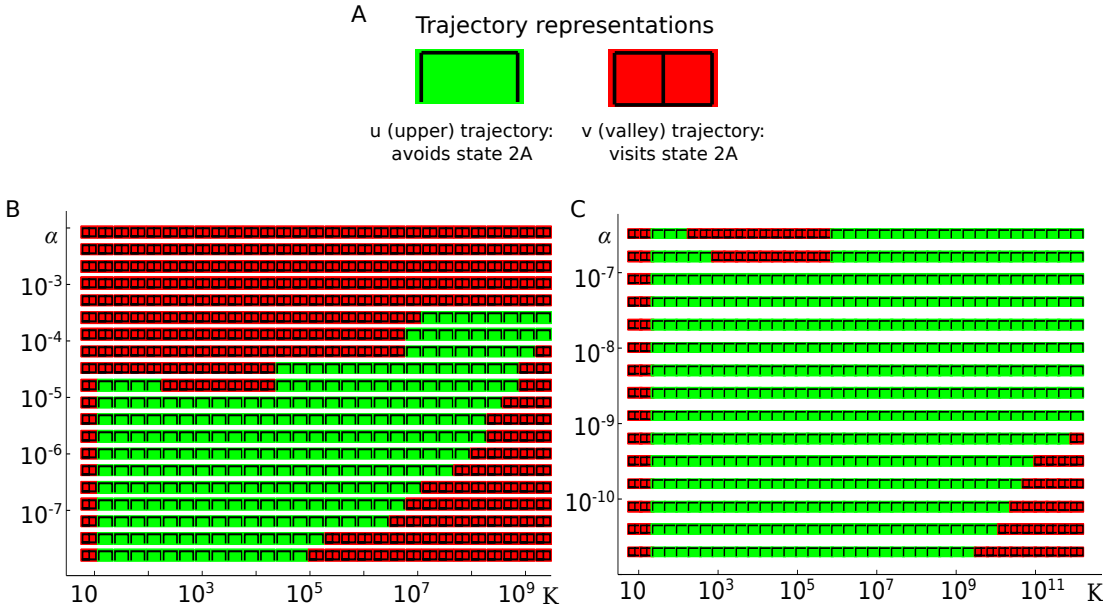

Figure 4.20 *Predicting when the optimal α range is expected to exist. (A) The symbols that identify whether a population is expected to visit state 2A in its evolution of a cell in state 3A. (B) and (C) show (K, α) space in which each point is represented by both a colour and a symbol, both of which identify whether successful cells are expected to have visited state 2A. The green region, identifying the beginning of the optimal α range, ends at $\alpha = \alpha_c$ when the approximation $T = \min[\mathrm{T_A}, \mathrm{T_B}]$ is predicted to break down. Parameters used are $\delta = 0.4, d = 0.1$ and $\mu = 10^{-6}$ for plot (B), and $\mu = 10^{-9}$ for plot (C).*

and fall on the valley floor of the optimal α range in a plot of $T(\alpha)$. Therefore we expect the green region of these plots to extend to larger α values in reality. Figure 4.20A uses the same parameter values as the plot of (K, α) space from simulations in Fig. 3.15B. We see good agreement between what is predicted there and in Fig. 4.20A. As we expected, the optimal α range in Fig. 3.15B extends to larger values of α than predicted in Fig. 4.20A.

4.10 Discussion and Conclusions

In this chapter we analytically studied the model that was introduced in Chapter 3. This model concerns how a haploid population of cells, that are able to switch phenotype, can overcome a fitness valley to evolve a compensatory double mutant. The aim throughout was to develop methods to calculate the adaptation time T. Once we could do this, we were able to search parameter space for the existence of the optimal α range, in which the evolutionary process can be improved by a population that can switch phenotypes.

The motivation for the approach taken in this chapter followed largely from the results of Chapter 3. In that chapter we identified the existence of an optimal range for α and an understanding of how the trajectories taken by successful cells vary with key parameters. However, in this chapter we sought to understand why these were our observations in Chapter 3. To do this we needed to consider the dynamics that a population of asexually reproducing cells are expected to have and the dependence of this on the parameters of our model. In doing this we were able to show mathematically why cells are likely to take different trajectories for different parameter values. For example, in the case of the competition between trajectories A and B (see Figs. 4.1A and B respectively) it is decided by which one has the lowest adaptation time. Alternatively a trajectory can become likely due to steps it contains becoming unlikely to be avoided. This is the case with increasing α values where it becomes unlikely the valley state 2A can be avoided, which results in trajectories with larger adaptation times becoming more likely. The mathematical formulations in this chapter to describe the population's dynamics in different dynamical regimes was integral to exploring the effect of stochastic phenotype switching at realistic parameter values.

Throughout this chapter our study successfully predicted the population to behave in a way consistent with results from Chapter 3. This encouraged us to use

these methods to make predictions for how a population will behave at biological parameter values, that we would otherwise be unable to simulate. Specifically, we found that when the mutation probability $\mu = 10^{-9}$, comparable with the probability of single nucleotide mutation measured in *E. coli* [47][116], evolution in this model is largely dependent on the existence of the second phenotype for a large range of parameters (see Fig. 4.20B).

We demonstrated that how a population behaves during its evolution is extremely sensitive to the model parameters, specifically those controlling the rate of mutant production. These differences made calculating a full general solution for the adaptation time T difficult, perhaps impossible. The procedure throughout this chapter was to consider each dynamical regime separately, in which the population was expected to behave in some way that could be described mathematically. With the exception of the sequential fixation (SF) regime, for which a solution for the full system is possible, we relied on using $T \approx \min[\mathrm{T_A}, \mathrm{T_B}]$ when $\alpha < \alpha_c$. This approximation greatly reduced the complexity of calculating T, turning it into calculating the adaptation time for two 1D sequences of mutations. Without this approximation, it may not have been possible to otherwise solve for T at intermediate values of α.

In each dynamical regime, numerous approximations were made for how the population is expected to behave. Despite doing this, it is remarkable just how well properties of the system could be reproduced. For example, Figs. 4.5B and 4.11 show very good agreement with observations from simulations for the adaptation time $T(\alpha)$. Having these individual solutions we were able to combine them to create a composite solution for the adaptation time T.

In considering the system's transition between dynamical regimes, we were able to satisfactorily predict where the boundaries between regimes are. In the composite solution, transitions between regimes can appear quite smooth. However, this is not often the case for the transition between the semi-deterministic (SD) and deterministic (Det) regimes. This can be seen in Fig. 4.16B, where there is a sizeable kink in the solution for T_B as it moves between the SD and Det regime. Ultimately this does not affect the smoothness of the composite solution in Fig. 4.16D, but it may for curves at other parameter values.

This kink between the SD and Det regimes indicates that stochasticity is still important in the system at the point that we start neglecting it. This suggests there may be a further dynamical regime between the SD and Det regime, with

which we could better describe the system in some other way. In [206] it is proposed that for a long sequence of mutations there are likely to be numerous SD regimes, in which the population growth at different states are treated deterministically, while the remainder are treated stochastically. In results that are not presented here, we attempted to find such an extra regime by treating the population growth at state 2B as deterministic, while the generation of a mutant at 3B and its subsequent growth is stochastic. However, the predicted solution did not match well with simulations.

For $\alpha > \alpha_c$, the only other suitable solution for T is found in the limit of large α. In this limit, the two-phenotype model maps well to that of a single phenotype with variable valley depth at the intermediate state. In the limit of $\alpha \to \infty$, it recovers well the limiting value of T observed in simulations. It also captures quite well how this limit is approached. This can be seen in Fig. 4.15, where the large α analytic solution for T matches reasonably well with the increase in T predicted by simulations. However, away from the large α limit, the justification for the mapping to a single phenotype model becomes less relevant. Therefore while results from the single phenotype model appear to capture well the increase in $T(\alpha)$ in Fig. 4.15, we cannot be confident that it still will at parameter values that we are unable to run simulations with to check. Therefore, for the final results in Fig. 4.18, it was not included to describe the main increase in $T(\alpha)$.

There remains a large range of α values in which we could make no approximations for the process. As a result, no adequate solution was found for T in this range. For example, see the broken curves in Fig. 4.18. However, the behaviour of the population in this regime is qualitatively well understood: upon increasing α, trajectories are unlikely to avoid visiting state 2A and therefore $T(\alpha)$ increases until the large α limit is reached.

In considering where this region begins, we have already discussed the shortcomings in the calculation of α_c. Thankfully, our calculations underestimate it and it can therefore still be used to identify if the curve of $T(\alpha)$ has decreased before $\alpha = \alpha_c$ is reached (thus whether the optimal α range exists or not). In the main text, we suggested that the calculation of α_c could be improved if, instead of testing if a cell is likely to have made the transition 2B$\to$2A$\to$2B, we could require this cell to go on to proliferate in the population at 2B. For small K, this is equivalent to conditioning the cell to reach some frequency in the population near fixation. The larger K is the longer this will take to happen. Therefore we can expect this change to mean, at small K, the upper boundary of the green

region in Fig. 4.20A will change to have a nonzero gradient. At larger K values, with a greater amount of cells switching 2B→2A→2B, it becomes less important that it be a single of these that proliferates in the population. Therefore for larger K we might expect the upper boundary of the green region in Fig. 4.20A to remain flat. This hypothetical change matches what is observed in the upper boundary of the green region in the simulation data in Fig. 3.15B.

Throughout this chapter we simplified things by setting the fitness cost $c = 0$. This was mainly done in order to simplify the final expressions into a presentable form and not because it affected the analysis. There is no reason the methods used here cannot be applied to the case of $c \neq 0$, provided the optimal α range remains. However, if it does not remain then the analysis becomes trivial as, as we saw in Chapter 3, the curve of $T(\alpha)$ will decrease monotonically from the $\alpha \to 0$ limit to the large α limit. An analysis of the system in both of these limits will be the same as we considered in this chapter.

Finally, it remains to be seen whether or not these methods can be used to study this model on an extended genotype space (i.e. one with more than 3 genotypes). While the methods themselves should still be applicable, there may be less opportunity to use them. With an increasing amount of intermediate genotypes there are more opportunities for a population following phenotype B to switch to phenotype A. When this happens the effectiveness of our analysis breaks down as we can no longer use the approximation $T \approx \min[\mathrm{T_A}, \mathrm{T_B}]$. Of course this all depends on the fitness landscapes used for each phenotype and how deleterious the intermediate states in phenotype A are. At the very least we would still be able to analyse the $\alpha \to 0$ and $\alpha \to \infty$ limits using the methods outlined in this chapter.

Chapter 5

Stochastic phenotype switching in an evolving population of sequences

5.1 Introduction

In Chapters 3 and 4 we studied the escape of an asexual haploid population from a local peak in a 1D fitness landscape. We saw there that the escape can be accelerated if the population is able to switch phenotype stochastically (to a phenotype with a uniform fitness landscape). In this chapter we undertake a numerical analysis into how robust this result is to changes in the size of genotype space and the fitness landscapes used.

The adaptive evolution of a population depends on both the dynamical parameters of the population and the topography of the fitness landscape. Recent experiments have probed subsets of real fitness landscapes [128, 198, 202, 207]. While this allows for evolutionary studies to be carried out on real landscapes [189], any findings are unlikely to help in predicting how the same population will behave on a different landscape. In this chapter we want to examine evolution over typical — rather than specific — fitness landscapes. Therefore all results will be averaged over an ensemble of fitness landscapes. These landscapes are randomly generated but have structures that reflect aspects of the real landscapes they are representing.

In this chapter, we again consider the evolution of an asexual haploid population. Each cell exists in a state that corresponds to a binary sequence of length L (its

genotype) and a phenotypic state (of which there are two: A and B). Each locus (i.e. site) in the sequence has 2 possible alleles. We assume that the genotype space is a hypercube, such that connected genotypes (through mutations) are those that differ by a single point mutation (i.e. at a single locus). The effect of the second phenotype is a doubling of state space, with each state now corresponding to a specific genotype/phenotype pairing. Therefore for a population of sequences of length L the state space is a composite hypercube of dimension $L + 1$. Whether states in the second phenotype can be accessed, and utilised, by an evolving population depends on the rate of stochastic phenotype switching α and the landscapes of both phenotypes.

The model in this chapter is an extension of the one studied in Chapters 3 and 4 and again models continuous microbial evolution in a chemostat environment. The specific process we are interested in is how a population of cells, beginning in the wild-type state, evolves the first cell in a chosen target state. As in the preceding chapters the focus is on understanding how the time taken for the process — the adaptation time T — is affected by the rate of phenotype switching α.

We will consider several pairings of random landscape types for both phenotypes. Initially we consider phenotype A to have a House of Cards (HoC) landscape, in which the fitnesses of genotypes are uncorrelated [101, 106] and phenotype B to have a uniform landscape. This is an approximate extension to higher dimensions of the 1D landscape that we studied in Chapters 3 and 4. We will then consider the case in which the landscapes for both phenotypes A and B are from the same class of fitness landscapes. We begin by considering them both to have HoC landscapes and then Rough Mount Fuji (RMF) landscapes. In RMF landscapes, fitness effects are (on average) additive in the neighbourhood of a local peak [9, 139].

For these models we will calculate the adaptation time T in several different ways. The first is by numerically solving the system of deterministic differential equations that describe the dynamics of the system in the limit of infinitely large populations. We will also consider results from stochastic simulations of the models, for small population sizes up to larger ones that are more applicable to microbial experiments.

For different values of dynamical parameters, the population can be in different *evolutionary regimes*. For moderate sized populations and low mutation probabil-

ities, the system may be in the *strong selection weak mutation* regime [74]. In this regime, the existence of *accessible paths* — along which the fitness never decreases — are important in the evolutionary process [62]. For much larger populations or higher mutation rates, *greedy dynamics* of the population can play an important role [92, 147].

The time required to simulate the evolutionary process increases rapidly with the sequence length L. This is particularly true when the aspect being studied is a population's attempt to overcome fitness barriers (i.e. deleterious states) as is often the case here. Therefore the results presented in this chapter are limited to small sequence lengths L. However, we hope the insight obtained from this study may be useful in future extensions of the work that may be capable of exploring larger values of L.

5.2 Background and motivation

Binary sequences can be used to represent real genotypes in many different ways. For example, in DNA sequences at the molecular level, the nucleotide bases adenine (A) and guanine (G) can be grouped together into *purines*, while thymine (T) and cytosine (C) can be grouped into *pyrimidines*. At a larger biological scale, such as sequences of genes, the 1's and 0's can identify the activation/inactivation of specific genes or important mutations in or across genes (e.g. mutations conferring antibiotic resistance). Therefore the space of binary sequences is a natural, albeit simplified, way of representing the genotype space. With links connecting genotypes that differ by a single point mutation (i.e. at a single locus) the structure of genotype space is a hypercube.

The Hamming distance h between two genotypes is the number of point mutations by which they differ. For the genotypes $\vec{\sigma} = \{\sigma_1, ..., \sigma_L\}$ and $\vec{\sigma}' = \{\sigma'_1, ..., \sigma'_L\}$, representing sequences of length L, this is given by

$$h(\vec{\sigma}, \vec{\sigma}') = \sum_{l=1}^{L} (1 - \delta_{\sigma_l, \sigma'_l}). \tag{5.1}$$

If the probability of incorrect replication of a nucleotide base during replication is μ, then the probability $Q(\vec{\sigma} \rightarrow \vec{\sigma}')$ that during replication genotype $\vec{\sigma} =$

$\{\sigma_1, ..., \sigma_L\}$ produces a mutant of genotype $\vec{\sigma}' = \{\sigma'_1, ..., \sigma'_L\}$ is

$$Q(\vec{\sigma} \to \vec{\sigma}') = \mu^{h(\vec{\sigma},\vec{\sigma}')}(1-\mu)^{(L-h(\vec{\sigma},\vec{\sigma}'))}, \tag{5.2}$$

Single point mutations (for which $h(\vec{\sigma}, \vec{\sigma}') = 1$) are therefore the only mutations of significant likelihood at small values of μ. In the models of this chapter we will therefore only consider single point mutations to be possible during replication.

A genotype space consisting of all possible genomic mutations would be astronomically large. Therefore experimental studies focus on the fitness effects of possible combinations (i.e. genotypes) of a small number of mutations of interest. So far, such studies have been carried out for genotypes featuring combinations of less than 10 specific point mutations in a single or a few different genes [199]. These studies have yielded empirical data on subsets of real fitness landscapes. Examples include the fungus *Aspergillus niger* [198], the fruit fly *Drosophila melanogaster* [207], and the evolution of antimicrobial resistance in *Escherichia coli* [128, 202].

On a hypercubic genotype space there are numerous possible trajectories that populations can take between any two genotypes. With each genotype connected to L nearest neighbours there are $L!$ shortest trajectories that connect any genotype to its antipodal genotype. This makes it difficult to predict how an evolving population will behave and the trajectory it will take. However, this behaviour becomes more predictable within *evolutionary regimes* [92, 93]. These are similar to the dynamical regimes that we considered in Chapter 4. However, in Chapter 4 the regimes described how a population acquires a fixed sequence of mutations (i.e. along a fixed trajectory). Here, the evolutionary regimes concern the trajectories that populations are expected to take over genotype space (or at least narrow them down by identifying what trajectories are unlikely).

In this section let N be the population number, u the rate of mutant production per cell (not to be confused with the mutation probability μ used in the model of this chapter) and s a measure of the typical selective advantage of neighbouring mutants over the existing population. In the *strong selection weak mutation* (SSWM) regime, occurring when $Nu \ll 1$ and $Ns \gg 1$, mutations are rare and unlikely to establish unless favourable [74, 75]. In the SSWM regime the population is constrained to move almost exclusively along paths for which the fitness never decreases [75]. These kinds of paths are called *accessible*. However, which neighbouring beneficial mutant (if there is more than one) will be acquired

by the population is a matter of chance, decided by which is produced first. Therefore uncertainty remains regarding the specific trajectory that will be taken. However, the existence of accessible paths are important in determining how *accessible* landscapes are to populations evolving in the SSWM regime.

At larger population sizes or mutation rates, when $Nu \sim L \gg 1$ and $Ns \gg 1$, the population undergoes the behaviour of *greedy dynamics* [92, 147]. The increased rate of mutations in the population means that mutants are expected to exist at all neighbouring genotypes to the main population simultaneously. The strong selection condition favours the fittest of these as being the one that is acquired by the population. Therefore the population remains localised about a single genotype (with nearest neighbour mutants) and sequentially moves to the neighbouring genotype that offers the greatest increase in fitness (hence the other name for this dynamics, that of *steepest ascent*). In this regime the dynamics are almost deterministic, in the sense that there is certainty in the trajectory a population is expected to take.

In the greedy dynamics regime, populations are more likely to become trapped at local fitness peaks, compared to smaller populations [92]. This trapping occurs if the population starts in the *basin of attraction* of a local peak [63]. This is the set of all genotypes from which a population will result, in this regime, trapped at that fitness peak.

Both the SSWM and greedy dynamics regimes can be used to quantify the accessibility of fitness landscapes [62, 63]. Knowing this accessibility can allow for predictions to be made on the outcome of evolutionary experiments and the repeatability of results.

Upon further increase of the population size N, the evolutionary behaviour becomes deterministic and can be described by the quasispecies model [27, 52, 143]. The evolution of self-replicating sequences was first studied in this context to model the evolution of prebiotic molecules [51, 53]. Here, the mutant production rate Nu is very large and as it increases the population experiences an increase in genetic heterogeneity to spread (like a cloud) over genotype space. This is the defining feature of a quasispecies, for which selection must be viewed as acting on the quasispecies as a whole (instead of on the individuals within it). This follows from a genotype's success (i.e. prevalence) in the population being more than a function of its own selective advantage (but depending on the success of others that can produce mutants at it).

The quasispecies model exhibits some interesting evolutionary behaviour such as a steady-state distribution that does not contain the global optimal genotype [144] and punctuated evolution [110]. Alternatively, if the mutation rate exceeds the *critical error threshold* u_c, the population loses genetic integrity and is unable to adapt (instead collapsing to spread out over genotype space) [27]. The value of the error threshold is a property of the landscape and not all landscapes have one. It can be regarded and studied as an equilibrium phase transition and the quasipecies model maps to various models in physics including the 2D Ising model [119, 120, 192], 1D quantum chain [12] and models of directed polymers [68]. In the simplest case of a fitness landscape with a single peak, the error threshold $\mu_c \sim 1/L$ [53].

The quasispecies concept is applicable to describing populations of asexually reproducing organisms if the mutation rate is large enough that significant diversity exists amongst the population. Owing to their large mutation rates, populations of RNA based viruses are often described as behaving like quasispecies [26, 43, 60, 115]. For them, the rate of mutation can be ~ 1 mutation per genome replication in riboviruses (e.g. *Influenza A*) [44, 45, 150] or higher in retroviruses such as *HIV-1* [156]. Such large mutation rates can make the infections caused by these viruses difficult to treat, as it allows them to evolve quickly to escape host immune responses or drug actions. As a result, there also exists a large degree of genetic variability in the same virus between hosts [180].

Bacterial populations have also been described as behaving like quasispecies [36]. In general they have lower mutation rates than many RNA based viruses [46]. However, they can experience increased mutation rates through, for example, mutator strains [182], localised hypermutable regions of DNA [135], or in the presence of antibiotics [76].

Our motivation in this chapter is to understand how the inclusion of stochastic phenotype switching affects the genetic evolution in the quasispecies model of self-replicating binary sequences. To do this we will consider two popular random landscape models, the first of which is the House of Cards (HoC) model [101, 106]. In the HoC model, the fitnesses of all genotypes are uncorrelated. This is equivalent to the Random Energy Model for spin glasses in statistical physics [41, 65] and properties of such landscapes are well understood [62, 101]. In these landscapes a single point mutation can lead to a drastically altered fitness and each genotype has the probability $1/(L+1)$ of being a local fitness peak, with $2^L/(L+1)$ peaks expected in total [101]. While real landscapes have been found to

exhibit a degree of ruggedness [82, 167], there is expected to exist some correlation between the fitnesses of genetically similar genotypes [9]. However, as a first order approximation to real landscapes — whose features still remain largely unknown — the HoC model is a useful model for consideration.

The second landscape model we will consider is the Rough Mount Fuji (RMF) model [9, 139]. Introduced in the context of protein evolution it is an extension of the earlier Mount Fuji model [7, 8] and assumes the effect of mutations to be approximately additive in the vicinity of a local fitness peak. In the RMF model the degree of landscape ruggedness can be tuned through the strength of stochastic fluctuations about the mean fitness values.

In the RMF model the fitness $r(\vec{\sigma})$ of genotype $\vec{\sigma}$ decreases monotonically with Hamming distance h from the optimal genotype $\vec{\sigma}_{\max}$ by

$$r_{\vec{\sigma}} = -\theta h(\vec{\sigma}, \vec{\sigma}_{\max}) + x. \tag{5.3}$$

Parameter θ is the average fitness decrease with the Hamming distance, while x is a randomly drawn noise, usually from a Gaussian distribution [9, 62]. When $\theta = 0$ the fitness function in (5.3) becomes that of the HoC model. Following [7, 139], the competition between the additive and random contributions to the fitness can be quantified by

$$\gamma = \frac{\theta}{\sqrt{Var(x)}}. \tag{5.4}$$

Equation (5.4) is a measure of the landscape's ruggedness γ, such that an increase in γ corresponds to a less rugged landscape.

Random landscape models can be classified by the expected statistics of their *accessible paths*, which populations are expected to travel by in the SSWM regime [62]. In such statistics, and in the work that follows, these are paths of shortest length (of which there are a possible $L!$) leading from the wild-type genotype to the antipodal genotype (which is the fitness maximum of the landscape). Statistics of interest are the probability that there are n accessible paths $p_n(L)$ and the expected number of accessible paths $\langle n_L \rangle = \sum_{n=0}^{L!} n p_L(n)$. For both the HoC and RMF landscapes $\langle n_L \rangle$ can be calculated directly [64] while numerical studies [62] have been the focus for calculating $p_L(n)$, which has recently been calculated analytically in the limit $L \to \infty$ [83].

In the HoC model, the expected number of accessible paths separating any state (i.e. not just the wild-type) from the global optimal is 1, regardless of L [64]. However, the probability of there being no accessible paths $p_L(0)$ tends to 1 for large L (when all states except the final one are random). When the HoC model is *constrained* the wild-type genotype is set to be the global fitness minimum (i.e. its fitness is set to zero). When this is the case $p_L(0)$ instead tends to 0 for large L. It is shown in [83] that for HoC landscapes there exists a threshold value for the wild-type genotype's fitness (being $\ln L/L$) that separates the landscapes from having the property $p_L(0) = 0$ or $p_L(0) = 1$.

Alternatively, in the RMF model, $\langle n_L \rangle$ scales with L^2 for large L when $\theta > 0$. The probability of there being no accessible paths $p_L(0)$ in the RMF model tends asymptotically to zero in the limit of large L. This feature is supported by numerical [62] and analytic studies [83].

5.3 Model

We now introduce the model that is studied in this chapter. It describes the evolution of an asexual haploid population over a hypercubic genotype space. There are two phenotypic states (A and B) which cells symmetrically switch between. The aim of the model is to study how the inclusion of a second phenotypic state affects how populations evolve over such a genotype space. This will be carried out numerically be calculating how the adaptation time T — the time it takes for the first cell to be produced in the designated target state — depends on the rate of switching α.

A cell in the population exists in the state $\vec{\sigma}^j = \{\sigma_1, ..., \sigma_L\}^j$. This consists of the vector $\vec{\sigma}$ that represent the genotype, in which σ_i, the value at locus i, can take one of two values (i.e. there are two different alleles). The subscript j in $\vec{\sigma}^j$ identifies the phenotype of the cell as either A or B. For example, in the following the wild-type state is always chosen to be $\{0, ..., 0\}^{\mathrm{A}}$, while the target is the antipodal state $\{1, ..., 1\}^{\mathrm{A}}$. The population begins at the value $(1 - d)K$ in the wild type state, where d and K are the death rate and carrying capacity respectively, and evolves until the first cell at the target is produced.

Cells undergo the same actions as we saw in the preceding two chapters. These are shown in Fig. 6.1 and correspond to successful replication, unsuccessful replication

(producing a mutant at a neighbouring genotype), switching phenotype and death. The parameters relating to these actions also remain the same (and can be seen in Table 3.1) except for when they are genotype specific, in which case a subscript identifies the relevant genotype, while a superscript identifies the phenotype. For example, r_i^{B} is the fitness of sequence i in phenotype B.

Each genotype has L nearest neighbours. At most, we consider a single point mutation as able to occur during each replication event. Therefore a replicating cell has the probability $L\mu$ of producing a mutant, with the probability μ that it is created at each nearest neighbour genotype.

We will identify the fitness landscapes for states in phenotype A and B as landscape A and B respectively. These will be randomly generated and all results will be averaged over different realisations of these landscapes.

We begin by considering the deterministic model for the population's evolution. Let N_i^{A} and N_i^{B} be the number of cells of genotype i in phenotype A and B respectively. Provided genotype i is not the target genotype, these obey the following deterministic differential equations

$$\frac{dN_i^{\mathrm{A}}}{dt} = \xi r_i^{\mathrm{A}}(1-L\mu)N_i^{\mathrm{A}} + \sum_{j\in\{n.n\}} \xi r_j^{\mathrm{A}}\mu N_j^{\mathrm{A}} - \alpha N_i^{\mathrm{A}} + \alpha N_i^{\mathrm{B}} - dN_i^{\mathrm{A}} \quad (5.5)$$

$$\frac{dN_i^{\mathrm{B}}}{dt} = \xi r_i^{\mathrm{B}}(1-L\mu)N_i^{\mathrm{B}} + \sum_{j\in\{n.n\}} \xi r_j^{\mathrm{B}}\mu N_j^{\mathrm{B}} - \alpha N_i^{\mathrm{B}} + \alpha N_i^{\mathrm{A}} - dN_i^{\mathrm{B}}. \quad (5.6)$$

Here $\xi = (1-(N_T/K))$ and the sums over j run over all the nearest neighbours of genotype i (i.e. those located a single point mutation away) that are not the target state $\{1,...,1\}^A$.

The populations at the target genotype in either phenotype, $N_{\mathrm{target}}^{\mathrm{A}}$ and $N_{\mathrm{target}}^{\mathrm{B}}$, obey the following differential equations

$$\frac{dN_{\mathrm{target}}^{\mathrm{A}}}{dt} = \sum_{j\in\{n.n\}} \xi r_j^{\mathrm{A}}\mu N_j^{\mathrm{A}} + \alpha N_i^{\mathrm{B}} \quad (5.7)$$

$$\frac{dN_{\mathrm{target}}^{\mathrm{B}}}{dt} = \xi r_i^{\mathrm{B}}(1-L\mu)N_i^{\mathrm{B}} + \sum_{j\in\{n.n\}} \xi r_j^{\mathrm{B}}\mu N_j^{\mathrm{B}} - \alpha N_i^{\mathrm{B}} - dN_i^{\mathrm{B}}. \quad (5.8)$$

The different equations for if the genotype is the target or not comes from requiring that the growth of $N_{\mathrm{target}}^{\mathrm{A}}$ is only due to mutations or phenotype switches to it. Therefore the population at $\{1,...,1\}^A$ cannot grow itself. Similarly $N_{\mathrm{target}}^{\mathrm{B}}$

cannot grow as a result of switches to it from the target state. This is similar to the deterministic analysis in Chapter 4 where, because we are interested in the first cell produced at the target, we choose to restrict small populations at it (such that $N^{\mathrm{A}}_{\mathrm{target}} < 1$) from growing or dying.

The adaptation time T is the time it takes for $N^{\mathrm{A}}_{\mathrm{target}} = 1$. In the following, for each realisation of the fitness landscapes, T is calculated and averaged over many landscape realisations. For the deterministic model of (5.5) to (5.8), this is calculated using an Euler update scheme. In the stochastic model it is calculated using either a KMC or τ leap algorithm.

We should be cautious of the results found by numerically solving the deterministic model of (5.5) to (5.8). Specifically, if the likelihood of a cell being created at a transient state i (by mutation or a phenotype switch) is very small then, unlike in the stochastic model, populations smaller than 1 can be produced there. These populations can grow themselves, which can lead to erroneous results (i.e. ones that the stochastic model cannot corroborate). Therefore in the following, when solutions of the deterministic model are presented we aim to corroborate their features through stochastic simulations.

5.3.1 House of Cards/Uniform landscapes

The first random landscape model we consider is the House of Cards (HoC) landscape. Here, fitnesses are uncorrelated and drawn randomly from the uniform distribution $(1-\chi, 1]$. The parameter χ controls the magnitude of the peaks and troughs in the landscape and we therefore term it the *ruggedness* of the landscape. Here ruggedness means the extent of the variability in the fitnesses about the mean fitness value (which will be $1 - (\chi/2)$).

We start by considering the HoC landscape for phenotype A, with the caveat that the wild-type state $\{0, ..., 0\}^{\mathrm{A}}$ and the target state $\{1, ..., 1\}^{\mathrm{A}}$ have fitnesses 1.0 and $1 + S$ respectively. The choice of S is arbitrary here and plays no role in the process until the target is reached. This landscape choice ensures there are no accessible paths connecting the wild-type and target states. A population traversing landscape A is therefore required to pass through at least one deleterious state to reach the target. Conversely, the landscape for phenotype B is uniform, with fitness $r^{\mathrm{B}}_i = 1$. Therefore cells in phenotype A can avoid deleterious states in the landscape by switching to phenotype B. For $L = 2$, if one

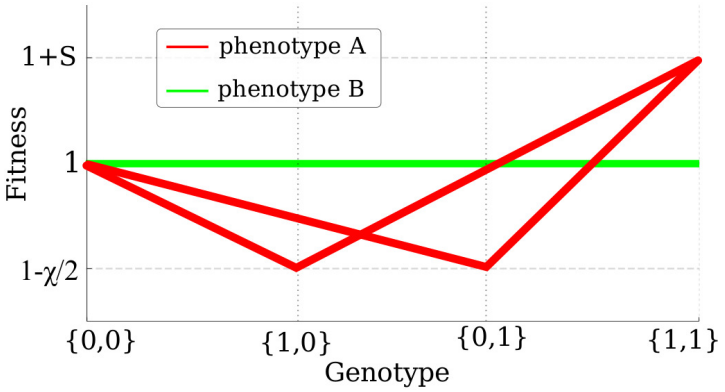

Figure 5.1 *The average fitness landscapes for the House of Cards(HoC)/Uniform random landscape model. Phenotype A has a HoC landscape with randomly drawn fitnesses at the intermediate states* $\{1,0\}^{\mathrm{A}}$ *and* $\{0,1\}^{\mathrm{A}}$*. These fitnesses are drawn (for each simulation) from a uniform distribution in the interval* $(1-\chi,1]$ *with an average value of* $(1-\chi/2)$*. Phenotype B has a uniform fitness landscape. Note that despite the landscape for phenotype B appearing as a straight line, the connectivity of the genotypes remain as for phenotype A (i.e. the states* $\{1,0\}^{\mathrm{B}}$ *and* $\{0,1\}^{\mathrm{B}}$ *are not connected by a single mutation).*

of the intermediate genotypes (i.e. 10 or 01) is made lethal in both phenotypes then these landscapes match those used in the 1D valley crossing problem of Chapters 3 and 4, except with a randomly drawn valley depth δ. This point can be seen in Fig. 5.1 which shows the fitness landscapes for phenotypes A and B. This can be compared with that of the 1D valley crossing problem in Fig. 3.1B.

Deterministic model

In the HoC/Uniform model (for landscapes A and B respectively) we first consider the numerical solution to the deterministic model of (5.5) to (5.8). The solution is the adaptation time T such that $N^{A}_{\mathrm{target}}(t=T)=1$.

Figure 5.2 shows plots of the adaptation time T as a function of the switching rate α. Figures 5.2A and 5.2B compare curves of different μ values for $L=2$ and $L=3$ respectively. At large α all curves tend towards the value for T in the single phenotype model with an HoC landscape and fitnesses in the range $(1-\chi/2]$. In this limit phenotype switching is sufficiently rapid that the average fitness of a population at any genotype is the average fitness of the genotype in both phenotypes. Therefore in this limit the two phenotype model can be

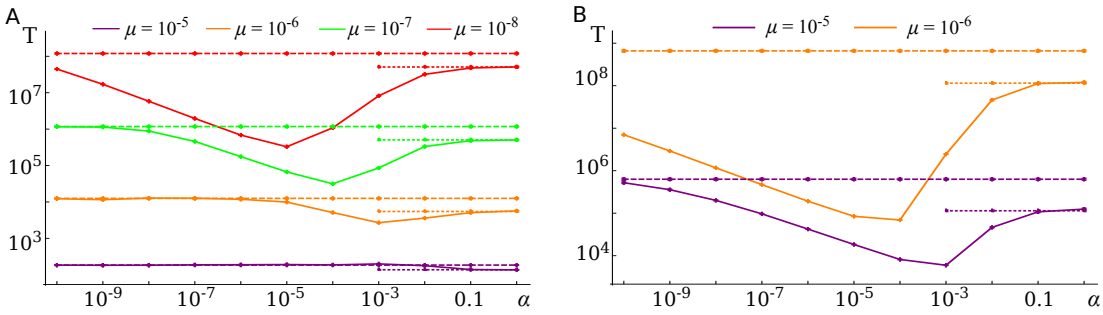

Figure 5.2 *The adaptation time T as a function of the switching rate α for the HoC/Uniform model. (A) and (B) compare curves of different values of the mutation probability μ, for sequence length $L = 2$ and $L = 3$ respectively. All curves (full lines) have a corresponding dashed line that identifies T when $\alpha = 0$, as well as a dotted line at high α that identifies T in the single phenotype model using a HoC landscape with fitnesses selected in the range $(1 - \chi/2, 1]$. The remaining parameter values are $K = 10^8, \chi = 0.4$ and $d = 0.1$. All results were collected using an Euler update algorithm and averaged over* 500 *fitness landscapes.*

mapped to the single phenotype model with halved ruggedness χ.

We observe in Fig. 5.2A that an optimal α range exists for curves with mutation probability $\mu < 10^{-5}$. When this occurs, the adaptation time T can be significantly lower than in the limits of $\alpha \to 0$ or $\alpha \to \infty$. As μ decreases this optimal range grows, both in depth and width, and the minimum of $T(\alpha)$ shifts to lower values of α. The shape of these curves are consistent with that which we observed for the 1D valley crossing model in Chapter 4 when studying it deterministically (see Fig. 4.4).

For the curve $\mu = 10^{-8}$, the minimum value of T in this optimal range is almost three orders of magnitude smaller than when $\alpha = 0$. However, for this value of μ, the rate of mutant production $\mu dK \ll 1$, for which the system may not be accurately described by the deterministic model of (5.5) to (5.8).

Figure 5.2B compares curves of $T(\alpha)$ for sequences of length $L = 3$. These curves show the same optimal α range as Fig. 5.2A but of a greater significance. Increasing the sequence length L by a single locus has resulted in a substantial increase in the depth of the $T(\alpha)$ curve for $\mu = 10^{-6}$ compared with Fig. 5.2A (and it now appears for $\mu = 10^{-5}$). The depths of this curve has increased from almost one to four orders of magnitude. The range of α values over which this range extends has also increased. While the curve for $\mu = 10^{-5}$ approaches its $T(\alpha = 0)$ limiting value at the lowest α value shown here, the curve of $\mu = 10^{-6}$

remains a large range of α from it.

These results predict the existence and growing significance of an optimal α range as the sequence length L increases by just a single locus. Therefore for such parameters an evolving population can benefit significantly from stochastic switching to a uniform secondary landscape. However, it remains to be seen if stochastic simulations predict the same behaviour of evolving populations. This is considered in the following sections.

Stochastic model - small population sizes

We now consider the stochastic simulation of population evolution using the HoC/Uniform model. We begin by looking at small population sizes with carrying capacity $K = 20$. Depending on the random landscape generated, it is possible that the population may behave locally at points on landscape A as in the *strong selection weak mutation* (SSWM) evolutionary regime [74, 75]. This depends on whether or not the random selective differences (i.e. fitnesses) between genotypes and their neighbours are great enough.

With no accessible trajectories connecting the wild-type and target states in Landscape A, we expect it will be time consuming for small populations to pass the deleterious states. Having access to landscape B provides neutral paths to the target state which may reduce the adaptation time T. However, the additional time it takes for a cell in a small population to undergo at least two phenotype switches may make this unlikely at low frequencies of switching.

Figure 5.3A shows the adaptation time T as a function of the switching rate α, comparing curves for different sequence lengths L. For all curves at low α we see that T is greater than in the absence of switching. Since T must tend to the $T(\alpha = 0)$ value as α approaches zero, this increase at low α must be part of a peak in which phenotype switching slows down the evolutionary process. This peak appears to increase in magnitude (relative to $T(\alpha = 0)$) with increasing L. For the largest L considered (a still small $L = 6$), evolution is slowed down at low frequency switching by almost an order of magnitude compared to without phenotype switching (i.e. $\alpha = 0$). We can hypothesise that this is due to populations of cells becoming trapped in phenotype B. Once there the waiting time to escape can be considerable at low α values, which can slow down the process of evolving a cell in state $\{1, .., 1\}^{\mathrm{A}}$.

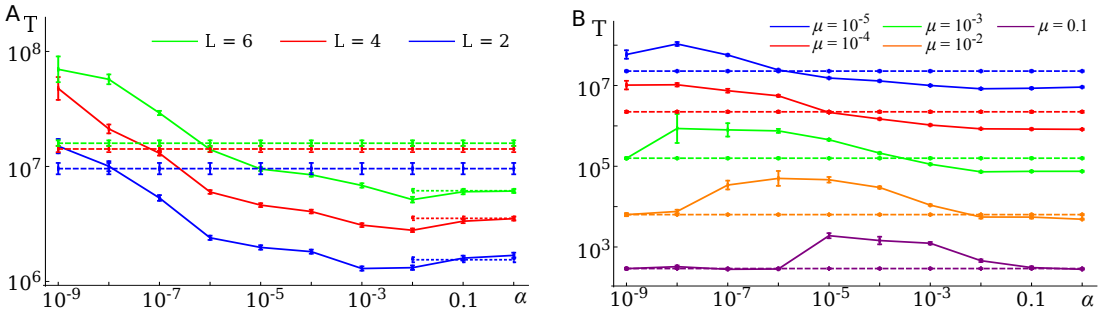

Figure 5.3 *The adaptation time T as a function of the switching rate α for the HoC/Uniform model. (A) A plot comparing curves for different sequence lengths L when $\mu = 10^{-5}$. For each L a dashed line identifies T when $\alpha = 0$. Also included is a dotted line at large α values that identifies T in the case of a single phenotype with HoC landscape and $\chi = 0.2$. (B) A plot comparing curves of different μ when $L = 7$. Dashed lines identify T when $\alpha = 0$ for each value of μ. The remaining parameters for both plots are $K = 20, \chi = 0.4$ and $d = 0.1$. All data is collected using a KMC algorithm and averaged over at least 500 fitness landscapes.*

There is an almost monotonic decrease in the curves of $T(\alpha)$ in Fig. 5.3A (although there are one or two data points in each curve at $\alpha \approx 10^{-2}$ which are below the large α values for T). The result is that for large α values T is lower than without phenotype switching. As discussed for Fig. 5.2, the large α limit of T is the same as T in the single phenotype model with HoC landscape and ruggedness χ halved. Other than this trivial reduction in T phenotype switching to a neutral phenotype does not appear to benefit these small populations.

Figure 5.3B examines how the peak in curves of $T(\alpha)$ versus α changes with mutation probability μ. It compares curves of $T(\alpha)$ for different values of μ and sequence length $L = 7$. The range of α values for which T increases above the $T(\alpha = 0)$ value extends to smaller α values as μ decreases, while the range of α values it spans is ~ 4 to 5 orders of magnitude. The height of the peak appears almost independent of μ, remaining approximately one order of magnitude greater than the value $T(\alpha = 0)$ in all curves. It is possible that there is a power law relationship between the peaks in the adaptation time T and α. However, to probe this it would first be necessary to gather more data in order to determine more precisely the location of each peak in the curves of $T(\alpha)$.

It may be surprising to see the peak existing in the curve of $T(\alpha)$ for $\mu = 0.1$ in Fig. 5.3B. For μ this large, mutants are produced at large enough rates that fitness barriers are less of an obstacle for the population than at lower μK. For this reason there is no observable difference between T in the large α limit and

the case without phenotype switching. That the peak is present here at the same magnitude as for other values of μ suggests that the entire population, not only some fraction of it, is stuck in phenotype B. Alternatively, if a fraction remained in phenotype A we would expect the target to be evolved quicker than we observe here. The intersection between the curves of $T(\alpha)$ and $T(\alpha = 0)$ increases by approximately an order of magnitude as μ increases by the same amount. This is because the process of evolving a cell in the target state takes less time at larger μ. Therefore the rate of phenotype switching can be comparably quicker and still manage to interfere with the evolutionary process in the same way.

The curves shown in Figs. 5.3A and B for low mutation probabilities μ are similar to the one that we observed for the 1D valley crossing model in Fig. 3.9A. In that case we observed a peak in the curve of the adaptation time $T(\alpha)$ followed by a moderate reduction in the limit of large α below the $T(\alpha = 0)$ value. This curve for $T(\alpha)$ then became one that contained the optimal α range following a reduction in the valley depth δ (see Fig. 3.9C). We can hypothesise that this may also occur for the curves shown in Figs. 5.3A and B if the ruggedness χ is increased. However, further work needs carried out in order to test this.

We consider now how results change at larger carrying capacities. For $K = 100$, Figs. 5.4A and B compare curves of T as a function of α for $\mu = 10^{-4}$ and $\mu = 10^{-5}$ respectively. Unlike in Fig. 5.3 both plots show a significant optimal α range emerging upon a reduction in μ. In Fig. 5.4A the reduction in T during the optimal range is almost 3 orders of magnitude compared with T at the lowest α value shown. The curves in Fig. 5.4B appear to show a smaller reduction in T in the optimal range. However, this is likely to be due to the $T(\alpha = 0)$ limit not having been reached yet at the lowest α values shown here. We saw earlier in Fig. 5.2 that the expected α value at which this limit is reached reduces with μ.

We can again observe similarities between the results of this model and those of the 1D valley crossing model of Chapters 3 and 4. This can be seen by comparing the curves for $L = 2$ in Figs. 5.4A and B with those of the 1D valley crossing model in Fig. 3.4A (specifically with the curves for $\mu = 9 \times 10^{-5}$ and $\mu = 10^{-5}$). The curves for $T(\alpha)$ in Fig. 3.4A show the same optimal α ranges existing as in Figs. 5.4A and B but at values of T approximately one order of magnitude greater. This is likely attributable to the smaller average fitness reductions we are considering at the intermediate states in the model of this chapter (where the ruggedness $\chi = 0.4$ is the maximum possible reduction in fitness rather than

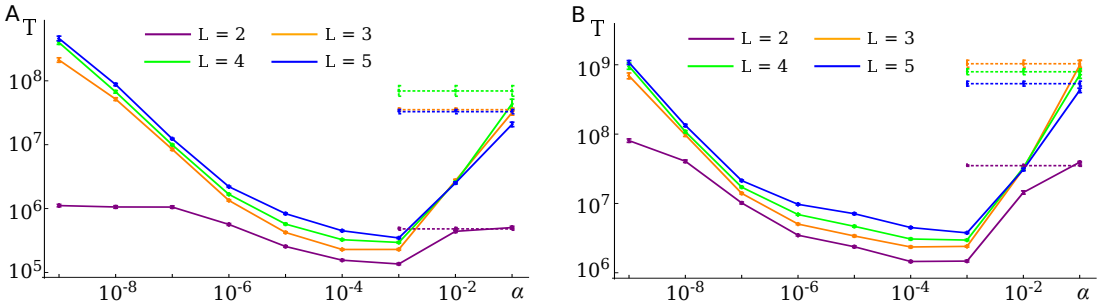

Figure 5.4 *The adaptation time T as a function of the switching rate α for the HoC/Uniform model. Plots (A) and (B) compare curves for different L when $\mu = 10^{-4}$ and $\mu = 10^{-5}$ respectively. Each curve in (A) has a dotted line which is the predicted large α limit for these curves. This is the T value in the single phenotype model with ruggedness χ halved. The remaining parameters used are $K = 100, \chi = 0.4$ and $d = 0.1$. All data is collected using a KMC algorithm and averaged over at least 500 fitness landscapes.*

the precise one used for the valley depth in Fig. 3.4A). However, the increased number of direct paths to the target state in the model of this chapter may also be significant in causing a general reduction in $T(\alpha)$.

Stochastic model - large population sizes

We now consider how the identified optimal range for the switching rate α depends on the size of the system (i.e. through the carrying capacity K). Results are shown in Fig. 5.5 which compares plots of $\Delta \log T = \log_{10}[T/T(\alpha = 0)]$ as a function of α for various K values. $\Delta \log T$ is the difference in adaptation time T (in orders of magnitude) between the T value being considered and the case without switching (i.e. $T(\alpha = 0)$). We examine this over the range of intermediate α values within which we expect the optimal range to be distinguishable. Figures 5.5B, C and D all differ from Fig. 5.5A by a single parameter.

In Fig. 5.5A the optimal α range appears for $K = 10^2$ and $K = 10^4$. In the former instance the adaptation time T is reduced during it by almost 2 orders of magnitude (compared with ~ 0.5 for the latter case). For the largest values of K shown ($K = 10^6$ and 10^8) there is no change with phenotype switching. With the system approaching the deterministic limit at these values, deleterious intermediate states become less of an obstacle. For the intermediate $K = 10^6$ there is a minor reduction at large α.

For Fig. 5.5B the landscape ruggedness χ is reduced by half compared with

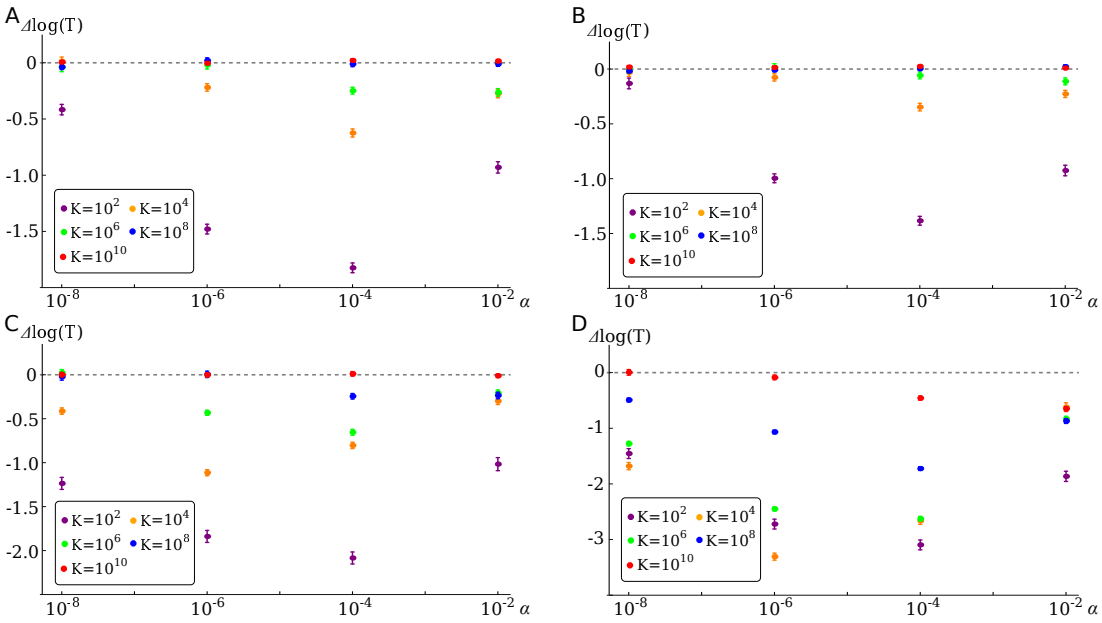

Figure 5.5 *Plots comparing the adaptation time difference* $\Delta \log T = \log_{10}[T/T(\alpha = 0)]$ *as a function of* α*, for different values of* K *in the HoC/Uniform model.* $\Delta \log T$ *is the difference (in orders of magnitude) of the adaptation time* T *compared to the case without switching (i.e. when* $\alpha = 0$ *which corresponds to the dashed line shown at* $\Delta T = 0$*). The sign of* $\Delta \log T$ *identifies whether* T *has increased or decreased with switching. All plots show points for the values* $K = \{10^2, 10^4, 10^6, 10^8, 10^{10}\}$*. The parameters used in (A) are* $\mu = 10^{-5}, L = 2, \chi = 0.4$ *and* $d = 0.1$*, while the remaining plots differ to (A) by a single parameter as follows: in (B) the landscape ruggedness* χ *is halved to* $\chi = 0.2$*, in (C) the mutation probability* μ *is reduced by an order of magnitude to* $\mu = 10^{-6}$ *and in (D) the sequence length* L *is increased by 1 to* $L = 3$*. All data is averaged over approximately 500 fitness landscapes and collected using a* τ*-leap algorithm.*

Fig. 5.5A. This reduces the magnitude of the fitness barriers in landscape A and the secondary phenotype becomes less beneficial to an evolving population. All of the T values therefore move closer to their $T(\alpha = 0)$ value (i.e. $\Delta \log T = 0$) with only points for $K = 10^2$ showing a significant benefit by switching (with a maximum improvement of around ~ 1.5 orders of magnitude reduction in T).

In Fig. 5.5C, the mutation probability μ is an order of magnitude lower than in Fig. 5.5A. This makes deleterious states in landscape A more time consuming to cross and the neutral trajectories in landscape B can benefit the population. This is observable here as optimal α ranges become more significant and extend to larger values of K than we have previously seen. For $K = 10^2$ and $K = 10^4$ the reduction in T with switching exceeds 2 and a single order of magnitude respectively. The optimal α range now appears for $K = 10^6$, while $K = 10^8$ experiences a reduction at large α. The only K value unaffected by switching is $K = 10^{10}$.

Finally, we see in Fig. 5.5D that the greatest change to the optimal α range follows an increase in the sequence length L (by a single locus compared with Fig. 5.5A). All K values experience a reduction in T from being able to switch phenotype, with the optimal α range existing now for $K \leq 10^8$. At its most significant, the adaptation time T for $K = 10^4$ reduces due to switching by over 3 orders of magnitude. All of the observations in Fig. 5.5 for $K = 10^8$ match with the predictions of the deterministic model in Fig. 5.2.

These observations may not be surprising given the nature of the HoC/Uniform model. The population in phenotype A, if it can switch quickly enough, will always have a beneficial landscape over which it can travel to the target genotype. This can involve travelling the whole of genotype space in phenotype B, or just a part of it when the local landscape in phenotype A is unfavourable. The growing significance of the optimal α range when L increases by a single locus is promising. However, it remains to be seen if this continues to grow as L is increased further. Figure 5.4 suggest that, for $K = 100$ at least, the significant difference in curves of $T(\alpha)$ for $L = 2$ and $L = 3$ does not continue as L increases to $L = 4$ and 5.

Extensions of this landscape pairing, for example including a fitness cost to the uniform landscape, are not expected to offer any new insight to the evolutionary process with phenotype switching. Therefore we will not consider them here. Instead we will now consider how results change with different landscape models, in which phenotype B is not engineered to provide such a clear benefit to a

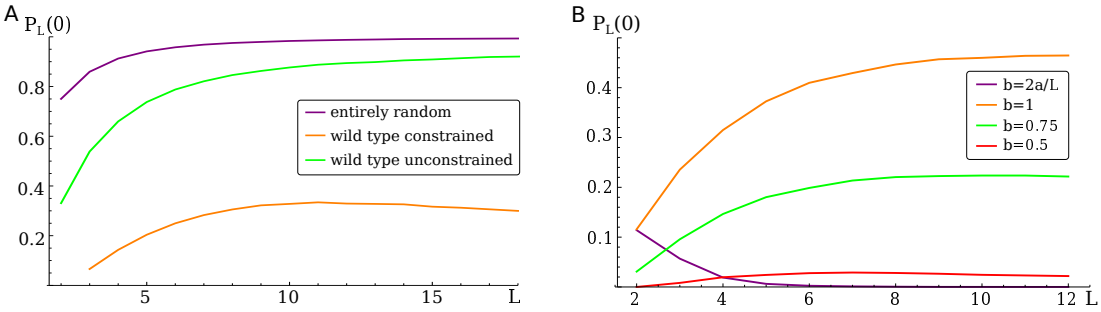

Figure 5.6 *Plots of the probability that randomly generated landscapes contain no accessible paths (of length L) connecting the wild type and antipodal target genotypes. Both plots shows curves of $P_L(0)$ — the probability that there are no accessible paths — as a function of L. (A) is for the House of Cards (HoC) random landscape model. The curves are "entirely random" in which all genotypes have random fitness, "wild type unconstrained" and "wild type constrained" in which the target genotype is assigned to be the global fitness maximum and the wild type genotype is random in the former case and assigned to be the fitness minimum in the latter case. (B) is for the Rough Mount Fuji (RMF) random landscape model as defined in (5.9). The curves compare different values of the landscape parameter b while $a = 1$. All results are averaged over 10^5 landscape realisations.*

population that is struggling to evolve on landscape A.

5.3.2 House of Cards/House of Cards landscapes

We now generalise the model to consider when both fitness landscapes A and B are randomly generated. We begin by looking at the case in which both use the House of Cards (HoC) model with the same value for the landscape ruggedness χ. Accessible pathways are expected to be increasingly rare in these landscapes with increasing L. This can be seen in Fig. 5.6A which, similarly to [62], plots the quantity $P_L(0)$ — the probability that there are no accessible paths of length L connecting the wild type genotype and target (antipodal) genotype in the landscape — as a function of sequence length L. Therefore in what follows we remove the restriction that landscape A contains no accessible path separating the wild-type state $\{0,..,0\}^{\mathrm{A}}$ to the target state $\{1,..,1\}^{\mathrm{A}}$. This is despite the fact that at low L, which we will often focus on in the following, there is still a significant probability that landscape A will contain accessible paths. For example, Fig. 5.6 predicts that when $L = 2$ this probability will be around 0.65.

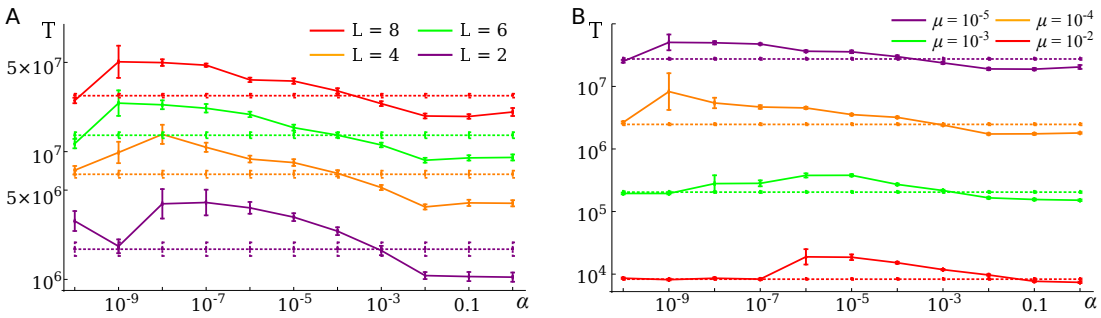

Figure 5.7 *The adaptation time T as a function of the switching rate α in the HoC/HoC model. Dashed lines identify T when $\alpha = 0$. (A) A plot comparing curves for different sequence lengths L when $\mu = 10^{-5}$. (B) A plot comparing curves of different μ when $L = 8$. The remaining parameters for both plots are $K = 20, \chi = 0.4$ and $d = 0.1$. All data is collected using a KMC algorithm and averaged over 500 fitness landscapes.*

Stochastic model - small population sizes

First we consider the stochastic evolution of small populations of size $K = 20$. Figure 5.7 shows plots of the adaptation time T as a function of the switching rate α. Figure 5.7A compares curves for different values of the sequence length L. As in Fig. 5.3, there is a peak in the curves at low values of α, in which phenotype switching slows down the process. A reduction in T occurs at the largest α values, as rapid switching lessens the effect of intermediate deleterious states. However, this reduction in T below the $T(\alpha = 0)$ value occurs at larger α values than we saw in Fig. 5.3A, at approximately the same point for all curves (except $L = 2$).

Figure 5.7B compares curves of $T(\alpha)$ for different values of the mutation probability μ. Again there are similarities between this plot and Fig. 5.3B. The peak appears smaller in Fig. 5.7B than Fig. 5.3B, although we should be careful with direct comparisons between these two plots as the L values differ by 1. A smaller peak may be because the landscape for phenotype B is not as advantageous as in the uniform case, so the population will be less likely to go into it and become trapped.

Stochastic model - large population sizes

We now consider the evolution of larger populations in the HoC/HoC model. Figure 5.8, as in Fig. 5.5, compares plots of $\Delta \log T = \log_{10}[T/T(\alpha = 0)]$ — the

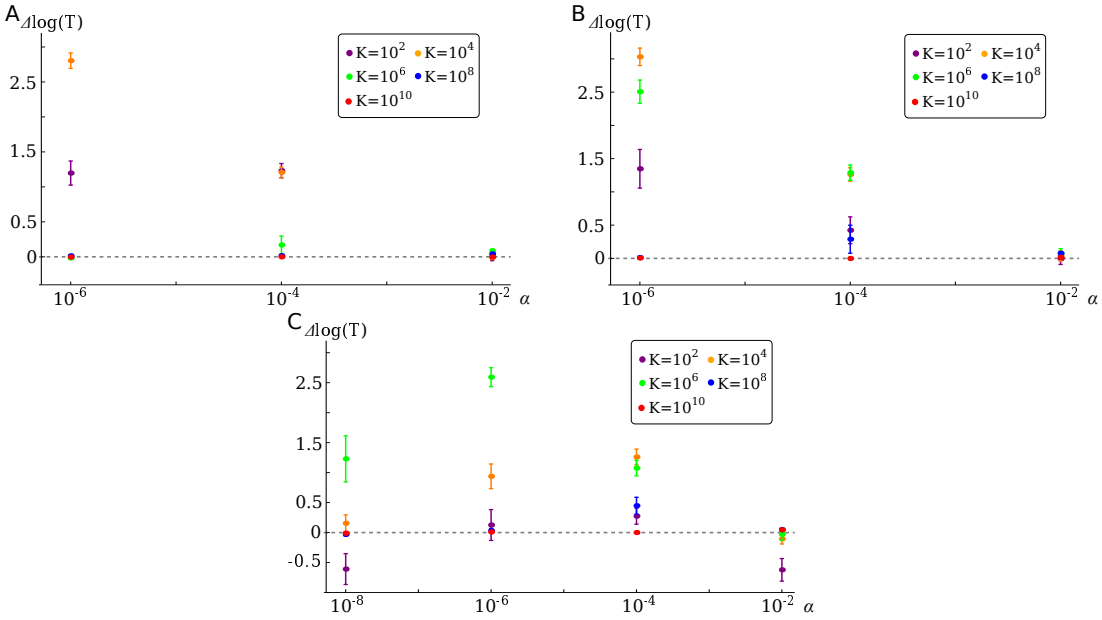

Figure 5.8 *Plots comparing the adaptation time difference* $\Delta \log T = \log_{10}[T/T(\alpha = 0)]$ *as a function of* α *for different values of* K *in the HoC/HoC model.* $\Delta \log T$ *measures the difference (in orders of magnitude) of the adaptation time* T *compared to the case without switching (i.e.* $T(\alpha = 0)$ *which corresponds to the dashed line at* $\Delta \log T = 0$*). The sign of* $\Delta \log T$ *identifies whether* T *has increased or decreased with phenotype switching. All plots compare points for* $K = \{10^2, 10^4, 10^6, 10^8, 10^{10}\}$*. The parameters used in (A) are* $\mu = 10^{-4}, L = 2, \chi = 0.4$ *and* $d = 0.1$*, while the remaining plots differ to (A) by a single parameter as follows: in (B) the mutation probability* μ *is reduced by an order of magnitude to* $\mu = 10^{-5}$ *and in (C) the sequence length* L *is increased by 1 to* $L = 3$ *. All data is averaged over at least 500 fitness landscapes and collected using a* τ*-leap algorithm.*

difference in adaptation time T (in orders of magnitude) between the T value being considered and $T(\alpha = 0)$ — as a function of α for various K values. We examine this for intermediate α values over which we expect the optimal range may exist. Figures 5.8A and 5.8B exclude results for $\alpha = 10^{-8}$ as they did not suitably converge. Figures 5.5B and C differ from Fig. 5.5A by a single parameter.

The most notable difference between the plots in Fig. 5.8 and those in Fig. 5.5 (i.e. from the HoC/Uniform model) is that here when phenotype switching impacts the process it is by slowing it down (while in Fig. 5.5 it accelerated it). It also appears in Fig. 5.8 that the reduction in T at rapid switching rates does not occur. However, this reduction is likely to be absent here simply because we do not consider large enough α to see it. For example, in this model when $K = 20$ we observed in Fig. 5.7A that the intersection between the curves of $T(\alpha)$ and

$T(\alpha = 0)$ occurs at larger α values than in the HoC/Uniform model (see Fig. 5.3A)

In Fig. 5.8A, only points for $K = 10^2$ and $K = 10^4$ are affected by phenotype switching. In both cases the adaptation time T is larger at the lowest frequencies of switching ($\alpha = 10^{-6}$ and $\alpha = 10^{-4}$). For $K = 10^4$ at $\alpha = 10^{-6}$ this increase is by almost three orders of magnitude. We will shortly consider why this happens.

The mutation probability μ is an order of magnitude lower in Fig. 5.8B than in Fig. 5.8A. Points for all K but the largest ($K = 10^{10}$) are now affected by phenotype switching. At the lowest switching frequency ($\alpha = 10^{-6}$) the process for $K = 10^2, 10^4$ and 10^6 are significantly slowed down (with $K = 10^6$ at $\alpha = 10^{-6}$ going from $\Delta \log T = 0$ to $\Delta \log T \approx 2.5$ between Fig. 5.8A and Fig. 5.8B). For all K its necessary that $\Delta \log T = 0$ as $\alpha \to 0$ and therefore these positive values of $\Delta \log T$ are part of a peak in the curve of $T(\alpha)$, like those shown in Fig. 5.7.

Finally, in Fig. 5.8C the sequence length L is larger than in Fig. 5.8A by a single locus. Again all K values except $K = 10^{10}$ experience some change in T amongst the considered frequencies of switching, with the most significant being $\Delta \log T \approx 2.5$ for $K = 10^6$ at $\alpha = 10^{-6}$. We can see here the peaked curves of $T(\alpha)$ reducing towards their $\alpha = 0$ values (as $\Delta \log T$ is reducing to zero) at the lower α values considered for $K = 10^4, 10^6$ and $K = 10^8$. Two points for $K = 10^2$ ($\alpha = 10^{-8}$ and $\alpha = 10^{-2}$) show the only reduction in T with phenotype switching in Fig. 5.8. In both instances $\Delta \log T \approx -0.5$ and it is not clear why this happens.

We now examine why the adaptation time T can increase significantly when cells are able to switch phenotype, as seen in Fig. 5.8. To do this we examine the underlying data that created two of the largest $\Delta \log T$ values in Fig. 5.8: that of ($\alpha = 10^{-6}, K = 10^4$) in Fig. 5.8A and ($\alpha = 10^{-6}, K = 10^6$) in Fig. 5.8B. For both of these points $\Delta \log T > 2$.

The adaptation time T is an average of the adaptation times collected in each simulation run, which we will call t. Each run uses a different realisation of the fitness landscape model. The distribution of times t in the underlying data reveals that the high values of T are due to a small fraction of particularly large t values (orders of magnitude greater than the average value T).

We will assume in the following that these large t values (i.e. the outliers) occur mainly due to the structure of the fitness landscapes selected for those simulation runs (and not on stochastic effects of the evolution). Figures 5.9A and B show

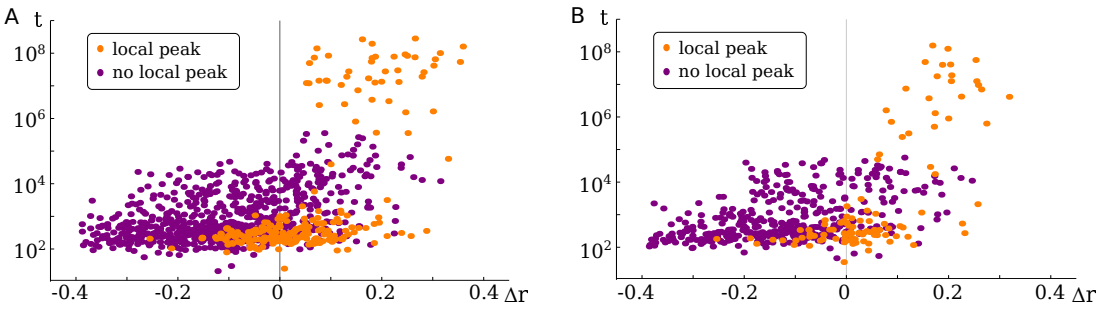

Figure 5.9 *Understanding why phenotype switching increases the average adaptation time T in the HoC/HoC model. (A) and (B) show scatter plots when $(\mu = 10^{-4}, K = 10^4)$ and $(\mu = 10^{-5}, K = 10^6)$ respectively. These plot the adaptation time t for individual simulation runs against the differences in fitness $\Delta r = r^{\mathrm{B}}_{\{0,0\}} - Max[r^{\mathrm{A}}_{\{1,0\}}, r^{\mathrm{A}}_{\{0,1\}}]$. Orange points identify when the state $\{0,0\}^B$ is a local peak (across both landscapes so its fitness is greater than the wild-type $\{0,0\}^A$ also). Purple points identify when $\{0,0\}^B$ is not a local peak. The remaining parameters used are $L = 2$ and $d = 0.1$.*

scatter plots for the points $(\alpha = 10^{-6}, K = 10^4)$ and $(\alpha = 10^{-5}, K = 10^6)$ from Figs. 5.8A and B respectively. These plot the individual times t against Δr, which is the fitness difference between the state $\{0,0\}^{\mathrm{B}}$ and the largest of $\{1,0\}^{\mathrm{A}}$ and $\{0,1\}^{\mathrm{A}}$ (i.e. $\Delta r = r^{\mathrm{B}}_{\{0,0\}} - \mathrm{Max}[r^{\mathrm{A}}_{\{1,0\}}, r^{\mathrm{A}}_{\{0,1\}}]$). Orange points identify simulation runs in which the landscapes have $\{0,0\}^B$ as a local peak in the composite $(L+1)$ dimensional landscape of both phenotypes (i.e. in which $r^{\mathrm{B}}_{\{0,0\}} > r^{\mathrm{A}}_{\{0,0\}}$ as well as $\{0,0\}^{\mathrm{B}}$ being a local peak in landscape B). Purple points identify runs in which $\{0,0\}^{\mathrm{B}}$ is not a local peak in the composite landscape.

Both plots in Fig. 5.9 show a similar result. The outlier points (defined here arbitrarily to be the points for which $t \geq 10^6$ in Fig. 5.9A and $t \geq 10^5$ in Fig. 5.9B) all correspond to the state $\{0,0\}^B$ being a local peak of the composite landscape (as all these points are orange). Therefore the increase in the adaptation time T may be due to individual runs in which the population is trapped at a local peak at state $\{0,0\}^{\mathrm{B}}$.

For all of the outlier points $\Delta r > 0$. Therefore for the population starting at state $\{0,0\}^{\mathrm{A}}$ the step to the local peak at $\{0,0\}^{\mathrm{B}}$ was the step of steepest ascent in fitness. This is similar to the behaviour associated with the greedy dynamics evolutionary regime. While the parameters for the points analysed in Fig. 5.9A do not quite match those associated with this regime, those of Fig. 5.9B may. Here the rate of mutant production $\alpha K = \mu d K = 1 \sim L$ while $(\mu d)^2 K \ll 1$, while $K\Delta r \gg 1$ ensuring an approximate form of the selection condition of this

regime is satisfied.

Often when $\{0,0\}^{\mathrm{B}}$ is both a local optimum and the step of steepest ascent from the wild-type (i.e an orange point such that $\Delta r > 0$) the times t are not outliers. In this case we assume that most of the population, despite it being the best step to make, did not travel to $\{0,0\}^{\mathrm{B}}$. This behaviour may occur due to the population either not satisfying the necessary conditions for the greedy regime or through stochastic effects. Note that the plots of Fig. 5.9 establish whether $\{0,0\}^{\mathrm{B}}$ is a local peak but not by how much compared to the neighbouring states of $\{0,0\}^{\mathrm{A}}, \{1,0\}^{\mathrm{B}}$ and $\{0,1\}^{\mathrm{B}}$. If the fitness of $\{0,0\}^{\mathrm{B}}$ is greater but comparable to the fitness of any of these states then the population may distribute itself between these states and not become entirely trapped at $\{0,0\}^{\mathrm{B}}$. This could lead to the target state $\{1,1\}^{\mathrm{A}}$ being evolved quicker.

Therefore stochastic phenotype switching can slow down the evolution of a population if the secondary landscape contains local peaks that can attract and trap the population. This is particularly a problem at larger population sizes, which due to greedy dynamics, are more likely to be trapped [92]. This may be why the increases in T in Fig. 5.8 can be much greater than those observed for small populations in Fig. 5.7. The results we examined here were for the smallest values of the sequence length L (i.e. $L = 2$ and $L = 3$). For larger L the number of evolutionary trajectories to the target and expected number of local optima will increase [101]. Additional work needs carried out to examine the effect this has on results.

5.3.3 Rough Mt Fuji landscapes

The final landscape model we will consider uses the Rough Mount Fuji (RMF) model for landscapes A and B. In this model the average fitness of a state increases the closer it is to the target state genotype, which is again $\{1,...,1\}^{\mathrm{A}}$, the antipodal state to the wild type $\{0,...,0\}^{\mathrm{A}}$. In the following the fitness of genotype $\vec{\sigma}$ (in either landscape) is randomly assigned by the following fitness function

$$r_i(\vec{\sigma}) = 1 + \left(\frac{a}{L}\right) h(\vec{\sigma}, \vec{\sigma}_{\text{wild-type}}) + x\left(-\frac{b}{2}, \frac{b}{2}\right), \tag{5.9}$$

where $h(\vec{\sigma}, \vec{\sigma}_{\text{wild-type}})$ is the Hamming distance between genotype i and the wild type genotype. The function $x(-\frac{b}{2}, \frac{b}{2})$ selects a uniformly distributed random number in the interval $[-\frac{b}{2}, \frac{b}{2}]$. The parameters a and b characterise the structure

of these landscapes, controlling the average fitness increase with Hamming distance and the degree of noise respectively.

Regardless of L the fitness function of (5.9) has the (average) upper limit of $1+a$. This was chosen so that the landscapes have an (average) fixed fitness maximum rather than an unbounded value. This means that as L changes the statistics of the landscapes change. Following [62] and using the fitness function defined in (5.9) the landscapes ruggedness γ (where γ was defined in 5.4) is

$$\gamma = \left(\frac{a}{L}\right)\sqrt{\frac{12}{b^3}} \tag{5.10}$$

$$= \sqrt{3} \quad \text{when} \quad b = \frac{2a}{L}. \tag{5.11}$$

The second line is true only when $b = 2a/L$, which will be our choice in the following. This choice for b ensures that an important feature of the landscape - the ruggedness - remains constant while we vary L. On the other hand the mean fitness change with Hamming distance decreases as L increases. As $L \to \infty$ the fitness landscapes given by (5.9) tend to the House of Cards model, with all fitnesses drawn randomly from the interval $[1 - \frac{b}{2}, 1 + \frac{b}{2}]$.

In the following we experiment with two scenarios in which the randomly generated RMF landscapes are (i) rejected if they contain accessible paths and (ii) always accepted. The likely scenario for RMF landscapes (for our choices for a and b) is that accessible paths exist that connect the wild-type state and the target. This can be seen in Fig. 5.6B, which plots $P_L(0)$ — the probability that there are no accessible paths in the landscape — as a function of the sequence length L. It compares curves of different fixed values of the parameter b, alongside a curve with the variable form of $b = 2a/L$. We can see that when $b = 2a/L$, the probability $P_L(0)$ decreases monotonically from ~ 0.1 when $L = 2$ to be approximately zero when $L = 6$.

Deterministic model

We begin the analysis of the RMF/RMF model with the numerical solutions to the deterministic model of (5.5) to (5.8). Figure 5.10 shows plots of the adaptation time T as a function of the switching rate α for different values of μ and sequence length L.

Figures 5.10A and B show results for $L = 2$ and $L = 3$ respectively when

landscapes with accessible paths are included. Both plots show the existence of the optimal range for α, in which T can be reduced by many orders of magnitude compared to $T(\alpha = 0)$. As we have come to expect, the valley only appears for small enough values of the mutation probability μ (for $\mu \leq 10^{-7}$ in both Figs. 5.10A and B) and increases in significance as μ reduces.

At low values of α, T can be larger than in the absence of switching which leads to a peak in the curves of $T(\alpha)$ at low frequencies of α. We also observed this happening in the HoC/HoC model in Section 5.3.2 where we analysed the peak (in Fig. 5.9) and concluded it was likely due to the population being trapped at a local peak in phenotype B. The smaller α is, the longer the escape from phenotype B (back to phenotype A) will take and hence T increases. However, as α increases escape from phenotype B (e.g. from a local peak) becomes less time consuming (and trapping is less likely to have occurred to begin with). This can be seen in the plots of Fig. 5.10 (particularly Figs. 5.10C and D) where, in general, the intersection of each curve of $T(\alpha)$ with the line of $T(\alpha = 0)$ increases by approximately an order of magnitude in α as μ increases by the same amount. The intersection between the two often occurs when $\alpha \approx \mu d$, i.e. when the rate of phenotype switching is comparable to the rate that genetic mutants are produced.

Figures 5.10C and D show results for $L = 2$ and $L = 3$ respectively when neither landscape contains accessible trajectories. These plots contain most of the same features as those in Figs. 5.10A and B, except there is a general increase in T. This is expected as the population must cross at least a single deleterious state in either landscape due to there being no accessible paths. By ensuring that there is an obstacle to evolution, populations benefit more from being able to switch phenotype. This leads to the optimal α range now being observable in curves from which it was absent in Figs. 5.10A and B. For example, this can be seen in the curves for $\mu = 10^{-6}$ in Figs. 5.10C and Fig. 5.10A.

Stochastic model

We now consider the stochastic evolution of the population in the RMF/RMF model. For this we consider simulation results for a range of population sizes (i.e. carrying capacities K). Figure 5.10 predicts that an optimal range for the switching rate α will exist at low enough values of the mutation probability μ. The RMF landscapes we use here (for both landscapes A and B) are ones that do not contain accessible paths (i.e landscapes with accessible paths are screened

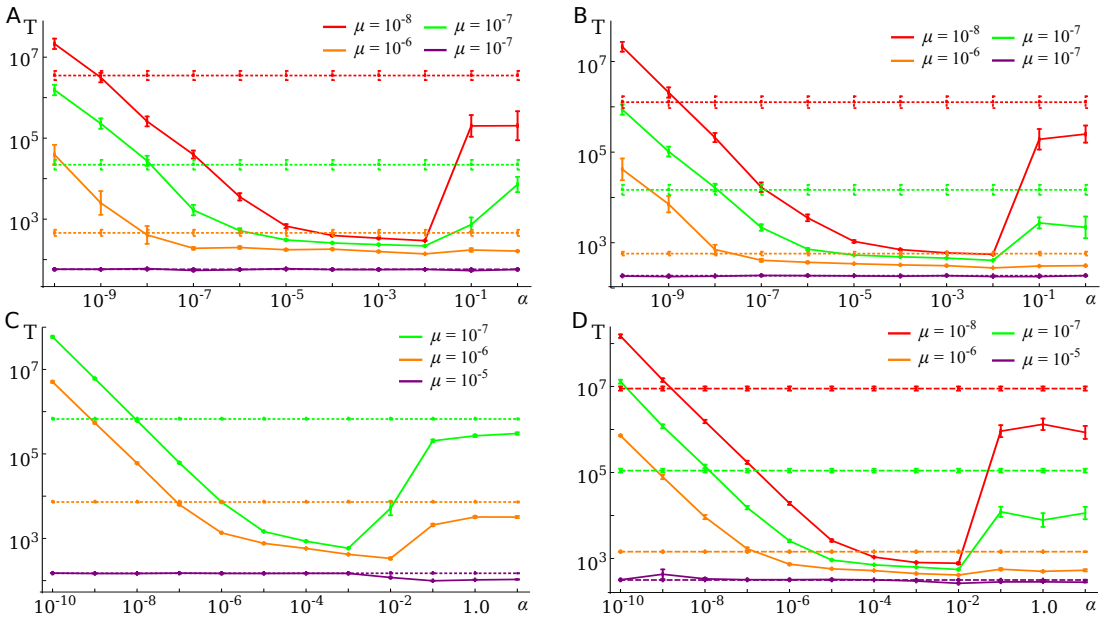

Figure 5.10 *Plots of the adaptation time T as a function of the switching rate α in the RMF/RMF model. All plots compare curves for different values of mutation probability μ. In (A) and (B) landscapes in either phenotype can contain accessible paths, while for (C) and (D) landscapes do not include accessible paths. $L = 2$ for (A) and (C) and $L = 3$ for (B) and (D). The remaining parameters are $K = 10^8, a = 1$ and $b = 2a/L$. Results were gathered using an Euler update algorithm and averaged over at least 500 fitness landscapes.*

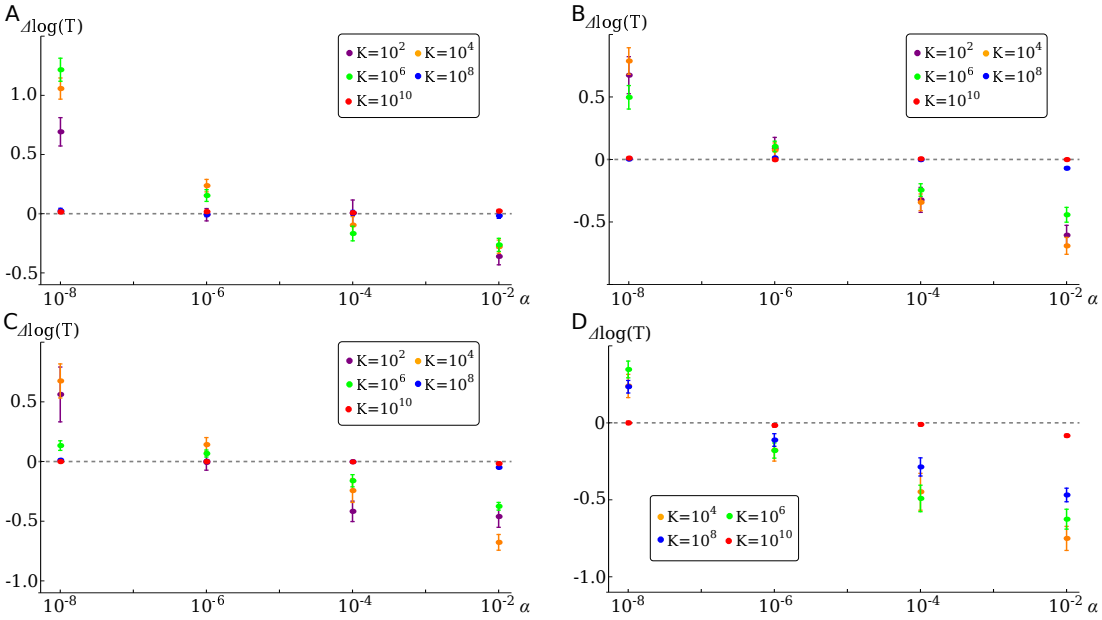

Figure 5.11 *Plots comparing the adaptation time difference* $\Delta \log T = \log_{10}[T/T(\alpha = 0)]$ *as a function of* α *for different values of* K *in the RMF/RMF model.* $\Delta \log T$ *measures the difference (in orders of magnitude) of the adaptation time* T *to the case without switching (i.e.* $T(\alpha = 0)$ *which corresponds to the dashed line at* $\Delta \log T = 0$*). The sign of* $\Delta \log T$ *identifies whether* T *has increased or decreased with phenotype switching. All plots compare points for different values of the carrying capacity* K*. The parameters used in (A) are* $\mu = 10^{-5}, L = 2, b = 2a/L$ *and* $d = 0.1$*, while the remaining plots differ to (A) as follows: in (B) and (C) the sequence length* L *is increased to* $L = 3$ *and* $L = 4$ *respectively, while in (D)* $L = 3$ *and the mutation probability* $\mu = 10^{-6}$*. All data is averaged over approximately 500 fitness landscapes and collected using a* τ*-leap algorithm.*

for and rejected). These are less likely to occur (see Fig. 5.6B) but according to Fig. 5.10 should result in the optimal α range appearing at larger values of μ.

Figure 5.11 compares plots of the difference in adaptation time $\Delta \log T = \log_{10}[T/T(\alpha = 0)]$ (i.e. in orders of magnitude relative to the case of $T(\alpha = 0)$) as a function of α. Each plot compares this for a range of K values. Figure 5.11D does not include points for $K = 10^2$ due to a problem with convergence.

Figure 5.11A shows results when the sequence length $L = 2$ and $\mu = 10^{-5}$. Points for the three smallest K values ($K = 10^2, 10^4$ and 10^6) are affected as a result of phenotype switching (the other K values are not). At low values of α they have $\Delta \log T > 0$. This indicates the existence of a peak in the curve of $T(\alpha)$ and a slowing down of the evolutionary process.

In Figs. 5.11B and C the sequence length L is increased by one and two loci respectively compared to Fig. 5.11A. According to the fitness landscape in (5.4) while the ruggedness remains the same under such a change the average increase with Hamming distance (from the wild-type genotype) decreases from $a/2$ to $a/3$ and $a/4$ respectively in these cases. With this change, only points for $K = 10^2, 10^4$ and 10^6 again show any change with phenotype switching. The magnitudes $|\Delta \log T|$ at high switching frequencies is slightly larger, indicating that phenotype switching is benefiting the population more. Conversely at low α, the magnitude of the peaks — at which the process is slowed down — are reducing in size compared to Fig. 5.11A. This may be because the peak in $T(\alpha)$ is shifting to lower α values or is vanishing altogether.

In Fig. 5.11D the mutation probability μ is an order of magnitude smaller than in Fig. 5.11B. In this instance, compared to Fig. 5.11B, all of the population sizes benefit from being able to switch phenotype at high frequencies (with $K = 10^{10}$ just beginning to leave the value $\Delta \log T = 0$). At the lowest switching frequency considered here ($\alpha = 10^{-8}$), a peak still exists in most curves of $T(\alpha)$ but these are smaller than they were when μ was greater in Fig. 5.11B. This matches with our observations in Figs. 5.10C and D that, as μ reduces, the intersection between the curves of T and $T(\alpha = 0)$ moves to lower values of α.

Although none of the plots in Fig. 5.11 confirm the existence of an optimal α range, they do show reductions in T at high frequencies of switching. They are also in approximate agreement with the results from the deterministic model in Fig. 5.10 (i.e. with the points for $K = 10^8$ in Fig. 5.11A, B and C). The results in Fig. 5.10 predict that as μ decreases further, the optimal α range comes into existence (both when the RMF landscapes include and exclude accessible paths). While we cannot be sure that the system of equations in (5.5) to (5.8) provides an adequate mean description of the stochastic behaviour at these parameters, we have seen nothing here to suggest they do not. Ultimately, further work is necessary to confirm the existence of an optimal α range in the RMF/RMF model.

5.4 Discussion and conclusions

In this chapter we carried out an exploratory study into the effect that stochastic phenotype switching (SPS) has on the evolution of populations of replicating binary sequences. These sequences evolve over multi-dimensional, randomly

generated fitness landscapes, which they symmetrically switch between. This analysis was carried out for different landscape models, which considered different random landscape types for the two fitness landscapes.

In the HoC/Uniform model we found that SPS can benefit evolving populations through the creation of an optimal range for the switching rate α. This was observed for all but the smallest population sizes ($K = 20$) considered. In this optimal range the adaptation time T can be significantly reduced. The largest reductions we saw were by almost four orders of magnitude in the deterministic model (see Fig. 5.2B) and three in the stochastic model (see Fig. 5.5D). The magnitude of the reduction in this optimal range increases with reducing mutation probability μ and increasing sequence length L. This latter point was shown to be very significant in the change from $L = 2$ to $L = 3$ (e.g. see Figs. 5.5A and D). We did not test if increasing L further continues such a significant change, due to how time consuming the simulations are for larger L. However, in Fig. 5.4 we considered simulation results for L up to $L = 5$ for small population sizes ($K = 100$). We found that while there is a large difference between the curves of $T(\alpha)$ for $L = 2$ and $L = 3$, the curves of $L = 3, 4$ and 5 are all similar.

The large reduction observed in T in the optimal α range may allow for fitness costs to be applied to phenotype B without loss of the optimal α range. This would make the model more applicable to many instances of stochastic phenotype switching, in which the second phenotypic state is more resistant to environmental stresses but has a reduced growth rate [16]. More work needs carried out to test if this is the case.

Throughout the analysis of the HoC/Uniform model we were able to compare many of the results to those of the 1D valley crossing model of Chapters 3 and 4. Similarities exist between the two models when we consider the sequence length $L = 2$ in the HoC/Uniform model. This comparison provided insights into understanding the form of the results we saw, as well as helped us to hypothesise why differences between results arose when they did.

We then proceeded to consider models in which landscapes A and B are both randomly generated. At low frequencies of switching we found that the population — or some fraction of it — can become trapped in landscape B. This can result in the adaptation time T increasing to values greater than in the absence of phenotype switching. This was observed for only the smallest population sizes in the HoC/Uniform model (see Fig. 5.3). However, in both the HoC/HoC and

RMF/RMF models this feature is also present at large values of K and can significantly slow down the evolutionary process. In Fig. 5.9, we concluded that this slowing down was there likely due to the population being trapped at a local peak in landscape B. Such local peaks do not exist in the HoC/Uniform model which may be why we did not observe this to occur in Fig 5.5. This feature is particularly harmful to larger populations in which the evolutionary behaviour of greedy dynamics can make it more likely for populations to become trapped [92].

In the HoC/HoC model we were unable to identify the existence of an optimal α range. However, this may be due to our study being over a very small region of parameter space (we discuss more on this point shortly). Also, in the HoC/HoC model we did not screen the random landscapes for accessible paths and instead argued that they were unlikely to exist according to Fig. 5.6A. While this is true for all but the smallest L values, our study primarily concerned $L = 2$ and $L = 3$ for which there is a high chance that accessible paths do exist (again see Fig. 5.6A). We have seen that the optimal α range is most significant when a population is struggling to evolve past fitness barriers. It is possible that such barriers often did not exist in our HoC/HoC model and this resulted in the absence of the optimal α range in our results.

Finally, for the RMF/RMF model we were able to identify that the optimal α range exists in the numerical solutions of the deterministic model (Fig. 5.10). These solutions predict that the optimal range will exist when accessible paths are both included and excluded. Stochastic simulations were able to confirm some of these predictions and showed that phenotype switching could speed up the process (see Fig. 5.11D). Whether or not this is due to the existence of an optimal α range, or a general speed-up at large α, still remains to be explored.

The work in this chapter contains a significant number of shortcomings and unfinished points that could be the focus of future work. As mentioned earlier, we only carried out simulations for a small set of parameter values. Most detrimental to this study was the limited values used for the sequence length L. The largest L we considered was $L = 8$ but we mostly focussed on when $L = 2$ and 3. With natural selection acting genome wide we are most interested in results when this quantity is very large. This point is frustrating but understandable given the waiting times required to simulate the model at larger values of L. Nevertheless, while some of the results we saw are promising we did not gain a sufficient understanding of how they scale with L. The statistical properties of random landscapes generated (such as the expected number of accessible paths

or local fitness peaks) vary significantly between $L = 2$ and 3 up to larger L [62, 63, 139]. How such changes affect the results shown here are unknown.

We also did not sufficiently explore the parameters that characterise the landscape models. We saw in Chapter 3 that for the optimal α range to exist, evolution over landscape A needed to be sufficiently obstructed by a fitness valley. We explored this feature in Chapter 3 with a valley depth of about $\sim 50\%$ the wild type's fitness. However, in this chapter none of the landscapes we used had intermediate states that were as deleterious as this. For example, fitnesses in the HoC landscapes were consistently selected in the range $(0.6, 1]$ (with $\chi = 0.4$). This value of χ may not be large enough to cause evolution over a single landscape to be obstructed enough to warrant the second phenotypic state. More work needs carried out to test a range of possible values for the landscape parameters.

The results of this chapter could be more accurate through averaging them over a greater number of landscape realisations (i.e. more simulation runs). In the results we averaged over at least 500 landscape generations but often no more than that. This low number was again due to how time consuming simulations of these types can be at certain parameter values. There were a number of instances in this chapter of results that are missing or incomplete due to the results failing to converge. It is likely that this failing was not of the numerical technique but that the stochasticity in the results was not sufficiently captured in only 500 runs to produce an accurate average.

Finally, as we discussed in Section 5.3 the accuracy of the system of differential equations of (5.5) to (5.8) in describing the dynamics of the population may be problematic. When the likelihood of the population transitioning to new states is extremely low (so when μ or α is very low) populations smaller than 1 can grow themselves at these new states. Describing low population numbers of mutants deterministically is never ideal but in this case it could lead to erroneous results (i.e. results a stochastic formulation of the system would not recover). Future work can reduce the likelihood of this happening by, e.g., introducing stochasticity into the existing deterministic model, or only allowing growth to occur at states when the population exceeds 1.

Chapter 6

Modelling the evolution of resistance in Escherichia coli to the antibiotic ciprofloxacin

6.1 Introduction

In this chapter we present a model of how a population of the bacterium *Escherichia coli* (*E. coli*) can evolve resistance upon exposure to the fluoroquinolone antibiotic *ciprofloxacin*. In experiments, *E. coli* is observed to acquire rapid resistance, over a matter of hours, to sub-lethal concentrations of ciprofloxacin [28, 218]. We would like to understand the importance of phenotype switching to a second, non-replicating phenotype, to the evolution of resistance.

The development of significant resistance of *E. coli* to the *fluoroquinolone* family of antibiotics (to which ciprofloxacin belongs) requires multiple mutations to occur in different genes [107]. These genes are primarily those that code for the (type-II) topoisomerase enzymes and those contributing to the abundance of drug-efflux pumps in the cell. Resistant cells often have combinations of a select few resistance-conferring mutations.

However, resistance to fluoroquinolones does not have to be genetical. In many bacterial species (e.g. *E. coli* [28], *Staphylococcus aureus* [126] and *Salmonella enterica* [183]), when exposed to stress, such as the presence of harmful chemicals (e.g. antibiotics), cells can induce a response that is collectively known as the

SOS response. This consists of the induction of as many as forty genes that are associated with DNA protection and repair [94]. Among those genes are those causing cell division arrest, such as *sulA* in *E. coli* [25]. During cell division arrest, cells can continue to grow and replicate genetic material, causing them to exist in a multi-nucleated filamentous state. Simultaneously, cells become less sensitive to the action of antimicrobial drugs.

Within this filamentous state, mutation rates can increase by as many as four orders of magnitude, following the induction of low fidelity replication polymerases [35] which are able to copy damaged DNA [194]. Meanwhile, the growth of filamentous cells can be interrupted by asymmetric division, producing small offspring cells — in a process known as *budding* — that may contain resistant mutations that will allow the cells to resume normal division [28].

The SOS response is different to the purely *stochastic phenotype switching* we have previously considered because it occurs in response to a stimulus (stress caused by the antibiotic). Nevertheless, it provides a secondary phenotype with reduced sensitivity to the antibiotic — a safe "niche" — in which cells can more easily explore genetic variants in order to accelerate the evolution of resistance. This is similar to the benefit that stochastic phenotype switching can bring to populations trapped at local fitness peaks, as studied in the preceding chapters.

The model considered in this chapter again has two phenotypic states; in one of these the cells can grow normally but there can be fitness barriers they must overcome, while in the other (the filamentous phenotype) the cells are unable to replicate but can explore genotype space through chromosomal mutations.

This work is motivated by a number of questions regarding how *E. coli* acquires rapid resistance to ciprofloxacin. The first is whether or not significant evolution of resistance can occur over short timescales without the inclusion of the filamentous phenotypic state. Experimental work on *E. coli* suggests it cannot [28, 35]. Another question regards the observation that certain mutations cause an increase in both fitness and resistance relative to the wild-type genotype [128]. This raises the possibility of populations of *E. coli* evolving resistance to ciprofloxacin in the absence of the drug. We will see if the model predicts that this is likely to happen.

Finally, inspired by some unpublished experimental work, we will look into the possibility of resistant bacteria "forgetting" their resistance, i.e. reverting back to a more sensitive genotype, when incubated for a few generations in the absence

Gene (bp/aa)	Function	Mutation	Effect
gyrA1	Codes for DNA Gyrase	S83L	Alters drug target
gyrA2	Codes for DNA Gyrase	D87N	Alters drug target
parC	Codes for topoisomerase IV	S80I	Alters drug target
acrR(648/215)	Represses *acrAB* gene	Knockout	Efflux pumps increase
marR(435/144)	Represses *marA* gene	Knockout	Efflux pumps increase

Table 6.1 *The resistance conferring mutations considered in the model*

of ciprofloxacin.

6.2 Background

Fluoroquinolones are an important family of synthetic antibacterial drugs. For example, they are the most widely used in treating urinary tract infections in North America and Western Europe [107]. They work by inhibiting the enzymes *DNA Gyrase* and *Topoisomerase IV* in the bacterial cell. Both of these enzymes are necessary in regulating the process of chromosomal supercoiling — and are vital for replication and transcription.

E. coli acquire resistance to fluoroquinolones in two main ways. The first is by mutations in the genes that code for DNA Gyrase and Topoisomerase IV. Such mutations, occurring at the "quinolone resistance determining regions" [107], strongly reduce the affinity of fluoroquinolones to these enzymes. The possible mutations of this type that we will consider are two occurring in the *gyrA* gene (which codes for one of the subunits of DNA Gyrase) and one in the *parC* gene (which codes for one of the subunits of Topoisomerase IV). These mutations are all of the type of amino acid substitutions.

The second common way for bacteria to acquire resistance to flouroquinolones is through mutations that reduce the concentration of drugs in the bacterial cytoplasm. Such mutations increase the activity of transmembrane efflux pumps, allowing the drug to be flushed out at a greater rate. The common mutations of this type that are observed in resistant *E. coli*, and that we will use in the following model, are knockout mutations of the *marR* and *acrR* genes [128]. Both of these genes are repressors, which, if mutated, increase the production rate of *AcrAB-TolC* multidrug efflux pumps. An overview of the five resistance conferring mutations that we consider can be seen in Table 6.1.

In the absence of antibiotics, the SOS genes are inhibited in *E. coli* by the repressor LexA, which binds to the promoter of the SOS genes [94]. Upon detection of DNA damage, LexA cleaves itself from the promoters of these genes, causing them to be expressed. The reason for this cleavage is the production of a nucleoprotein complex called the *RecA filament*. The RecA filament does two things; it induces the cleaving of LexA and is involved in catalyzing strand exchange during homologous recombination (a process that repairs DNA double strand breaks). The RecA filament consists of the protein RecA which is bound to a single-stranded DNA (ssDNA). DNA damage can result in ssDNA and therefore the creation of RecA filaments and the induction of the SOS response. For example, in *E. coli*, UV exposure can create single-strand gaps in DNA [171], while antibiotics such as ciprofloxacin, acting to inhibit topoisomerase enzymes, can cause DNA double strand breaks and expose ssDNA [130].

6.3 Model

In the model we consider there to be as many genotypes as there are possible combinations of the five mutations in Table 6.1. By representing the presence and absence of these mutations as 1's and 0's respectively, genotypes can be represented as binary sequences of length $L = 5$ and the genotype space is a 5D hypercube. In this representation, each mutation is assigned to the following locus: $\{gyrA1, gyrA2, parC, marR, acrR\}$. Including the second phenotypic state the space of all possible genotype/phenotype combinations consists of 64 states. For consistency with the preceding chapters, the normal replicating phenotype will be referred to as phenotype A, while the filamentous, non-growing phenotype will be phenotype B.

As in the models of the preceding chapters, cells can mutate during replication (by at most a single point mutation at a time). However, unlike before, the likelihood of producing mutants will now depend on what genotype the mutant is. This is motivated by the five possible mutations (see Table 6.1) having different likelihoods of occurrence. For example, the mutations in the *gyrA* or *parC* genes, in which 0→1 at either loci 1,2 or 3 in the genotype sequence, arise from particular amino acid substitutions taking place. These changes can be brought about by only a few nucleotide substitutions that cause a different codon — the sequence of 3 nucleotides that code for specific amino acids or "stop" signals during protein synthesis — to be produced at a point in the sequence. As the genetic code is

degenerate (i.e. the same amino acid can be be coded for by more than one codon) we will assign each of these mutations a probability of approximately $5\times$ the probability of single nucleotide mutation μ. This factor that multiplies the mutation probability will be referred to throughout as the *mutation coefficient* λ. This is equal to the expected number of ways single nucleotide substitutions can cause the mutation in question, and will differ for different mutation types.

Consider now the mutation coefficients for the mutations in the *marR* and *acrR* genes. These are knockout mutations (i.e. loss of function mutations) that can occur as a result of many single nucleotide mutations such as frameshift mutations, insertion or deletion mutations or the creation of nonsense codons. Therefore these mutations, in which $0\rightarrow1$ at loci 4 or 5 in the genotype sequence, have a far greater likelihood of occurrence than the mutations in the *gyrA* and *parC* genes. This must be reflected in the value of the mutation coefficients for these knockout mutations. In the following we consider these knockout mutations as able to occur in as many ways as are equal to the length of the gene. Therefore the mutation coefficients for the *marR* and *acrR* mutations are 450 and 650 respectively (see the bp length of the genes in Table 6.1). In work that is not presented, smaller mutation coefficients were considered for these mutations — an order of magnitude smaller — and no unexpected changes were observed in the results.

While we can estimate the rate with which the forward mutations $0\rightarrow1$ occur at each locus, it is more difficult to estimate the rate with which the back mutations $1\rightarrow0$ occur. For example, not knowing specifically how the *marR* and *acrR* genes were knocked out makes it difficult to estimate how likely they would be to regain function. However, back mutations for the mutations in the *gyrA* and *parC* genes are simple substitutions of the original nucleotide, or a different one that results in the same codon. Therefore back mutations will sometimes be included for these mutations (with equal mutation coefficients to the forward mutations) but not for those in the *marR* and *acrR* genes. In what follows, whether or not back mutations are included will always be identified alongside any results.

The actions available to cells in the model can be seen in Fig. 6.1, which is separated into actions involving cells in phenotype A and B. Cells in phenotype A have most of the same actions as cells had in the preceding chapters: they can successfully replicate, unsuccessfully replicate (producing a mutant) and switch phenotype. As the antibiotic affects only a cell's growth rate there is no "death" action in the model. As we introduced above in the discussion of mutation

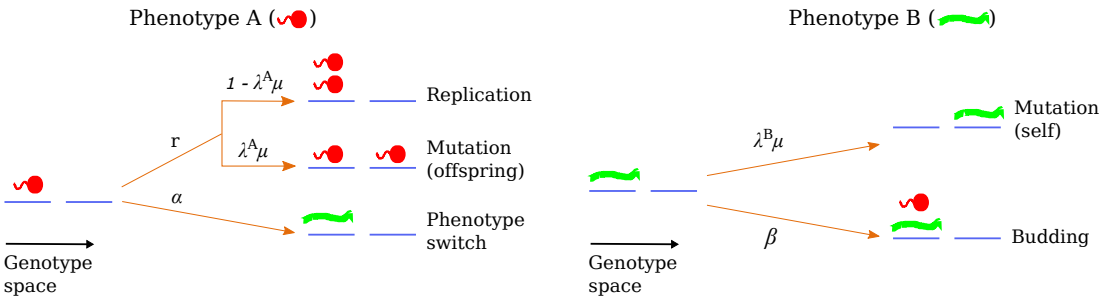

Figure 6.1 *The actions available to cells in phenotypic states A and B in the model, identified by red circular cells and green filamentous cells respectively. Included for each action is the parameters that control the rate with which they occurs; most often these will depend on the genotype in question and any neighbouring genotype that the action involves. Cells in phenotype A can undergo three possible actions: replication, mutation (to each of its neighbouring genotypes) and switching phenotype. Cells in phenotype B can only undergo two actions: mutation of its own genotype and producing budded offspring in phenotype A.*

coefficients, the probability that a cell in genotype i produces a mutant in state j is now $\lambda_{ij}^{\mathrm{A}}\mu$, where $\lambda_{ij}^{\mathrm{A}}$ is the mutation coefficient for this particular mutation. Therefore the probability of mutation-free replication of a cell at genotype i is now $(1-\lambda_i^{\mathrm{A}}\mu) = (1-\sum_j \lambda_{ij}^{\mathrm{A}}\mu)$ where j runs over all nearest neighbour genotypes to i and λ_i^{A} is the *total mutation coefficient* for genotype i.

For cells in phenotype B, Fig. 6.1 shows the two possible available actions: mutation and the production of offspring in phenotype A. We refer to this latter action as the budding process and assume it to occur at rate β. For a cell in phenotype B, mutation corresponds to incorrect DNA replication within the filamentous cell and does not result in the production of offspring. Therefore there can be no population growth from cells in phenotype B; however, they can still explore genotype space through the incorrect replication of their own genotype.

The probability of mutation from genotype i to j in phenotype B is equal to $\lambda_{ij}^{\mathrm{B}}\mu$, where $\lambda_{ij}^{\mathrm{B}}$ is the mutation coefficient for the mutation between genotypes i and j. We assume the mutation coefficients for phenotype B to be three orders of magnitude greater than those for phenotype A (i.e $\lambda_{ij}^{\mathrm{B}} = 10^3\lambda_{ij}^{\mathrm{A}}$). This is because cells in the filamentous phenotype (phenotype B) have been observed to have increased rates of mutation, by as many as four orders of magnitude compared with mutations in the non-filamentous phenotype [28, 35].

The experiment we model here is a serial transfer experiment, which cultures

bacteria during the exponential (log) phase of their growth. Their rate of division is greatest in this phase and is therefore best for viewing evolution over short timescales. However, unbounded growth cannot last forever and a bacterial culture will eventually reach the stationary phase of growth. This can occur due to the exhaustion of nutrients, physical space or the accumulation of inhibitory metabolites or end products in the culture. In a serial transfer experiment, when the stationary phase is reached, a small fraction of the population is transferred to seed a new culture, in which exponential growth can continue. This process can be repeated for as many transfers as the experiment requires. The size of the transferred population must be large enough for genetic diversity to remain, allowing this method to be used in the study of adaptive evolution [18].

In our model, the population starts in the wild-type state (state 00000 in phenotype A) with the total population size $N_T = 10^7$. Growth continues until $N_T = 10^9$ is reached. At this point 1% of the population (rounding population numbers to the nearest integer values) is transferred to a new culture and growth begins again. Each culture therefore starts from the population size $N_T = 10^7$ but the genetic diversity can be different in each one. In the following results, this process is normally repeated for 4 or 5 culture transfers.

A new parameter in the model is the antibiotic concentration C, which affects a cell's mutation and growth rate. Specifically, these will now depend on the fitness of its genotype in the absence of antibiotics (i.e. when $C = 0$ ng/ml), as well as its *minimum inhibitory concentration* (*MIC*) value, a measure of its resistance to the antibiotic.

In our simulations the replication rate of a cell of the wild-type genotype, when $C = 0$ ng/ml, is approximately 1 (simulation time unit)$^{-1}$. Therefore 1 simulation time unit is the average cellular doubling time (i.e. generational time). In *E. coli* this is on average $\sim$ 20 minutes [61], which allows us to infer an approximate physical time from the upcoming results. As we are interested in the evolution of resistance over small timescales (i.e. hours) we only consider results for less than 24 hours.

6.3.1 Growth rates and sensitivities of different genotypes

For the properties of the considered genotypes we use experimental data taken from [128], which is contained in Appendix E. This includes information on the

average fitness and *MIC* values for a particular strain of *E. coli* (MG1655). This data is calculated in [128] for all but three of the possible genotypes we consider. The parameter values for the "missing" three genotypes (00111, 00101 and 00110) are estimated by assuming the level of resistance (i.e. *MIC* value) to be additive in mutation combinations, while the fitness is the minimum fitness of the less mutated neighbouring genotypes. Specifics on the values chosen for these missing genotypes can be found in Appendix E. In work that will not be presented, when these missing genotypes are made lethal — i.e. their fitnesses are set to zero — there is no observable difference in the results. This suggests they are not important and we proceed under this assumption.

Figure 6.2 presents diagrams of the fitnesses (Fig. 6.2A) and *MIC* values (Fig. 6.2B) of all the genotypes we consider. These diagrams show the space of all possible genotypes, with links connecting those that differ by a single point mutation. Each genotype is represented by a circle which contains within it the binary sequence it corresponds to. The background colour of these circles communicate the value of the quantity under consideration, in which a bar legend shows the corresponding numerical values (note the logarithmic scale in the legend of Fig. 6.2B). In these diagrams the wild-type genotype (00000) is located at the bottom. With every row above the wild-type there can be found genotypes with a Hamming distance further away from it. Therefore the genotype at the top of the diagrams — in a row by itself — is the furthest mutated (i.e. 11111) relative to the wild-type. Note that due to the concentrations of *ciprofloxacin* used in the experiment, the errors in the *MIC* values in Fig. 6.2B are ± 1 half doubling step of the *MIC* values that are reported. As suggested in [128] we will consider significant changes in *MIC* to be those that are at least 2-fold. The implications of these errors will be discussed at a later point.

In Fig. 6.2A we see that, in the absence of antibiotics, many of the genotypes with the greatest fitnesses are near the wild-type; three are only a single point mutation away from it (i.e. 10000, 01000 and 00100). The fitnesses of these states are comparable to the wild-type's and therefore — while there are equally fit genotypes elsewhere (e.g. 11100) — there is no significant selective pressure for a population starting at the wild-type to leave the vicinity of it. Therefore we expect, especially over the short timescales we are concerned with here, that the population will remain in the wild-type state. This situation can be contrasted with that of the *MIC* values in Fig. 6.2B. Here we find that, in general, genotypes in the vicinity of the wild-type have low resistance (i.e. low *MIC* values) and that

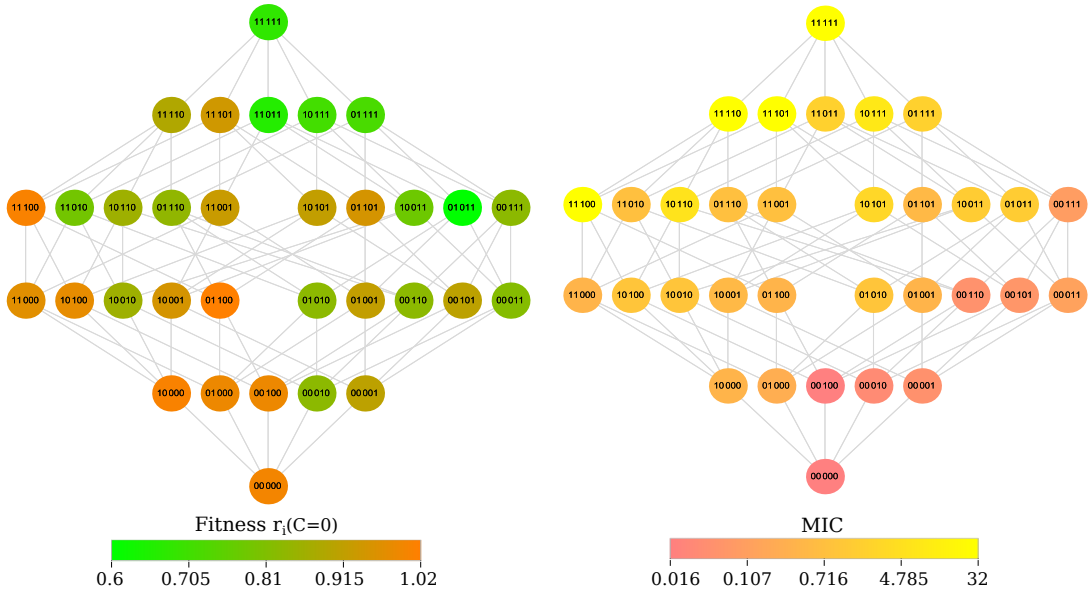

Figure 6.2 *Diagrams presenting the empirical data that is used to calculate the fitness landscape of phenotype A. Both diagrams show the space of all possible genotypes in which links connect genotypes that differ by a single point mutation. Each genotype is represented as a circle with the binary sequence it corresponds to written within it. For each circle the background colour identifies in (A) the fitness and in (B) the MIC value of that genotype. Legends are included that show how the colours translate to numerical values. Note that while the legend for (A) is linear, that for (B) is logarithmic.*

the most resistant genotypes (including the "super-resistant" yellow ones with $MIC = 32\mu$g/ml) are at least three point mutations away.

As expected, we observe in Fig. 6.2 that most genotypes with an increased *MIC* value have a reduction in fitness relative to the wild-type. However, this is not always the case and in some instances both the *MIC* value and fitness increase. This can be seen to greatest effect in genotype 11100 which is super-resistant while having a 1% increase in fitness over the wild-type. However, this fitness increase may not be statistically significant as it is within the error bars of the wild-type's fitness. Similarly genotype 10000 experiences a slight increase in fitness (which again may not be statistically significant), along with a marked increase in *MIC*.

We now specify how the fitness (i.e. growth rate) of each genotype depends on the antibiotic concentration C, its *MIC* value and its fitness in the absence of antibiotics. We assume that in the absence of antibiotics a genotype's growth rate is equal to its fitness $r_i^0 = r_i(C = 0)$ in Fig. 6.2A. From experiments, the growth rate as a function of *ciprofloxacin* concentration C is sigmoidal, such that

it is plateaued for $C \ll MIC$ and drops off rapidly as $C \approx MIC$ [161]. For $C > MIC$ we assume that growth is no longer possible. We therefore use the following function for the fitness r_i of genotype i, with fitness r_i^0 when $C = 0$, minimum inhibitory concentration MIC_i and antibiotic concentration C in the medium:

$$r_i = \begin{cases} r_i^0 \left[1 - \left(\frac{C}{MIC_i}\right)^2\right] & \text{if } C < MIC_i \\ 0 \quad \text{otherwise} \end{cases} \tag{6.1}$$

Using this function we look now at the fitness landscape for a non-zero value of C. Fig. 6.3 shows this for $C = 15$ ng/ml, which is presented in the same way as Fig. 6.2A. This value of C is just below the reported MIC value of the wild-type genotype (which is 16 ng/ml). We see that the fitness of the wild-type is now 10% of what it is when $C = 0$ ng/ml. The only other genotype that is as deleterious as this is 00100. Many of the genotypes appear to have similarly moderate to high fitnesses, which is understandable as they consist of combinations of mutations that are expected to be beneficial when $C \neq 0$. When $C = 15$ ng/ml, following the significant reduction in fitness of the wild-type genotype (relative to other genotypes), we can expect rapid evolution away from the wild-type.

The genotype statistics of Fig. 6.2 only apply to cells that replicate, i.e. those in phenotype A. Cells in phenotype B do not replicate, but we will assume they bud at a rate that depends on their MIC value and the antibiotic concentration C. Furthermore, we will assume that the mutation rate is the same for all genotypes in phenotype B, with only the mutation coefficients changing depending on the specific mutation (i.e. *gyrA*,*marR*,..). This can be considered equivalent to phenotype B having a uniform fitness landscape.

6.4 Single phenotype model

We begin by looking at how the population evolves when confined to phenotype A (i.e. there is no phenotype switching). We carry this out in order to explore the timescales and evolutionary trajectories the population is expected to follow in the absence of the filamentous phenotypic state. We will consider two cases: $C = 0$ and $C \neq 0$ ng/ml.

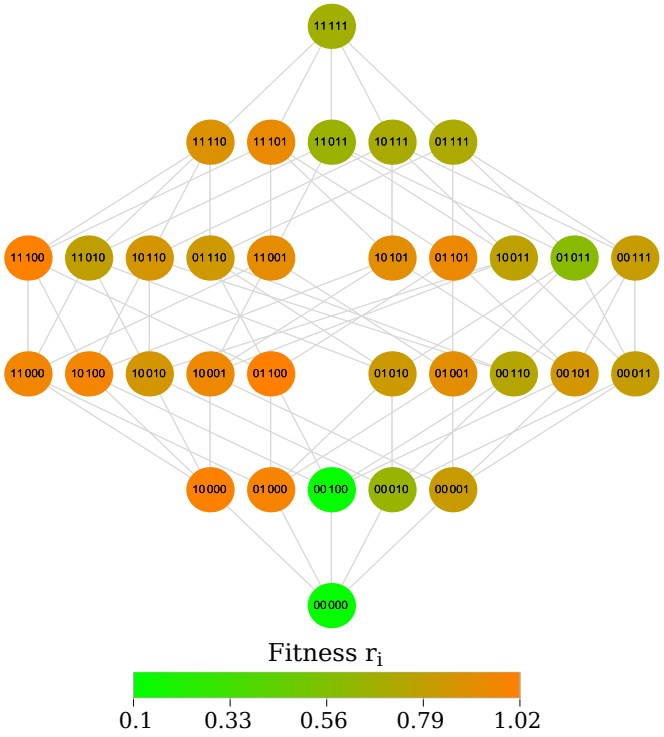

Figure 6.3 *The fitness landscape when the antibiotic concentration* $C = 15$ *ng/ml. The diagram shows the space of all possible genotypes in which links connect genotypes that differ by a single mutation. Each genotype is represented as a circle with the sequence that it corresponds to written within it. The background colour of each circle identifies the fitness* r_i *for that genotype (see the bar legend).*

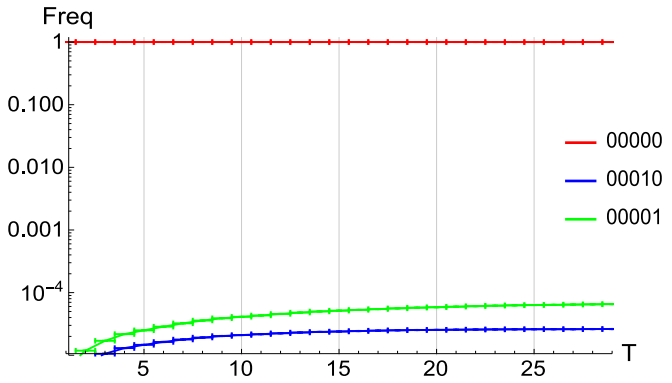

Figure 6.4 *The evolution of the population in the single phenotype model in the absence of antibiotics ($C = 0$ ng/ml). The plot show curves of the genotype populations (expressed as a frequency of the total population) as a function of time T (in generations). Genotypes that are absent never had a frequency as large as 10^{-5}. Vertical lines indicate the points at which culture transfer took place, in which 1% of the population seeds a new culture which continues to evolve. Back-mutations were not considered here. All results were gathered using a KMC algorithm, for mutation probability $\mu = 10^{-8}$, and averaged over 100 runs.*

6.4.1 Evolution in the absence of antibiotics

We first consider what evolution occurs in the absence of antibiotics, i.e. when $C = 0$ ng/ml. Figure 6.4 shows a plot of how the population at each genotype (expressed as a frequency of the total population) evolves as a function of time. Any genotype that is not represented in the plot may still have been present but at fractions lower than 10^{-5} of the total population size. Vertical lines indicate the points at which culture transfers have taken place. This result is for the scenario that excludes back mutations. This is the only scenario we consider for $C = 0$ ng/ml as it is the one that is most likely to induce the population to leave the wild-type genotype.

We observe in Fig. 6.4 that when $C = 0$ ng/ml there is approximately no change to the genetic composition of the population over the time considered. Due to the large mutation coefficients of the knockout mutations — those affecting the final two loci of a genotype sequence — genotypes 00010 and 00001 are the most abundant non-wild-type genotypes in the population. However, as they offer no growth advantage to the population their abundances remain low.

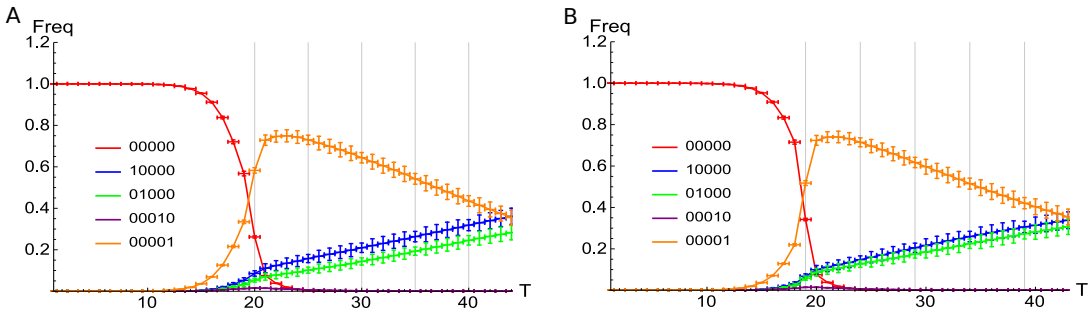

Figure 6.5 *The evolution of the population in the single phenotype model at sub-MIC ($C = 15$ ng/ml) concentrations of ciprofloxacin. All plots show curves of the average frequency of genotype populations as a function of time T (in generations). Genotypes that are absent never attained a frequency in the population as large as 10^{-3}. Vertical lines indicate the points at which culture transfer took place, in which 1% of the population was used to seed a new culture. For (A) back mutations were not possible (i.e no 1→0 mutations) while for (B) they were possible at loci 1,2 and 3. All results were gathered using a KMC algorithm, with mutation probability $\mu = 10^{-8}$, and averaged over 100 runs.*

6.4.2 Evolution in sub-MIC concentrations of antibiotics

We now consider how the population evolves when $C \neq 0$ and is just below the MIC value of the wild-type genotype (which is 16 ng/ml). Figure 6.5 shows results when $C = 15$ ng/ml, for which the fitness landscape is that seen earlier in Fig. 6.3.

Both plots in Fig. 6.5 show how the average genotype populations (expressed as a frequency of the total population) vary as a function of time T. This is shown across 5 culture transfers, so the growth of 6 colonies can be seen in each plot. Figure 6.5A shows results for the scenario with no back mutations (so no mutations going 1→0 at any locus). However, this is relaxed in Fig. 6.5B which allows for back mutations at the first three loci (so the *gyrA* and *parC* genes).

Both plots in Fig. 6.5 show approximately the same results, indicating that back mutations are not important in the adaptive evolution over these timescales. The results show the beginning of the process in which the genotypes 10000 and 01000 become significant in the population. Evolution begins with the wild-type genotype quickly being outcompeted at $T \sim 20 \approx 7$ hours, due to its reduced growth rate when $C \neq 0$. It is first outcompeted by the genotype 00001 which has a knocked out *acrR* gene and the largest mutation coefficient. The genotype

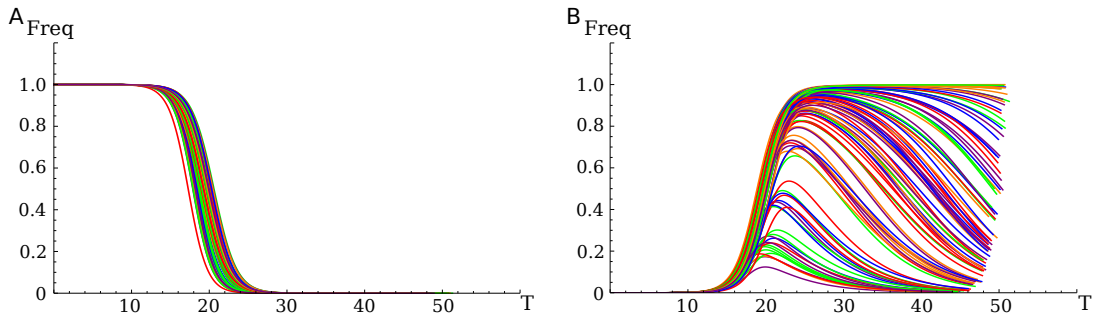

Figure 6.6 *The evolution of the population in individual simulation runs at sub-MIC ($C = 15$ ng/ml) concentrations of ciprofloxacin. (A) and (B) show the frequency of the populations at genotypes 00000 and 00001 respectively as a function of time T (in generations), for* 100 *individual simulation runs. Results were gathered using a KMC algorithm, with mutation probability $\mu = 10^{-8}$.*

featuring the other knockout mutation, 00010, appears also and increases to a small percentage of the population of $\sim 1\%$ before vanishing.

When the wild-type population later produces the genotypes 01000 and 10000, they compete with 00001 for dominance in the population. They have greater growth rates and by the end of the time considered ($\sim$ 16 hours) are at equal frequencies to the 00001 genotype but look set to outcompete it.

The evolution that the population undergoes in the plots of Fig. 6.5 makes qualitative sense. However, there is significant variability in the observed evolution over even these short timescales. To illustrate this, Fig. 6.6 shows data for each individual simulation run that we averaged over to produce the first culture section of the curves in Fig. 6.5A. Figures 6.6A and B show the frequency in the population of the wild-type genotype (00000) and 00001 respectively as a function of time. In Fig. 6.6A, the decaying population frequency appears almost deterministic. However, the stochasticity inherent in the process is apparent in Fig. 6.6B. The maximum abundance of the population at 00001 in different simulation runs, ranges from a small amount ($< 20\%$ of the population) to taking over the population. If the latter outcome occurs then the eventual evolution will follow a different path to the genotypes 10000 and 01000 being created, as these cannot be reached from 00001 without considering back mutations.

We can hypothesise that the stochasticity evident in Fig. 6.6B arises due to the variation in rates with which the population at the wild-type genotype (00000) produces mutants of genotype 00001 compared to mutants of genotypes 10000 or

01000. On average, mutants of the former type occur approximately one hundred times quicker but will be outcompeted by those of type 10000 and 01000 once they appear in the population. Through the lower production rate of the latter mutants we expect both a greater time and a wider distribution of times over which they will first be produced compared with the 00001 mutants. Until this happens a mutant population at 00001 will be left to outcompete the population at 00000 and grow to a significant fraction of the population. Further to this, the larger the population at 00001 becomes the longer it will take, on average, for the eventual mutant population produced at 10000 or 01000 to grow to the same significance in the population (when compared with the time it would take if they were competing with the wild-type genotype 00000). This can be considered an instance of *clonal interference*, discussed in Chapter 2, in which multiple fit genotypes competing for dominance of a population can result in the slowing down of the adaptation process as a whole. As a result we can hypothesise that if either genotypes 10000 and 01000 had a greater fitness (or alternatively if 00001 was less fit) then there would be less stochasticity in the trajectories in Fig. 6.6B. Finally, the narrow (almost deterministic) distribution of trajectories in Fig. 6.6A is due to the rapid rate with which mutants are produced from a population at 00000. A mutant being produced at any genotype (excluding 00100 which has a similarly low fitness compared with 00000) will result in the rapid growth of this mutant population and subsequent rapid decay of the 00000 population frequency, consistent with Fig. 6.6A.

6.4.3 Subsequent evolution upon removal of the antibiotic

One of the questions we are interested in exploring with this model is the following: If we remove the antibiotic (i.e. set $C = 0$ ng/ml) from a population that has evolved resistance in the presence of it, will the population evolve back towards the wild-type, thus "forgetting" its evolved resistance?

We consider this by taking an evolved distribution of the population from Fig. 6.5B and using it to seed a new culture in a serial transfer process (in which $C = 0$ ng/ml). In order for backwards evolution to be possible we must consider the scenario that includes back mutations (at only the first 3 loci). Upon removal of the antibiotic the fitness landscape reverts back to that shown in Fig. 6.2A.

Figure 6.7 shows results, with plots again comparing curves of the average population frequency at each genotype as a function of time T. Note, that the

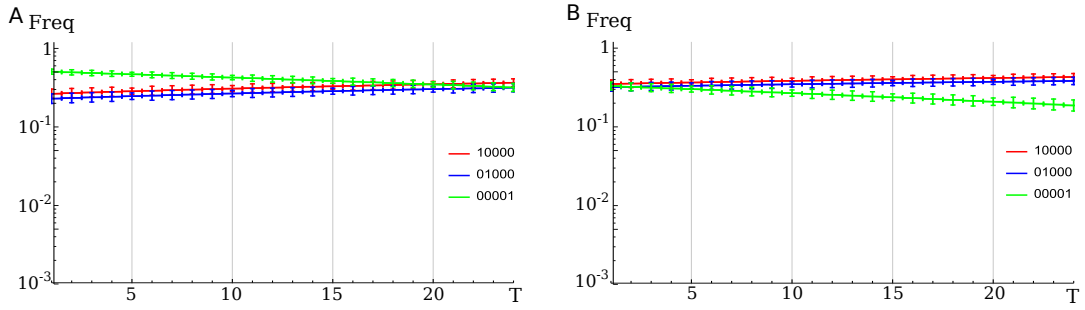

Figure 6.7 *The evolution of a resistant population upon removal of the antibiotic, in the single phenotype model. The plots show curves of average genotype frequency in the population as a function of time T (in generations). Missing genotypes never reached a frequency as large as 10^{-3}. (A) and (B) show evolution following the transfer of the population to an environment with $C = 0$ ng/ml, seeded with the final population distributions from the fourth and sixth cultures in Figs. 6.5B respectively. All results were gathered using a KMC algorithm, with mutation probability $\mu = 10^{-8}$ and averaged over* 100 *runs.*

frequency axis has a logarithmic scale so that small frequencies, which must still be greater than 10^{-3}, can be seen. Figures 6.7A and B show results when the transfer to an environment with $C = 0$ ng/ml occurs using the final population distributions of the fourth and sixth cultures in Fig. 6.5B respectively.

In both plots in Fig. 6.7, the three genotypes present at the point in which the antibiotic is removed (i.e. 100000, 01000 and 00001) continue to be the only ones present over the time considered. Their abundances change in a way that is consistent with how the evolution looked like it was proceeding when the antibiotics were present. There is nothing to indicate that the wild-type will be recovered over the timescales considered.

However, it might be possible that back mutations of the knockout genes will cause recovery of the wild-type, as the genotypes 00001 and 00010 have reduced growth rates relative to the wild-type when $C = 0$ ng/ml (see Fig. 6.2). However, without including these back mutations the genotypes 10000 and 01000 that dominate when $C = 15$ ng/ml have large growth rates which are comparable to the wild-type even when $C = 0$ ng/ml. Therefore it is not surprising that in the scenario we considered there is no recovery of the wild-type genotype.

6.5 Two phenotype model

We now add the second (filamentous) phenotypic state to the model and observe how it affects the evolution of the population. It is unknown what the relationship is between the switching rate α, the antibiotic concentration C and resistance (MIC value) of the genotype in question. What factors influence the budding rate β is also unknown. To make progress, we will consider the simple case in which α and β are genotype dependent (with which genotype they refer to identified in a subscript) and can each take one of two values only; $\alpha = \{\alpha_{\min}, \alpha_{\max}\}$ and $\beta = \{\beta_{\min}, \beta_{\max}\}$, such that $\alpha_{\min} < \alpha_{\max}$ and $\beta_{\min} < \beta_{\max}$. The rates assigned to genotype i, in the system with antibiotic concentration C, are

$$\alpha_i = \begin{cases} \alpha_{\min} & \text{if } \; C \leq \epsilon MIC_i \\ \alpha_{\max} & \text{if } \; C > \epsilon MIC_i \end{cases} \qquad \beta_i = \begin{cases} \beta_{\max} & \text{if } \; C \leq \epsilon MIC_i \\ \beta_{\min} & \text{if } \; C > \epsilon MIC_i \end{cases} \tag{6.2}$$

where ϵ is the threshold value that defines where the step occurs in the functions α and β (set to $\epsilon = 0.5$ in the following). The choice of a step function for α and β is the simplest way to acknowledge their dependence on the concentration C and the MIC value of the genotype. The SOS response is induced in *E. coli* following the cleavage of the *LexA* repressor due to DNA damage in the cell. Therefore for C below some threshold value, which we select to be $MIC/2$, we assume there has not been enough damage to cause this cleavage, or what little damage there has been can be repaired quickly, in order for a cell of this genotype to exist mainly in phenotype A. This is achieved through an asymmetry in the pair of rates $(\alpha_{\min}, \beta_{\max})$ such that $\alpha_{\min}/\beta_{\max} \ll 1$. Conversely, for C greater than $MIC/2$, cells are expected to suffer substantial DNA damage, which induces the SOS response and puts them in phenotype B, where they spend time recovering and replicating chromosomes. This is reflected by an asymmetry in the pair of rates $(\alpha_{\max}, \beta_{\min})$ such that $\alpha_{\min}/\beta_{\max} \gg 1$, favouring cells of low-resistance genotypes existing in the filamentous state. In Appendix G we consider briefly how results change for a smaller choice of ϵ. In the following results we use the values $\alpha_{\min} = \beta_{\min} = 0.01$ and $\alpha_{\max} = \beta_{\max} = 1$.

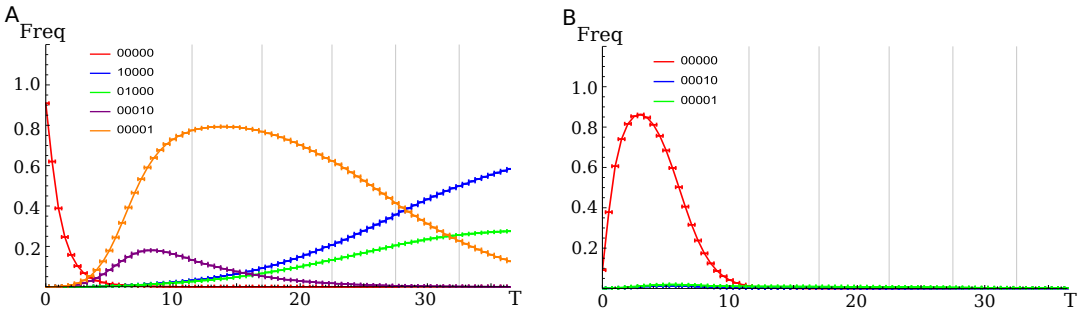

Figure 6.8 *The evolution of the population in the two phenotype model at sub-MIC ($C = 15ng/ml$) concentrations of antibiotics. The plots show curves of the average population frequency at states (i.e. genotype/phenotype pairs) as a function of time T (in generations). States that are absent never reached a frequency as large as 10^{-3}. Vertical lines indicate the points at which culture transfer took place, in which 1% of the population was used to seed a new culture. (A) shows states in phenotype A while (B) shows states in phenotype B. The parameters used are mutation probability $\mu = 10^{-8}, \epsilon = 0.5, \alpha_{min} = \beta_{min} = 0.01$ and $\alpha_{max} = \beta_{max} = 1$. All results are gathered using a KMC algorithm and averaged over 100 runs.*

6.5.1 Evolution in sub-MIC concentrations of antibiotics

We consider now how the population, with access to two phenotypic states, evolves when the antibiotic concentration $C = 15$ ng/ml. The fitness landscape in this case is again that of Fig. 6.3. Figure 6.8 shows plots of the populations at each state (expressed as a fraction of the total population) as a function of the time T. Figures 6.8A and B are results from the same simulations, showing curves for states in different phenotypes (Fig. 6.8A shows states in phenotype A, while Fig. 6.8B is for phenotype B). The scenario we consider here excludes back mutations. However, in results that are not shown, when back mutations are included the results are indistinguishable from those seen here.

For the scenario in Fig. 6.8, we observe that evolution away from the wild-type genotype (i.e. 00000) is quicker than in Fig. 6.5A (it is $\sim 4\times$ as quick for 50% of the population to leave the wild-type genotype). This is due to most of the population at the wild-type state (0000 in phenotype A) switching to the filamentous phenotype (see the red curves in Fig. 6.8B) where the mutation rate is increased. This allows for quicker evolution of resistant genotypes for which growth can continue.

Once a cell, at the wild-type state in phenotype B, evolves to a more resistant

genotype its budded offspring can grow in phenotype A. Four of the genotypes that are a single point mutation away from the wild-type are resistant enough for growth to occur when $C = 15$ ng/ml. Therefore with the exception of the accelerated initial stage of evolution — owing to the second phenotype — the population continues the same course of adaptive evolution that we observed in Fig. 6.5. In order to see any significant difference, or the evolution of super-resistance cells over short times, we need to look at larger antibiotic concentrations that exceed the MIC value of the wild-type.

Note that we will not consider here how the resistant population evolves upon removal of the antibiotic. When $C = 0$ ng/ml, according to (6.2) and our choice that $\alpha_{\min}/\beta_{\max} \ll 1$, cells are expected to exist out of the filamentous phenotype. Therefore the evolution observed will be approximately the same as in the case of a single phenotype. We have already looked at single phenotype evolution upon removal of the antibiotic (see Fig. 6.7A) and observed nothing of interest. A look at how the result of Fig. 6.8 changes when the mutation probability is reduced to $\mu = 10^{-9}$ can be found in Appendix F.

6.5.2 Evolution in antibiotic concentrations $C > MIC_{\text{wild-type}}$

We look now at the evolution of the population when the antibiotic concentration C exceeds the MIC value of the wild-type genotype (so when $C > 16$ ng/ml). We will consider this when $C = 50$ ng/ml and when $C = 1$ μg/ml, for which the fitness landscapes are shown in Fig. 6.9A and B respectively. These landscapes differ to the earlier fitness landscape for $C = 15$ ng/ml (see Fig. 6.3) in that some of the genotypes are represented by black circles. These are "lethal" genotypes that are assigned a growth rate of zero according to (6.1). If a cell is in one of these lethal genotypes then it cannot replicate while in phenotype A.

Consider first the fitness landscape of Fig. 6.9A for $C = 50$ ng/ml. This contains 5 lethal states, including the wild-type. With growth no longer able to occur at these states in phenotype A we expect them to no longer appear at significant frequencies in the population. Results for evolution over this fitness landscape can be seen in Fig. 6.10. These plots show curves of the average population frequency at states as a function of time T. Figures 6.10A and B show this for states in phenotype A and B respectively, for the scenario in which back mutations are excluded.

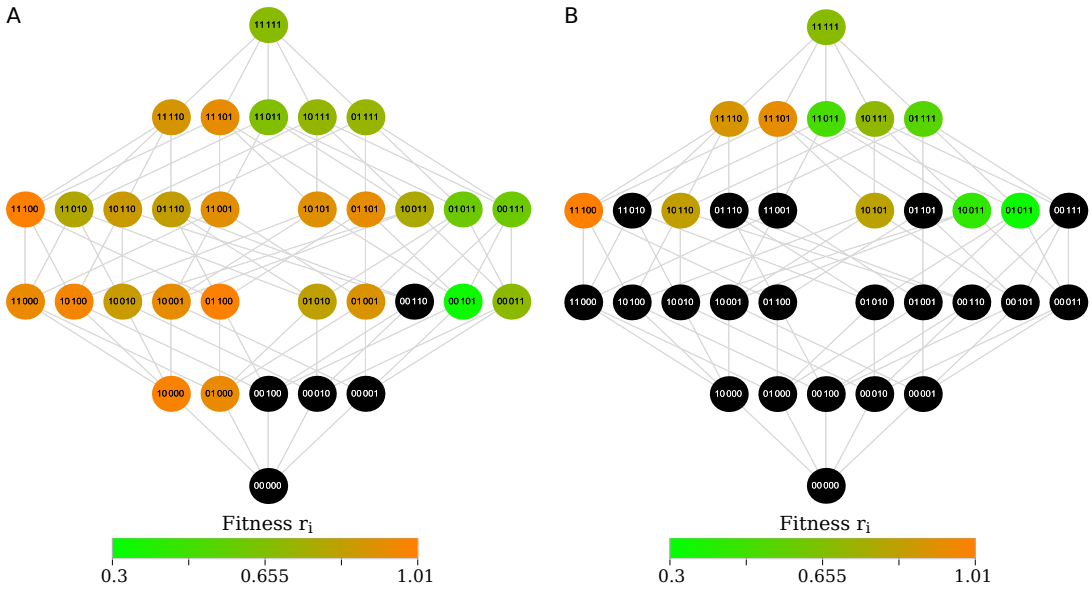

Figure 6.9 *Fitness landscapes when the antibiotic concentration C exceeds the MIC of the wild-type. These landscapes are for (A) $C = 50$ ng/ml and (B) $C = 1$ $\mu g/ml$. Each diagram shows the space of all possible genotypes in which links connect those that differ by a single point mutation. Each genotype is represented by a circle with the sequence written inside that it corresponds to. The background colour of each circle identifies the fitness r_i for that genotype (see the bar legend). Genotypes with black circles are lethal — i.e. they have zero growth rate.*

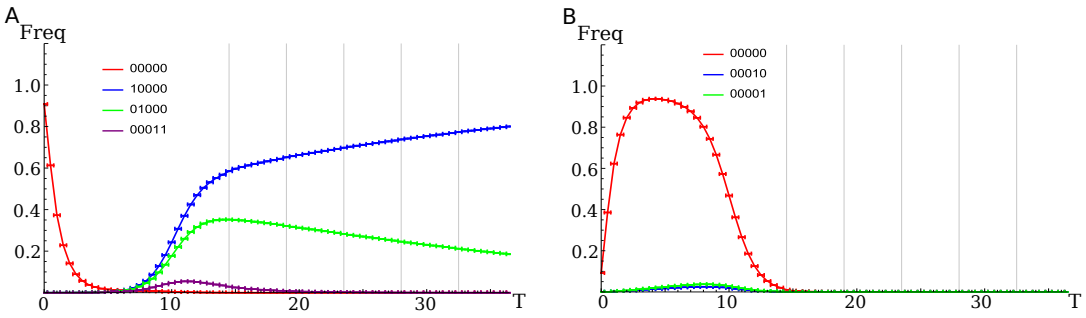

Figure 6.10 *The evolution of the population in the two phenotype model at antibiotic concentration $C = 50$ ng/ml. All plots show curves of the average population frequency at each state (i.e. genotype/phenotype pair) as a function of the time T (in generations). States that are absent never had a frequency as large as 10^{-3}. Vertical lines indicate the points at which culture transfer took place, in which 1% of the population was used to seed a new culture. (A) and (B) show results for states in phenotype A and B respectively. Back mutations were excluded in the model. The remaining parameters used are mutation probability $\mu = 10^{-8}, \epsilon = 0.5, \alpha_{min} = \beta_{min} = 0.01$ and $\alpha_{max} = \beta_{max} = 1$. All results are gathered using a KMC algorithm and averaged over 100 runs.*

At $C = 50$ ng/ml, both knockout mutation genotypes (i.e. 00001 and 00010) are lethal. Therefore in Fig. 6.10, both evolve quickly in phenotype B (see the green and blue curves in Fig. 6.10B) but are not resistant and therefore do not produce buds that will replicate in phenotype A. This is unlike the case for $C = 15$ ng/ml (see Fig. 6.8), in which 00001 became initially abundant in the population. Instead, here the genotypes 00001 and 00010 in phenotype B facilitate the evolution of the first observed double-mutant at 00011 (see the purple curve in Fig. 6.10A). This double mutant is resistant and therefore able to bud and grow to a significant amount ($\sim 5\%$ of the total population) in phenotype A. However, this genotype is still not as fit as 10000, which again takes over the population.

Compared with when $C = 15$ ng/ml (see Fig. 6.8), the evolution in Fig. 6.10 has accelerated but is maintaining the same general trajectory in genotype space over these short timescales. Figure 6.10 predicts that genotype 10000 becomes significant in the population ($\sim 50\%$ of it) after $T \sim 12 \approx 4$ hours, compared to it taking almost $3\times$ this time when $C = 15$ ng/ml in Fig. 6.8.

Consider now the fitness landscape when $C = 1\ \mu g/ml$, which is shown in Fig. 6.9B. In this case the majority of the genotypes are lethal, leaving the super-resistant genotype 11100 ($MIC = 32$) as the clear optimal state in the landscape. As we saw above for $C = 50$ ng/ml, the effect of lethal intermediate genotypes is that they induce the population to explore further mutations in the filamentous phenotype (than they would otherwise evolve over the same time in phenotype A).

The results for $C = 1\ \mu g/ml$ can be seen Fig. 6.11, for the scenario including back mutations (at the first 3 loci). All non-lethal genotypes at this value of antibiotic concentration C are necessarily very resistant. Nevertheless the results predict the evolution of the optimal (super-resistant) genotype at 11100 (see the blue curve beginning to appear in Fig. 6.11A). Following its establishment this genotype is expected to take over the population at larger values of T than we consider here. Nevertheless our observation that the super-resistant genotype 11100 appear at $T \sim 30$ simulation time units translates to around 10 hours.

Understandably, the population spends a greater initial amount of time in the filamentous phenotype, while it explores mutations until viable (i.e. non-lethal) genotypes are found. This results in the largest initial culture time (around 10 hours) of all the results considered in this chapter.

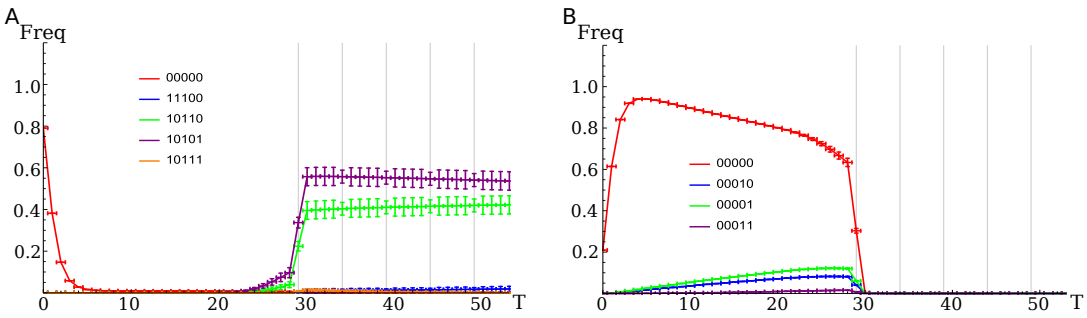

Figure 6.11 *The evolution of the population in the two phenotype model at antibiotic concentration $C = 1$ $\mu g/ml$. Plots show curves of the average population frequency of each state (i.e. genotype/phenotype pair) as a function of the time T (in generations). States that are absent never reached a frequency as large as 10^{-3}. Vertical lines indicate the points at which culture transfer took place, in which 1% of the population was used to seed a new culture. (A) and (B) show results for the states in phenotype A and B respectively. Results are for the scenario that includes back mutations at loci 1,2 and 3 in the model. The remaining parameters used are mutation probability $\mu = 10^{-8}, \epsilon = 0.5, \alpha_{min} = \beta_{min} = 0.01$ and $\alpha_{max} = \beta_{max} = 1$. All results are gathered using a KMC algorithm and averaged over 100 runs.*

6.6 Discussion and conclusion

In this chapter we considered simulation results from a model that describes how a population of *E. coli* develops resistance to the antibiotic *ciprofloxacin*. This model considered resistance to arise through combinations of 5 experimentally observed mutations [128] which either reduce the affinity of *ciprofloxacin* to bind with (type-II) topoisomerase enzymes or lead to an increased level of drug efflux pumps in the cell. We were interested in probing the importance of cells being able to switch to a secondary filamentous phenotypic state (as part of the SOS response) in accounting for the short timescales over which *E. coli* is observed to develop resistance experimentally [28, 35, 128]. Empirical data was used to construct realistic fitness landscapes over which the adaptive evolution of populations of *E. coli* could be tested.

We began the analysis with a single phenotype model without the filamentous phenotype. This should be valid at low values of antibiotic concentration C for which the SOS response will not be initiated. We showed that in the absence of antibiotics (i.e. $C = 0$ ng/ml) no significant evolution is predicted to occur for a population starting at the wild-type state that is left to evolve over ~ 10

hours (see Fig. 6.4). We then considered a non-zero antibiotic concentration $C < MIC_{\text{wild-type}}$ ($C = 15$ ng/ml) and observed the evolution of more resistant genotypes to occur over the same time range (with the majority of the population no longer of the wild-type genotype after about 7 hours) (see Fig. 6.5). The average change to the population over the time considered is the evolution of the genotypes 01000 and 10000 (which both correspond to single mutations in the *gyrA* genes). The latter mutant looks set to dominate the population at times immediately larger than we considered.

When the second (filamentous) phenotypic state is included in the model, the time taken to evolve resistance decreases further. The filamentous state provides the population with a "safe niche" within which mutant genotypes can evolve faster. At the concentration $C = 15$ ng/ml) it took approximately $4\times$ less time for 50% of the population to evolve from the wild-type genotype (Fig. 6.8) than in the single phenotype model.

We then proceeded to look at when the antibiotic concentration $C > MIC_{\text{wild-type}}$ (which is 16 ng/ml). For $C = 50$ ng/ml, evolution of 50% of the population to genotype 10000 occurs very quickly ($\sim$ 4 hours compared to the $\sim$ 10 hours it took when $C = 15$ ng/ml) (See Fig. 6.10). Upon further increase of C to $C = 1\ \mu g/ml$, we observed the rapid evolution over ~ 10 hours of mutants that are at least 3 point mutations from the wild-type (which were not present in any other simulations) (See Fig. 6.11). This includes the evolution of the super-resistant state 11100 with $MIC = 32\ \mu$g/ml. All mutations with less point mutations are lethal, which induces the population to remain in the filamentous phenotypic state from which super-resistant genotypes can be quickly evolved.

The model in this chapter therefore succeeds in demonstrating qualitatively the result of rapidly accelerated evolution of resistant cells, as a result of a secondary filamentous phenotypic state and a sufficient concentration of antibiotics. However, the quantitative results of the model are unlikely to be realistic and the model requires further work in order to rectify this. The first thing that is necessary is a tuning of the model's parameters to values seen experimentally.

A large assumption of the model was that the rates of phenotype switching and budding (α and β respectively) in (6.2) behave as step functions with respect to the concentration C. These forms were selected in the absence of empirical data suggesting an alternative form that is more suitable. The point of transition

between the maximum and minimum values of the functions were decided by the threshold value ϵ. The value $\epsilon = 0.5$ was used for all results in this chapter. However, according to observations in [28], in which 95% of cells were estimated to be in the filamentous state when $C = 0.125 \times MIC_{\text{wild-type}}$, $\epsilon = 0.5$ is likely to be too great a value. In Appendix G we tested a smaller value ($\epsilon = 0.1$) and found that the results are sensitive to ϵ, significantly varying the average trajectory that the population takes through genotype space (but still predicting the rapid evolution of resistant genotypes).

In order to determine a biologically realistic value for ϵ, as well as to test whether or not the step functions in (6.2) are suitable to describe the rates α and β, it is necessary to perform experimental work. This work would test the proportion of cells existing in the filamentous state (at short enough times that they are not expected to have genetically mutated) and how this changes with the antibiotic concentration C.

Another aim of this chapter was to test a recent observation from unpublished experimental work in which resistant cells "forgot" their resistance upon the removal of antibiotics (by evolving back towards the wild-type genotype). This behaviour seems possible given the structure of the growth function used in (6.1). For example, consider the genotype 01001 which has a large growth rate when $C =$ 15 ng/ml (see Fig. 6.3) and a low one when $C = 0$ ng/ml (see Fig. 6.2A). If the population is at 01001, then in the absence of antibiotics selection would favour the wild-type over genotype 01001 and its evolution may be likely. However, in our results a recovery of the wild-type was not observed when the antibiotics were removed following periods of growth in $C = 15$ ng/ml (see Fig. 6.7). This was due to the evolved genotypes 10000 and 01000 having comparable fitnesses to the wild-type genotype when $C = 0$. However, this result may change if we allow for back step mutations to occur in the knockout mutations (in the example we have just considered of genotype 01001, the wild-type could not be recovered otherwise). In results that are not included, back mutations were considered for the knockout mutations and recovery of the wild-type was still not observed.

A major shortcoming of the model is that it excludes the possibility of cell death (i.e. irreparable damage to the cell). In experiments with the same strain of *E. coli* that we use the empirical results for in this chapter, an antibiotic concentration of $C = 40$ ng/ml was enough to kill 99% of cells over a 24 hour period [35]. Experimentally this results in a far smaller pool of bacteria (1%) from which resistance can evolve, if it does so at all. This smaller population

may result in a slower evolution of resistance. Alternatively, populations that have survived may have done so precisely because they were so quick to evolve key mutations necessary for resistance. With fewer cells in total there would also be less competition for a resistant sub-population to take over once it arises. A more realistic version of the model is necessary to explore these possibilities. This new model would include the possibility of irreparable cellular damage occurring, the likelihood of which should depend on a genotype's MIC value and the antibiotic concentration C. In work that is not included in this thesis this extension was made to the model. However, results from it are forthcoming and remain the focus of future work. Nevertheless it is clear that this inclusion is necessary to improve the ability of the model to make any real world predictions.

Another improvement that can be made to the model concerns the selection of the 1% of the population that seeds the next culture in the serial transfer process. In the existing model this 1% is selected by dividing all of the genotype populations by 10^3 and then rounding these values to the nearest integer. Therefore the presence of small non-zero populations (i.e. $< 5 \times 10^6$ cells) are wiped out upon transfer to a new culture. To allow the chance of these small populations appearing in the seed of a new batch (which is a possibility in the experiment being modelled) we could introduce stochasticity into the selection process to decide the make-up of the seed population for the next culture.

The empirical results used in this chapter for the fitness and MIC values have errors which are reported in the raw data in Appendix E. However, these errors were ignored throughout this chapter and while the largest fitness error is 15%, those for the MIC values are larger, being ± 1 half doubling step of the reported values. We briefly consider here how the errors in the MIC values could affect the results we observed. Over the timescales we were interested in, for all but the largest non-zero antibiotic concentration C considered, we mainly observed the competition for dominance of the population to be between genotypes which are a single mutation from the wild-type (00000). There are significant enough differences in the MIC values of these genotypes with respect to 00000 (and each other) to suggest the observed behaviour is resistant to changes in MIC values within the error intervals. For example, the genotypes 00010 and 00001 are always expected to be produced first and while the difference between their MIC values is not significant, we expect the greater fitness of 00001 will result in a sub-population first building up at this genotype (provided C is not too great to make 00001 lethal). Later, when mutants arise at 10000 or 01000 (both of which have

MIC values which are significantly greater than 00000 and the remaining single-mutant genotypes) they will outcompete any mutant population at 00001. Note however, the difference in MIC values of 10000 and 01000 is not a significant one when the errors are included (the same is true for their fitness values). Therefore genotype 01000 could provide greater competition with 10000 to take over the population than we observed throughout this chapter. Nevertheless over the same short timescales we can expect the behaviour of the population to be similar to that observed in this chapter. However, over longer timescales this is unlikely to be the case and future studies would benefit from more precise experimental data.

Finally, the accuracy of results could be improved by running more simulations. As the changing population numbers at $2 \times 2^5 = 64$ states in time needed stored the results in this chapter are averaged over a modest 100 runs. In general, this number of runs was suitable, with small errors predicted in most results. However, the results shown in Fig. 6.11 showed an increase in variability and could benefit from more simulation runs. These simulations are not time consuming (occurring in the exponential phase of growth and without any consideration of cell "death") and there is no reason that this cannot be carried out to greater numbers in the future.

Chapter 7

Conclusions

In this thesis we have considered numerous models that describe the stochastic evolution of asexually reproducing populations of cells. The aim in all of them was to understand how the evolution of the population is affected by the inclusion of a secondary phenotypic state that cells are able to switch to. This results in there being a secondary fitness landscape that cells can exist on and allows for evolutionary trajectories that span both landscapes. If fitness barriers are slowing down evolution upon one landscape, then switching to the other landscape could lessen, or eliminate, those fitness barriers and allow for evolution to proceed faster.

The work undertaken was largely exploratory in nature, focussing on models that describe a small number of popular evolutionary scenarios. Results from these models confirmed our hypothesis that phenotype switching can speed up evolution. Yet there remains many unanswered questions and directions of study that future work could take. The main mechanism of phenotype switching that we were interested in was *stochastic phenotype switching* (SPS). This was the mechanism of switching considered in the models of Chapters 3, 4 and 5. Alternatively, in Chapter 6 we considered a model with a responsive mechanism for switching — that of the *SOS response* — which is initiated upon the detection of DNA damage in the cell following exposure to, e.g. antibiotic agents. If the evolutionary advantage to phenotype switching is significant enough, then positive selection for the existence of such mechanisms is possible. While the SOS response is clearly beneficial for the survival of cells, it is not always clear when this is the case for SPS. While SPS has been shown to benefit the survival of populations in fluctuating environments and in static environments through

division of labour [3], we sought to understand whether it could also facilitate genetic evolution when the environment is static.

This study began in Chapter 3, with a model of how an evolving population of haploid cells can escape from a local peak in a 1D fitness landscape (in which the secondary phenotypic state has a uniform fitness landscape). We demonstrated here that — provided the fitness barrier is high enough — there exists an optimal range of values for the rate of phenotype switching. Within this optimal range, the time taken for the evolutionary process (to reach the target optimal state) can be reduced by many orders of magnitude. By studying the trajectories that cells in the population are likely to take, we established that this optimal range coincides with when a new evolutionary trajectory becomes viable. This trajectory avoids the deleterious valley state entirely (by switching to the secondary phenotypic state) and optimises the time taken to escape from the local fitness peak. We observed this optimal trajectory to be a persistent feature in simulations, across a wide range of parameters. This model was then extended to allow cells (beginning with approximately no phenotype switching) to evolve their rates of SPS, while still attempting to escape from the local peak as part of the same evolutionary process. The model predicted that the benefit of the optimal switching range to the evolutionary process was great enough to support the possibility of SPS emerging in populations due to this benefit it confers in facilitating genetic evolution in static environments.

We undertook further study of this model in Chapter 4, where we sought to analytically understand and verify the results of the preceding numerical study. The key to achieving this was to exploit the observed competition between two evolutionary trajectories that the population is most likely to follow at low to intermediate rates of phenotype switching. This greatly simplified the problem to one of calculating the time (the adaptation time) it takes an evolving population to acquire a fixed set of mutations. This is a common problem in population genetics which we were able to tackle analytically. Without this simplification the model would not be analytically solvable, for any rate of phenotype switching other than the limits of low and high switching frequencies (for which the model maps to that of a single phenotype).

The focus of Chapter 4 was therefore on calculating the adaptation time for both of these trajectories in different possible dynamical regimes. For each of these we calculated both the adaptation time and the boundaries for that regime. For parameters of the model that don't conform to this two-trajectory competition

approximation we were unable to solve for the adaptation time other than in the limit of high frequency switching. Nevertheless, we obtained a qualitative understanding of the behaviour of the model in this quantitatively unknown region. Thankfully the uncertainty here did not affect calculations to determine if the optimal range for the rate of phenotype switching exists. Therefore we were able to proceed and search for this optimal range at any given set of parameters.

This approach allowed us to produce composite solutions — made up of numerous individual solutions for the different dynamical regimes and limits of the model — to explore the relationship between the adaptation time, the expected trajectory taken and the rate of phenotype switching in the model. Through these composite solutions we verified numerous results from Chapter 3 and explored new parameter values that we otherwise would not be able to study by simulations. We verified that when the mutation probability is as small as the values typically found in bacteria (i.e. $\sim 10^{-9}$ per nucleotide base [46, 116]) the optimal switching rate range is still predicted to exist. What is more, we predicted it to occur up to (and beyond) population sizes that are consistent with the typical sizes of microbial populations encountered in laboratory experiments ($\sim 10^6$ to 10^{10} bacteria).

We next sought to test how resilient the existence of an optimal range for the rate of phenotype switching is to more realistic genotype spaces and fitness landscapes. We did this in Chapter 5, by carrying out an exploratory study into the effect of stochastic phenotype switching in models of evolving binary sequences. Three different evolutionary models were studied, that used different random landscape models for the two fitness landscapes required. The first model we considered used the House of Cards (HoC) model for the original landscape. The secondary phenotype had a uniform fitness landscape, as in the 1D model of the preceding chapters, which provides a clear benefit to SPS for populations that are struggling to evolve on the HoC landscape. Unsurprisingly yet promisingly, this resulted in the existence, for all but the smallest population sizes considered (around 20 cells), of an optimal range for the rate of phenotype switching, within which the adaptation time can be reduced by orders of magnitude.

It is not unrealistic to imagine that two phenotypic states, between which stochastic phenotype switching occurs, can have different suitabilities to a given environment, which results in one being distinctly beneficial. For example, consider persister cells in the presence of antibiotics [16] or the numerous phase variant structures that aid pathogenic bacteria's survival against an immune

response [213]. However, in the next two models of Chapter 5 we sought to test if the potential benefit of stochastic phenotype switching was more general than in this situation alone. Therefore we tested if it could also aid evolution if neither phenotype was engineered to have a distinct advantage, but were instead assigned different realisations of the same random landscape model. We first tested this for a model in which both landscapes had uncorrelated HoC landscapes and then a model in which they both had Rough Mount Fuji (RMF) landscapes.

For both of these models we observed that the adaptation time can increase by the inclusion of phenotype switching. An analysis into individual simulation runs revealed that this was likely a result of the populations becoming trapped at local fitness maxima in the second phenotype. How likely this is to happen depends on both the random landscapes generated and the dynamical parameters, such as the mutation rate, strength of selection and population size. This problem was exacerbated at low frequencies of switching where the long waiting times for cells to switch back to the original phenotype (which contained the target state) slowed down the process even more.

This increase in adaptation time with SPS persisted across results for the HoC and RMF models, at all parameter values except in the limit of high frequency switching. In this limit the magnitude of fitness fluctuations away from the mean value are dampened, resulting in consistently reduced adaptation times across all models. However, in the deterministic RMF model, we observed the optimal range for phenotype switching was predicted to occur at lower values of the mutation probability than we had looked at. While we did not verify this feature in any stochastic simulations, what results we did compare between the stochastic and deterministic models approximately agreed. This was promising but more work needs carried out on these models to answer conclusively on whether or not SPS can benefit the evolving populations in these two models. As we detailed extensively in the chapter, there remained several unfinished bits of work and shortcomings in the models, that could be the focus of future work. Most detrimental to our understanding of the results, is how they vary with the length of sequences that the genotypes represent. The presented results only considered the smallest lengths, which were simpler to simulate.

Finally, in Chapter 6 we presented a model of how populations of *E. coli* evolve resistance to the antibiotic *ciprofloxacin*. This work was motivated by the experimental observation that *E. coli* can evolve rapid resistance upon exposure to the antibiotic *ciprofloxacin* [28, 35]. The model was successful in demonstrating

how the rapid evolution of resistant cells, over a matter of hours, is able to take place. We demonstrated that these low timescales can be due entirely to the presence of the filamentous (and error-prone) phenotypic state that cells entered as part of the SOS response. Through entering this "safe niche" — in which the environment for genetic evolution was improved — the necessary genetic evolution for resistance is able to occur more quickly. This is analogous to the scenario of escape from a local peak form our earlier models, in which the secondary phenotype provided a situation more amenable to genetic mutations.

Despite the success of this model in demonstrating qualitatively the process of accelerated evolution, more work needs to be carried out for it to be of any predictive use. This includes incorporating the possibility of irreparable cellular damage occurring in cells, which is observed to be significant experimentally [35]. As well as this, experimental work needs to be carried out in order to obtain biologically realistic values for numerous parameters used in the model, that we demonstrated results to be sensitive to. For example, measuring the fraction of cells (of the same genotype) that switch to the filamentous phenotype at different antibiotic concentrations. If this can be done, then perhaps this model could be tuned to make specific predictions about how *E. coli* develops resistance, regarding the timescales and evolutionary trajectories, that could be tested experimentally.

In conclusion the numerous models of this thesis have demonstrated the potential of phenotype switching to facilitate genetic evolution in static environments. This is particularly true when the second phenotype is more resilient to pressures of the current environment. The models themselves were drastic simplifications of the complex process of biological evolution, from which it was therefore difficult to arrive at any quantitative results that real biological systems could test. Nevertheless, as a qualitative exploration into whether or not stochastic phenotype switching could theoretically arise as a means to aid populations struggling to evolve in a static environment (e.g. by escaping from a local fitness peak), our findings suggest that it could. Further work is warranted to more fully explore the models under consideration, and to explore the best way to realise our findings experimentally.

Appendix A

The solution for $N_{3\mathrm{A}}(t)$ for trajectory B in the deterministic regime

The following presents the solutions to the system of deterministic differential equations in (4.26) to (4.30), describing how the population at states 1A, 1B, 2B, 3B and 3A change in time. All of the following solutions contain the fitnesses at the individual states (i.e. r_i for state i). However, it should be noted that for trajectory B, $r_{1\mathrm{A}} = r_{1\mathrm{B}} = r_{2\mathrm{B}} = r_{3\mathrm{B}} = 1$. This is used in the following solutions only when it makes a significant simplification of results.

First, we define the following quantities which will be used in the following solutions:

$$g_1 = \xi r_{1\mathrm{A}}(1-\mu) - \alpha - d \approx -\mu d - \alpha \tag{A.1}$$

$$g_2 = \xi r_{1\mathrm{B}}(1-\mu) - d \approx -\mu d \tag{A.2}$$

$$g_3 = \xi r_{2\mathrm{B}}(1-2\mu) - d \approx -2\mu d \tag{A.3}$$

$$g_4 = \xi r_{3\mathrm{B}}(1-\mu) - \alpha - d \approx -\mu d - \alpha \tag{A.4}$$

$$C_0 = \left(1 - \frac{d}{r_{1\mathrm{A}}}\right) K = (1-d)K \tag{A.5}$$

where for the approximated final forms we have substituted in $\xi = (1 - (N_T/K))K \approx d$ and set all the fitnesses equal to one for trajectory B. The

solutions for the population at states 1A and 1B are

$$N_{1\mathrm{A}}(t) = C_0 e^{g_1 t} \tag{A.6}$$

$$N_{1\mathrm{B}}(t) = C_0[e^{g_2 t} - e^{g_1 t}], \tag{A.7}$$

while for the remaining solutions it is necessary to consider the relationship between μ and α. When $\alpha \neq \mu d$ the solutions are

$$N_{2\mathrm{B}}(t) = \frac{\epsilon_2}{\xi\mu}[e^{g_3 t} - e^{g_1 t}] + C_0[e^{g_2 t} - e^{g_3 t}] \tag{A.8}$$

$$N_{3\mathrm{B}}(t) = \epsilon_1 e^{g_4 t} - \epsilon_2 t e^{g_1 t} + \epsilon_3 e^{g_2 t} - \epsilon_4 e^{g_3 t} \tag{A.9}$$

$$N_{3\mathrm{A}}(t) = \frac{\alpha\epsilon_1}{g_4} e^{g_4 t} - \alpha\epsilon_2 \left(\frac{t}{g_1} - \frac{1}{g_1^2}\right) e^{g_1 t} + \frac{\alpha\epsilon_3}{g_2} e^{g_2 t} - \frac{\alpha\epsilon_4}{g_3} e^{g_3 t} + K_1, \tag{A.10}$$

in which

$$K_1 = -\alpha\left[\left(\frac{\epsilon_1}{g_4}\right) + \left(\frac{\epsilon_2}{g_1^2}\right) + \left(\frac{\epsilon_3}{g_2}\right) - \left(\frac{\epsilon_4}{g_3}\right)\right] \tag{A.11}$$

$$\epsilon_1 = \xi r_{2\mathrm{B}} \mu C_0 \left[\frac{\alpha}{(\alpha - \xi r_{2\mathrm{B}}\mu)^2} - \frac{1}{\alpha}\right] \tag{A.12}$$

$$\epsilon_2 = \frac{\xi^2 r_{1\mathrm{B}} r_{2\mathrm{B}} \mu^2 C_0}{\xi r_{1\mathrm{A}}\mu - \alpha} \tag{A.13}$$

$$\epsilon_3 = \frac{\xi r_{2\mathrm{B}} \mu C_0}{\alpha} \tag{A.14}$$

$$\epsilon_4 = \frac{\alpha\xi r_{2\mathrm{B}} \mu C_0}{(\alpha - \xi r_{2\mathrm{B}}\mu)^2} \tag{A.15}$$

While if $\alpha = \mu d$, the solutions are

$$N_{2\mathrm{B}}(t) = \frac{\xi r_{1\mathrm{B}} \mu C_0}{(g_2 - g_3)}[e^{g_2 t} - e^{g_3 t}] - \xi r_{1\mathrm{B}} \mu C_0 t e^{g_1 t} \tag{A.16}$$

$$N_{3\mathrm{B}}(t) = \omega_1[e^{g_2 t} - e^{g_4 t}] - \omega_2 t^2 e^{g_1 t} - \omega_3 t e^{g_3 t} \tag{A.17}$$

$$N_{3\mathrm{A}}(t) = \alpha\omega_1\left[\frac{e^{g_2 t}}{g_2} - \frac{e^{g_4 t}}{g_4}\right] - \alpha\omega_2\left[\frac{t^2}{g_1} - \frac{2t}{g_1^2} + \frac{2}{g_1^3}\right] e^{g_1 t} - \alpha\omega_3\left[\frac{t}{g_3} - \frac{1}{g_3^2}\right] e^{g_3 t} + K_2 \tag{A.18}$$

in which

$$K_2 = \frac{2\alpha\omega_2}{g_1^3} - \alpha\omega_1\left[\frac{1}{g_2} - \frac{1}{g_4}\right] - \frac{\alpha\omega_3}{g_3^2} \tag{A.19}$$

$$\omega_1 = \frac{\xi r_{2\mathrm{B}}\mu C_0}{\alpha} \tag{A.20}$$

$$\omega_2 = \frac{\xi^2 r_{1\mathrm{B}} r_{2\mathrm{B}}\mu^2 C_0}{2} \tag{A.21}$$

$$\omega_3 = \xi r_{2\mathrm{B}}\mu C_0 \tag{A.22}$$

Appendix B

Transition rates in the SF regime

In the following we consider the transition rates between states that were used for the calculations in the sequential fixation (SF) regime in Section 4.4.2. These are for when the fitness cost $c = 0$. Figure 4.6 shows all of the possible transitions that exist in the system.

All transition rates are of the form:

$$\text{population size} \times \text{mutation rate} \times \text{probability of success} \tag{B.1}$$

For the population size at state i we use the saturation value $N_i^* = (1 - \frac{d}{r_i})K$ from (4.8), in which $R = r_i$ as we expect the population to be localised at state i. For the transitions 2A→3A and 3B→3A the probability of success equals one as the target is the creation of an individual cell in state 3A.

First we consider the (non-extinction) transition rates:

$$W_{1\mathrm{A}\to 2\mathrm{A}} = N^*_{1\mathrm{A}}\left(1-\frac{N^*_{1\mathrm{A}}}{K}\right) r_{1\mathrm{A}}\mu\left(\frac{1-e^{\delta}}{1-e^{\delta N^*_{1\mathrm{A}}}}\right) = \frac{N^*_{1\mathrm{A}} d\mu(1-e^{\delta})}{1-e^{\delta N^*_{1\mathrm{A}}}} \quad \text{(B.2)}$$

$$W_{1\mathrm{A}\to 1\mathrm{B}} = W_{1\mathrm{A}\to 1\mathrm{B}} = N^*_{1\mathrm{A}}\alpha\left(\frac{1}{N^*_{1\mathrm{B}}}\right) = \alpha \quad \text{(B.3)}$$

$$W_{2\mathrm{A}\to 1\mathrm{A}} = N^*_{2\mathrm{A}}\left(1-\frac{N^*_{2\mathrm{A}}}{K}\right) r_{2A}\mu\left(\frac{1-e^{-\delta}}{1-e^{-\delta N_{2\mathrm{A}^*}}}\right) = \frac{N^*_{2\mathrm{A}} d\mu(1-e^{-\delta})}{1-e^{-\delta N^*_{2\mathrm{A}}}} \quad \text{(B.4)}$$

$$W_{2\mathrm{A}\to 3\mathrm{A}} = N^*_{_{2\mathrm{A}}}\left(1-\frac{N^*_{2\mathrm{A}}}{K}\right) r_2\mu = N^*_{2\mathrm{A}} d\mu \quad \text{(B.5)}$$

$$W_{2\mathrm{A}\to 2\mathrm{B}} = N^*_{2\mathrm{A}}\alpha\left(\frac{1-e^{-\delta}}{1-e^{-\delta N^*_{2\mathrm{A}}}}\right) \quad \text{(B.6)}$$

$$W_{1\mathrm{B}\to 2\mathrm{B}} = N^*_{1\mathrm{B}}\left(1-\frac{N^*_{1\mathrm{B}}}{K}\right) r_{1B}\mu\left(\frac{1}{N^*_{2\mathrm{B}}}\right) = d\mu \quad \text{(B.7)}$$

$$W_{2\mathrm{B}\to 1\mathrm{B}} = W_{1\mathrm{B}\to 2\mathrm{B}} = W_{2\mathrm{B}\to 3\mathrm{B}} = W_{3\mathrm{B}\to 2\mathrm{B}} \quad \text{(B.8)}$$

$$W_{2\mathrm{B}\to 2\mathrm{A}} = N^*_{2\mathrm{B}}\alpha\left(\frac{1-e^{\delta}}{1-e^{\delta N^*_{2\mathrm{B}}}}\right) \quad \text{(B.9)}$$

$$W_{3\mathrm{B}\to 3\mathrm{A}} = N^*_{3\mathrm{B}}\alpha \quad \text{(B.10)}$$

Now consider calculating the extinction rate from state i: $W_{i\to \mathrm{E}}$. This is the inverse of the mean time it takes the total population size N_T (all at state i in this regime, starting from the saturation value N^*_T) to undergo a random walk and be absorbed at the boundary state $N_T = 0$. The other boundary, $N_T = K$ is reflective.

To calculate this mean time we use the equation in (4.54) from [138]. As a reminder this allows us to solve for $\bar{t}_{N_T=i,N_T=j}$, which is the mean first passage time for a 1D random walker, with position N_T, and asymmetric hopping rates to be absorbed at state j given it starts at i (which is a reflecting boundary). With this we can calculate the quantities $\bar{t}_{N_T=K,N_T=0}$ and $\bar{t}_{N_T=K,N_T=N^*_T}$, where N^*_T is for the population at state i.

To calculate these quantities using (4.54), we need to know the (state dependent) rates with which N_T decreases and increases by one, being p_i and q_i respectively.

For a population at state i, with size $N_T = (K - j)$, these are

$$p_j = (K-j)d \tag{B.11}$$

$$q_j = \begin{cases} (K-j)r_i(1-\frac{K-j}{K})(1-\mu) & \text{for } i = \{1\text{A}, 1\text{B}, 3\text{B}\} \\ (K-j)r_i(1-\frac{K-j}{K})(1-2\mu) & \text{for } i = \{2\text{A}, 2\text{B}\} \end{cases} \tag{B.12}$$

By substituting these into (4.54), both $\bar{t}_{N_T=K,N_T=0}$ and $\bar{t}_{N_T=K,N_T=N_T^*}$ can be calculated (which we do with *Mathematica* in our results). Once we have these quantities, the extinction rate $W_{i\to\text{E}}$ can be calculated by

$$W_{i\to E} = \frac{1}{\bar{t}_{N_T=K,N_T=0} - \bar{t}_{N_T=K,N_T=N^*}} \tag{B.13}$$

Appendix C

The method of characteristics

We consider here how to solve the differential equation in Eq. 4.89 using the method of characteristics. The equation is of the form

$$\frac{\partial \Phi_i}{\partial t} - \beta \frac{\partial \Phi_i}{\partial x} = 0, \tag{C.1}$$

with the initial condition $\Phi_i(x, y, 0) = e^{-x}$ and

$$\beta = -d_i e^x - b_i e^{-x} + d_i + b_i + y \tag{C.2}$$

We have no information about Φ_i's dependence on y and hence we will treat it as a fixed parameter throughout (which satisfies our eventual replacement of y with η_i). The characteristics are curves in the xt-plane, described in terms of the parameter s such that $x = x(s), t = t(s), \Phi_i = \Phi_i(s)$ and

$$\frac{dt}{ds} = 1 \qquad \frac{dx}{ds} = -\beta(s) \qquad \frac{d\Phi_i}{ds} = 0. \tag{C.3}$$

From the first of these $t = s + c_1$, while from the second we get

$$ds = -\frac{dx}{\beta} = \frac{-dx}{-d_i e^x - b_i e^{-x} + d_i + b_i + y}. \tag{C.4}$$

Changing variables from x to u by $u = e^{-x}$ gives us

$$ds = \frac{-du}{b_i(u - \sigma_i^+)(u - \sigma_i^-)}, \tag{C.5}$$

where

$$\sigma_i^{\pm} = \frac{(d_i + y + b_i) \pm \sqrt{(d_i + y + b_i)^2 - 4d_i b_i}}{2b_i}. \tag{C.6}$$

Splitting up the factors in this, integrating and returning the variable to x gives us

$$s = \frac{-1}{b_i(\sigma_i^+ - \sigma_i^-)} \ln\left(\frac{e^{-x} - \sigma_i^+}{e^{-x} - \sigma_i^-}\right) + c_2. \tag{C.7}$$

Now combining this with $t = s + c_1$, that we found from the first equation in (C.3), gives

$$t = \frac{-1}{b_i(\sigma_i^+ - \sigma_i^-)} \ln\left(\frac{e^{-x} - \sigma_i^+}{e^{-x} - \sigma_i^-}\right) + (c_1 + c_2). \tag{C.8}$$

If we define the constant $K = (c_1 + c_2)$ this is equal to

$$K = \left(\frac{e^{-x} - \sigma_i^+}{e^{-x} - \sigma_i^-}\right) \exp(-b_i(\sigma_i^+ - \sigma_i^-)t). \tag{C.9}$$

Therefore along each characteristic curve, the combination of x and t are constant according to (C.9). The final differential equation in (C.3) tells us that $\Phi_i = c_3$ which will be a function of K, i.e. $\Phi_i = F(K)$. To find the form of the function F we use the initial condition $\Phi_i(x, y, 0) = F(K)|_{t=0} = e^{-x}$. A function of K that satisfies this is

$$F(K) = \frac{\sigma_i^+ K - \sigma_i^-}{K - 1}, \tag{C.10}$$

which yields the following solution for $\Phi_i(x, y, t)$

$$\Phi_i(x, y, t) = \frac{\sigma_i^+(e^{-x} - \sigma_i^-)e^{-b_i(\sigma_i^+ - \sigma_i^-)t} - \sigma_i^-(e^{-x} - \sigma_i^+)}{(e^{-x} - \sigma_i^-)e^{-b_i(\sigma_i^+ - \sigma_i^-)t} - (e^{-x} - \sigma_i^+)}. \tag{C.11}$$

Substituting $y = \eta_i$ into (C) produces the solution in (4.90).

Appendix D

The solution for trajectory B in the ST regime

The following is a list of the quantities found in the solution for T_B in the ST regime (see (4.103)). It assumes the bulk of the population remains in state $1A$ or alternatively that there is no observable difference in the saturation value of the population as it moves along states 1B, 2B and 3B. This will always be the case when the cost $c = 0$.

We begin with the birth rates b_i for each state; these are the rates that a cell at each state successfully replicates with.

$$b_{1A} = (1 - \frac{N_T}{K}) r_{1A}(1 - \mu) \approx d(1 - \mu) \tag{D.1}$$

$$b_{1B} = (1 - \frac{N_T}{K}) r_{1B}(1 - \mu) \approx d(1 - \mu) \left(\frac{r_{1B}}{r_{1A}} \right) \tag{D.2}$$

$$b_{2B} = (1 - \frac{N_T}{K}) r_{2B}(1 - 2\mu) \approx d(1 - 2\mu) \left(\frac{r_{2B}}{r_{1A}} \right) \tag{D.3}$$

$$b_{3B} = (1 - \frac{N_T}{K}) r_{3B}(1 - \mu) \approx d(1 - \mu) \left(\frac{r_{3B}}{r_{1A}} \right) \tag{D.4}$$

The approximated form for these uses the commonly made substitution that $(1 - N_T/K) \approx d$.

We consider now the mutation rates; these are the rates with which a cell at each

state produces a successful mutant at the next state in the considered sequence. These are

$$\eta_{1A\to 1B} = \alpha P_{1B} \tag{D.5}$$

$$\eta_{1B\to 2B} = (1-\frac{N_T}{K})r_{1B}\mu \approx d\mu\left(\frac{r_{1B}}{r_{1A}}\right)P_{2B} \tag{D.6}$$

$$\eta_{2B\to 3B} = (1-\frac{N_T}{K})r_{2B}\mu \approx d\mu\left(\frac{r_{2B}}{r_{1A}}\right)P_{3B} \tag{D.7}$$

$$\eta_{3B\to 1A} = \alpha, \tag{D.8}$$

where P_{iB} is the probability that a mutant created at state i will be successful.

Now consider the $\sigma^{\pm}$ values for states 1B, 2B and 3B, which appear in the solution in (4.103).

$$\sigma^{\pm}_{3B} = \frac{(d+\eta_{3B\to 3A}+b_{3B}) \pm \sqrt{(d+\eta_{3B\to 3A}+b_{3B})^2-4db_{3B}}}{2b_{3B}} \tag{D.9}$$

$$= \frac{(1+\frac{\alpha}{d})r_{1A}+r_{3B}(1-\mu)}{2r_{3B}(1-\mu)} \pm \frac{\sqrt{\left[(1+\frac{\alpha}{d})r_{1A}+r_{3B}(1-\mu)\right]^2-4r_{1A}r_{3B}(1-\mu)}}{2r_{3B}(1-\mu)} \tag{D.10}$$

$$\sigma^{\pm}_{2B} = \frac{(d+\eta_{2B\to 3B}+b_{2B}) \pm \sqrt{(d+\eta_{2B\to 3B}+b_{2B})^2-4db_{2B}}}{2b_{2B}} \tag{D.11}$$

$$= \frac{\frac{r_{1A}}{r_{2B}}+(1-2\mu)+\mu P_{3B}}{2(1-2\mu)} \pm \frac{\sqrt{\left[\frac{r_{1A}}{r_{2B}}+(1-2\mu)+\mu P_{3B}\right]^2-\frac{4r_{1A}(1-2\mu)}{r_{2B}}}}{2(1-2\mu)} \tag{D.12}$$

$$\sigma_{1B}^{\pm} = \frac{(d+\eta_{1B\to 2B}+b_{1B}) \pm \sqrt{(d+\eta_{1B\to 2B}+b_{1A})^2 - 4db_{1A}}}{2b_{1A}} \quad \text{(D.13)}$$

$$= \frac{\frac{r_{1A}}{r_{1B}} + (1-\mu) + \mu P_{2B}}{2(1-\mu)} \quad \text{(D.14)}$$

$$\pm \frac{\sqrt{\left[\frac{r_{1A}}{r_{1B}} + (1-\mu) + \mu P_{2B}\right]^2 - \frac{4r_{1A}(1-\mu)}{r_{1B}}}}{2(1-\mu)}$$

Using these, the probability that a mutant is successful at state i is simply $P_i = (1-\sigma_i^-)$.

Appendix E

Growth rates and sensitivities of different genotypes

We consider here the empirical data that is used to create the fitness landscapes in Chapter 6. This data is contained in Fig. E.1, which shows a table of results taken from [128]. This shows the measured fitness and susceptibility (i.e. *MIC* value) of *E. coli* mutants (of the wild-type strain MG1655) in the absence of antibiotics. Fitness is expressed as a fraction of the fitness of the wild-type genotype 00000.

Figure E.1 is missing data on three genotypes: 00101, 00110 and 00111. In estimating the values for these we will assume that the resistance of a genotype is additive in the resistance of its less mutated nearest neighbours (i.e. $MIC(00101) = MIC(00100) + MIC(00001)$), while the fitness takes the minimum value of them (i.e. $g(00101) = \mathrm{Min}[g(00100), g(00001)]$). This respects the general trend for the acquisition of resistance, while acknowledging our expectation that these missing genotypes do not confer a significant increase in fitness over their less mutated neighbours (otherwise they would be expected to be observed more in experiments). This leads to the estimated values for the fitness and MIC of the missing genotypes shown in Table E.1.

Table 1. Genotypes, susceptibility, and fitness of isogenic strains.

Strain	*gyrA*1	*gyrA*2	*parC*	*marR*	*acrR*	MIC[b]	Fitness (SD)[c]	P[d]	N[e]
MG1655	-	-	-	-	-	0.016	1.00 (0.01)	-	5
LM378	S83L	-	-	-	-	0.38	1.01 (0.03)	0.37	6
LM534	-	D87N	-	-	-	0.25	0.99 (0.03)	0.57	7
LM792	-	-	S80I	-	-	0.016	0.99 (0.01)	0.59	5
LM202	-	-	-	Δ	-	0.032	0.83 (0.03)	<0.0001	5
LM351	-	-	-	-	Δ	0.047	0.91 (0.02)	<0.0001	5
LM625	S83L	D87N	-	-	-	0.38	0.97 (0.03)	0.04	8
LM862	S83L	-	S80I	-	-	1	0.98 (0.03)	0.18	6
LM421	S83L	-	-	Δ	-	1	0.86 (0.03)	<0.0001	5
LM647	S83L	-	-	-	Δ	0.5	0.95 (0.04)	0.02	11
LM1124	-	D87N	S80I	-	-	0.38	1.02 (0.02)	0.04	8
LM538	-	D87N	-	Δ	-	1	0.83 (0.03)	<0.0001	5
LM592	-	D87N	-	-	Δ	0.38	0.92 (0.03)	0.0001	10
LM367	-	-	-	Δ	Δ	0.125	0.82 (0.04)	<0.0001	5
LM693	S83L	D87N	S80I	-	-	32	1.01 (0.02)	0.48	13
LM695	S83L	D87N	-	Δ	-	0.75	0.79 (0.03)	<0.0001	10
LM691	S83L	D87N	-	-	Δ	0.75	0.93 (0.03)	0.0002	13
LM871	S83L	-	S80I	Δ	-	6	0,86 (0.03)	<0.0001	10
LM873	S83L	-	S80I	-	Δ	3	0.92 (0.04)	0.0005	10
LM882	-	D87N	S80I	Δ	-	0.75	0.84 (0.05)	<0.0001	14
LM1125	-	D87N	S80I	-	Δ	0.5	0.95 (0.01)	<0.0001	8
LM709	S83L	-	-	Δ	Δ	1.5	0.78 (0.04)	<0.0001	5
LM595	-	D87N	-	Δ	Δ	1.5	0.60 (0.09)	<0.0001	10
LM701	S83L	D87N	-	Δ	Δ	2	0.66 (0.07)	<0.0001	10
LM707	S83L	D87N	S80I	Δ	-	32	0.89 (0.03)	<0.0001	10
LM703	S83L	D87N	S80I	-	Δ	32	0.94 (0.03)	0.0009	14
LM875	S83L	-	S80I	Δ	Δ	8	0.71 (0.04)	<0.0001	5
LM878	-	D87N	S80I	Δ	Δ	2	0.72 (0.05)	<0.0001	10
LM705	S83L	D87N	S80I	Δ	Δ	32	0.68 (0.07)	<0.0001	5

[a]Genotype. Strains are isogenic to MG1655 and carry only the mutations shown.
[b]MIC for ciprofloxacin (μg/ml).
[c]Fitness. Mean fitness per generation, relative to wild-type, SD, standard deviation (within parentheses) measured in pair wise competition against the isogenic wild-type (Δ*araBC*).
[d]P. Statistical significance of difference in fitness relative to the wild-type (Students t-test (95% confidence limit, two-tailed P-value).
[e]N. Number of independent competition experiments on which the fitness value is based.
doi:10.1371/journal.ppat.1000541.t001

Figure E.1 *Experimental data on the measured fitness and susceptibility of E. coli mutants to the MG1655 strain. Taken from [128]*

Genotype	Fitness	MIC(ng/ml)
00101	0.91	0.063
00110	0.83	0.048
00111	0.83	0.095

Table E.1 *The estimated fitness and susceptibility of the missing genotypes. Fitness is expressed as a fraction of the wild-type fitness (i.e. that of 00000)*

Appendix F

A lower probability of mutation in the two phenotype model

We consider here how a result of Chapter 6 changes when the mutation probability μ is lowered to $\mu = 10^{-9}$, making it comparable to the experimentally measured probability of mutation in *E. coli* [46, 116]. We consider this for antibiotic concentration $C = 15$ ng/ml, for which results can be compared with those in Fig. 6.8, in which μ was an order of magnitude greater.

Figure F.1 shows plots of how the average frequencies of the population at each genotype (for phenotypes A and B) vary as a function of the time T. Comparing this with Fig. 6.8 we can see that the population follows a very similar evolutionary trajectory. The only difference between the results are the timescales in which they occur, in particular for the first culture. As is expected, due to the lower μ value, the results in Fig. F.1 show the population initially taking longer to evolve more resistant genotypes away from the wild-type. Genotype 00001 is evolved first before it begins to be outcompeted by the genotypes 10000 and 01000, as is the case in Fig. 6.8. Subsequent cultures appear to take similar times (~ 5 simulation time units) and there is otherwise no significant difference by reducing μ by an order of magnitude.

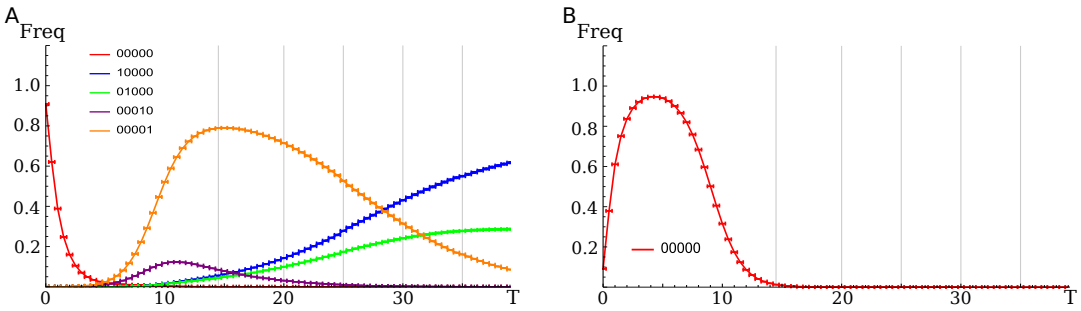

Figure F.1 *The evolution of the population in the two phenotype model at antibiotic concentration $C = 15$ ng/ml. All plots show curves of the average population frequency at each state (i.e. genotype/phenotype pair) as a function of the time T (in generations). States that are absent never had a frequency as large as 10^{-3}. Vertical lines indicate the points at which culture transfer took place, in which 1% of the population was used to seed a new culture. (A) and (B) show results for states in phenotype A and B respectively. Back mutations were excluded in the model. The remaining parameters used are mutation probability $\mu = 10^{-9}, \epsilon = 0.5, \alpha_{min} = \beta_{min} = 0.01$ and $\alpha_{max} = \beta_{max} = 1$. All results are gathered using a KMC algorithm and averaged over 100 runs.*

Appendix G

A lower threshold value ϵ in the two phenotype model

We consider here how the results in Chapter 6 change when the threshold value ϵ — defined in (6.2) — is reduced. This is motivated by the observation in [28] that when the antibiotic concentration $C = 0.125 \times MIC_{\text{wild-type}}$, that 99.5% of cells were observed to be in the filamentous state. This was measured using a different strain of *E. coli* than we consider in Chapter 6. Nevertheless it suggests that the value $\epsilon = 0.5$, used for all results in Chapter 6, may be too high to be consistent with experimentally observed behaviour. Therefore we examine here how results change when $\epsilon = 0.1$. The consequence of reducing ϵ in the model is that it lowers the amount of DNA damage (due to antibiotic action) that can occur in a cell before it triggers the SOS response (and becomes filamentous).

Figure G.1 shows plots of how the average frequencies of the population at each genotype (for phenotypes A and B) vary as a function of the time T. These results are for when the antibiotic concentration $C = 50$ ng/ml, allowing for direct comparison with the results in Fig. 6.10 for which $\epsilon = 0.5$. The genotypes 10000 and 01000, which were both important to the evolution in Fig. 6.10, have MIC values that favour cells of these types existing in the filamentous state when $\epsilon = 0.1$.

The evolution of more mutated genotypes therefore occurs faster when $\epsilon = 0.1$. We can see this in Fig. G.1 in the rapid evolution of double mutants (i.e. those with two point mutations relative to the wild-type genotype) occurring over ~ 4 hours. This can be compared with Fig. 6.10 which shows only single mutation

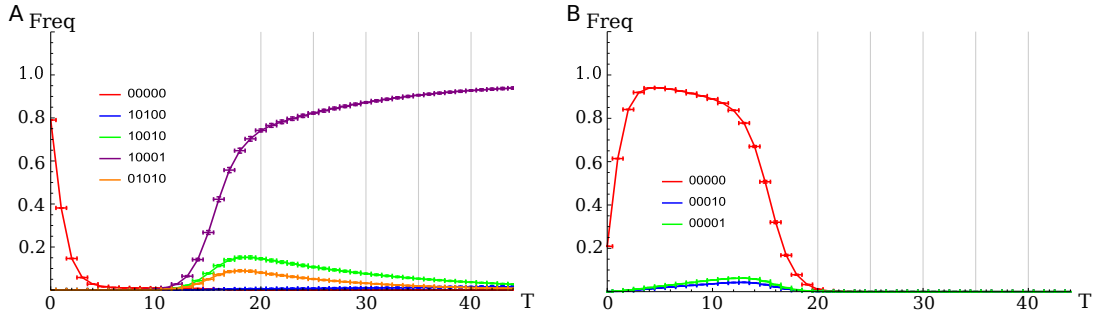

Figure G.1 *The evolution of the population in the two phenotype model at antibiotic concentration* $C = 50$ *ng/ml. All plots show curves of the average population frequency at each state (i.e. genotype/phenotype pair) as a function of the time* T *(in generations). States that are absent never had a frequency as large as* 10^{-3}*. Vertical lines indicate the points at which culture transfer took place, in which* 1% *of the population was used to seed a new culture. (A) and (B) show results for states in phenotype A and B respectively. Back mutations were excluded in the model. The remaining parameters used are mutation probability* $\mu = 10^{-8}, \epsilon = 0.1, \alpha_{min} = \beta_{min} = 0.01$ *and* $\alpha_{max} = \beta_{max} = 1$*. All results are gathered using a KMC algorithm and averaged over* 100 *runs.*

genotypes reaching considerable frequencies over $\sim$ 12 hours. In Fig. G.1 the mutant 10001 quickly comes to dominate the population by $\sim$ 6 hours and remains dominant for the remaining time considered. By the absence of the genotype 10000 (which came to dominate the results in Fig. 6.10 when $\epsilon = 0.5$) the population is now taking a different evolutionary trajectory over the space of possible genotype/phenotype pairs. Therefore the results of this model are sensitive to the value of ϵ.

Bibliography

[1] "Genetic Science Learning Center. "Why Clone?" Learn.Genetics. University of Utah." http://learn.genetics.utah.edu/content/cloning/whyclone, . Accessed: 19-10-2016.

[2] Ackermann, M. "Microbial individuality in the natural environment." *The ISME Journal* 7, 3: (2013) 465–467.

[3] ———. "A functional perspective on phenotypic heterogeneity in microorganisms." *Nature Reviews Microbiology* 13, 8: (2015) 497–508.

[4] Ackermann, M., and L. Chao. "DNA sequences shaped by selection for stability." *PLoS Genetics* 2, 2: (2006) 224–230.

[5] Ackermann, M., B. Stecher, N. E. Freed, P. Songhet, W.-D. Hardt, and M. Doebeli. "Self-destructive cooperation mediated by phenotypic noise." *Nature* 454, 7207: (2008) 987–90.

[6] Adiciptaningrum, A. M., I. C. Blomfield, and S. J. Tans. "Direct observation of type 1 fimbrial switching." *EMBO reports* 10, 5: (2009) 527–532.

[7] Aita, T., and Y. Husimi. "Adaptive Walks by the Fittest among Finite Random Mutants on a Mt. Fuji-type Fitness Landscape." *Journal of Theoretical Biology* 193, 3: (1998) 383–405.

[8] ———. "Fitness Spectrum Among Random Mutants on Mt. Fuji-Type Fitness Landscape." *Journal of Theoretical Biology* 182, 4: (1996) 469–485.

[9] Aita, T., H. Uchiyama, T. Inaoka, M. Nakajima, T. Kokubo, and Y. Husimi. "Analysis of a local fitness landscape with a model of the rough Mt. Fuji-type landscape: Application to prolyl endopeptidase and thermolysin." *Biopolymers* 54, 1: (2000) 64–79.

[10] Alberts, B., A. Johnson, J. Lewis, M. Raff, K. Roberts, and P. Walter. *Molecular biology of the cell*. Garland Science, 2008, fifth edition.

[11] Aldridge, B. B., M. Fernandez-suarez, D. Heller, V. Ambravaneswaran, D. Irimia, M. Toner, and S. M. Fortune. "Asymmetry and

Aging of Mycobacterial Cells Lead to Variable Growth and Antibiotic Susceptibility." *Science (New York, N.Y.)* 529, 2006.

[12] Ancliff, M., and J. M. Park. "Spin Coherent State Representation of the Crow-Kimura and Eigen Models of Quasispecies Theory." *Journal of Statistical Physics* 143, 4: (2011) 636–656.

[13] Ansel, J., H. Bottin, C. Rodriguez-Beltran, C. Damon, M. Nagarajan, S. Fehrmann, J. François, and G. Yvert. "Cell-to-cell stochastic variation in gene expression is a complex genetic trait." *PLoS Genetics* 4, 4.

[14] Arnoldini, M., I. A. Vizcarra, R. Peña-Miller, N. Stocker, M. Diard, V. Vogel, R. E. Beardmore, W. D. Hardt, and M. Ackermann. "Bistable expression of virulence genes in salmonella leads to the formation of an antibiotic-tolerant subpopulation." *PLoS Biology* 12, 8.

[15] Baake, E., M. Baake, and H. Wagner. "Ising Quantum Chain is Equivalent to a Model of Biological Evolution." *Physical Review Letters* 78, 3: (1997) 559–562.

[16] Balaban, N., J. Merrin, R. Chait, L. Kowalik, and S. Leibler. "Bacterial persistence as a phenotypic switch." *Science (New York, N.Y.)* 305, 5690: (2004) 1622–5.

[17] Bar-Even, A., J. Paulsson, N. Maheshri, M. Carmi, E. K. O'Shea, Y. Pilpel, and N. Barkai. "Noise in protein expression scales with natural protein abundance." *Nature Genetics* 38, 6: (2006) 636–643.

[18] Barrick, J. E., and R. E. Lenski. "Genome dynamics during experimental evolution." *Nature reviews. Genetics* 14, 12: (2013) 827–39.

[19] Barton, N. H., and S. Rouhani. "The frequency of shifts between alternative equilibria." *Journal of Theoretical Biology* 125: (1987) 397–418.

[20] Bayliss, C. D., W. A. Sweetman, and E. R. Moxon. "Mutations in Haemophilus influenzae Mismatch Repair Genes Increase Mutation Rates of Dinucleotide Repeat Tracts but Not Dinucleotide Repeat-Driven Pilin Phase Variation Rates." *Journal of Bacteriology* 186, 10: (2004) 2928–2935.

[21] Bayliss, C. D., T. van de Ven, and E. R. Moxon. "Mutations in polI but not mutSLH destabilize Haemophilus influenzae tetranucleotide repeats." *The EMBO journal* 21, 6: (2002) 1465–76.

[22] Beaumont, H. J., J. Gallie, C. Kost, G. C. Ferguson, and P. B. Rainey. "Experimental evolution of bet hedging." *Nature* 462, 1476-4687 (Electronic): (2009) 90–93.

[23] Becskei, a., and L. Serrano. "Engineering stability in gene networks by autoregulation." *Nature* 405, June: (2000) 590–593.

[24] Berestycki, J., E. Brunet, and Z. Shi. "The number of accessible paths in a hypercube." *Bernoulli* 22, 2: (2016) 653–680.

[25] Bi, E., and J. Lutkenhaus. "Cell division inhibitors SulA and MinCD prevent formation of the FtsZ ring." *Journal of Bacteriology* 175, 4: (1993) 1118–1125.

[26] Biebricher, C. K., M. Eigen, and W. C. Gardiner. "Kinetics of RNA Replication: Competition and Selection among Self-Replicating RNA Species." *biochemistry* 24: (1985) 6550–6560.

[27] Biebricher, C., and M. Eigen. "What is a quasispecies?" In *Current topics in microbiology and immunology*, 2006, volume 299, 1–31.

[28] Bos, J., Q. Zhang, S. Vyawahare, E. Rogers, S. M. Rosenberg, and R. H. Austin. "Emergence of antibiotic resistance from multinucleated bacterial filaments." *Proceedings of the National Academy of Sciences of the United States of America* 112, 1: (2015) 178–83.

[29] ———. "Emergence of antibiotic resistance from multinucleated bacterial filaments." *Proceedings of the National Academy of Sciences of the United States of America* 112, 1: (2015) 178–83.

[30] Breidenstein, E. B. M., C. de la Fuente-Nunez, and R. E. W. Hancock. "Pseudomonas aeruginosa: All roads lead to resistance." *Trends in Microbiology* 19, 8: (2011) 419–426.

[31] Burch, C., and L. Chao. "Evolution by small steps and rugged landscapes in the RNA virus phi6." *Genetics* 151, 3: (1999) 921–7.

[32] Cao, Y., D. T. Gillespie, and L. R. Petzold. "Efficient step size selection for the tau-leaping simulation method." *The Journal of chemical physics* 124, 4: (2006) 044,109.

[33] Carter, A. J. R., and G. P. Wagner. "Evolution of functionally conserved enhancers can be accelerated in large populations: a population-genetic model." *Proceedings. Biological sciences / The Royal Society* 269, 1494: (2002) 953–60.

[34] Choi, P. J., L. Cai, K. Frieda, and X. S. Xie. "A Stochastic Single-Molecule Event Triggers Phenotype Switching of a Bacterial Cell." *Science* 322, 5900: (2008) 442–446.

[35] Cirz, R. T., J. K. Chin, D. R. Andes, V. De Crécy-Lagard, W. A. Craig, and F. E. Romesberg. "Inhibition of mutation and combating the evolution of antibiotic resistance." *PLoS Biology* 3, 6: (2005) 1024–1033.

[36] Covacci, A., and R. Rappuolit. "Helicobacter pylori: molecular evolution of a bacterial quasi-species." *Current Opinion in Microbiology* 1: (1998) 96–2.

[37] Darwin, C. *Journal of researches into the natural history and geology of the countries visited during the voyage of H.M.S. Beagle round the world.* 1845.

[38] ———. *On the origin of species.* Oxford University Press, 1859.

[39] De Bolle, X., C. D. Bayliss, D. Field, T. Van De Ven, N. J. Saunders, D. W. Hood, and E. R. Moxon. "The length of a tetranucleotide repeat tract in Haemophilus influenzae determines the phase variation rate of a gene with homology to type III DNA methyltransferases." *Molecular Microbiology* 35, 1: (2000) 211–222.

[40] Deng, W., V. Burland, G. P. Iii, A. Boutin, G. F. Mayhew, P. Liss, N. T. Perna, J. Debra, B. Mau, S. Zhou, D. C. Schwartz, D. Fetherston, L. E. Lindler, R. R. Brubaker, G. V. Plano, S. C. Straley, A. Kathleen, M. L. Nilles, J. S. Matson, R. Frederick, R. D. Perry, D. J. Rose, J. D. Fetherston, K. a. Mcdonough, and F. R. Blattner. "Genome Sequence of Yersinia pestis KIM ." *Journal of Bacteriology* 184, 16: (2002) 4601–4611.

[41] Derrida, B. "Random-energy model: An exactly solvable model of disordered systems." *Physical Review B* 24, 5: (1981) 2613–2626.

[42] Dixon, K., C. D. Bayliss, K. Makepeace, E. R. Moxon, and D. W. Hood. "Identification of the functional initiation codons of a phase-variable gene of Haemophilus influenzae, lic2A, with the potential for differential expression." *Journal of Bacteriology* 189, 2: (2007) 511–521.

[43] Domingo, E. "Quasispecies and the implications for virus persistence and escape." *Clinical and Diagnostic Virology* 10, 2-3: (1998) 97–101.

[44] Drake, J. W. "Rates of spontaneous mutation among RNA viruses." *Proceedings of the National Academy of Sciences of the United States of America* 90, 9: (1993) 4171–4175.

[45] Drake, J. W., and J. J. Holland. "Mutation rates among RNA viruses." *Proceedings of the National Academy of Sciences of the United States of America* 96, 24: (1999) 13,910–3.

[46] Drake, J. W., B. Charlesworth, D. Charlesworth, and J. F. Crow. "Rates of spontaneous mutation." *Genetics* 148, 4: (1998) 1667–1686.

[47] Drake, J. W. "A constant rate of spontaneous mutation in DNA-based microbes." *Proceedings of the National Academy of ...* 88, 16: (1991) 7160–4.

[48] Drenkard, E. "Antimicrobial resistance of Pseudomonas aeruginosa biofilms." *Microbes and Infection* 5, 13: (2003) 1213–1219.

[49] Durrett, R., and D. Schmidt. "Waiting for two mutations: with applications to regulatory sequence evolution and the limits of Darwinian evolution." *Genetics* 180, 3: (2008) 1501–9.

[50] Eckburg, P. B., P. B. Eckburg, E. M. Bik, C. N. Bernstein, E. Purdom, L. Dethlefsen, M. Sargent, S. R. Gill, K. E. Nelson, and D. A. Relman. "Diversity of the Human Intestinal Microbial Flora." *Science* 1635, 2005: (2013) 1635–1639.

[51] Eigen, M. "Selforganization of matter and the evolution of biological macromolecules." *Die Naturwissenschaften* 58, 10: (1971) 465–523.

[52] Eigen, M., J. McCaskill, and P. Schuster. "Molecular Quasi-Species." *Journal Physical Chemistry* 92, 1: (1988) 6881–6891.

[53] Eigen, M., and P. Schuster. "The Hypercyde Emergence of the Hypercycle." *Die Naturwissenschaften* 64: (1977) 541–565.

[54] Elena, S., and R. Lenski. "Evolution experiments with microorganisms: the dynamics and genetic bases of adaptation." *Nature reviews. Genetics* 4, 6: (2003) 457–69.

[55] Elowitz, M. B. "Stochastic Gene Expression in a Single Cell." *Science* 297: (2002) 1183–1186.

[56] Ewens, W. J. *Mathematical population genetics.* Springer, 2004, second edition.

[57] Feller, W. *An introduction to probability theory and its applications.* Wiley, 1950, second edition.

[58] Fexby, S., T. Bjarnsholt, P. Ø. Jensen, V. Roos, N. Høiby, M. Givskov, and P. Klemm. "Biological trojan horse: Antigen 43 provides specific bacterial uptake and survival in human neutrophils." *Infection and Immunity* 75, 1: (2007) 30–34.

[59] Fisher, R. A. *The genetical theory of natural selection.* Oxford University Press, 1930, first edition.

[60] Fishman, S. L., and A. D. Branch. "The quasispecies nature and biological implications of the hepatitis C virus." *Infection, Genetics and Evolution* 9, 6: (2009) 1158–1167.

[61] Fossum, S., E. Crooke, and K. Skarstad. "Organization of sister origins and replisomes during multifork DNA replication in Escherichia coli." *The EMBO Journal* 26, 21: (2007) 4514–4522.

[62] Franke, J., A. Klözer, J. A. G. M. de Visser, and J. Krug. "Evolutionary accessibility of mutational pathways." *PLoS computational biology* 7, 8.

[63] Franke, J., and J. Krug. "Evolutionary Accessibility in Tunably Rugged Fitness Landscapes." *Journal of Statistical Physics* 148, 4: (2012) 705–722.

[64] Franke, J., G. Wergen, and J. Krug. "Records and sequences of records from random variables with a linear trend." *Journal of Statistical Mechanics: Theory and Experiment* 10013: (2010) 21.

[65] Franz, S., L. Peliti, and S. Franz. "Error threshold in simple landscapes An evolutionary version of the random energy model." *Journal of Physics A* 26: (1993) 1195—-1199.

[66] Fraser, H. B., A. E. Hirsh, G. Giaever, J. Kumm, and M. B. Eisen. "Noise minimization in eukaryotic gene expression." *PLoS Biology* 2, 6: (2004) 834–838.

[67] Fudenberg, D., and L. Imhof. "Phenotype switching and mutations in random environments." *Bulletin of mathematical biology* 74, 2: (2012) 399–421.

[68] Galluccio, S. "Exact solution of the quasispecies model in a sharply peaked fitness landscape." *Physical Review E* 56, 4: (1997) 4526–4539.

[69] Garcia, C., D. A. Moreno, A. Ballester, M. L. Blazquez, and F. Gonzalez. "Bioremediation of an industrial acid mine water by metal-tolerant sulphate-reducing bacteria." *Minerals Engineering* 14, 9: (2001) 997–1008.

[70] Gardiner, C. *Stochastic methods*. Springer, 2009, fourth edition.

[71] Gavrilets, S. "Evolution and speciation on holey adaptive landscapes." *Trends in Ecology and Evolution* 12, 8: (1997) 307–312.

[72] Gillespie, D. T. "Approximate accelerated stochastic simulation of chemically reacting systems." *Journal of Chemical Physics* 115, 4: (2001) 1716–1733.

[73] ———. "General Method for Numerically Simulating Stochastic Time Evolution of Couple Chemical Reactions." *Journal of Computational Physics* 22, 4: (1976) 1–32.

[74] Gillespie, J. "Some properties of finite populations experiencing strong selection and weak mutation." *American Naturalist* 121, 5: (1983) 691–708.

[75] ———. "Molecular evolution over the mutational landscape." *Evolution* 38, 5: (1984) 1116–1129.

[76] Gillespie, S. H., S. Basu, A. L. Dickens, D. M. O'Sullivan, and T. D. McHugh. "Effect of subinhibitory concentrations of ciprofloxacin on Mycobacterium fortuitum mutation rates." *Journal of Antimicrobial Chemotherapy* 56, 2: (2005) 344–348.

[77] Griffiths, D. F., and D. J. Higham. *Numerical methods for ordinary differential equations*. Springer, 2010.

[78] Haldane, J. B. S. *The causes of evolution*. Longmans, Green and Co, 1932, first edition.

[79] van Ham, S. M., L. van Alphen, F. R. Mooi, and J. P. M. van Putten. "Phase variation of H. influenzae fimbriae: Transcriptional control of two divergent genes through a variable combined promoter region." *Cell* 73, 6: (1993) 1187–1196.

[80] Hartl, D. L., and A. G. Clark. *Principles of population genetics*. Sinauer Associates, Inc., 2007, fourth edition.

[81] Hasman, H., M. A. Schembri, and P. Klemm. "Antigen 43 and type 1 fimbriae determine colony morphology of Escherichia coli K-12." *Journal of Bacteriology* 182, 4: (2000) 1089–1095.

[82] Hayashi, Y., T. Aita, H. Toyota, Y. Husimi, I. Urabe, and T. Yomo. "Experimental rugged fitness landscape in protein sequence space." *PLoS ONE* 1, 1.

[83] Hegarty, P., and A. Martinsson. "On the existence of accessible paths in various models of fitness landscapes." *The Annals of Applied Probability* 24, 4: (2014) 1375–1395.

[84] Hermisson, J., O. Redner, H. Wagner, and E. Baake. "Mutation-selection balance: ancestry, load and maximum principle." *Theoretical Population Biology* 62: (2002) 9–46.

[85] High, N. J., M. P. Jennings, and E. R. Moxon. "Tandem repeats of the tetramer 5'-CAAT-3' present in lic2A are required for phase variation but not lipopolysaccharide biosynthesis in Haemophilus influenzae." *Molecular microbiology* 20, 1 996: (1996) 165–174.

[86] Holland, J. J., E. Domingo, J. C. de la Torre, and D. A. Steinhauer. "Mutation frequencies at defined single codon sites in vesicular stomatitis virus and poliovirus can be increased only slightly by chemical mutagenesis." *Journal of virology* 64, 8: (1990) 3960–2.

[87] Hood, D. W., M. E. Deadman, T. Allen, H. Masoud, a. Martin, J. R. Brisson, R. Fleischmann, J. C. Venter, J. C. Richards, and E. R. Moxon. "Use of the complete genome sequence information of Haemophilus influenzae strain Rd to investigate lipopolysaccharide biosynthesis." *Molecular microbiology* 22, 5: (1996) 951–65.

[88] Huh, D., and J. Paulsson. "Non-genetic heterogeneity from stochastic partitioning at cell division." *Nature Genetics* 43, 2: (2011) 95–100.

[89] Iwasa, Y., F. Michor, and M. a. Nowak. "Evolutionary dynamics of invasion and escape." *Journal of Theoretical Biology* 226, 2: (2004) 205–214.

[90] ———. "Stochastic tunnels in evolutionary dynamics." *Genetics* 166, 3: (2004) 1571–9.

[91] Jain, K., and J. Krug. "Adaptation in simple and complex fitness landscapes." *Structural approaches to sequence evolution* .

[92] Jain, K., J. Krug, and S. Park. "Evolutionary advantage of small populations on complex fitness landscapes." *Evolution; international journal of organic evolution* 65, 7: (2011) 1945–55.

[93] Jain, K., and J. Krug. "Deterministic and stochastic regimes of asexual evolution on rugged fitness landscapes." *Genetics* 175, 3: (2007) 1275–88.

[94] Janion, C. "Inducible SOS response system of DNA repair and mutagenesis in Escherichia coli." *International Journal of Biological Sciences* 4, 6: (2008) 338–344.

[95] John E. McGowan, J. "Antimicrobial Resistance in Hospital Organisms and Its Relation to Antibiotic Use." *Reviews of Infectious Diseases* 5, 6: (1983) 1033–1048.

[96] Justice, S. S., D. A. Hunstad, P. C. Seed, and S. J. Hultgren. "Filamentation by Escherichia coli subverts innate defenses during urinary tract infection." *Proceedings of the National Academy of Sciences of the United States of America* 103, 52: (2006) 19,884–9.

[97] Kallmeyer, J., R. Pockalny, R. R. Adhikari, D. C. Smith, and S. D'Hondt. "From the Cover: Global distribution of microbial abundance and biomass in subseafloor sediment." *Proceedings of the National Academy of Sciences* 109, 40: (2012) 16,213–16,216.

[98] Karlin, S., and J. a. N. Mra. "Compositional biases of bacterial genomes and evolutionary implications . Compositional Biases of Bacterial Genomes and Evolutionary Implications." *Journal of bacteriology* 179, 12: (1997) 3899–3913.

[99] Kashiwagi, A., I. Urabe, K. Kaneko, and T. Yomo. "Adaptive response of a gene network to environmental changes by fitness-induced attractor selection." *PLoS ONE* 1, 1.

[100] Kauffman, S., and E. D. Weinberger. "The NK model of rugged fitness landscapes and its application to maturation of the immune response." *Journal of Theoretical Biology* 141: (1989) 211–246.

[101] Kauffman, S., and S. Levin. "Towards a general theory of adaptive walks on rugged landscapes." *Journal of Theoretical Biology* 128: (1987) 11–45.

[102] Kearns, D., and R. Losick. "Cell population heterogeneity during growth of Bacillus subtilis." *Genes & development* 3083–3094.

[103] Kimura, M. "Evolutionary rate at the molecular level." *Nature* 217, 5129: (1968) 624–626.

[104] ———. "On the probability of fixation of mutant genes in a population." *Genetics* 47, 391: (1962) 713–719.

[105] ———. "The role of compensatory neutral mutations in molecular evolution." *Journal of Genetics* 64, 1: (1985) 7–19.

[106] Kingman, J. "A simple model for the balance between selection and mutation." *Journal of applied probability* 15, 1: (1978) 1–12.

[107] Komp Lindgren, P., A. Karlsson, and D. Hughes. "Mutation rate and evolution of fluoroquinolone resistance in Escherichia coli isolates from patients with urinary tract infections." *Antimicrobial agents and chemotherapy* 47, 10: (2003) 3222–3232.

[108] Korona, R., C. Nakatsu, L. Forney, and R. Lenski. "Evidence for multiple adaptive peaks from populations of bacteria evolving in a structured habitat." *Proceedings of the National Academy of Sciences of the United States of America* 91, 19: (1994) 9037–41.

[109] Krug, J., and K. Jain. "Breaking records in the evolutionary race." *Physica A: Statistical Mechanics and its Applications* 358, 1 SPEC. ISS.: (2005) 1–9.

[110] Krug, J., and C. Karl. "Punctuated evolution for the quasispecies model." *Physica A: Statistical Mechanics and its Applications* 318, 1-2: (2003) 137–143.

[111] Kussell, E., and S. Leibler. "Phenotypic Diversity , Population Growth , and Information in Fluctuating Environments." *Science* 309, 5743: (2005) 2075–2078.

[112] Kuwahara, H., and O. S. Soyer. "Bistability in feedback circuits as a byproduct of evolution of evolvability." *Molecular systems biology* 8, 564: (2012) 1–11.

[113] Lachmann, M., and E. Jablonka. "The inheritance of phenotypes: an adaptation to fluctuating environments." *Journal of theoretical biology* 181, 1: (1996) 1–9.

[114] ed. by Lassig, M., and A. Valleriani. *Biological evolution and statistical physics*. Springer, 2002, first edition.

[115] Lauring, A., and R. Andino. "Quasispecies theory and the behavior of RNA viruses." *PLoS pathogens* 6, 7: (2010) e1001,005.

[116] Lee, H., E. Popodi, H. Tang, and P. L. Foster. "Rate and molecular spectrum of spontaneous mutations in the bacterium Escherichia coli as determined by whole-genome sequencing." *Proceedings of the National Academy of Sciences* 109, 41: (2012) E2774–E2783.

[117] Lehner, B. "Selection to minimise noise in living systems and its implications for the evolution of gene expression." *Molecular systems biology* 4, 170: (2008) 170.

[118] Lenz, P., and L. Søgaard-Andersen. "Temporal and spatial oscillations in bacteria." *Nature reviews. Microbiology* 9, 8: (2011) 565–577.

[119] LeuthÄusser, I. "Statistical mechanics of Eigen's evolution model." *Journal of Statistical Physics* 48, 1-2: (1987) 343–360.

[120] Leuthausser, I. "An exact correspondence between Eigen's evolution model and a two-dimensional Ising system." *The Journal of Chemical Physics* 84, 3: (1986) 1884.

[121] Levin, B. R., and C. T. Bergstrom. "Bacteria are different: observations, interpretations, speculations, and opinions about the mechanisms of adaptive evolution in prokaryotes." *Proceedings of the National Academy of Sciences of the United States of America* 97, 13: (2000) 6981–5.

[122] Libby, E., and P. B. Rainey. "Exclusion rules, bottlenecks and the evolution of stochastic phenotype switching." *Proceedings. Biological sciences / The Royal Society* 278, 1724: (2011) 3574–83.

[123] Liu, Y., N. F. Tsinoremas, C. H. Johnson, N. V. Lebedeva, S. S. Golden, M. Ishiura, and T. Kondo. "Circadian orchestration of gene expression in cyanobacteria." *Genes and Development* 9, 12: (1995) 1469–1478.

[124] Lozovsky, E. R., T. Chookajorn, K. M. Brown, M. Imwong, P. J. Shaw, S. Kamchonwongpaisan, D. E. Neafsey, D. M. Weinreich, and D. L. Hartl. "Stepwise acquisition of pyrimethamine resistance in the malaria parasite." *Proc Natl Acad Sci U S A* 106, 29: (2009) 12,025–12,030.

[125] Maamar, H., A. Raj, and D. Dubnau. "Noise in Gene Expression Determines Cell Fate in Bacillus subtilis." *Science* 317, 5837: (2007) 1–9.

[126] Maiques, E., C. Úbeda, S. Campoy, Í. Lasa, R. P. Novick, J. Barbé, J. R. Penadés, N. Salvador, U. Carles, J. Barbe, and R. Penade. "β -Lactam Antibiotics Induce the SOS Response and Horizontal Transfer of Virulence Factors in Staphylococcus aureus -Lactam Antibiotics Induce the SOS Response and Horizontal Transfer of Virulence Factors in Staphylococcus aureus I n." *Journal of Bacteriology* 188, 7: (2006) 2726–2729.

[127] Maisnier-Patin, S., O. G. Berg, L. Liljas, and D. I. Andersson. "Compensatory adaptation to the deleterious effect of antibiotic resistance in Salmonella typhimurium." *Molecular Microbiology* 46, 2: (2002) 355–366.

[128] Marcusson, L. L., N. Frimodt-Møller, and D. Hughes. "Interplay in the selection of fluoroquinolone resistance and bacterial fitness." *PLoS pathogens* 5, 8: (2009) e1000,541.

[129] Massey, R. C., A. Buckling, and S. J. Peacock. "Phenotypic switching of antibiotic resistance circumvents permanent costs in Staphylococcus aureus." *Current Biology* 11, 22: (2001) 1810–1814.

[130] Michel, B. "After 30 years of study, the bacterial SOS response still surprises us." *PLoS Biology* 3, 7: (2005) 1174–1176.

[131] Miller, C., L. E. Thomsen, C. Gaggero, R. Mosseri, H. Ingmer, and S. N. Cohen. "SOS response induction by beta-lactams and bacterial defense against antibiotic lethality." *Science (New York, N.Y.)* 305, 5690: (2004) 1629–31.

[132] Miralles, R., P. Gerrish, A. Moya, and S. Elena. "Clonal interference and the evolution of RNA viruses." *Science* 285: (1999) 1745–1747.

[133] Moore, F., and S. Tonsor. "A simulation of Wright's shifting-balance process: migration and the three phases." *Evolution* 48, 1: (1994) 69–80.

[134] Moran, P. "Random Processes in Genetics." , April: (1957) 60–71.

[135] Moxon, R., C. Bayliss, and D. Hood. "Bacterial contingency loci: the role of simple sequence DNA repeats in bacterial adaptation." *Annual review of genetics* 40: (2006) 307–33.

[136] Mrázek, J., X. Guo, and A. Shah. "Simple sequence repeats in prokaryotic genomes." *Proceedings of the National Academy of Sciences of the United States of America* 104, 20: (2007) 8472–8477.

[137] Murray, J. *Mathematical biology.* Springer, 2002, third edition.

[138] Murthy, K., and K. Kehr. "Mean first-passage time of random walks on a random lattice." *Physical Review A* 40, 4: (1989) 2082–2087.

[139] Neidhart, J., I. G. Szendro, and J. Krug. "Adaptation in tunably rugged fitness landscapes: The rough Mount Fuji model." *Genetics* 198, 2: (2014) 699–713.

[140] New, A. M., B. Cerulus, S. K. Govers, G. Perez-Samper, B. Zhu, S. Boogmans, J. B. Xavier, and K. J. Verstrepen. "Different Levels of Catabolite Repression Optimize Growth in Stable and Variable Environments." *PLoS Biology* 12, 1: (2014) 17–20.

[141] Newman, C. M., J. E. Cohen, and C. Kipnis. "Neo-darwinian evolution implies punctuated equilibria." *Nature* 315: (1985) 400–401.

[142] Newman, J. R. S., S. Ghaemmaghami, J. Ihmels, D. K. Breslow, M. Noble, J. L. DeRisi, and J. S. Weissman. "Single-cell proteomic analysis of S. cerevisiae reveals the architecture of biological noise TL - 441." *Nature* 441 VN -, 7095: (2006) 840–846.

[143] Nowak, M. "What is a quasispecies?" *Trends in ecology & evolution* 7, 4.

[144] Nowak, M. A. *Evolutionary Dynamics.* The Belknap Press of Harvard University Press, 2006.

[145] O'Neill, J. "Antimicrobial Resistance : Tackling a crisis for the health and wealth of nations." Technical Report December, 2014.

[146] Organization, W. H. "Antimicrobial resistance: global report on surveillance." Technical report, 2014.

[147] ORR, H. "A Minimum on the Mean Number of Steps Taken in Adaptive Walks." *Journal of Theoretical Biology* 220, 2: (2003) 241–247.

[148] Ozbudak, E., M. Thattai, and H. Lim. "Multistability in the lactose utilization network of Escherichia coli." *Nature* 4680, 1982: (2004) 4677–4680.

[149] Ozbudak, E. M., M. Thattai, I. Kurtser, A. D. Grossman, and A. van Oudenaarden. "Regulation of noise in the expression of a single gene." *Nature genetics* 31, 1: (2002) 69–73.

[150] Parvin, J. D., A. Moscona, W. T. Pan, J. M. Leider, and P. Palese. "Measurement of the mutation rates of animal viruses: influenza A virus and poliovirus type 1." *Journal of virology* 59, 2: (1986) 377–83.

[151] Pericone, C. D., D. Bae, M. Shchepetov, T. McCool, and J. N. Weiser. "Short-sequence tandem and nontandem DNA repeats and endogenous hydrogen peroxide production contribute to genetic instability of Streptococcus pneumoniae." *Journal of Bacteriology* 184, 16: (2002) 4392–4399.

[152] Philippi, T., and J. Seger. "Hedging one's evolutionary bets, revisited." *Trends in Ecology and Evolution* 4, 2: (1989) 41–44.

[153] Pine, L., and C. J. Boone. "Comparative cell wall analyses of morphological forms within the genus Actinomyces." *Journal of Bacteriology* 94, 4: (1967) 875–883.

[154] Poelwijk, F., S. Tnase-Nicola, D. Kiviet, and S. Tans. "Reciprocal sign epistasis is a necessary condition for multi-peaked fitness landscapes." *Journal of theoretical biology* 272, 1: (2011) 141–4.

[155] Press, W. H., S. A. Teukolsky, W. T. Vetterling, and B. P. Flannery. *Numerical recipes in C*. Cambridge University Press, 2002, second edition.

[156] Preston, B. D., B. J. Poiesz, and L. A. Loeb. "Fidelity of HIV-1 reverse transcriptase." *Science* 242, 4882: (1988) 1168–1171.

[157] Rainey, P., H. Beaumont, G. Ferguson, J. Gallie, C. Kost, E. Libby, and X. Zhang. "The evolutionary emergence of stochastic phenotype switching in bacteria." *Microbial cell factories* 10 Suppl 1, Suppl 1: (2011) S14.

[158] Raser, J. M., and E. K. O'Shea. "Noise in gene expression: origins, consequences, and control." *Science (New York, N.Y.)* 309, 5743: (2005) 2010–3.

[159] Redner, S. *A guide to first-passage processes.* Cambridge University Press, 2001.

[160] Reeve, J. N., J. Nolling, R. M. Morgan, and D. R. Smith. "Bmp4 and Morphological Variation of Beaks in Darwin's Finches." *Science* 305, September: (2004) 1462–1465.

[161] Regoes, R. R., C. Wiuff, R. M. Zappala, N. Kim, F. Baquero, B. R. Levin, and K. N. Garner. "Pharmacodynamic Functions : a Multiparameter Approach to the Design of Antibiotic Treatment Regimens Pharmacodynamic Functions : a Multiparameter Approach to the Design of Antibiotic Treatment Regimens." *Antimicrobial agents and chemotherapy* 48, 10: (2004) 3670–3676.

[162] Reuven, P., and A. Eldar. "Macromotives and microbehaviors: The social dimension of bacterial phenotypic variability." *Current Opinion in Genetics and Development* 21, 6: (2011) 759–767.

[163] Riley, K., M. Hobson, and S. Bence. *Mathematical methods for physics and engineering.* Cambridge University Press, .

[164] Ritz, D. "Conversion of a Peroxiredoxin into a Disulfide Reductase by a Triplet Repeat Expansion." *Science* 294, 5540: (2001) 158–160.

[165] Rosqvist, R., M. Skurnik, and H. Wolf-Watz. "Increased virulence of Yersinia pseudotuberculosis by two independent mutations." *Nature* 334, 6182: (1988) 522–4.

[166] Rotem, E., A. Loinger, I. Ronin, I. Levin-Reisman, C. Gabay, N. Shoresh, O. Biham, and N. Q. Balaban. "Regulation of phenotypic variability by a threshold-based mechanism underlies bacterial persistence." *Proceedings of the National Academy of Sciences of the United States of America* 107, 28: (2010) 12,541–12,546.

[167] Rowe, W., M. Platt, D. C. Wedge, P. J. Day, D. B. Kell, and J. Knowles. "Analysis of a complete DNA-protein affinity landscape." *Journal of The Royal Society Interface* 7, 44: (2010) 397–408.

[168] Ryan, D. M., and D. Monsey. "Bacterial filamentation and in vivo efficacy: a comparison of several cephalosporins." *Journal of Antimicrobial Chemotherapy* 7, 1: (1981) 57–63.

[169] Salathé, M., J. Van Cleve, and M. Feldman. "Evolution of stochastic switching rates in asymmetric fitness landscapes." *Genetics* 182, 4: (2009) 1159–64.

[170] Sanchez, G. V., R. N. Master, R. B. Clark, M. Fyyaz, P. Duvvuri, G. Ekta, and J. Bordon. "Klebsiella pneumoniae antimicrobial drug resistance, United States, 1998-2010." *Emerging Infectious Diseases* 19, 1: (2013) 133–136.

[171] Sassanfar, M., and J. Roberts. "Nature of the SOS-inducing signal in Escherichia coli. The involvement of DNA replication." *Journal of Molecular Biology* 212: (1990) 79–96.

[172] Schembri, M. A., L. Hjerrild, M. Gjermansen, and P. Klemm. "Differential expression of the Escherichia coli autoaggregation factor antigen 43." *Journal of Bacteriology* 185, 7: (2003) 2236–2242.

[173] Schmiegelt, B., and J. Krug. "Evolutionary accessibility of modular fitness landscapes." *Journal of Statistical Physics* 154: (2014) 334–355.

[174] Schrag, S. J., V. Perrot, and B. R. Levin. "Adaptation to the fitness costs of antibiotic resistance in Escherichia coli." *Proc Biol Sci* 264, 1386: (1997) 1287–1291.

[175] Schrag, S. J., and V. Perrot. "Reducing antibiotic resistance." *Nature* 381: (1996) 120–121.

[176] Serra, M. C., and P. Haccou. "Dynamics of escape mutants." *Theoretical population biology* 72, 1: (2007) 167–78.

[177] Shimizu, Y., S. Tsuru, Y. Ito, B. Ying, and T. Yomo. "Stochastic switching induced adaptation in a starved Escherichia coli population." *PloS one* 6, 9: (2011) e23,953.

[178] Shin, T., D. Kraemer, J. Pryor, L. Liu, J. Rugila, L. Howe, S. Buck, K. Murphy, L. Lyons, and M. Westhusin. "A cat cloned by nuclear transplantation." *Nature* 415, 6874: (2002) 859.

[179] Silander, O. K., N. Nikolic, A. Zaslaver, A. Bren, I. Kikoin, U. Alon, and M. Ackermann. "A genome-wide analysis of promoter-mediated phenotypic noise in Escherichia coli." *PLoS Genetics* 8, 1.

[180] Simmonds, P., P. Balfe, C. a. Ludlam, J. O. Bishop, and a. J. Brown. "Analysis of sequence diversity in hypervariable regions of the external glycoprotein of human immunodeficiency virus type 1." *Journal of virology* 64, 12: (1990) 5840–50.

[181] Smith, J. M. "Natural selection and the concept of a protein space." *Nature* 225, 5232: (1970) 563–564.

[182] Sniegowski, P. D., P. J. Gerrish, and R. E. Lenski. "Evolution of high mutation rates in experimental populations of E . coli." *Nature* 387: (1997) 703–705.

[183] Stackhouse, R. R., N. G. Faith, C. W. Kaspar, C. J. Czuprynski, and A. C. L. Wong. "Survival and virulence of Salmonella enterica serovar enteritidis filaments induced by reduced water activity." *Applied and Environmental Microbiology* 78, 7: (2012) 2213–2220.

[184] Stern, A., M. Brown, P. Nickel, and T. F. Meyer. "Opacity genes in Neisseria gonorrhoeae: Control of phase and antigenic variation." *Cell* 47, 1: (1986) 61–71.

[185] Stewart, M. K., L. A. Cummings, M. L. Johnson, A. B. Berezow, and B. T. Cookson. "Regulation of phenotypic heterogeneity permits Salmonella evasion of the host caspase-1 inflammatory response." *Proceedings of the National Academy of Sciences* 108: (2011) 20,742–20,747.

[186] Süel, G. M., R. P. Kulkarni, J. Dworkin, J. Garcia-Ojalvo, and M. B. Elowitz. "Tunability and noise dependence in differentiation dynamics." *Science (New York, N.Y.)* 315, 5819: (2007) 1716–9.

[187] Sweetman, W. A., E. R. Moxon, and C. D. Bayliss. "Induction of the SOS regulon of Haemophilus influenzae does not affect phase variation rates at tetraneucleotide or dinucleotide repeats." *Microbiology* 151, 8: (2005) 2751–2763.

[188] Szendro, I., M. Schenk, and J. Franke. "Quantitative analyses of empirical fitness landscapes." *Journal of Statistical Mechanics: Theory and Experiment* .

[189] Szendro, I. G., J. Franke, J. A. G. M. de Visser, and J. Krug. "Predictability of evolution depends nonmonotonically on population size." *Proceedings of the National Academy of Sciences of the United States of America* 110, 2.

[190] Taddei, F., M. Radman, J. Maynard-Smith, B. Toupance, P. H. Gouyon, and B. Godelle. "Role of mutator alleles in adaptive evolution." *Nature* 387, 6634: (1997) 700–702.

[191] Tadrowski, A. C., M. R. Evans, and B. Waclaw. "Phenotypic switching can speed up biological evolution of microbes." *arXiv preprint* 1–11.

[192] Tarazona, P. "Error thresholds for molecular quasispecies as phase transitions." *Physical Review A* 45, 8: (1992) 6038–6050.

[193] Thattai, M., and A. van Oudenaarden. "Stochastic gene expression in fluctuating environments." *Genetics* 167, 1: (2004) 523–30.

[194] Tippin, B., P. Pham, and M. F. Goodman. "Error-prone replication for better or worse." *Trends in Microbiology* 12, 6: (2004) 288–295.

[195] Tran, H. T., J. D. Keen, M. Kricker, M. a. Resnick, and D. a. Gordenin. "Hypermutability of homonucleotide runs in mismatch repair and DNA polymerase proofreading yeast mutants." *Molecular and cellular biology* 17, 5: (1997) 2859–2865.

[196] Veening, J.-W., O. a. Igoshin, R. T. Eijlander, R. Nijland, L. W. Hamoen, and O. P. Kuipers. "Transient heterogeneity in extracellular protease production by Bacillus subtilis." *Molecular systems biology* 4, 184: (2008) 184.

[197] de Visser, J. A., S. C. Park, and J. Krug. "Exploring the effect of sex on empirical fitness landscapes." *Am Nat* 174 Suppl, July 2009: (2009) S15–30.

[198] de Visser, J. A. G. M., R. F. Hoekstra, and H. van den Ende. "Test of Interaction Between Genetic Markers That Affect Fitness in Aspergillus niger." *Evolution* 51, 5: (1997) 1499.

[199] de Visser, J. A. G. M., and J. Krug. "Empirical fitness landscapes and the predictability of evolution." *Nature reviews. Genetics* 15, 7: (2014) 480–90.

[200] Waters, C. M., and B. L. Bassler. "Quorum Sensing : Communication in Bacteria." *Annual Reviews in Cell Development Biology* 21, 1: (2005) 319–346.

[201] Weinreich, D. M., and L. Chao. "Rapid evolutionary escape by large populations from local fitness peaks is likely in nature." *Evolution; international journal of organic evolution* 59, 6: (2005) 1175–82.

[202] Weinreich, D. M., N. F. Delaney, M. a. Depristo, and D. L. Hartl. "Darwinian Evolution Can Follow Only Very Few Mutational Paths to Fitter Proteins." *Science* 3, 2004.

[203] ———. "Darwinian evolution can follow only very few mutational paths to fitter proteins." *Science* 3, 2004.

[204] Weinreich, D. M., R. A. Watson, and L. Chao. "Perspective:Sign Epistasis and Genetic Constraint on Evolutionary Trajectories." *Evolution* 59, 6: (2005) 1165.

[205] Weiser, J. N., J. M. Love, and E. R. Moxon. "The molecular mechanism of phase variation of H. influenzae lipopolysaccharide." *Cell* 59, 4: (1989) 657–665.

[206] Weissman, D. B., M. M. Desai, D. S. Fisher, and M. W. Feldman. "The rate at which asexual populations cross fitness valleys." *Theoretical population biology* 75, 4: (2009) 286–300.

[207] Whitlock, M. C., and D. Bourguet. "Factors affecting the genetic load in Drosophila: synergistic epistasis and correlations among fitness components." *Evolution* 54, 5: (2000) 1654–1660.

[208] Whitlock, M. C., P. C. Phillips, F. B. Moore, J. Stephen, and M. C. Whitlock. "Multiple Fitness Peaks and Epistasis." *Annual Review of Ecology and Systematics* 26, 1995: (2016) 601–629.

[209] Whitman, W. B., D. C. Coleman, and W. J. Wiebe. "Prokaryotes: the unseen majority." *Proc Natl Acad Sci U S A* 95, 12: (1998) 6578–6583.

[210] Wolf, D. M., V. V. Vazirani, and A. P. Arkin. "Diversity in times of adversity: Probabilistic strategies in microbial survival games." *Journal of Theoretical Biology* 234, 2: (2005) 227–253.

[211] Wolff, A., and J. Krug. "Robustness and epistasis in mutation-selection models." *Physical Biology* 6, 6.

[212] van der Woude, M. W., and I. R. Henderson. "Regulation and function of Ag43 (flu)." *Annual review of microbiology* 62: (2008) 153–69.

[213] Woude, M. W. V. D., and A. J. Bäumler. "Phase and Antigenic Variation in Bacteria." *Clinical Microbiology Reviews* 17, 3: (2004) 581–611.

[214] Wright, S. "Evolution in Mendelian populations." *Genetics* 16: (1931) 97–159.

[215] ———. "The roles of mutation, inbreeding, crossbreeding and selection in evolution.", 1932.

[216] Yvert, G., S. Ohnuki, S. Nogami, Y. Imanaga, S. Fehrmann, J. Schacherer, and Y. Ohya. "Single-cell phenomics reveals intra-species variation of phenotypic noise in yeast." *BMC systems biology* 7, 1: (2013) 54.

[217] Zaleski, P., M. Wojciechowski, and A. Piekarowicz. "The role of Dam methylation in phase variation of Haemophilus influenzae genes involved in defence against phage infection." *Microbiology* 151, 10: (2005) 3361–3369.

[218] Zhang, Q., G. Lambert, D. Liao, H. Kim, K. Robin, C.-k. Tung, N. Pourmand, and R. H. Austin. "Acceleration of Emergence of Bacterial Antibiotic Resistance in Connected Microenvironments." *Science* 333, 2011: (2011) 1764–1767.

[219] Zhang, Z., W. Qian, and J. Zhang. "Positive selection for elevated gene expression noise in yeast." *Molecular systems biology* 5, 299: (2009) 299.

[220] Zobell, C. E., and A. B. Cobet. "Filament formation by escherichia coli at increased hydrostatic pressures." *Journal of bacteriology* 87, 3: (1964) 710–719.